Spectroscopic Analysis of Hot (Pre-) White Dwarfs

Dissertation

der Mathematisch-Naturwissenschaftlichen Fakultät
der Eberhard Karls Universität Tübingen

zur Erlangung des Grades eines
Doktors der Naturwissenschaften
(Dr. rer. nat)

vorgelgt von
Nicole Reindl
aus Oberviechtach

2015

The cover picture shows a image of the newly discovered planetary nebula Kronberger 61. The composite color image consists of two narrow-band images ([O III] in blue and H α in red) obtained with the Gemini Multi-Object Spectrograph on the Gemini North telescope on Mauna Kea in Hawai'i (see Gemini Office press release http://www.gemini.edu/node/11656)

Gedruckt mit Genehmigung der Mathematisch – Naturwissenschaftlichen Fakultät der Eberhard Karls Universität Tübingen.

Tag der mündlichen Qualifikation:	26.03.2015
Dekan:	Prof. Dr. Wolfgang Rosenstiel
1. Berichterstatter:	Prof. Dr. Klaus Werner
2. Berichterstatter:	Dr. Thorsten Nagel

Contents

Zusammenfassung

In dieser Arbeit wurden verschiedene Arten von (Prä-) Weißen Zwergen (WZ) mittels statischen und expandierenden non-LTE Modellatmosphären analysiert mit dem Ziel, ein besseres Verständnis der späten, heißen Stadien der Sternentwicklung zu erhalten.
In der ersten Arbeit, Reindl *et al.* (2014c), wurde zum ersten Mal die zeitliche Entwicklung der Sternparameter des sich ungewöhnlich schnell entwicklenden, wasserstoffreichen Zentralsterns eines Planetarischen Nebels (ZSPN) SAO 244567 quantitativ bestimmt. Wir bestätigen, dass es sich um einen Stern mit geringer Masse ($M < 0.55\,M_{\odot}$) handeln muss. Somit stehen die schnelle Entwicklung von SAO 244567 und sein junger PN im starken Widerspruch zur klassischen Entwicklungstheorie. Wir glauben, dass der Stern vor Kurzem einen späten thermischen Puls erlitten hat. Alternativ könnte SAO 244567 auch das Endprodukt einer engen Doppelsternentwicklung sein. Damit wäre er ein Vorläufer eines massearmen ($0.35\,M_{\odot}$) Helium-WZ, der kürzlich eine Common-Envelope-Phase durchlebt hat, bei der der PN abgestoßen wurde.
Das Ziel der Arbeit Reindl *et al.* (2014b) war es, Anhaltspunkte für die Entwicklung der exotischen O(He)-Sterne zu erhalten. Neue optische Beobachtungen erlaubten uns eine bessere Bestimmung der atmosphärischen Parameter der ZSPN K 1−27 und LoTr 4. Zudem wurden Obergrenzen für die Massenverlustraten von K 1−27, LoTr 4, HS 1522+6615, und HS 2209+8229 bestimmt. Die Elementhäufigkeiten der O(He)-Sterne wurden mit denen anderer Sternklassen sowie Sternentwicklungsrechnungen verglichen, um eine heliumdominierte Entwicklungssequenz zu erklären.
In Reindl *et al.* (2014a) wurden 24 DO-WZe, die wir in der zehnten Datenveröffentlichung des Sloan Digital Sky Survey gefunden hatten, zum ersten Mal mit non-LTE Modellatmosphären analysiert. Zwei der Objekte sind die kühlsten DO-WZe, die noch beträchtliche Mengen an Kohlenstoff aufweisen, und stehen damit im starken Widerspruch zu Diffusionsrechnungen. Ein schwacher Sternwind könnte die hohen Kohlenstoffhäufigkeiten aber erklären. Des Weiteren stimmt die Massenverteilung der DO-WZe nach dem Windlimit nicht mit der der Objekte vor Windlimit überein. Wir führen diese Diskrepanz auf verschiedene evolutionäre Eingangskanäle zurück. Zur wasserstoffarmen WZ Sequenz tragen post-EHB-Sterne zu 13% bei und PG 1159- und O(He)-Sterne im jeweils etwa gleichem Ausmaß.
Die letzte Arbeit, De Marco *et al.* (2015), trägt zur Suche nach engen Doppelsternsystemen unter den ZSPN bei. Dazu wurden die Keplerlichtkurven von fünf ZSPN auf photometrische Variabilität untersucht. Mein Beitrag zu dieser Arbeit bestand in der Spektralanalyse dreier ZSPN. Dadurch konnten wir Pa 5 als zehntes Mitglied der O(He)-Sterne nachweisen. Obwohl nur bei einem Objekt die photometrische Variabilität eindeutig auf einen nahen Begleiter zurückzuführen ist, schlussfolgern wir, dass der Anteil von kurzperiodischen ZSPN sehr viel größer sein muss als der gegenwärtig geschätzte Anteil von 15%.

Summary

In this work, different kinds of hot (pre-) white dwarfs (WD) were analyzed by means of static and expanding non-LTE model atmospheres to obtain a better understanding of the late, hot stages of stellar evolution.
In the first paper, Reindl *et al.* (2014c), we derived for the first time the temporal evolution of the atmospheric parameters of the unusually quick evolving, hydrogen-rich central star of planetary nebula (CSPN) SAO 244567. We confirm that SAO 244567 must be a low-mass star ($M < 0.55\,M_{\odot}$). The slow evolution of the respective canonical stellar evolutionary models is, however, in strong contradiction to the observed fast evolution and the young planetary nebula. We speculate that the star could be a late He-shell flash object. Alternatively, it could be the outcome of a close-binary evolution. Then SAO 244567 would be a low-mass ($0.35\,M_{\odot}$) helium pre-WD after the common-envelope phase, during which the planetary nebula was ejected.
The paper Reindl *et al.* (2014b) aimed to obtain clues about the nature of the exotic O(He) stars. The new optical spectra allowed a more precise determination of the atmospheric parameters of the two CSPNe K 1−27 and LoTr 4. Furthermore, upper limits for the mass-loss rates of K 1−27, LoTr 4, HS 1522+6615, and HS 2209+8229 were derived. Finally, the atmospheric parameters of the O(He) stars were compared to those of other helium-dominated stars and stellar evolution calculations in order to explain a helium-dominated stellar evolution sequence.
In Reindl *et al.* (2014a), we identified 24 DO WDs in the tenth data release of the Sloan Digital Sky Survey and analyzed them for the first time by means of non-LTE model atmospheres. Two of our objects are the coolest DO WDs ever discovered that still show a considerable amount of carbon in the atmosphere. This is in strong contradiction with diffusion calculations and we suggested that a weak mass-loss is present in DO WDs. The mass distribution of DO WDs beyond the wind limit strongly deviates from the mass distribution of the objects before the wind limit. We address this phenomenon to different evolutionary input channels. We argue that the DO WD channel may be fed by about 13% by post-extreme-horizontal branch stars and that PG 1159 stars and O(He) stars may contribute in a similar extent to the non-DA WD channel.
The final paper, De Marco *et al.* (2015), contributes to the search for close binary CSPNe. We examined the Kepler lightcurves of five CSPNe and searched for photometric variabilities. My contribution to this paper was the determination of the atmospheric parameters of three CSPNe. By that, we could identify Pa 5 as the tenth known O(He) star. Although the photometric variability of only one CSPN can certainly be ascribed to a close companion, we conclude that there are a lot more short periodic close binaries than the currently estimated fraction of 15%.

Preface

The precise knowledge of the properties and evolution of stars is of central importance to astrophysics. The study of stars provides not only the understanding of different stellar populations' properties, but offers us also knowledge about cosmological basic principles, e.g., on the chemical evolution of the Universe or important standard candles such as Cepheid variables or progenitor systems of type Ia supernovae.

Figure 0.1: Artist's impression of Tycho Brahe observing of a "new star" (a supernova) on November 11, 1572. From Flammarion's Astronomie Populaire (1880), reproduced in Sky and Telescope, November 1998.

Over a human life span, stars seem to undergo no changes, therefore they were considered as immutable for a long time. In fact, in Europe this idea held up until 1572 when Tycho Brahe observed a very bright star, now named Supernova 1572, which had unexpectedly appeared in the constellation Cassiopeia (Fig. 0.1). He found that this object does not show any parallax against the background of the fixed stars over several months and thus, he concluded that this star must belong to the fixed stars (Gingerich, 2005). This discovery fundamentally changed the astronomical world view, because fixed stars were now not longer considered as unchangeable objects. In the meantime it is well established that stars are actually born, live their life and die.

Studying the evolution of stars is, however, not an easy task, since the long stellar evolutionary time scales make it in general impossible for an astronomer to directly "watch" a star evolving. Therefore we are normally restricted to observe at a given time the characteristics of a large sample of stars and trying to reconstruct the main phases of their evolution by comparing their observed properties (Mowlavi, 1999). For this purpose stellar evolution is often depicted in the Hertzsprung-Russell diagram (HRD, Fig. 0.2), which gives the relationship between the stars' luminosities versus their effective temperatures[1]. Because a star stays at its position in the HRD up to billions of years, the evolution through the HRD normally cannot be seen directly. In this way misleading conclusions can sometimes be drawn. The most popular example might be the main sequence, which was firstly thought to represent the evolution of one star that radiates energy by converting gravitational energy into radiation through the Kelvin-Helmholtz mechanism. Only when nuclear fusion was identified as the source of stellar energy, it became clear, that the main sequence is actually a mass sequence of stars that are fusing hydrogen in their cores. Still today, our knowledge about stellar evolution depends on our understanding of the underlying physics, the amount and quality of the observations, and also the computing power to analyse the data or to simulate various evolutionary mechanisms.

In a few cases, however, the evolution of the surface properties of a given star occurs on a time scale shorter than a human life-time, and can thus be witnessed by careful observations performed at different times. This provides a unique way to gain a direct knowledge of stellar evolution and defines stellar evolution in real-time (Mowlavi, 1999). This phenomenon can not only be seen at the end of the life of massive stars (e.g. luminous blue variables, supernovae) but has also been observed amongst intermediate mass stars. Some of the latter will be discussed in Sect. 1.1.3.

In the context of this thesis both methods are used to deepen our knowledge about stellar evolution. The focus of the work lies on the late, hot stages of intermediate mass stars. They are located around the knee of the evolutionary tracks (upper left corner) in the HRD, so they are stars which are in their planetary nebula (PN) phase and/or stars which are just about to enter or just entered the white dwarf cooling sequence. In particular, the thesis aims to provide a better understanding of hot, hydrogen-deficient stars and one unusually quickly evolving hydrogen-rich central star of a planetary nebula (CSPN). Finally, the thesis contributes to the search for close binary systems amongst CSPNe.

In the following Chapter 1, I give firstly an introduction on the evolution of intermediate mass stars (Sect. 1.1). In Sect. 1.2, I describe the detection of hot (pre-) white dwarfs (WDs) in large sky surveys and finally note some analysis issues of these objects in Sect. 1.3. The aim of Chapter 2 is to describe the connections between the content of this thesis and the current state of research as well as the motivation for the work. In

[1] The effective temperature of a star is the temperature of a black body with the same luminosity per surface area as the star ($T_{\rm eff}$).

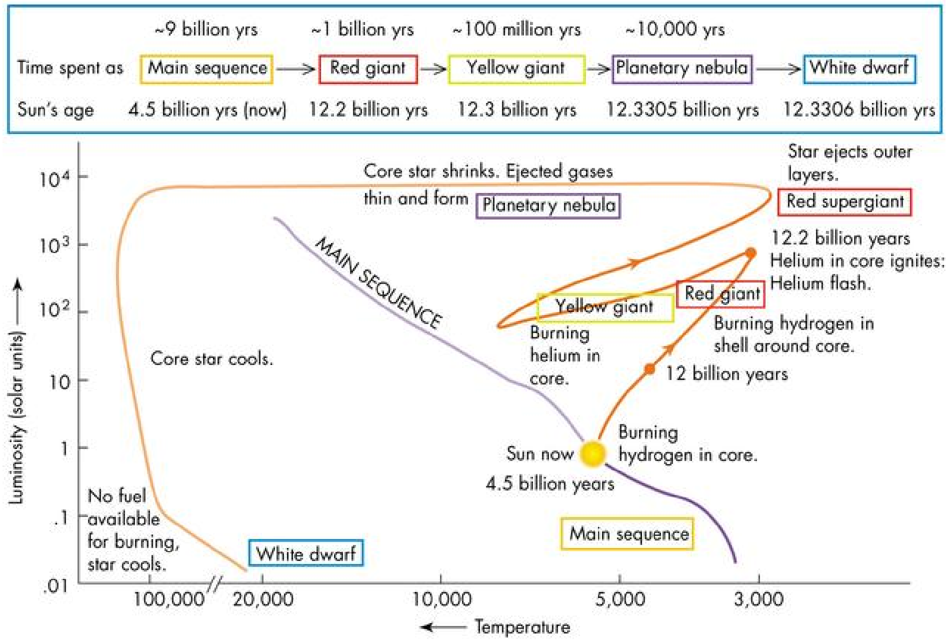

Figure 0.2: Hertzsprung-Russell diagram showing the evolution of a star with an initial mass of one solar mass ($M_{\odot}$), http://skyserver.sdss.org/dr1/en/astro/stars/stars.asp .

Chapter 3 the publications written during this thesis work are presented. Chapter 4 summarizes the results of the four papers. Finally, Chapter 5 gives an outlook on future work.

1 Introduction

1.1 On the evolution of intermediate mass stars

1.1.1 Canonical stellar evolution

It is believed that 97% of the stars in the Galaxy will eventually end up as WDs (Fontaine *et al.*, 2001). Most of them have initial masses between $0.8 - 8\,M_{\odot}$ and after depleting all the hydrogen and helium in the core, these stars will go through the Asymptotic Giant Branch (AGB) stage. During this phase stars will become extremely luminous and cool and will, consequently, undergo very strong mass-loss that can expel up to 90% of their initial mass to the interstellar medium. Due to this strong mass reduction the star will depart from the AGB evolving to form first a dust enshrouded post-AGB star then, when the ejected material is ionized by its strong UV radiation, a CSPN. The post-AGB star moves blueward at constant bolometric luminosity until it reaches its maximum effective temperature. When nuclear burning ceases, the star enters the WD cooling sequence as a carbon-oxygen WD (CO-WD) with a mass between $0.5\,M_{\odot}$ and $1.2\,M_{\odot}$. Canonical stellar evolution predicts that throughout all evolutionary phases the stars retain hydrogen-rich envelopes which, however, can become contaminated by processed material from the interior by dredge-up events occurring in the Red Giant Branch (RGB) and the AGB stages (Werner and Herwig, 2006). This classical picture is thought to account for the evolution of the vast majority of intermediate mass stars and directly connects the hydrogen-rich CSPNe to WDs with a hydrogen-rich atmosphere, corresponding to the DA spectral type.

1.1.2 Hydrogen-deficient post-AGB stars

Greenstein (1958) was the first who pointed out that the spectra of WDs subdivide into two well marked types – with and without hydrogen lines, whereas the latter corresponds to the non-DA type. The prototype of the hottest subclass of the non-DA WDs, the DO WDs, is HZ 21 (e.g., Eggen and Greenstein 1965). The optical spectra of the hot DO WDs show basically only broad He II lines, whereas in the spectra of the cooler DO WDs, He I lines can also be seen. Heap (1975) was one of the first reporting about a CSPN, (NGC 246), that exhibits only carbon, oxygen, and probably helium lines, what was already suggesting the existence of hydrogen-deficient post-AGB stars. She described the exciting star of NGC 246 as "the fulfillment of the theoretician's dream, in the sense providing observational evidence of the triple-α process". Later it turned out that NGC 246 belongs to the group of the PG 1159 stars, named after its prototype PG 1159−035, which was discovered – among many other hot, hydrogen-deficient (pre-) WDs – in the Palomar-Green Survey (Wesemael *et al.*, 1985; Green *et al.*, 1986). The optical spectra of these stars are characterized by weak and broad absorption lines of He II and C IV, sometimes with central emission reversals. In contrast to the hydrogen-rich post-AGB stars, PG 1159 stars do not exhibit just traces of intershell matter in their photospheres, but their outer layers are essentially made up of intershell matter. Therefore they indeed offer the possibility to study intershell abundances directly and understand also the physical processes leading to the composition.

The hydrogen-deficient and helium, carbon, and oxygen-rich atmospheres of PG 1159 stars (typically He : C : O = $(0.30 - 0.85) : (0.15 - 0.60) : (0.02 - 0.20)$ by mass, Werner and Herwig, 2006), can be explained by a (very) late thermal pulse ((V)LTP) that occurs either during the blueward excursion of the post-AGB star (LTP), or during its early WD cooling phase (VLTP, Fig. 1.1). The release of nuclear energy by the flashing helium-shell forces the already very compact star to expand back to giant dimensions - the so-called born-again scenario. This scenario was first explored in detail by Fujimoto (1977) and Schönberner (1979) and later invoked to explain the hydrogen-deficiency observed in some hot post-AGB stars (Iben *et al.*, 1983).

Carbon-rich Wolf-Rayet-type CSPNe are believed to be the direct progenitors of the PG 1159 stars, because of their strong similarities in derived atmospheric compositions. As a consequence of the higher mass-loss rates compared to PG1159 stars, they show essentially pure emission line spectra, mainly presenting broad and bright lines of helium, carbon, and oxygen. There are also some [WC]-PG 1159 transition objects known (e.g., Abell 30, Abell 78), which show mixed absorption/emission line spectra.

As a PG 1159 star cools down, gravitational settling removes heavy elements from the photosphere and turns it into a DO WD (unless it is of the subtype hybrid-PG 1159, then it turns into a DA WD, Unglaub and Bues 2000). With further cooling, the star will then first become a DB WD until around $T_{\mathrm{eff}} \approx 12\,000$ K dredge-up becomes important and the star will turn into a carbon-dominated, hot DQ WD (Brassard *et al.*, 2007). The carbon pollution will decrease again with further cooling, mainly because carbon sinks back into the star as a result of its partial recombination and the star finally becomes a helium-dominated DQ WD (Pelletier *et al.*, 1986).

Besides the carbon-dominated PG 1159 stars, there exists another class of very hot, hydrogen-deficient post-AGB stars, namely the O(He) stars. The spectral sub-type O(He) was introduced by Méndez *et al.* (1986) for CSPNe showing an almost pure He II absorption-line spectrum in the optical wavelength range. From their effective temperatures and surface gravities, these stars are found in the hot post-AGB region of the $\log T_{\mathrm{eff}} - \log g$ diagram, just amongst the luminous PG 1159 stars, and hydrogen-rich CSPNe. Closely related to the O(He) stars are R Coronae Borealis (RCB) stars, extreme helium (EHe) stars, [WN]-type central stars and helium-rich subdwarf O (He-sdO) stars, whose atmospheres are dominated by helium as well (He $\geq 90\%$, by mass). An extensive discussion about these objects can be found in Reindl *et al.* (2014b) and will not be repeated here.

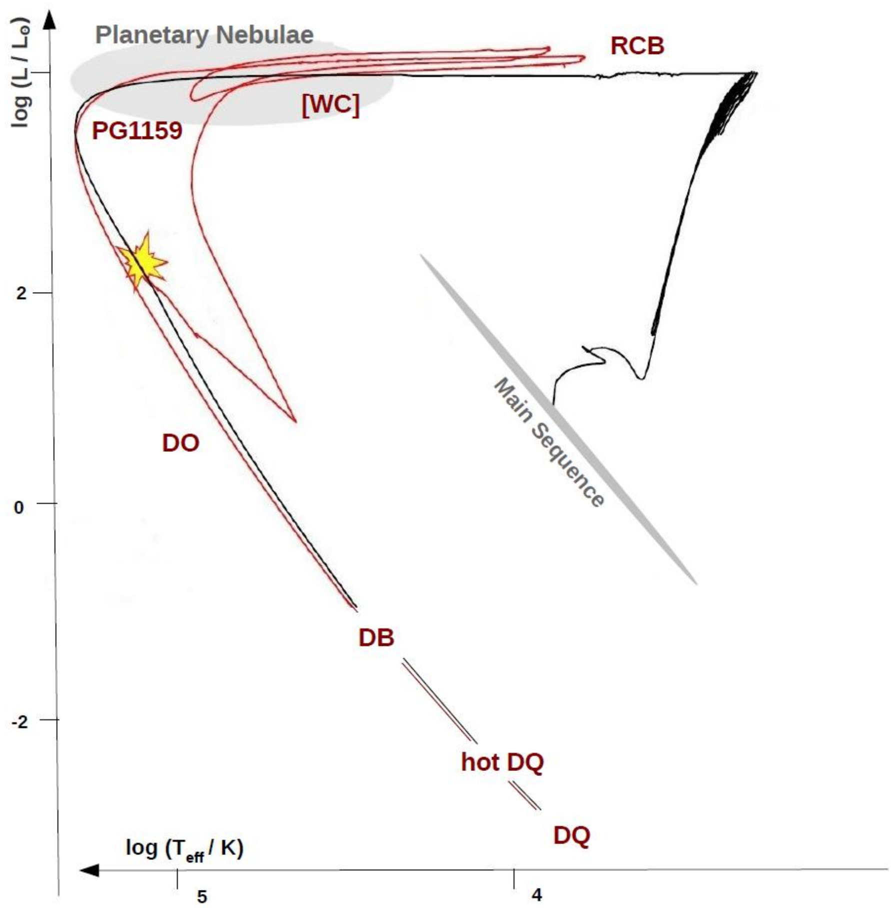

Figure 1.1: VLTP evolution of a star with an initial mass of $2\,M_{\odot}$ in the HRD. The black curve represents a canonical evolutionary track. When the star suffers a VLTP during its early WD cooling phase (yellow flash symbol) it will evolve back to the AGB, and after a second loop it will cool down as a hydrogen-deficient WD (red curve).

1.1.3 Real-time stellar evolution objects

During a late thermal pulse, the evolution through the HRD is extremely fast (decades). Well known examples for "caught in the act" born-again stars are V605 Aql (e.g. Clayton *et al.* 2006), V4334 Sgr (Sakurai's object, e.g., Hajduk *et al.* 2005) and FG Sge (e.g., Jeffery and Schönberner 2006).
V605 Aql, the central star of the planetary nebula A58, was discovered in 1919 and firstly classified as a slow nova, but is now considered to be in a post born-again stage. Within only a few years it turned into a born-again giant and remained as a giant with a hydrogen-poor and carbon-rich atmosphere with the spectral appearance of an RCB star for a further couple of years. As expected theoretically, recontraction occurred on a longer timescale. At present, V605 Aql is a hot ($\approx 95\,000\,$K), luminous [WC] central

star and about to complete its first born-again loop (Schönberner, 2008).
V4334 Sgr was detected in the 1990s and showed a remarkably rapid cooling of 1460 K/yr in 1996/1997 (Duerbeck *et al.*, 1997), accompanied by a reduction of the already small atmospheric hydrogen content from 0.04 to 0.004 (mass fractions, Asplund *et al.* 1999). During the second half of 1998, an optically thick dust shell obscured Sakurai's Object, causing a rapid decrease in visibility of the star, until in 1999 it disappeared completely. Van Hoof *et al.* (2007) reported an increasing radio flux of the shell since 2006, which they attributed to a stellar temperature rise to about 12 000 K.
FG Sge has been transformed over an interval of 120 years from a hot, hydrogen-rich post-AGB star into a very luminous cool supergiant. The cooling rate (≈ 350 K/yr) was lower than in the case of V4334 Sgr and since about 1980 the temperature remained constant at ≈ 5500 K. A study of the surface abundances has revealed that hydrogen has been depleted and s-process element abundances have generally maintained a steady enhancement of around 1–2 dex between about 1960 and 1995. While V605 Aql and V4334 Sgr are considered to have undergone a VLTP, which produces a hydrogen-free stellar surface already during the flash, this scenario cannot account for the hydrogen-rich surface of FG Sge. FG Sge must instead have experienced a LTP. Within this scenario, the convective shell triggered by excessive helium burning is not able to penetrate the hydrogen-rich envelope from below because the entropy jump across the helium/hydrogen interface is too large. Only when the star evolves back to its Hayashi limit on the AGB ($T_{\rm eff} \lesssim 7000$ K), envelope convection sets in again (Blöcker and Schönberner, 1996, 1997; Schönberner, 2008).
The detection and the repeated observation of such quickly evolving objects makes it possible to derive the temporal evolution of their stellar parameters and offer a unique opportunity to directly test the accuracy of stellar evolution modeling under extreme conditions.

1.1.4 AGB-manqué stars

WDs with masses smaller than about $0.5\,M_\odot$ cannot have been produced by the above mentioned evolutionary scenario, because the respective low-mass progenitor stars would not have finished their main sequence evolution yet[1,2]. However, hot subdwarfs lie between the main sequence and the WD sequence and far beyond the horizontal branch – a region which is not covered by the canonical evolutionary tracks for stellar masses which agree with the age of the universe. These stars are expected to have undergone a strong mass-loss already on the RGB. The mass-loss rate, $\dot{M}$, along the RGB can be parameterized by the empirical Reimers (1975) formula,

$$\dot{M} = -4 \times 10^{-13}\,\eta_{\rm R}\,\frac{L}{g\,R}\,\frac{M_\odot}{yr},$$

[1] The oldest globular clusters in the Galactic halo are currently producing $0.53\,M_\odot$ WDs (Kalirai *et al.*, 2009).

[2] The main-sequence time of a star with an initial mass of $0.5\,M_\odot$ is about 50 billion years, which is about 3.6 times the age of the Universe.

where L , g, and R are the stellar luminosity, gravity, and radius in solar units, and $\eta_{\rm R}$ is the Reimers mass-loss parameter. The driving mechanism behind RGB mass-loss is not well understood, different metallicities, initial helium abundances, rotational velocities, or binary interactions may, in principle, produce enhanced mass-loss rates (Miller Bertolami *et al.*, 2008). Evolutionary calculations of Brown *et al.* (2001) for example showed that for a star with an initial mass of $0.862\,M_\odot$, the models remain tightly bound to the RGB until the central helium flash as long as $\eta_{\rm R} \leq 0.740$ (case a in Fig. 1.2). However, depending on the amount of mass-loss, the star will reach a different zero-age horizontal branch (ZAHB) position (the higher $\eta_{\rm R}$, the hotter the ZAHB position becomes). Still, the envelope mass of the $\eta_{\rm R} \leq 0.740$ models is sufficient to let the star evolve to the AGB after the central helium burning phase. These stars will evolve as described in Sect. 1.1.1. For $0.740 < \eta_{\rm R} < 0.937$, the stars will leave the RGB and ignite helium while evolving to or descending the WD cooling curve (cases b and c in Fig. 1.2). These stars fail to evolve to the AGB and instead experience a post-extreme horizontal branch (post-EHB) evolution. For even higher values of $\eta_{\rm R}$, stars fail to ignite helium and instead directly evolve to become helium core WDs (He-WDs, post-RGB evolution, case d in Fig. 1.2). In the following, the latter two scenarios will be described more in detail.

Post-EHB stars

Canonical EHB models (e.g., Dorman *et al.* 1993) are characterized by a core mass of nearly half a solar mass and a tiny inert hydrogen-rich envelope. The core mass of a RGB star is fixed at the onset of the helium core-flash (HeCF) at the tip of the RGB and depends only slightly on metallicity and helium abundance. This restricts the mass of EHB stars to a very narrow range from 0.46 to $0.5\,M_\odot$ (Heber, 2009). If the star experiences the HeCF after departing from the RGB tip, during the evolution at constant luminosity in the HRD (early hot flasher scenario, case b in Fig. 1.2), it will become a hot subdwarf with a hydrogen-rich envelope. The high helium-burning luminosity at the peak of the helium core flash ($L_{\rm He} = 10^{10}\,L_\odot$) drives a temporary convection zone that extends from the site of the flash outward through the core (Heber, 2009). Ordinarily, the flash convection zone does not penetrate into the hydrogen envelope because of the high entropy of the hydrogen-burning shell (Lanz *et al.*, 2004). However, when the HeCF happens on the WD cooling curve (case c in Fig. 1.2), it does so in the presence of a much weaker hydrogen-burning shell. The associated entropy barrier is then lower and can be overcome, allowing the flash convection zone to penetrate into the hydrogen envelope. The thin hydrogen envelope is then quickly mixed into the helium-burning core. Hence, hydrogen might be mixed into hotter layers and be burnt there, leading to a helium-enriched surface (Lanz *et al.*, 2004).

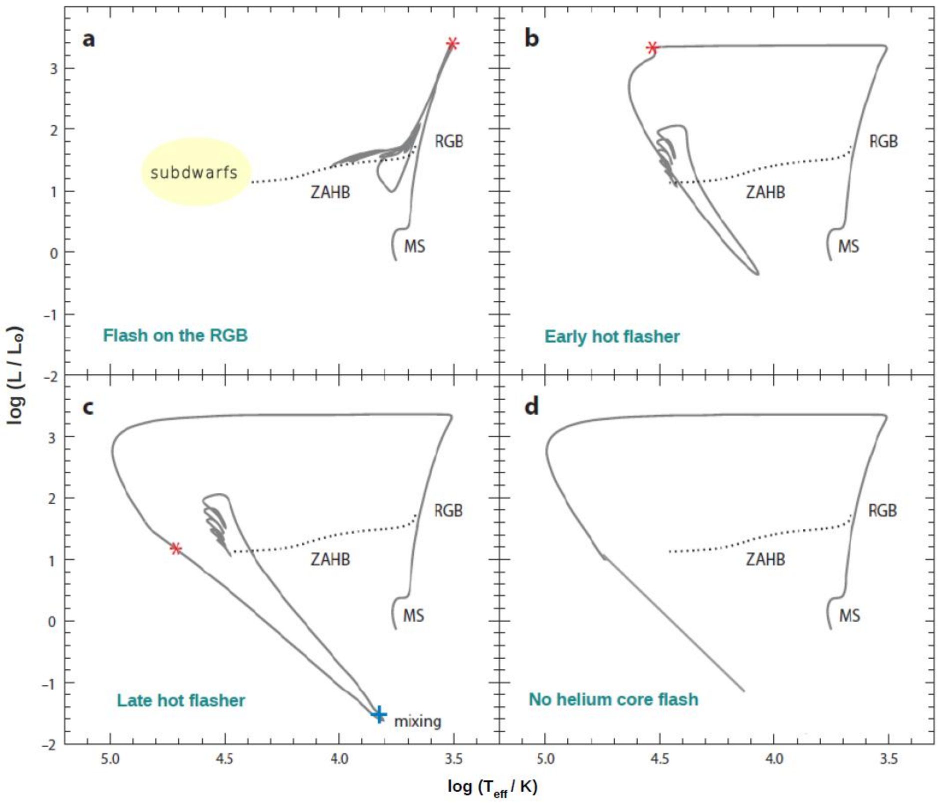

Figure 1.2: Evolution of a star from the main sequence (MS) through the helium flash to the ZAHB (dotted curve) for different amounts of mass-loss on the RGB. For sufficiently large mass-loss, a star evolves off the RGB to high effective temperatures before igniting helium. The peak of the helium flash is indicated by a red asterisk. Flash mixing does not occur for the sequences in panels a and b. In panel c, the flash convection zone reached the hydrogen envelope at the plus sign. In panel d, the star does not ignite helium and becomes a He-WD. Figure taken from Heber (2009) and modified.

Post-RGB stars

In the case of post-RGB evolution, the resulting WDs can have extremely low masses (below $0.2\,M_{\odot}$), which are commonly referred to as extremely low-mass (ELM) WDs. They are believed to be the result of a compact binary evolution, during which the envelope of a RGB star was removed via a common envelope (CE) evolution before the core reached enough mass to ignite helium. Thanks to the result of many surveys, e.g. the SPY and ELM survey and the WASP surveys (see Koester *et al.* 2009; Brown *et al.* 2010, 2012; Maxted *et al.* 2011), the number of detected WDs with very low stellar masses has increased considerably in the recent years. The recent discovery of pulsating He-WDs with stellar masses below $0.23\,M_{\odot}$ and effective temperatures below 10 000 K (Hermes *et al.*, 2012, 2013), was a big step towards the understanding of the formation and evolution of ELM WDs. Many ELM WDs are indeed found in close binary systems, several of them have even millisecond radio pulsars companions (Lorimer, 2008). With respect to our understanding the PNe phase and their central stars, it is also worth to mention the work of Hall *et al.* (2013). They showed for the first time that not only post-AGB stars may have a planetary nebula phase, but also post-RGB stars with masses greater than about $0.3\,M_\odot$ and that leave the CE phase in thermal equilibrium.

1.1.5 Post-merger evolution

Following orbital decay by gravitational-wave radiation, very close (periods less than a few hours) WD binary systems may merge within a Hubble time and form a single star if

$$q \equiv \frac{m_2}{m_1} \geq q_{\mathrm{crit}} = \frac{5}{6} + \frac{\zeta(m_2)}{2}\,,$$

where m_2 and m_1 are the masses of stars in the binary, and $\zeta(m_2) \equiv \mathrm{d}\ln r/\mathrm{d}\ln m$ is obtained from the WD mass-radius relation (Zhang *et al.*, 2014). As a consequence of the transfer of angular momentum, the radius of the larger (less massive) WD will increase more quickly than the separation leading to unstable mass transfer on a dynamical time-scale (a few seconds, Zhang and Jeffery 2012b). Stable mass transfer will occur for $q \leq q_{\mathrm{crit}}$ and possibly lead to the formation of an AM Canum Venaticorum (AM CVn) binary[3]. If the system contains two sufficiently massive WDs, this evolutionary path can lead to a type Ia supernova (Webbink, 1984). Because the total mass of the merging system can vary significantly, the luminosity of the supernovae can vary considerably, too. Hence, this evolutionary channel is in particular important to understand in view of the applicability of type Ia supernovae as standard candles. If the total mass of the two merging WDs does not exceed the Chandrasekhar limit, RCB stars, EHe stars, He-sdO stars or O(He) stars may be produced. In Fig. 1.3, the rates of different, possible double WD mergers for a single starburst (normalized to $10^{11}\,M_\odot$) are shown. These systems include only mergers arising from WD binaries which fill their Roche lobes within a Hubble time.

The hydrodynamics of the merger process remains difficult to compute, however, it is possible to compute the evolution of a double WD merger following the destruction of one component. Such calculations became available only recently (e.g., Staff *et al.* 2012; Zhang and Jeffery 2012b,a; Zhang *et al.* 2014) and they are discussed in Reindl *et al.* (2014b) in regard to explain a helium-dominated stellar evolutionary sequence.

[3] AM CVn binaries are a rare group of hydrogen-deficient, ultrashort period, mass-transferring WD binaries.

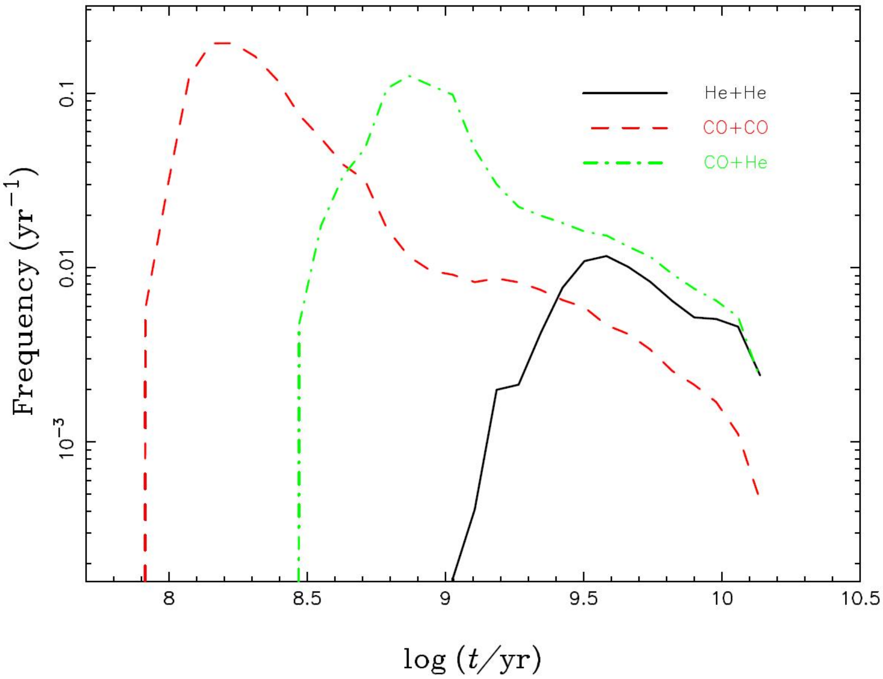

Figure 1.3: Frequency of possible mergers from CO+CO, CO+He and He+He WD systems for a single starburst (normalized to $10^{11}\,M_{\odot}$). Figure taken from Zhang *et al.* (2014).

1.2 Astronomy in times of large sky surveys

Before hot, hydrogen-deficient stars in the post-AGB region enter the WD cooling sequence they are in their most luminous (they have a few 10^3 to 10^4 times the solar luminosity) evolutionary state and thus they allow us observe them in a huge space volume (several kpc^3). However, their evolutionary time scales are rather short. Depending on their mass, the transition time from the AGB to the knee in the HRD lasts only about 10^3 to a few 10^5 years. The typical lifetime of a DO WD is a few million years, but as the star cools down its luminosity decreases to a few percent of the solar luminosity[4] until it reaches the DB region. Besides that, only about 20% of the stars in the post-AGB region are expected to be hydrogen-deficient. That is why large surveys are needed to improve the statistics of these rare objects and to understand their origin. As already mentioned above, many PG 1159 stars and DO white dwarfs were discovered by the Palomar-Green Survey. Of the 1874 objects in the Palomar-Green catalog of ultraviolet (UV) excess stellar objects, 1715 comprise a statistically complete sample that covers 10 714 deg^2 of sky down to an average limiting magnitude $B = 16.1$ (Green *et al.*, 1986). Another survey contributing to the number of known hot and hydrogen-deficient

[4]Time scales and luminosity as they can be derived from evolutionary calculations of Blöcker (1995) and Althaus *et al.* (2009).

(pre-) WDs was the Hamburg Quasar Survey (Hagen *et al.*, 1995). This wide-angle objective prism survey aimed to find bright, high-redshift quasars in an area of about 14 000 deg^2, but also provided a rich source of faint ($13 \lesssim B \lesssim 18$) blue stars.
Finally, the data from the Sloan Digital Sky Survey (SDSS, York *et al.* 2000; Yanny *et al.* 2009; Eisenstein *et al.* 2011; Dawson *et al.* 2013) have more than doubled the number of known hot, hydrogen-deficient (pre-) WDs. The SDSS is a multi-filter imaging and spectroscopic survey using a 2.5 m wide-angle optical telescope at Apache Point Observatory (APO) in New Mexico, USA and has continuously operated since 2000.

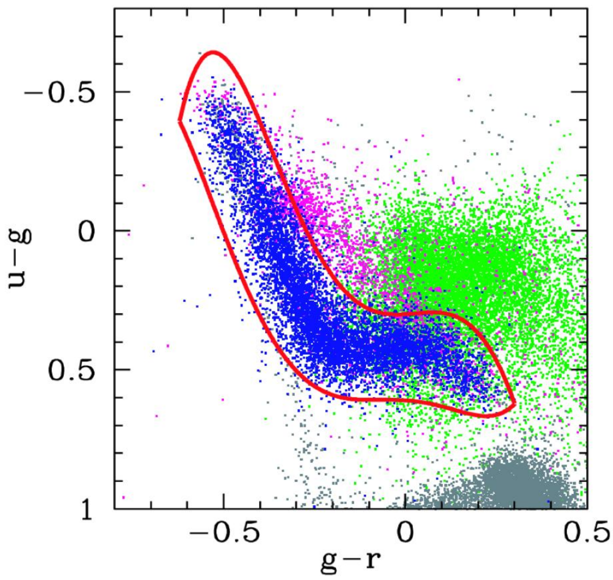

Figure 1.4: ($u - g$, $g - r$) color-color plot illustrating the location of SDSS DR7 spectroscopic objects. The locations of DA WDs (blue), non-DA WDs (magenta), quasars (green) and main sequence stars (grey) are shown. Figure taken from Girven *et al.* (2011).

The basic procedure of the SDSS is the following: after imaging the sky in five passbands (u, g, r, i, z), potential targets are selected for spectroscopic follow-up based on the five-band photometry. This spectroscopic selection process is referred to as "targeting", and many different targeting categories are used to fill all the fibers available on each 640 fiber spectroscopic plate. Where there are not enough primary targets (i.e., galaxies, quasars, etc.) to fill a given plate, the lower priority targeting categories (which may include various stellar categories) get to allocate fibers (Kleinman *et al.*, 2004). Thus there are many Galactic spin-off projects resulting from the survey, although the main focus of the SDSS was extragalactic during its early phase.
In a color-color diagram, as shown in Fig 1.4, hot WDs can be found relatively easy at the upper left end of the WD banana (red curve). Fortunately, hot WDs fall into the hot standard star criterion in the region of the Legacy survey, which comprises bright ($14 < g < 19$), isolated, hot ($-1.5 < (u{-}g)_0 < 0$ and $-1.5 < (g{-}r)_0 < 0$) stars. Because

of the relative rarity of these objects in the sky and their importance in calibration, the SDSS gave hot standard stars the highest priority in assigning fibers. Their completeness can be expressed as a function of Galactic latitude and object brightness and is about 77 % for the DR4 (Krzesiński *et al.*, 2009). However, in the SEGUE survey the hot standard class was not tiled, which decreases the completeness (e.g. Girven *et al.* 2011 estimated the overall spectroscopic completeness of DA WDs in the SDSS DR7 to 44.3%).

1.3 Spectral analysis of hot (pre-) WDs

Quantitative analysis of stellar spectra is one of the most important tools of modern astrophysics, because all our knowledge about the structure and evolution of stars is primarily based on the interpretation of their electromagnetic spectrum. The observed spectrum stems from the star's photosphere, a very thin layer at the surface of the star. To derive the basic photospheric parameters, the temperature and pressure stratification of the atmosphere needs to be calculated, which then allow the computation of synthetic spectra that can be compared with the observations.
The classical stellar atmosphere problem requires the solution of the radiation-transfer equations simultaneously with the equations for hydrostatic, radiative, and statistical equilibrium. A stellar atmosphere is an open thermodynamic system and by that it is not in thermodynamic equilibrium (TE) and cannot be characterized by a single temperature. If the atomic transition collision rates dominate radiative rates and photon-mean-free-paths are small, the atmosphere may be assumed to be in local thermodynamic equilibrium (LTE), which means that small volume elements can be considered to be in TE. This holds for high-gravity and low-temperature objects (e.g. cool WDs or main sequence stars with spectral type B or later, see Fig. 1.5).

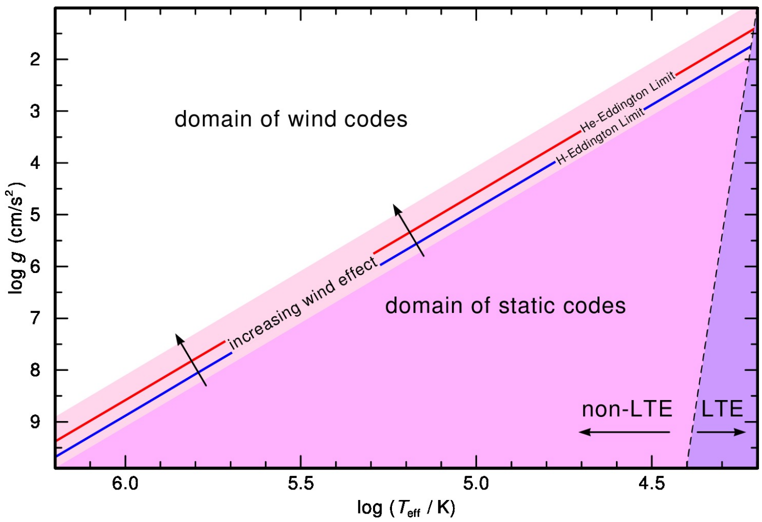

Figure 1.5: Domains of static LTE and non-LTE codes and domain of wind codes. The Eddington limits for pure hydrogen (blue) and pure helium (red) atmospheres are marked. Figure taken from Rauch (2012) and modified.

The spectral analysis of hot post-AGB stars is, however, a more complex task, because it requires the calculation of non-local thermal equilibrium (non-LTE) model atmospheres. The abandonment of the LTE assumption leads to a much more difficult model-atmosphere problem, because of subtle couplings between the radiation-transfer and atomic rate-equations (see Werner *et al.* 2003 for a review). The numerical solution of this coupled, non-linear problem occasionally causes convergence problems, which

may hinder the spectral analysis of hot objects.
The occurrence of the so-called Balmer line problem further complicates the analysis of hot stars. It describes the failure to achieve a consistent fit to the Balmer line spectrum of hot subdwarfs, CSPNe, DA and DAO WDs whose effective temperature exceeds $\approx$ 70 000 K. Because metal opacities are time-consuming to deal with, non-LTE models used to derive their basic stellar atmospheric parameters (effective temperature, surface gravity, and the hydrogen to helium ratio), traditionally contained exclusively hydrogen and helium. Werner (1996) showed that the Balmer line problem can be solved when surface cooling by photon escape from the Stark wings of CNO lines is accounted for. However, the inclusion of the CNO elements only is not sufficient to overcome this problem in the case of the O(He) stars (Reindl 2012, see also Reindl *et al.* 2014b). While the addition of Ne to the models could solve zhe problem, it was however shown that the opacities of other elements can have a significant influence on the temperature structure of the entire atmosphere and thus on the resulting line profiles of optical He II and Balmer lines as well (e.g., Preval *et al.* 2014; Reindl and Rauch 2014; Reindl *et al.* 2014a; Latour *et al.* 2013). The impact of Mg, Ne, Na or iron-group elements (at solar abundances) on the temperature structure of a DA WD with $T_{\rm eff}$ = 100 kK and $\log g = 7.0$ is shown in Fig. 1.6. While the impact of Na is small, Ne, Mg, and the iron-group elements have a significant influence on the temperature structure of the entire atmosphere. These elements cause a backwarming effect and the resonance lines of Ne, Na, and Mg additionally cause a strong decrease of the temperature in the outer atmosphere ($\log m \leq -3$).

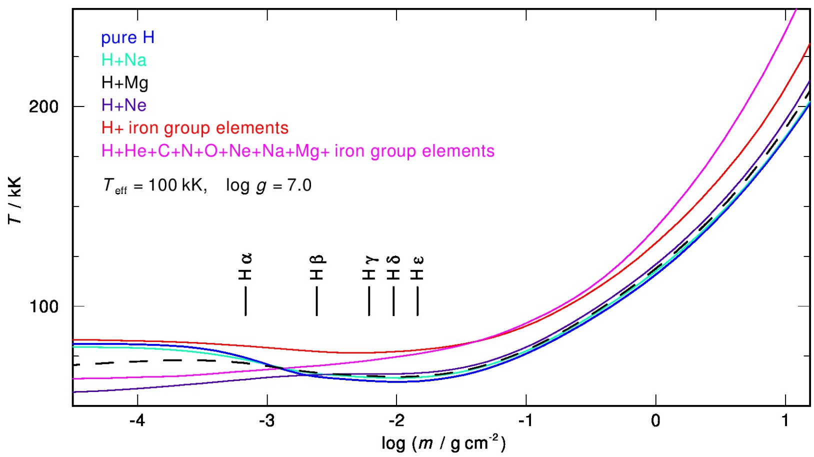

Figure 1.6: Temperature as function of the column mass m that is measured from the outer boundary of the model atmospheres. The impact of different elements on the temperature structure for $T_{\rm eff}$ = 100 kK and $\log g$ = 7.0. Formation depths of the Balmer line cores are marked.

Finally, some of these hot stars still show some residual wind, as indicated by the presence of P-Cygni profiles in their UV spectra or strong emission lines in their optical spectra. These lines can only be modeled using a code for an expanding model-atmosphere.

Besides the effective temperature, surface gravity and the chemical composition, these codes need additional physical input parameters (e.g., the luminosity of the star, mass-loss rate, terminal-wind velocity, velocity law, clumping and filling factors) which even further complicates the analysis.

2 Work in context

2.1 The rapid evolution of the exciting star of the Stingray Nebula

SAO 244567, the exciting star of the Stingray Nebula, is an unusually fast evolving star that offers us the unique opportunity to study stellar evolution in real time. Based on a spectral classification of the optical spectrum obtained in 1971, SAO 244567 was found to be a B1 or B2 supergiant (Parthasarathy *et al.*, 1995). Optical spectra in 1990 and 1992 as well as the IUE[1] spectra (1992–1996) however display many nebula emission lines, indicating that SAO 244567 has turned into a CSPN within twenty years only. Previous analyses suggested that it has heated up from an effective temperature of about 21 kK in 1971 to over 50 kK in the 1990s. From the H β flux, the luminosity, and by that the mass of the CSPN can be estimated. Parthasarathy *et al.* (1993) and Bobrowsky (1994) found that it must be below $0.60\,M_\odot$, however the slow evolution of the canonical post-AGB stellar evolutionary models is in strong contrast to the observed fast evolution. Recentely, Arkhipova *et al.* (2013) performed an analysis of the nebula spectra taken in 1990, 1992, and 2011 and found significant changes in the relative line intensities. Using a formula of Kaler (1978), they estimated that T_eff decreased from $T_\mathrm{eff} = 57$ kK (1990) to $T_\mathrm{eff} = 40$ kK (2011).
Fortunately, SAO 244567 was observed with various space-based telescopes from 1988 to 2006. However, these spectra have not yet been analyzed quantitatively. The aim of this work was therefore to derive the chemical composition of the atmosphere, as well as the temporal change of effective temperature, surface gravity, mass-loss rate, and terminal-wind velocity by means of static and expanding non-LTE model atmospheres. The derived parameters should provide a better understanding of the evolutionary status of this object.

2.2 On helium-dominated stellar evolution: the mysterious role of the O(He)-type stars

As already mentioned in Sect. 1.1.2, O(He) stars form an exotic group of extremely hot stars with helium-dominated atmospheres. For more than 15 years, only the two CSPNe K 1−27 and LoTr 4, as well as HS 1522+6615, and HS 2209+8229 were known

[1] International Ultraviolet Explorer.

(Rauch *et al.*, 1994, 1996, 1998). The evolutionary status of these objects has been studied only rarely. Rauch *et al.* (1998) proposed that O(He) stars might be successors of the luminous He-rich sdO stars and that due to ongoing mass-loss, the low-gravity O(He) stars might evolve into PG 1159 stars. This possibility was studied by Miller Bertolami and Althaus (2006). However, they had to assume mass-loss rates, that were higher than predicted by radiation-driven wind theory to turn O(He) stars into helium-enriched PG 1159 stars. An alternative scenario was suggested by Rauch *et al.* (2006). They invoked the idea that the O(He) stars could also be the offspring of a merging event of two white dwarfs and thus, the direct descendants of RCB stars.
The spectral analysis of O(He) stars was already subject of my master thesis (Reindl, 2012) in which I analyzed the UV and optical spectra of the O(He) stars and discussed possible evolutionary channels. I found, that O(He) stars can not be explained by a (V)LTP scenario, because these evolutionary models predict higher carbon and oxygen abundances than observed in the O(He) stars. Instead, I suggested that O(He) stars might be the outcome of a double He-WD merger process. Evolutionary models for this scenario became first available in January 2012 (Zhang and Jeffery, 2012b), and they indeed predict helium dominated atmospheres as well as carbon, nitrogen, and oxygen abundances as they are found amongst the O(He) stars. At about the same time Miszalski *et al.* (2012) reported about the first unambiguous [WN]-type CSPN. One year later another object, Abell 48, was also identified as [WN]-type CSPN (Todt *et al.*, 2013; Frew *et al.*, 2014). Because of the strong similarity of the element abundances of [WN] stars and nitrogen-enriched O(He) stars, it was then believed that analog to the hydrogen-deficient, but carbon-dominated post-AGB sequence [WCL] → [WCE] → PG 1159 (e.g. Werner and Herwig, 2006), a second, hydrogen-deficient sequence, [WN] → O(He) could exist (cf. Werner, 2012). Recently, Werner *et al.* (2014) found four additional O(He) stars in the SDSS DR10. They also pointed out that KPD 0005+5106 is actually not a DO WD but a pre-WD as it has not yet entered the WD cooling sequence. Because of the helium-rich surface composition of KPD 0005+5106 (98% by mass, Wassermann *et al.* 2010), it is now reclassified as an O(He) star.
During the work of the present thesis, we obtained new optical spectra of K 1-27 and LoTr 4, which should provide a more precise determination the atmospheric parameters. This is crucial to also precisely derive other parameters of a star, for instance its mass or spectroscopic distance. Another important goal was to derive the mass-loss rates (or at least upper limits) of the O(He) stars by examining all wind lines that are located in the FUSE[2] and HST/COS[3] wavelength ranges. This was important to investigate on the possibility, that O(He) stars could have lost their hydrogen-rich envelope via enhanced mass-loss and/or the possibility that they could be the progenitor of some PG 1159 stars. Finally, a broader comparison of the atmospheric parameters of other helium-dominated stars with the ones of the O(He) stars should give clues about how the helium-dominated stellar evolution sequence could look like.

[2]Far Ultraviolet Spectroscopic Explorer.
[3]Cosmic Origins Spectrograph on board of the Hubble Space Telescope.

2.3 Analysis of cool DO-type white dwarfs from the Sloan Digital Sky Survey Data Release 10

DO WDs represent the beginning of the hydrogen-deficient WD cooling sequence and they are believed to be the direct successors of O(He) stars and PG 1159 stars. The latter can display extremely high carbon abundances, while DO WDs have a nearly pure helium atmosphere, with only relatively few showing weak metal lines. Their surface composition is controlled by the competition between gravitational settling and radiative levitation, as well as possible weak mass-loss. Thus, DO WDs are particularly interesting to study the chemical evolution of hot WDs and to place constraints on possible progenitors and successors of DO WDs. The transition of PG 1159 stars into DO WDs can be understood when at a certain point of their evolution gravitational settling overcomes radiation-driven mass-loss and heavy elements are removed from the photosphere. However, this process is far from being understood quantitatively. Several works (e.g., Chayer *et al.* 1995; Dreizler 1999) showed that the observed metal abundances do not fit theoretical predictions. However, the number of DO WDs is rather small, and only for a few of them metal abundances were derived and thus it is very desirable to increase their statistics.
In some cases a detailed study of DO WDs even allows the detection of trans-iron elements, which were not discovered previously in any other white dwarf (e.g., krypton and xenon, Werner *et al.* 2012). In addition hot WDs can be used as plasma laboratory to investigate on atomic data of highly ionized species, that are a pre-requisite for precise stellar-atmosphere modeling (Rauch *et al.*, 2012, 2014b,a).
The analysis of DO WDs is furthermore an important groundwork for the determination of the WD luminosity function (WDLF) and the space density of WDs. These provide not only constraints on the star formation rate and thus on the history of our Galaxy, but they can also be used to help determine the role of weakly interacting particles in WD cooling (Isern *et al.*, 2008) and thus their ages. Especially the shape of the hot end of the WDLF turned out to be an excellent tool for constraining the emission of particles in the core of hot WDs and to check for the possible existence of DFSZ axions, a proposed but not yet detected type of weakly interacting particle which is still a conjectural non-baryonic particle considered as candidate for dark matter (Miller Bertolami *et al.*, 2014; Miller Bertolami, 2014).
As mentioned in Sect. 1.2, the SDSS is a rich source of hot WD spectra. Werner *et al.* (2014) detected 21 new, hydrogen-deficient, hot (pre-) WDs in the SDSS DR10. However, their search was restricted to objects showing no He I lines. The aim of this work was to find also the cooler DO WDs (which also show He I lines) in the SDSS DR10 and to derive their atmospheric parameters. Based on the increased number of hot, hydrogen-deficient objects, their mass distribution as well as the ratio of hot DA WDs to hot non-DA WDs should be derived.

2.4 Identifying close binary central stars of PN with Kepler

A major issue in PN research is to explain the asymmetrical shapes of PNe. The great majority of PNs (80–85%, Parker *et al.* 2006) display axial symmetries and point symmetries, sometimes with the addition of jetlike structures. Until today there exists no satisfactory physical explanation for how single stars can create asymmetrical shapes. The so called binary hypothesis (De Marco *et al.*, 2009) states that a companion is needed to account for the shapes of non-spherical PNe, and several groups are trying to determine the true frequency of binary CSPNe and the properties of these systems. The only well constrained binary fraction is that of very close (typical orbital periods below one day) binary CSPNe and is rather low ($\approx 15\%$). These systems were detected via periodic flux variability due to eclipses, irradiation, and/or ellipsoidal deformation (Bond, 2000; Miszalski *et al.*, 2009). Almost all the known binary CSPNe were detected in this way, however, this technique is biased against binaries with periods longer than about two weeks, against binaries with high inclination angles, and against companions with small radii. The photometric variables detected in this way usually have amplitudes larger than 0.1 mag, and it has therefore been asked how many binary systems have remained undetected because of photometric accuracy limits of ground based telescopes. The scientific objective of the Kepler Mission is to explore the structure and diversity of planetary systems and it is able to detect flux variabilities in the 0.1‰ range. Thus, it is about 100–1000 times more sensitive than ground based observations. At the time of launch, only three PNe were known in the Kepler field of view. Two additional PNe were discovered by the Deep Sky Hunters amateur collaboration while an additional object was recently found by Aller *et al.* (2013).
The goal of this paper (De Marco *et al.*, 2015) was to check all known CSPNe within the Kepler field for photometric variability and to derive their periods if possible. The detection of even one binary CSPN, which could not have been detected from the ground, would indicate that such binaries exist and motivate further studies to quantify how much larger the binary fraction of CSPNe is than the 15% currently known. My contribution to this paper was to analyze the spectra of the central stars to obtain clues about their nature.

3 Publications

In this chapter, the publications written during my thesis are presented. They are in the order of publication date.

Reindl *et al.* (2014c):
N. Reindl, T. Rauch, M. Parthasarathy, K. Werner, J. W. Kruk, W.-R. Hamann, A. Sander and H. Todt: The rapid evolution of the exciting star of the Stingray nebula, 2014, *A&A*, **565**, A40

Reindl *et al.* (2014b):
N. Reindl, T. Rauch, K. Werner, J. W. Kruk and H. Todt: On helium-dominated stellar evolution: the mysterious role of the O(He)-type stars, 2014, *A&A*, **566**, A116

Reindl *et al.* (2014a):
N. Reindl, T. Rauch, K. Werner, S. O. Kepler, B. T. Gänsicke and N. P. Gentile Fusillo: Analysis of cool DO-type white dwarfs from the Sloan Digital Sky Survey data release 10, 2014, *A&A*, **572**, A117

De Marco *et al.* (2015):
O. De Marco, J. Long, G. H. Jacoby, T. Hillwig, M. Kronberger, S. B. Howell, N. Reindl and S. Margheim: Identifying close binary central stars of PNe with Kepler, submitted to *MNRAS*

The first three papers are published in Astronomy & Astrophysics. They are reproduced with permission from Astronomy & Astrophysics, ©ESO. The last one is currently in review for publication in the Monthly Notices of the Royal Astronomical Society.

A&A 565, A40 (2014)
DOI: 10.1051/0004-6361/201323189

Astronomy & Astrophysics

The rapid evolution of the exciting star of the Stingray nebula★,★★,★★★

N. Reindl[1], T. Rauch[1], M. Parthasarathy[2], K. Werner[1], J. W. Kruk[3], W.-R. Hamann[4], A. Sander[4], and H. Todt[4]

[1] Institute for Astronomy and Astrophysics, Kepler Center for Astro and Particle Physics, Eberhard Karls University, Sand 1, 72076 Tübingen, Germany,
e-mail: reindl@astro.uni-tuebingen.de
[2] Inter-University Centre for Astronomy and Astrophysics, Post Bag 4, Ganeshkhind, 411007 Pune, India
[3] NASA Goddard Space Flight Center, Greenbelt MD 20771, USA
[4] Institute for Physics and Astronomy, University of Potsdam, Karl-Liebknecht-Str. 24/25, 14476 Potsdam, Germany

Received 4 December 2013 / Accepted 12 March 2014

ABSTRACT

Context. SAO 244567, the exciting star of the Stingray nebula, is rapidly evolving. Previous analyses suggested that it has heated up from an effective temperature of about 21 kK in 1971 to over 50 kK in the 1990s. Canonical post-asymptotic giant branch evolution suggests a relatively high mass while previous analyses indicate a low-mass star.

Aims. A comprehensive model-atmosphere analysis of UV and optical spectra taken during 1988–2006 should reveal the detailed temporal evolution of its atmospheric parameters and provide explanations for the unusually fast evolution.

Methods. Fitting line profiles from static and expanding non-LTE model atmospheres to the observed spectra allowed us to study the temporal change of effective temperature, surface gravity, mass-loss rate, and terminal wind velocity. In addition, we determined the chemical composition of the atmosphere.

Results. We find that the central star has steadily increased its effective temperature from 38 kK in 1988 to a peak value of 60 kK in 2002. During the same time, the star was contracting, as concluded from an increase in surface gravity from $\log g = 4.8$ to 6.0 and a drop in luminosity. Simultaneously, the mass-loss rate declined from $\log(\dot{M}/M_\odot\,\mathrm{yr}^{-1}) = -9.0$ to -11.6 and the terminal wind velocity increased from $v_\infty = 1800\,\mathrm{km\,s}^{-1}$ to $2800\,\mathrm{km\,s}^{-1}$. Since around 2002, the star stopped heating and has cooled down again to 55 kK by 2006. It has a largely solar surface composition with the exception of slightly subsolar carbon, phosphorus, and sulfur. The results are discussed by considering different evolutionary scenarios.

Conclusions. The position of SAO 244567 in the $\log T_\mathrm{eff}$–$\log g$ plane places the star in the region of sdO stars. By comparison with stellar-evolution calculations, we confirm that SAO 244567 must be a low-mass star ($M < 0.55\,M_\odot$). However, the slow evolution of the respective stellar evolutionary models is in strong contrast to the observed fast evolution and the young planetary nebula with a kinematical age of only about 1000 years. We speculate that the star could be a late He-shell flash object. Alternatively, it could be the outcome of close-binary evolution. Then SAO 244567 would be a low-mass ($0.354\,M_\odot$) helium pre-white dwarf after the common-envelope phase, during which the planetary nebula was ejected.

Key words. stars: abundances – stars: evolution – stars: AGB and post-AGB – stars: individual: SAO 244567 – stars: fundamental parameters – planetary nebulae: individual: Stingray nebula (Henize 3-1357)

1. Introduction

The long stellar evolutionary time scales mean it is in general impossible for an astronomer to "watch" a star evolving in real time. Intermediate-mass stars ($M_\mathrm{ZAMS} = 0.8$–$8\,M_\odot$) experience their most rapid evolution close to the end of their nuclear-burning phase. Observing stars during this period provides the unique opportunity to investigate on the stellar asymptotic giant branch (AGB) and post-AGB evolution, including the AGB mass-loss phase, and the ejection, shaping, and excitation of planetary nebulae (PNe) – phases that are still not fully understood.

SAO 244567, the exciting star of the Stingray nebula (Henize 3-1357, Henize 1976), is an unusually fast evolving star. It was first classified to be a hot post-AGB star (Parthasarathy & Pottasch 1989) based on the discovery of a circumstellar dust shell with far-IR (IRAS) colors and flux distribution similar to that of PNe. Based on a spectral classification of the optical spectrum obtained in 1971, Parthasarathy et al. (1995) concluded that the star was a B1 or B2 supergiant. From the UBV colors and the 1971 spectrum, they estimated $T_\mathrm{eff} = 21$ kK. However, they found that the optical spectra from 1990 and 1992 as well as the IUE[1] spectra (1992–1996) display many nebular emission lines, indicating that SAO 244567 has turned into a central star of a PN (CSPN) within a time span of only 20 years. Furthermore, when comparing the IUE spectra from 1988 and 1995 Parthasarathy et al. (1995) discovered it is the only known CSPN that faded by a factor of 2.83 in its flux level within seven years. In addition, it was possible for them to observe how the stellar wind gradually decreased. From the IUE spectrum obtained

★ Based on observations with the NASA/ESA *Hubble* Space Telescope, obtained at the Space Telescope Science Institute, which is operated by the Association of Universities for Research in Astronomy, Inc., under NASA contract NAS5-26666.

★★ Based on observations made with the NASA-CNES-CSA Far Ultraviolet Spectroscopic Explorer.

★★★ Tables 1 and 3, and Figs. 4–9 are available in electronic form at http://www.aanda.org

[1] International Ultraviolet Explorer.

in 1988, Parthasarathy et al. (1995) measured a terminal wind velocity of $\upsilon_\infty = 3500\,\mathrm{km\,s^{-1}}$ from the C IV resonance doublet. The IUE spectrum in 1994 showed that the stellar wind vanished. Based on the IUE spectra, they estimated that $T_{\rm eff}$ must be around 55 kK. Assuming a distance of 5.6 kpc (Kozok 1985b) and an expansion velocity of $8\,\mathrm{km\,s^{-1}}$, Parthasarathy et al. (1993) found that the post-AGB time of SAO 244567 is about 2700 years. Furthermore, they estimated the luminosity and core mass of the CS to be 3000 $L_\odot$ and 0.55 $M_\odot$, respectively.

The first optically resolved images of the Stingray nebula were presented by Bobrowsky (1994) and Bobrowsky et al. (1998) using the Wide Field and Planetary Camera 1 (WFPC1) and WFPC2, respectively. Bobrowsky (1994) found that in Hβ, the Stingray nebula appears to have an equatorial ring of enhanced density tilted approximately 56° from the line of sight. In addition, he found bubbles of gas above and below the ring with areas of decreased brightness near the poles where a fast stellar wind has broken through the red giant envelope. From the Hβ flux, he derived an ionized mass of 0.2 $M_\odot$, $L = 5000\,L_\odot$ and a stellar core mass of 0.59 $M_\odot$. Thanks to the superior spatial resolution of the WFPC2 Bobrowsky et al. (1998) found evidence of collimated outflows, which are focused by the nebula bubbles and function like nozzles, with gas leaving through the polar holes. They also report a possible detection of a late type companion star at a distance of 2200 AU from the central star.

Umana et al. (2008) present the first detailed radio study of the Stingray nebula by using the Australian Telescope Compact Array (ATCA). They find that the Stingray nebula is still embedded in the dusty remnant of the AGB phase. Depending on their models, they derived an ionized mass of 0.057–0.07 $M_\odot$ and a total dust mass of $2 \times 10^{-4}\,M_\odot$ in the case of silicates and $7.5 \times 10^{-5}\,M_\odot$ in case of graphite.

Arkhipova et al. (2013) performed an analysis of the nebula spectra taken in 1990, 1992, and 2011. They find significant changes in the relative line intensities. The low-excitation [O I], [O II], and [N II] lines became stronger relative to Hβ by a factor of two, while the [O III] lines weakened by a factor of ≈2. Using a formula of Kaler (1978), they estimated that $T_{\rm eff}$ decreased from 1990 ($T_{\rm eff}$ = 57 kK) to 2011 ($T_{\rm eff}$ = 40 kK).

Parthasarathy et al. (1995) first discovered that the observed properties of SAO 244567, e.g. the rapid changes in $T_{\rm eff}$ and the drop of luminosity, contradict with canonical post-AGB evolution. For such a rapid evolution, the core mass should be 0.8 $M_\odot$ or even more (Parthasarathy et al. 1995; Bobrowsky et al. 1998). The evolutionary time scales for CSs with core masses of 0.6 $M_\odot$ or less are predicted to be much longer (Blöcker 1995).

To address the evolution of the properties of SAO 244567 quantitatively for the first time, we carried out a spectral analysis based on all available spectra from 1988 until 2006 taken with IUE, FUSE[2], HST/STIS[3], and HST/FOS[4]. The comparison of the results to different evolutionary models should help provide conclusions on the nature of SAO 244567.

This paper is organized as follows. In Sect. 2, we describe the observations. The spectral analysis follows in Sect. 3. In Sect. 4, we summarize our results and derive the distance and the mass of SAO 244567. We discuss possible stellar evolutionary scenarios and compare SAO 244567 to other low-mass CSPNe. We conclude in Sect. 5.

[2] Far Ultraviolet Spectroscopic Explorer.

[3] *Hubble* Space Telescope/Space Telescope Imaging Spectrograph.

[4] Faint Object Spectrograph.

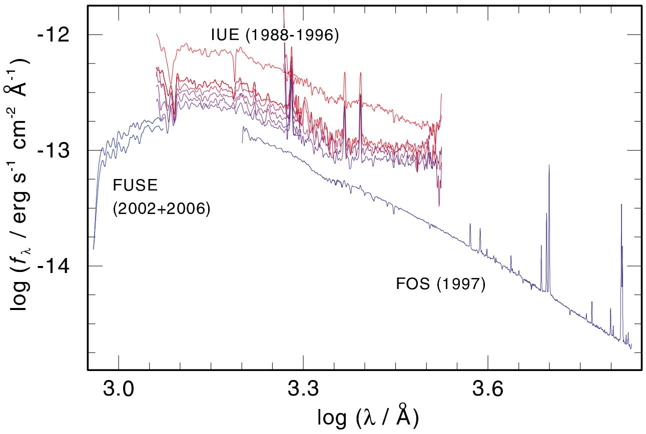

Fig. 1. All reliably flux-calibrated observations of SAO 244567.

2. Observations

SAO 244567 was observed with various telescopes (Table 1). Parthasarathy et al. (1995) reported the decrease in the flux level of the IUE observations by a factor of 2.83. We found that SAO 244567 has faded even more; e.g., we found a decrease by a factor of five by comparing the IUE observation from 1988 to the FOS observation in 1997. In Fig. 1, we show all available, reliable flux-calibrated observations of SAO 244567. The STIS observations are not photometric because of the narrow slit width used and therefore are not shown in Fig. 1. Comparing the FOS observation in 1997 to the FUSE observations in 2002, we found that the flux must have increased slightly. Comparing the flux level of the FUSE spectrum from 2002 to the one in 2006, we found a decrease of 15%. We mention all the available spectra and their special features in Sect. 2.1. The determination of the interstellar reddening follows in Sect. 2.2.

2.1. Description of the spectra

IUE spectra were taken from 1988 to 1996. All these observations but SWP51772 and SWP55690 were obtained in low-resolution mode. The main features in the spectra are nebular emission lines (from 1992 on) and the C IV and N V resonance doublets that are blue shifted and show P-Cygni profiles (Sect. 3.4).

The HST/FOS spectra were obtained in 1997 using the G190H, G270H, G400H, and G570H gratings (total exposure time ≈4600 s, ProgID 6039). The observations cover a wavelength range from ≈1600 to 6800 Å.

SAO 244567 was observed with HST/STIS in 1998 (ProgID 7652), 1999 (ProgID 7652, 7653), and 2001 (ProgID 8929) using the $52'' \times 0\farcs05$ aperture. These observations cover a total wavelength range from 1540 to 6000 Å and from 9050 to 9650 Å. In the optical wavelength range (3200 to 6800 Å), the HST/FOS and HST/STIS spectra show many nebular emission lines, but also some photospheric He II lines (partially blended by the nebula emission lines). The NUV spectra turned out to be more useful for the spectral analysis, because of the He II lines ($n \rightarrow n' = 3 \rightarrow 6, ..., 14$), which could be used to determine $\log g$, $T_{\rm eff}$, and the H/He ratio. We identified C III and C IV lines which allowed us a more precise determination of $T_{\rm eff}$ by evaluation of the C III/C IV ionization equilibrium (see Sect. 3.2). Apart from the photospheric lines, we found some interstellar Fe II, Mg II, and Mn II lines.

FUV spectra were taken with FUSE in 2002 and 2006 (total exposure time: 31 ksec, ProgIDs Q304 and U109) using the

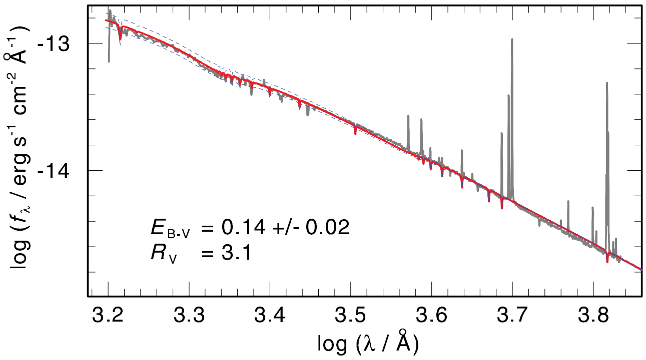

Fig. 2. Example for the determination of E_{B-V} for SAO 244567. The FOS observation (gray) is compared to TMAW model fluxes with different corrections for the interstellar reddening. The thick (red in online version) line represents the TMAW model corrected with $E_{B-V} = 0.14$, the dashed lines (blue) indicate the error limits.

LWRS aperture. These spectra show many interstellar lines, but also photospheric H I, He II, C III, C IV, N III (2002 only), N IV, O III, O IV, Si IV, P V, S IV, S V, S VI, Fe V, and Fe VI lines. Furthermore, the O VI doublet lines show weak P-Cygni profiles. We checked the FUSE observations for relative motion of interstellar and photospheric lines, but we could not find any hint of velocity shifts either by comparing the observation from 2002 and 2006, or in the individual exposures of the corresponding years. This indicates (except in case of a very high inclination angle) the probability of a close companion is rather unlikely. All these space-based observations were retrieved from the MAST archive.

2.2. Interstellar reddening

We derived the interstellar reddening for each observation. The flux shape of the IUE, STIS, and FOS spectra can only be reproduced using the LMC reddening law of (Howarth 1983). The FUSE observations could be fitted with the reddening law of Fitzpatrick (1999). Figure 2 shows the determination of E_{B-V} for the FOS observation. Since the impact of the interstellar reddening is negligible in the infrared, the TMAW model flux of our best fit model to the FOS observation ($T_{\rm eff} = 50$ kK, $\log g = 5.5$, Sect. 3.2) was firstly normalized to the reddest part of the spectrum. Then, we corrected the model flux for different values of E_{B-V} to fit the model flux to the observation.

We confirm the variations in E_{B-V} found by Arkhipova et al. (2013), who measured the reddening from the Hβ line intensity, using the simple relation, $E_{B-V} = 0.68 \times c(\mathrm{H}\beta)$, with the extinction coefficient c(Hβ). In Table 2, we compare our values with those of other authors.

3. Spectral analysis

The procedure of our spectral analysis is the following. First, we derived $T_{\rm eff}$, $\log g$, and the abundances (or at least upper limits) of the elements H, He, C, N, O, Ne, Si, P, S, Fe, and Ni with the Tübingen NLTE model-atmosphere package (TMAP[5], Werner et al. 2003; Rauch & Deetjen 2003) from the FOS, STIS, and FUSE spectra. The mass-loss rate of SAO 244567 during those years, in which these observations were taken, is negligible and therefore it is justified to use a code for hydrostatic atmospheres. We compared the PoWR[6] (Potsdam Wolf-Rayet model-atmosphere code, Gräfener et al. 2002; Hamann & Gräfener 2003, 2004) and TMAP models for the FUSE observations and found that apart from the O VI P Cygni profiles, the spectral lines are reproduced equally well. The TMAP analysis is described in Sect. 3.1. To study the mass-loss rates and terminal wind velocities from the P Cygni profiles found in the IUE and FUSE spectra and to determine $T_{\rm eff}$ in the years of the IUE observations, we used PoWR. The description of this analysis can be found in Sect. 3.4.

Table 2. Interstellar reddening of SAO 244567.

Year	Telescope	E_{B-V}	Method
1980	61 cm ESO	0.18	UBV photometry[d]
1988	IUE	0.18	LMC reddening law[a]
1988		0.20	Seaton reddening law[c]
1990	1.5 m ESO	0.18	Hβ line intensity[b]
		0.18	Hβ line intensity[c]
		0.14	Balmer decrement[3]
1992	1.5 m ESO	0.13	Hβ line intensity[b]
1993	IUE	0.17	LMC reddening law[a]
1994	IUE	0.19	LMC reddening law[a]
1995	IUE	0.20	LMC reddening law[a]
1996	IUE	0.20	LMC reddening law[a]
1997	FOS	0.14	LMC reddening law[a]
1999	STIS	0.18	LMC reddening law[a]
2002	FUSE	0.11	Fitzpatrick reddening law[a]
2006	FUSE	0.11	Fitzpatrick reddening law[a]
2011	1.9 m SAAO	0.24	Hβ line intensity[b]

Notes. Typical errors for E_{B-V} are ±0.02. [(a)] This work. [(b)] Arkhipova et al. (2013). [(c)] Parthasarathy et al. (1993). [(d)] Kozok (1985a).

3.1. TMAP model atmospheres

We used TMAP to compute non-LTE, plane-parallel, fully metal-line blanketed model atmospheres in radiative and hydrostatic equilibrium. The final models included opacities of the elements H, He, C, N, O, Ne, Si, P, S, Fe, and Ni. The model atoms for this analysis were taken from the Tübingen model-atom database TMAD[7] and calculated (Fe, Ni) via the Tübingen iron-group opacity interface TIRO[8] (Müller-Ringat 2013). It has been developed recently in the framework of the Virtual Observatory (VO[9]) and is provided as a registered service by the German Astrophysical Virtual Observatory (GAVO[10]). The statistics of the model atoms used in this analysis are summarized in Table 3. All spectral energy distributions that were calculated for this analysis are available via the registered GAVO service TheoSSA[11].

In a standard procedure (e.g. Ziegler et al. 2012), we modeled both, the photospheric and the interstellar line-absorption spectrum, to correctly identify the stellar lines. We employed the OWENS program to model the ISM line absorption with several ISM clouds with different parameters (radial and turbulent velocities, temperatures, and column densities of the individual ions). In the following, we describe our photospheric analysis.

[5] http://astro.uni-tuebingen.de/~TMAP

[6] http://www.astro.physik.uni-potsdam.de/~wrh/PoWR/

[7] http://astro.uni-tuebingen.de/~TMAD

[8] http://astro.uni-tuebingen.de/~TIRO

[9] http://www.ivoa.net

[10] http://www.g-vo.org

[11] http://dc.g-vo.org/theossa

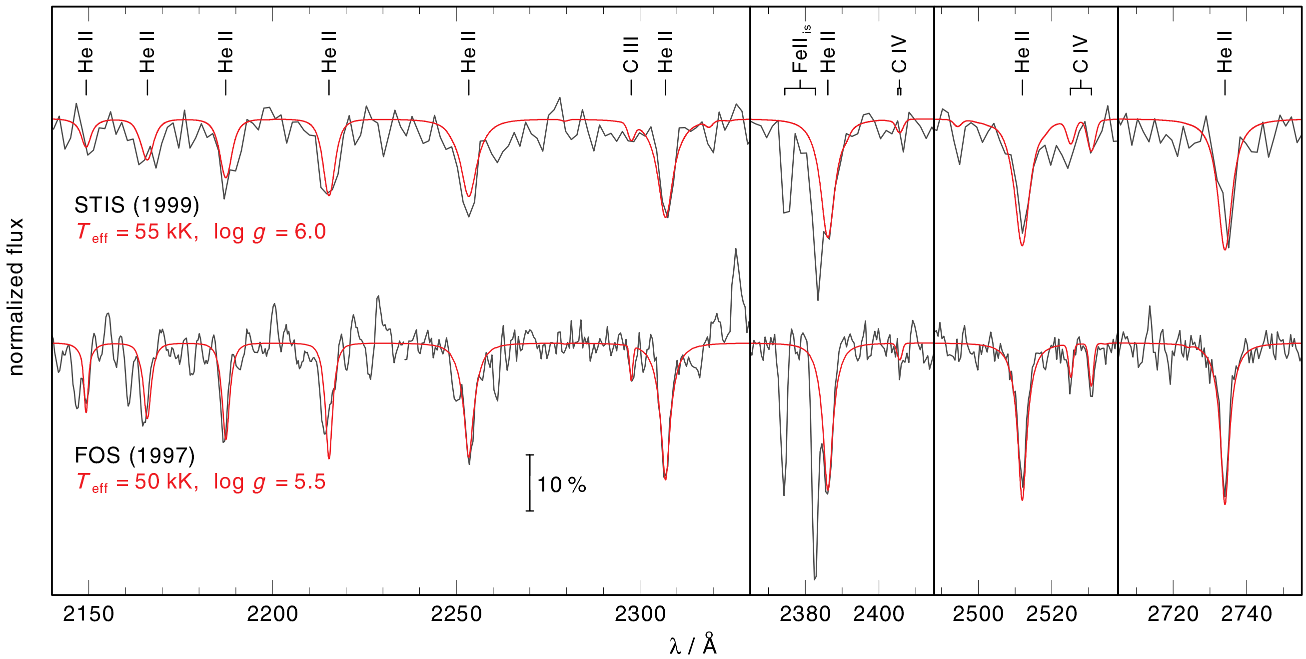

Fig. 3. Comparison of our best-fit TMAP models (black, red in online version) to the FOS and STIS observation (gray). He II, C III–IV, and interstellar Fe II lines are marked. The vertical bar indicates 10% of the continuum flux.

3.2. Effective temperature, surface gravity, H/He ratio, C abundance

Based on the IUE spectrum in 1995, Parthasarathy et al. (1995) estimated $T_{\rm eff} \approx 55$ kK. Starting with this value, we computed a grid of H+He composed model atmospheres ($T_{\rm eff}$ = 40–70 kK, 10 kK steps), $\log g$ = 4.0–7.0, 0.5 steps), H/He abundance ratios (by mass) of 9/1, 3/1 (i.e. solar), and 2/3 for a preliminary $T_{\rm eff}$ and $\log g$ determination. The synthetic spectra of these models were then compared to the observed He line profiles in the STIS and FOS spectra.

He II λ 2723.2 Å is much too strong in all H/He = 2/3 models so we can rule out He enrichment. The H/He = 9/1 models show that SAO 244567 is not He-poor because it is not possible to match the strengths and wings of the He II lines. All line profiles are reproduced well with a solar H/He ratio at $\log g = 6.0$ and $T_{\rm eff} = 50, 60, 70$ kK for the STIS spectrum. For the FOS observations the best fit was found for $\log g = 5.5$ and $T_{\rm eff} = 40, 50, 60$ kK. We adopted this abundance ratio for our analysis.

We identified several C III and C IV lines in the FUSE, STIS and FOS spectra. Consequently, we included C in our models to evaluate the C III/C IV ionization equilibrium and to determine the C abundance. For the determination of the C abundance, we used C III $\lambda\lambda$ 1165.6–1165.9, 1174.9–1176.4 Å and C IV $\lambda\lambda$ 1107.6–1108.0, 1168.8–1169.0 Å in the FUSE spectrum and C III λ 2297.6 Å and C IV $\lambda\lambda$ 2336.7–2337.1, 2405.1–2405.9, 2524.41–2530.7 Å in the STIS and FOS spectra. The C IV $\lambda\lambda$ 1548.2, 1550.8 Å resonance doublet is contaminated by the respective interstellar lines, hence not suited to determine the C abundance. The best agreement with the observation was found at C = 5.0×10^{-4}, which is 0.2× solar (solar values according to Asplund et al. 2009) in all spectra. Simultaneously, we refined our model grid ($T_{\rm eff}$ step 5 kK). In Fig. 3, we show the best-fit models for the FOS observation in 1997 and the STIS observation in 1999. We discovered that the ionization equilibrium and also the surface gravity have changed with time. While we determined $T_{\rm eff}$ = 50 kK and $\log g = 5.5$ for the FOS observation, the STIS observation is best reproduced by $T_{\rm eff}$ = 55 kK and $\log g = 6.0$.

In the FUSE spectra, we evaluated ionization equilibria of C III/C IV, N III/N IV (FUSE 2002 only), O III/O IV, and S IV/S V/S VI to derive $T_{\rm eff}$. In Fig. 4, we show the different ionization equilibria of the FUSE observation in 2002. The model with $T_{\rm eff}$ = 60 kK matches the observations. In the 55 kK model, the O III and S IV lines are too strong, whereas the S VI line is too weak. In the 65 kK model, the N III, O III, S IV, and C III lines are too weak and the S VI line is too strong. Comparing the FUSE observations from 2002 and 2006, we found that the O III and S IV lines became slightly stronger. Figure 5 shows that the best agreement in 2006 is obtained for $T_{\rm eff}$ = 55 kK. The value of $\log g = 6.0 \pm 0.5$ was confirmed using the He II line wings. In Table 4, we list the values of $T_{\rm eff}$ and $\log g$ that we found from this analysis.

Table 4. Temporal evolution of the atmospheric parameters as derived from our spectral analysis.

Year	$T_{\rm eff}$ [kK]	$\log g$ [cm/s^2]	$\log \dot{M}$ [$M_\odot$/yr]	v_∞ [km s^{-1}]	Code
1988	38	4.8	−9.0	1800	PoWR
1992	43	5.0	−9.0	1800	PoWR
1993	44	5.0	−9.1	2100	PoWR
1994	48	5.2	−10.0	2100	PoWR
1995	50	5.2	−10.0	2400	PoWR
1996	50	5.2	−10.0	2800	PoWR
1997	50	5.5			TMAP
1999	55	6.0			TMAP
2002	60	6.0	−11.3	2800	TMAP/PoWR
2006	55	6.0	−11.6	2800	TMAP/PoWR

Notes. Typical errors are $\Delta T_{\rm eff} = \pm 5$ kK, $\Delta \log g = \pm 0.5$, $\Delta \dot{M} = \pm 0.2$ dex, and $\Delta v_\infty = \pm 200$ km s^{-1}.

3.3. Element abundances

For determining the abundances of N, O, Si, P, S, and Ni, we used the respective lines found in the FUSE spectra. To derive upper limits, we compared our models to FOS spectra. For the determination of the element abundances, we adopted the values of $T_{\rm eff}$ and $\log g$ found for each epoch (Sect. 3.2). The He and C abundances were already achieved as a byproduct of the $T_{\rm eff}$ and $\log g$ determination (see above). To calculate the SAO 244567 model grids in a reasonable time, we only included H, He, C, N, and O and added the trace elements Ne, Mg, Si, P, S, Fe, and Ni in a subsequent line-formation calculation; i.e., we kept the atmospheric structure fixed and calculated NLTE occupation numbers only for newly introduced species. This is justified by the comparison of temperature structures of a HHeCNO and a complete, final HHeCNONeSiPSFeNi model, with $T_{\rm eff} = 60$ kK and $\log g = 6.0$, where the atmospheric structure is calculated with all these elements. Figure 6 demonstrates that the temperature structures are almost identical in the line-formation region ($-4 \lesssim \log m \lesssim 1$). All abundances found from line-formation calculations are verified with our final models.

Nitrogen and oxygen. The N abundance of SAO 244567 is solar (N $= 6.9 \times 10^{-4}$). It was measured using N III $\lambda\lambda$ 1183.0−1184.6 Å, N IV $\lambda\lambda$ 1123.5−1133.1 Å, and N IV λ 1183.0 Å lines in the FUSE spectrum. The O abundance was derived from the O III $\lambda\lambda$ 1149.6−1153.8 Å, and O IV $\lambda\lambda$ 1045.4−1050.5, 1167.8−1168.0 Å lines identified in the FUSE spectrum (Fig. 4). We found a solar value (O $= 5.6 \times 10^{-3}$).

Neon, sodium, magnesium, silicon, phosphor, and sulfur. The only Ne line that was prominent in our models is Ne III λ 2678.7 Å. It would emerge from the STIS and FOS spectra above an upper abundance limit of five times the solar value (Ne $\lesssim 6.2 \times 10^{-3}$). Using Na III $\lambda\lambda$ 2012.5, 2031.8 Å, we derive an upper limit for sodium of ten times the solar value (Na $\lesssim 2.9 \times 10^{-4}$). For magnesium, we derive an upper limit (solar, Mg $\lesssim 7.1 \times 10^{-4}$) using Mg III $\lambda\lambda$ 2134.7, 2178.4 Å. For the determining the Si abundance we used the Si III λ 1113.2 Å and Si IV λ 1128.3 Å lines. All other Si lines are contaminated by interstellar absorption lines. As illustrated in Fig. 7, the best fit is obtained at a solar Si abundance (Si $= 6.7 \times 10^{-4}$). For lower/higher Si abundances the modeled Si lines are too weak/strong. P V $\lambda\lambda$ 1118.0, 1128.0 Å were used to determine the P abundance (Fig. 8) which is 0.1× solar (P $= 5.8 \times 10^{-7}$). We identified S IV $\lambda\lambda$ 1073.0, 1073.5 Å, S V λ 1039.9 Å, and S VI λ 1117.8 Å and determined the S abundance to be 0.5× solar (S $= 1.6 \times 10^{-4}$).

Iron and nickel. Some Fe lines could be identified in the FUSE spectra (Fe V $\lambda\lambda$ 999.6−1001.1 Å, Fe VI $\lambda\lambda$ 1165.7, 1167.7 Å). The Fe abundance was found to be solar (Fe $\lesssim 1.3 \times 10^{-3}$). The Fe V/Fe VI ionization equilibrium also confirms $T_{\rm eff} = 60$ kK (Fig. 9). The quality of the available FUSE spectra is not sufficient to unambiguously identify individual Ni lines. Therefore, we could only derive a (solar) upper limit for the Ni (Ni $\lesssim 7.1 \times 10^{-5}$) abundance (Fig. 9). We summarize the abundances in Table 5. Their error limits are ±0.3 dex.

3.4. Stellar wind

Parthasarathy et al. (1993) found that in the IUE spectra of 1988 and 1992 the C IV and N V resonance doublets are blue-shifted and they show P-Cygni profiles. Looking more carefully, we found that all the spectra show P-Cygni profiles in these lines. While in 1988 the P-Cygni profile of N V is quite weak and C IV strong, this changes from 1992 on, which indicates that the star's $T_{\rm eff}$ has increased. Furthermore, we found in the FUSE spectra that the O VI $\lambda\lambda$ 1031.9, 1037.6 Å resonance lines show P-Cygni profiles, too.

Table 5. Photospheric abundances of SAO 244567.

Element	log mass fraction	log number fraction	$\log \epsilon$	[X]
H	−0.13	−0.04	12.01	0.00
He	−0.60	−1.11	10.94	0.00
C	−3.30	−4.28	7.77	−0.68
N	−3.16	−4.21	7.84	0.00
O	−2.25	−3.35	8.70	0.00
Ne	<−2.21	<−3.41	<8.64	<0.70
Na	<−3.53	<−4.80	<7.26	<1.00
Mg	<−3.15	<−4.44	<7.61	<0.00
Si	−3.18	−4.53	7.52	0.00
P	−6.24	−7.63	4.42	−1.00
S	−3.81	−5.22	6.83	−0.30
Fe	−2.89	−4.54	7.51	0.00
Ni	<−4.15	<−5.82	<6.23	<0.00

Notes. [X] denotes log (abundance/solar abundance). $\log \varepsilon_X$ are normalized to $\log \sum \mu_X \varepsilon_X = 12.15$, where μ_X is the atomic weight.

To measure the mass-loss rate and $T_{\rm eff}$ of SAO 244567, we used PoWR. It solves the NLTE radiative transfer in a spherically expanding atmosphere simultaneously with the statistical-equilibrium equations and accounts at the same time for energy conservation. Iron-group line blanking is treated by means of the superlevel approach (Gräfener et al. 2002), and a wind clumping in first-order approximation is taken into account (Hamann & Gräfener 2004). We do not calculate hydrodynamically consistent models, but assume a velocity field following a β-law with $\beta = 1$. For the PoWR models, we adopted the elemental abundances that we found in our TMAP analysis. We extrapolated the mass and the luminosity of SAO 244567 using the evolutionary tracks from Hall et al. (2013) and found $M = 0.36\,M_\odot$ and $\log(L/L_\odot) = 2.5$. We also calculated models with $M = 0.47\,M_\odot$ and $\log(L/L_\odot) = 2.2$ (values extrapolated from the tracks by Driebe et al. 1998), but we found that the line profiles change only slightly with M and L. This agrees with Herald & Bianchi (2007) who report that wind features are not very sensitive to the gravity, which is in the case of the PoWR code an equivalent input parameter.

Based on these assumptions, we varied the terminal wind velocity v_∞, mass-loss rate $\dot{M}$, and $T_{\rm eff}$ in our models. The relative strengths of N V/C IV turned out to be very sensitive to $T_{\rm eff}$, so that we can achieve an error of only $\Delta T_{\rm eff} = \pm 3$ kK. The sensitvity to $T_{\rm eff}$ can be clearly seen by comparing the best-fit models for 1988 and 1992, where the only difference of these models is $T_{\rm eff}$. In the $T_{\rm eff} = 38$ kK model for 1988, C IV is relatively stronger than N V, whereas the opposite holds for the $T_{\rm eff} = 43$ kK model for 1992. The mass-loss rate was derived from the strengths of the P-Cygni profiles. As the P-Cygni profiles broaden as v_∞ increases, v_∞ can be measured not only from the blue edge of the absorption component of the P-Cygni profiles, but also from the shape of the emission peak.

The best-fit models are shown in Figs. 10 (IUE spectra) and 11 (FUSE). The P-Cygni profile of O VI λ 1037.6 Å in the PoWR models is blended by interstellar H_2 and is therefore not visible in the observation. Furthermore, we found that the absorption components of O VI $\lambda\lambda$ 1031.9, 1037.6 Å must have an interstellar origin. Table 4 lists the parameters that we found from this analysis. The resulting surface gravities are also given.

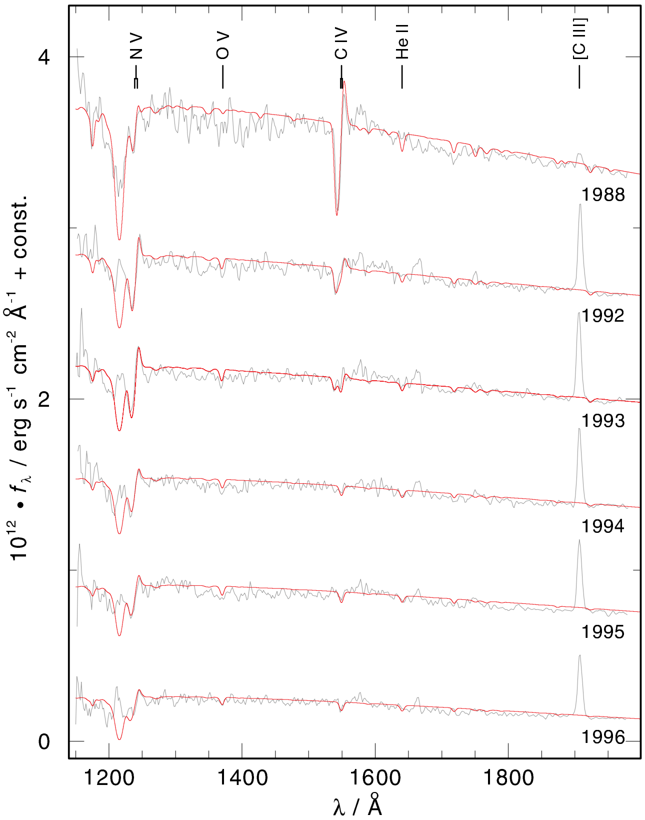

Fig. 10. Comparison of the IUE spectra taken from 1988 to 1996 (thin, gray) with the best-fit PoWR model (thick, red). All but the 1988 observation are shifted for clarity.

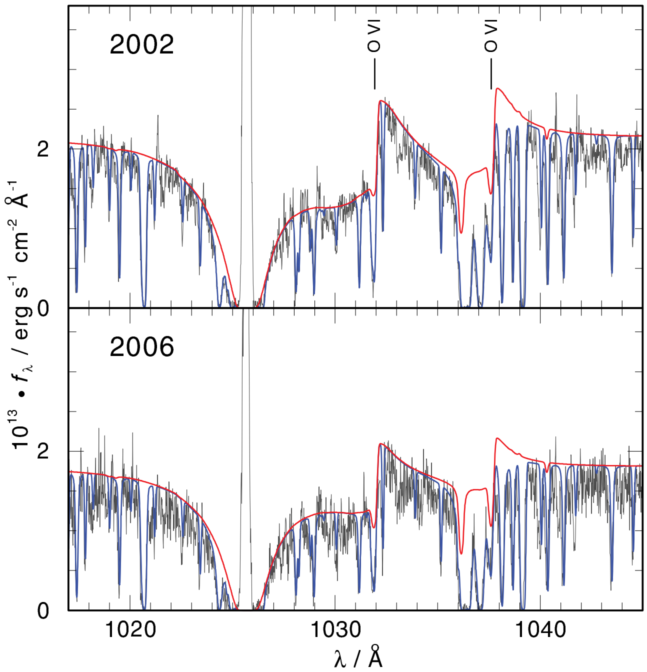

Fig. 11. Comparison the FUSE spectra taken in 2002 and 2006 (gray) with the best-fit PoWR model (thick, red). The blue line (thin) indicates the combined stellar and ISM spectrum.

Table 6. Comparison of the element abundances (number fractions relatively to H) of SAO 244567 (CS) as derived by our analysis and of its PN as derived by analysis of the spectrum in 1990 (Parthasarathy et al. 1993), 1992, and 2011 (Arkhipova et al. 2013).

	CS		PN	
		2011	1992	1990
He/H	8.50×10^{-2}	9.60×10^{-2}	9.30×10^{-2}	1.03×10^{-1}
C/H	5.69×10^{-5}		7.59×10^{-5}	
N/H	6.69×10^{-5}	5.75×10^{-5}	6.45×10^{-5}	6.50×10^{-5}
O/H	4.84×10^{-4}	1.91×10^{-4}	2.46×10^{-4}	3.00×10^{-4}
Ne/H	$< 3.59 \times 10^{-4}$	3.47×10^{-5}	5.75×10^{-5}	9.20×10^{-5}
S/H	6.03×10^{-6}	2.40×10^{-6}	6.03×10^{-6}	2.20×10^{-6}

We point out that these values refer to the models with $M = 0.36\,M_\odot$, the resulting values for the surface gravity from the $M = 0.47\,M_\odot$ models were about 0.1–0.2 dex higher.

We find that the mass-loss rate decreased continuously from $\log(\dot{M}/M_\odot\,\mathrm{yr}^{-1}) = -9.0$ in 1988 to $\log(\dot{M}/M_\odot\,\mathrm{yr}^{-1}) = -11.6$ in 2006. The previously published value ($v_\infty = 3500\,\mathrm{km\,s^{-1}}$, Parthasarathy et al. 1995) turned out to be an overestimate. We find that the terminal wind velocity has steadily increased from $v_\infty = 1800\,\mathrm{km\,s^{-1}}$ in 1988 to $v_\infty = 2800\,\mathrm{km\,s^{-1}}$ in 2006.

4. Results and discussion

We analyzed the high-resolution UV spectra taken with FUSE, STIS, FOS, and IUE by means of non-LTE line blanketed model atmospheres. The values of T_{eff} were derived with high precision by evaluating the ionization equilibria of C III/C IV (FOS, STIS and FUSE spectra), O III/O IV, S IV/S V/S VI (FUSE spectra), and N III/N IV (FUSE 2002 spectra). From the IUE spectra, we derived T_{eff} using the relative strength of N V/C IV.

Both the surface gravity and the H/He ratio (solar) were obtained by an analysis of the He II lines found in the STIS and FOS spectra. For the FOS observations, the best fit was found with $\log g = 5.5$, while for the STIS observation the model with $\log g = 6.0$ fits better. This value of $\log g = 6.0$ was confirmed by the wings of the He II lines in the FUSE spectra.

SAO 244567 exhibits solar abundances of H, He, O, and N. The C abundance is definitely subsolar. This indicates that the AGB phase of the star was terminated before the third dredge-up (Mello et al. 2012). P and S were found to be subsolar, the Si and Fe abundances are solar. For Ne, Mg, and Ni, we could only derive upper limits (five times solar for Ne, ten times solar for Na, solar for the rest). We could not find any hint of a change in the chemical abundances during the years. Within the error limits (typically ±0.3 dex) the abundances found for the CS are in good agreement with the nebula abundances (Table 6) determined by Arkhipova et al. (2013) and Parthasarathy et al. (1993).

The temporal evolution of the atmospheric parameters of SAO 244567 is summarized in Table 4 and Fig. 12. We found that compared to the temperature found from the spectrum in 1971 (Sect. 1) SAO 244567 has increased its T_{eff} by about 40 kK within only thirty years. The peak T_{eff} of 60 kK was reached in 2002, and the 2006 observations suggest that it is now decreasing. We cannot confirm the values for T_{eff} found by Arkhipova et al. (2013). They find the peak T_{eff} in 1990 ($T_{\mathrm{eff}} = 57$ kK), i.e. about 10 kK higher than our analysis from spectra taken at that time. We want to point out, that the formalism of Kaler (1978) used by Arkhipova et al. (2013) might not provide good estimates for the CS temperature. Comparing the T_{eff} of Kaler (1978) found for his sample of CSPNe, shows often big deviations from recent literature values (e.g. NGC 6543: Kaler 1978 found $T_{\mathrm{eff}} = 45$ kK while Herald & Bianchi 2011 found $T_{\mathrm{eff}} = 60$ kK). However, evaluation of the ionization equilibria found in the FUSE spectra shows T_{eff} declining from 2002

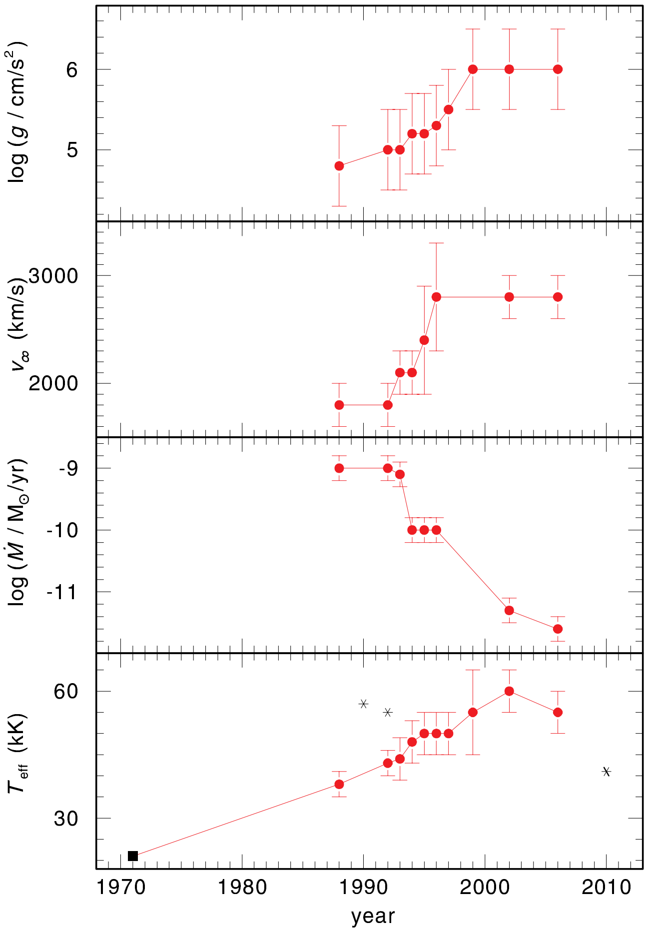

Fig. 12. Temporal evolution of $T_{\rm eff}$, $\log g$, mass-loss rate $\dot{M}$, and the terminal wind velocities v_∞ as derived in our analysis (red). The black stars in the *bottom panel* show the $T_{\rm eff}$ as derived by Arkhipova et al. (2013), the black square indicates the $T_{\rm eff}$ estimate when SAO 244567 was still a B-type supergiant (1971).

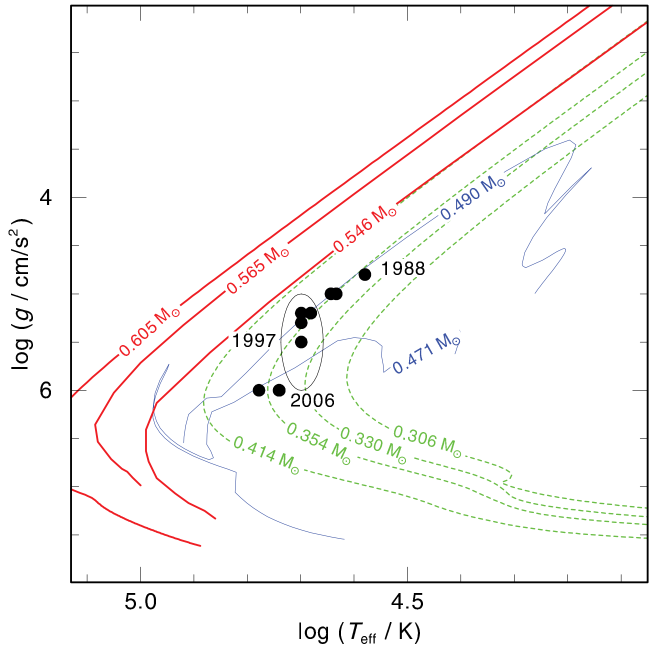

Fig. 13. Evolution of SAO 244567 (black dots) in the $\log T_{\rm eff}$–$\log g$ plane compared to post-AGB (red, thick) by Blöcker (1995), post-EHB (blue, thin) by Dorman et al. (1993), and post-RGB (green, dashed) evolutionary tracks by Hall et al. (2013) The tracks are labeled with stellar masses. The ellipse indicates the errors of $T_{\rm eff}$ and $\log g$ in 1997.

on, supporting the contention by Arkhipova et al. (2013) that $T_{\rm eff}$ has recently peaked and has begun to decline.

By examining the P-Cygni profiles of the C IV and N V resonance doublets in the IUE spectra from 1988 to 1996 and the P-Cygni profiles of O VI in the FUSE spectra, we derived the mass-loss rates and terminal wind velocities as a function of time. We found a steady decrease in the mass-loss rate (from $\log(\dot{M}/M_\odot\,{\rm yr}^{-1}) = -9.0$ in 1988 to $\log(\dot{M}/M_\odot\,{\rm yr}^{-1}) = -11.6$ in 2006) and the steady increase in the terminal wind velocity (from $v_\infty = 1800\,{\rm km\,s}^{-1}$ in 1988 to $v_\infty = 2800\,{\rm km\,s}^{-1}$ in 2006). To compare the mass-loss rate with predictions from radiative-driven wind theory, we used Eq. (5) in Vink & Cassisi (2002) with $L = 2.5\,L_\odot$, $M = 0.354\,M_\odot$, $T_{\rm eff} = 38$ kK, and $Z = 2$ to derive the theoretical value of the mass-loss rate in 1988. We found $\log \dot{M} = -8.8 \pm 0.3$, which is in good agreement with the observed value. However, we note that the formula given by Vink & Cassisi (2002) might not give the right predictions, since it is meant for a slightly different parameter space in L, $T_{\rm eff}$, and M.

The decrease in flux with a simultaneous increase of $T_{\rm eff}$ from 1988 to 1999 can be explained by the contraction of the star ($L \propto R^2 T_{\rm eff}{}^4 \propto g^{-1} T_{\rm eff}{}^4$). This is consistent with the increase in $\log g$ as seen in the FOS (1997) and STIS (1999) observations, and consistent with the increase in v_∞ which is proportional to $v_{\rm esc} \propto g$. The decrease in flux from 2002 to 2006 can be explained by a decrease in $T_{\rm eff}$ as seen in the FUSE spectra.

4.1. Distance

The distance of SAO 244567 was estimated first by Kozok (1985b) using UBV photometry and the assumption of a typical absolute magnitude of a Be star, leading to $d = 5.64$ kpc. Arkhipova et al. (2013) argues that Kozok (1985b) overestimated the absolute magnitude of SAO 244567 since it was not a main sequence star at that time. Using the estimates of Parthasarathy et al. (1993) for $T_{\rm eff} = 37.5$ kK and $\log g = 4.0$, they estimated $M \approx 0.55\,M_\odot$ and derived $d = 1.8$ kpc. We calculated the spectroscopic distance of SAO 244567 using the flux calibration of Heber et al. (1984) for $\lambda_{\rm eff} = 5454$ Å,

$$d[{\rm pc}] = 7.11 \times 10^4 \cdot \sqrt{H_\nu \cdot M \times 10^{0.4 m_{V_0} - \log g}},$$

with $m_{V_0} = m_V - 2.175c$, $c = 1.47 E_{B-V}$, and the Eddington flux H_ν (7.15×10^{-4} erg/cm^2/s/Hz) at 5454 Å of our model atmosphere ($T_{\rm eff} = 50$ kK and $\log g = 5.5$). The visual brightness ($m_V = 14.9$) was extracted from the FOS spectrum, so we used all the model parameters found for this year. We assumed $E_{B-V} = 0.14$ (Sect. 2.2) and a stellar mass of $M = 0.354^{+0.14}_{-0.05}\,M_\odot$ (Sect. 4.2). We derived $d = 1.6^{+0.8}_{-1.2}$ kpc which leads to a height above the Galactic plane of $z = 0.3 \pm 0.2$ kpc. These values are in good agreement with the estimates of Arkhipova et al. (2013). From the angular diameter of 2.″3, a linear radius of the PN of $R = 0.009^{+0.004}_{-0.007}$ pc results. With the expansion velocity of $8.4\,{\rm km\,s}^{-1}$ (Arkhipova et al. 2013), the kinematic age of the PN is only about 1013^{+488}_{-793} years. We note that different masses, which we derive from various evolutionary scenarios, hardly affect the distance determination and that the large errors are mainly due to the uncertainties in $\log g$.

4.2. Mass and evolutionary status

In Fig. 13, we compare the time-dependent location of SAO 244567 in the $\log T_{\rm eff}$–$\log g$ plane with H-rich post-AGB evolutionary tracks by Blöcker (1995), post-EHB-tracks by Dorman et al. (1993), and post-RGB-tracks by Hall et al. (2013). The last represent the evolution of post-common envelope remnants of post-RGB stars that will not ignite He and become low-mass white dwarfs with a He core. The determination of the mass of SAO 244567 would only be possible, if the evolutionary status of this object is known. For that reason, we give only the mass estimates valid for a certain evolutionary scenario below.

The position of SAO 244567 in the log $T_{\rm eff}$–log g plane places the star in the region of sdO stars. Since SAO 244567 does not match the 0.546 $M_\odot$ track within the error ranges, it may either be a very low-mass post-AGB star with a mass of about 0.53 $M_\odot$ or even an AGB-manqué star, which never reaches the AGB.

The existence of the PN around SAO 244567 suggests that it is more likely a post-AGB star than an AGB-manqué star because – in general – only these stars are expected to eject a PN. If we consider SAO 244567 as a 0.53 $M_\odot$ post-AGB star, it evolves much more quickly than predicted by theory. Comparing $T_{\rm eff}$ = 21 kK estimated for 1971 to the peak value of $T_{\rm eff}$ = 60 kK in 2002, SAO 244567 increased its temperature to 40 kK within only 30 years. According to Fig. 6 in Blöcker (1995) such a rapid evolution ($\log({\rm d}t/{\rm d}T_{\rm eff}/{\rm yr K}^{-1}) = -3$) would be expected only for a 0.87 $M_\odot$ star with an initial mass of about 6 $M_\odot$. For a 0.55 $M_\odot$ star it would take 130 000 years to heat up from $T_{\rm eff}$ = 21 kK to $T_{\rm eff}$ = 60 kK.

An alternative to the canonical post-AGB evolution is a late thermal pulse (LTP, e.g. Blöcker 2001). The evolutionary speed of objects, which are considered to have undergone a (very) late He-shell flash (V605 Aql, e.g., Clayton et al. 2006; V4334 Sgr, e.g., Hajduk et al. 2005; and FG Sge, e.g., Jeffery & Schönberner 2006), is very high (decades). A very late thermal pulse can be ruled out because this scenario produces a hydrogen-free stellar surface, whereas a normal surface composition is typical of a LTP in the phase relevant to SAO 244567. The LTP occurs when the star evolves with roughly constant luminosity from the AGB towards the white dwarf domain. The convective shell triggered by excessive helium burning is not able to penetrate the hydrogen-rich envelope from below because the entropy jump across the helium/hydrogen interface is too large. Only when the star evolves back to its Hayashi limit on the AGB ($T_{\rm eff} \lesssim 7000$ K), envelope convection sets in again (Blöcker & Schönberner 1996, 1997; Schönberner 2008). Therefore, the surface abundances of SAO 244567 are in agree with the LTP scenario. The evolutionary calculations of Blöcker (2001) for a 0.625 $M_\odot$ LTP star predict that the solar surface composition of the star holds up after the LTP. Only when the star has cooled down to $T_{\rm eff}$ = 10 kK, the H abundance decreases while the He and C abundances increase. The LTP scenario is able to explain the rapid evolution (increase in $T_{\rm eff}$ and drop in luminosity). It would predict a decrease in $T_{\rm eff}$ (the FUSE observation in 2006 already suggests that) and an increase in the brightness within the next decades (similar to the evolution of FG Sge). The LTP is a good candidate for explaining the evolutionary status of SAO 244567; however, concrete evolutionary models that match the position of SAO 244567 in the log $T_{\rm eff}$–log g plane, are missing to prove this scenario.

Considering SAO 244567 as an AGB-manqué star, which ignited central He-burning, we derive a mass of 0.49 $M_\odot$ according to the tracks of Dorman et al. (1993). Within this scenario the existence of the PN and the short evolutionary time scales are even more difficult to explain. Even if the RGB precursor would have ejected a PN, it should have disappeared a long time ago since the horizontal branch (HB) evolution lasts $\approx 10^8$ years. It is worthwhile mentioning that the mass of the remaining H layer ($\leq 0.001\,M_\odot$) of extended horizontal branch (EHB) stars is much too low to produce a nebula at the end of the HB stage. We can also rule out an early hot-flasher scenario. Brown et al. (2001) found that as the Reimers mass-loss parameter $\eta_{\rm R}$ increases, the peak of the main helium core flash shifts to higher temperatures, and the subsequent zero age horizontal branch (ZAHB) position becomes hotter. However their models never produced stars with a ZAHB position hotter than $T_{\rm eff}$ = 31.5 kK.

Recently Hall et al. (2013) have proposed that it is possible that at least some PNe are composed of matter ejected from a binary star system during common envelope (CE) evolution. For these PNe, the ionizing component is the hot and luminous remnant of a giant that had its envelope ejected by a companion in the process of spiraling in to its current short-period orbit. A large fraction of CE phases that end with ejection of the envelope are thought to be initiated by low-mass red giants, giants with inert, degenerate helium cores. In their calculations Hall et al. (2013) find, that PNe are expected in post-CE systems with core masses greater than about 0.3 $M_\odot$ if remnants end the CE phase in thermal equilibrium. Considering this scenario for SAO 244567, we estimate a mass of 0.354 ± 0.03 $M_\odot$. The rapid evolution of SAO 244567, though, is also not predicted in their models. A higher mass-loss rate might increase the evolutionary speed, but there are no hints of any enhanced mass loss in the observations. However, if the remnant is in thermal non-equilibrium after the CE ejection, it might evolve rapidly enough (Philip Hall, priv. comm.).

The current decrease in $T_{\rm eff}$ of SAO 244567 from 2002 on found in our work and also by Arkhipova et al. (2013) argues for post-RGB evolution instead of the post-EHB evolution, since the H-shell-burning models cool down directly, whereas the He-core burning post-EHB models become even hotter (Fig. 13).

The bipolar shape of the PN is most likely due to some kind of binary interaction of a RGB or AGB star with either a stellar or substellar companion. This was already suggested by Bobrowsky (1994) to explain the axisymmetric structure of SAO 244567. Soker (1997) proposed that bipolar structures of PNe, as seen in SAO 244567, can be explained by close binary interactions that avoid a CE phase, or they entered this phase only in their late evolution. The gravitational interaction between the companion and the PN progenitor and/or their winds are non-negligible. The companion's tidal force can spin up the primary and enhance the mass-loss rate or the companion can accrete mass from the primary's wind. This accretion process is likely to result in a high mass-loss rate in the equatorial plane, leading to a bipolar PN. The possible companion detected by Bobrowsky et al. (1998), however, is too far away (638 AU at a distance of 1.6 kpc) for significant interaction with SAO 244567. But it might be possible that SAO 244567 has another, hitherto undetected companion.

4.3. Comparison with other low-mass CSPNe

SAO 244567 is not the only low-mass CSPN. Napiwotzki (1999) found five such candidates (HDW 11, K 2–2, GD 561, PHL 932, and DeHt 5) that are not in accordance with post-AGB evolution. For the DA-type WD DeHt 5 (M = 0.414 $M_\odot$), they considered a post-RGB evolution as the kinematical age of the PN (≈129 000 yrs) is in good agreement with the post-RGB age (≈100 000 yrs) estimated from the calculations of Driebe et al. (1998). The two DAO-type WDs K 2–2 (M = 0.39 $M_\odot$) and HDW 11 (M = 0.38 $M_\odot$) are also candidates for this evolutionary scenario.

For PHL 932 and EGB 5, an object with similar parameters, the post-RGB times corresponding to the tracks of Driebe et al. (1998) are much longer than the ages of the PNe. The PN EGB 5 is believed to be a remnant of an ejected CE. Geier et al. (2011) discovered a close low-mass companion orbiting the sdB central star and thus EGB 5 is considered to be a good candidate for a post-CE object. Napiwotzki (1999) considered PHL 932 ($M = 0.28\,M_{\odot}$) to be the outcome of a CE event of a star with a degenerate CO core as calculated by Iben & Tutukov (1985) or even as the result of a merger within a common envelope (Méndez et al. 1988b). However Frew et al. (2010) convincingly demonstrate that the nebula around PHL 932 is not a PN, but rather a Strömgren sphere in the ambient ISM. Also EGB 5 has recently been classified as an ionized H II region (Frew et al. 2013). The same holds for the nebulae around the DAO-type WDs GD 561 and BD-22°3467 (Ziegler et al. 2012), which Frew & Parker (2010) also consider to be Strömgren spheres. Other objects of this type are the sdO stars HD 497898, LSS 630, LSE 44, LSE 153, SB 705, and KPD 0720−0003 around which nebulosities were detected that are not believed to be ejected by or physically associated with the corresponding stars (Méndez et al. 1988a). This can clearly not be true for SAO 244567 owing to its complex nebula structure and the expansion velocity.

A multi-shell planetary nebula around the hot sdO star 2MASS J19310888+4324577 has recently been detected (Aller et al. 2013). The morphology of the nebula (bipolar and elliptical shell, whose major axes are oriented perpendicular to each other) strongly resembles the one of the Stingray nebula. The complex nebula structure and the fact that 2MASS J19310888+4324577 was found to be in a binary system (Jacoby et al. 2012) suggest that it might have formed through binary star evolution.

5. Conclusions

SAO 244567 is a rapidly evolving object. Its evolutionary status remains unclear. The most reasonable explanations are a late He-shell flash or CE evolution with a remnant that is in thermal non-equilibrium after the CE ejection. However, respective models are lacking that match the position of SAO 244567 in the $\log T_{\rm eff}$–$\log g$ plane. The contradiction between observations and theory make SAO 244567 particularly interesting. Its fast evolution gives us the unique opportunity to study stellar evolution in real time and establishes constraints for stellar evolutionary theory. Further observations, in the next years, decades and even centuries, are essential for monitoring whether the rapid evolution of SAO 244567 is still going on and to see if it is directly evolving to the white dwarf domain or back to the AGB. The detection of a close binary would support the scenario of a CE ejection, whereas an increase in brightness and decrease in $T_{\rm eff}$ over the next decades, would indicate an evolution back to the AGB and hence speak for a LTP scenario.

Acknowledgements. N.R. is supported by the German Research Foundation (DFG, grant WE 1312/41-1), TR by the German Aerospace Center (DLR, grant 05 OR 0806). We thank Marcelo Miguel Miller Bertolami and Philip Hall for helpful discussions and comments. M.P. is grateful to Profs. Ajit K. Kembhavi, Kandaswamy Subramanian and T. Padmanabhan for their kind encouragement, support, and hospitality. This research has made use of the SIMBAD database, operated at the CDS, Strasbourg, France. This research made use of NASA's Astrophysics Data System. This work used the profile-fitting procedure OWENS developed by M. Lemoine and the French FUSE Team. Some of the data presented in this paper were obtained from the Mikulski Archive for Space Telescopes (MAST). STScI is operated by the Association of Universities for Research in Astronomy, Inc., under NASA contract NAS5-26555. Support for MAST for non-HST data is provided by the NASA Office of Space Science via grant NNX13AC07G and by other grants and contracts.

References

Aller, A., Miranda, L. F., Ulla, A., et al. 2013, A&A, 552, A25
Arkhipova, V. P., Ikonnikova, N. P., Kniazev, A. Y., & Rajoelimanana, A. 2013, Astron. Lett., 39, 201
Asplund, M., Grevesse, N., Sauval, A. J., & Scott, P. 2009, ARA&A, 47, 481
Blöcker, T. 1995, A&A, 299, 755
Blöcker, T. 2001, Ap&SS, 275, 1
Blöcker, T., & Schönberner, D. 1996, Mem. Soc. Astron. It., 67, 665
Blöcker, T., & Schönberner, D. 1997, A&A, 324, 991
Bobrowsky, M. 1994, ApJ, 426, L47
Bobrowsky, M., Sahu, K. C., Parthasarathy, M., & García-Lario, P. 1998, Nature, 392, 469
Brown, T. M., Sweigart, A. V., Lanz, T., Landsman, W. B., & Hubeny, I. 2001, ApJ, 562, 368
Clayton, G. C., Kerber, F., Pirzkal, N., et al. 2006, ApJ, 646, L69
Dorman, B., Rood, R. T., & O'Connell, R. W. 1993, ApJ, 419, 596
Driebe, T., Schönberner, D., Blöcker, T., & Herwig, F. 1998, A&A, 339, 123
Fitzpatrick, E. L. 1999, PASP, 111, 63
Frew, D. J., & Parker, Q. A. 2010, PASA, 27, 129
Frew, D. J., Madsen, G. J., O'Toole, S. J., & Parker, Q. A. 2010, PASA, 27, 203
Frew, D. J., Bojičić, I. S., & Parker, Q. A. 2013, MNRAS, 431, 2
Geier, S., Napiwotzki, R., Heber, U., & Nelemans, G. 2011, A&A, 528, L16
Gräfener, G., Koesterke, L., & Hamann, W.-R. 2002, A&A, 387, 244
Hajduk, M., Zijlstra, A. A., Herwig, F., et al. 2005, Science, 308, 231
Hall, P. D., Tout, C. A., Izzard, R. G., & Keller, D. 2013, MNRAS, 435, 2048
Hamann, W.-R., & Gräfener, G. 2003, A&A, 410, 993
Hamann, W.-R., & Gräfener, G. 2004, A&A, 427, 697
Heber, U., Hunger, K., Jonas, G., & Kudritzki, R. P. 1984, A&A, 130, 119
Henize, K. G. 1976, ApJS, 30, 491
Herald, J. E., & Bianchi, L. 2007, ApJ, 661, 845
Herald, J. E., & Bianchi, L. 2011, MNRAS, 417, 2440
Howarth, I. D. 1983, MNRAS, 203, 301
Iben, Jr., I., & Tutukov, A. V. 1985, ApJS, 58, 661
Jacoby, G., De Marco, O., Howell, S., & Kronberger, M. 2012, in AAS Meeting Abstracts, 219, 41802
Jeffery, C. S., & Schönberner, D. 2006, A&A, 459, 885
Kaler, J. B. 1978, ApJ, 220, 887
Kozok, J. R. 1985a, A&AS, 62, 7
Kozok, J. R. 1985b, A&AS, 61, 387
Mello, D. R. C., Daflon, S., Pereira, C. B., & Hubeny, I. 2012, A&A, 543, A11
Méndez, R.-H., Gathier, R., Simon, K. P., & Kwitter, K. B. 1988a, A&A, 198, 287
Méndez, R. H., Kudritzki, R. P., Groth, H. G., Husfeld, D., & Herrero, A. 1988b, A&A, 197, L25
Müller-Ringat, E. 2013, Dissertation, University of Tübingen, Germany, http://tobias-lib.uni-tuebingen.de/volltexte/2013/6774/
Napiwotzki, R. 1999, A&A, 350, 101
Parthasarathy, M., Garcia-Lario, P., de Martino, D., et al. 1995, A&A, 300, L25
Parthasarathy, M., & Pottasch, S. R. 1989, A&A, 225, 521
Parthasarathy, M., Garcia-Lario, P., Pottasch, S. R., et al. 1993, A&A, 267, L19
Rauch, T. & Deetjen, J. L. 2003, in Stellar Atmosphere Modeling, eds. I. Hubeny, D. Mihalas, & K. Werner, ASP Conf. Ser., 288, 103
Schönberner, D. 2008, in Hydrogen-Deficient Stars, eds. A. Werner, & T. Rauch, ASP Conf. Ser., 391, 139
Soker, N. 1997, ApJS, 112, 487
Umana, G., Trigilio, C., Cerrigone, L., Buemi, C. S., & Leto, P. 2008, MNRAS, 386, 1404
Vink, J. S., & Cassisi, S. 2002, A&A, 392, 553
Werner, K., Deetjen, J. L., Dreizler, S., et al. 2003, in Stellar Atmosphere Modeling, eds. I. Hubeny, D. Mihalas, & K. Werner, ASP Conf. Ser., 288, 31
Ziegler, M., Rauch, T., Werner, K., Köppen, J., & Kruk, J. W. 2012, A&A, 548, A109

Pages 10 to 14 are available in the electronic edition of the journal at http://www.aanda.org

Table 1. Observations of SAO 244567.

Instrument/ telescope	ObsId	Aperture/ grating	Start time (UT)	Exposure time (s)
B & C, ESO 1.5 m			1990-06	1-600
B & C, ESO 1.5 m			1992-08	1-600
IUE	SWP33954LL	large	1988-07-21 23:44:32	1800
	LWP13715LL	large	1988-07-22 00:34:19	1200
	SWP33955LL	large	1988-07-22 01:05:33	1800
	LWP22874LL	large	1992-04-23 04:19:56	600
	SWP44459LL	large	1992-04-23 03:52:00	1200
	LWP25397LL	large	1993-04-23 05:06:09	600
	SWP47530LL	large	1993-04-23 05:23:38	1200
	SWP50589LL	large	1994-04-19 08:13:06	1200
	LWP27971LL	large	1994-04-23 01:56:53	600
	SWP51772HL	large	1994-08-11 01:52:34	25 200
	SWP51852LL	large	1994-08-20 09:40:09	900
	LWP30479LL	large	1995-04-19 02:31:12	600
	SWP54463LL	large	1995-04-19 01:59:00	1200
	SWP54465LL	large	1995-04-19 08:18:31	1800
	LWP30490LL	large	1995-04-20 01:45:20	1800
	SWP55690HL	large	1995-08-24 18:23:29	22 920
	LWP32551LL	large	1996-08-10 20:08:00	1200
	LWP32552LL	large	1996-08-10 21:54:07	1800
	SWP57774LL	large	1996-08-10 19:31:12	1800
	SWP57775LL	large	1996-08-10 20:55:02	3000
FOS, HST	Y3415205T	$0\farcs3$, G190H	1997-02-03 11:21:13	180
	Y341520BT	$0\farcs3$, G400H	1997-02-03 12:25:41	950
	Y341520CT	$0\farcs3$, G570H	1997-02-03 12:48:27	1500
	Y341520KT	$0\farcs3$, G270H	1997-02-03 15:38:38	1650
STIS, HST	O4NH01030	$52'' \times 0\farcs05$, G750M	1998-03-07 22:58:48	708
	O4NH01040	$52'' \times 0\farcs05$, G430L	1998-03-07 23:15:55	840
	O4NH02030	$52'' \times 0\farcs05$, G230LB	1999-02-05 18:13:25	1978
	O4C562020	$52'' \times 0\farcs05$, G230L	1999-04-12 01:22:42	900
	O4C562030	$52'' \times 0\farcs05$, G140M	1999-04-12 01:45:28	862
	O6IH20020	$52'' \times 0\farcs05$, G430M	2001-09-16 02:35:05	900
	O6IH20060	$52'' \times 0\farcs05$, G430M	2001-09-16 03:20:42	1080
	O6IH30020	$52'' \times 0\farcs05$, G750M	2001-09-24 08:55:01	1080
	O6IH30060	$52'' \times 0\farcs05$, G750M	2001-09-24 10:32:46	1080
FUSE	Q3040101000	LWRS	2002-04-12 02:00:59	8240
	Q3040102000	LWRS	2002-06-16 22:12:47	15 268
	U1093201000	LWRS	2006-06-23 04:02:36	15 824
	U1093202000	LWRS	2006-06-24 11:12:43	2862

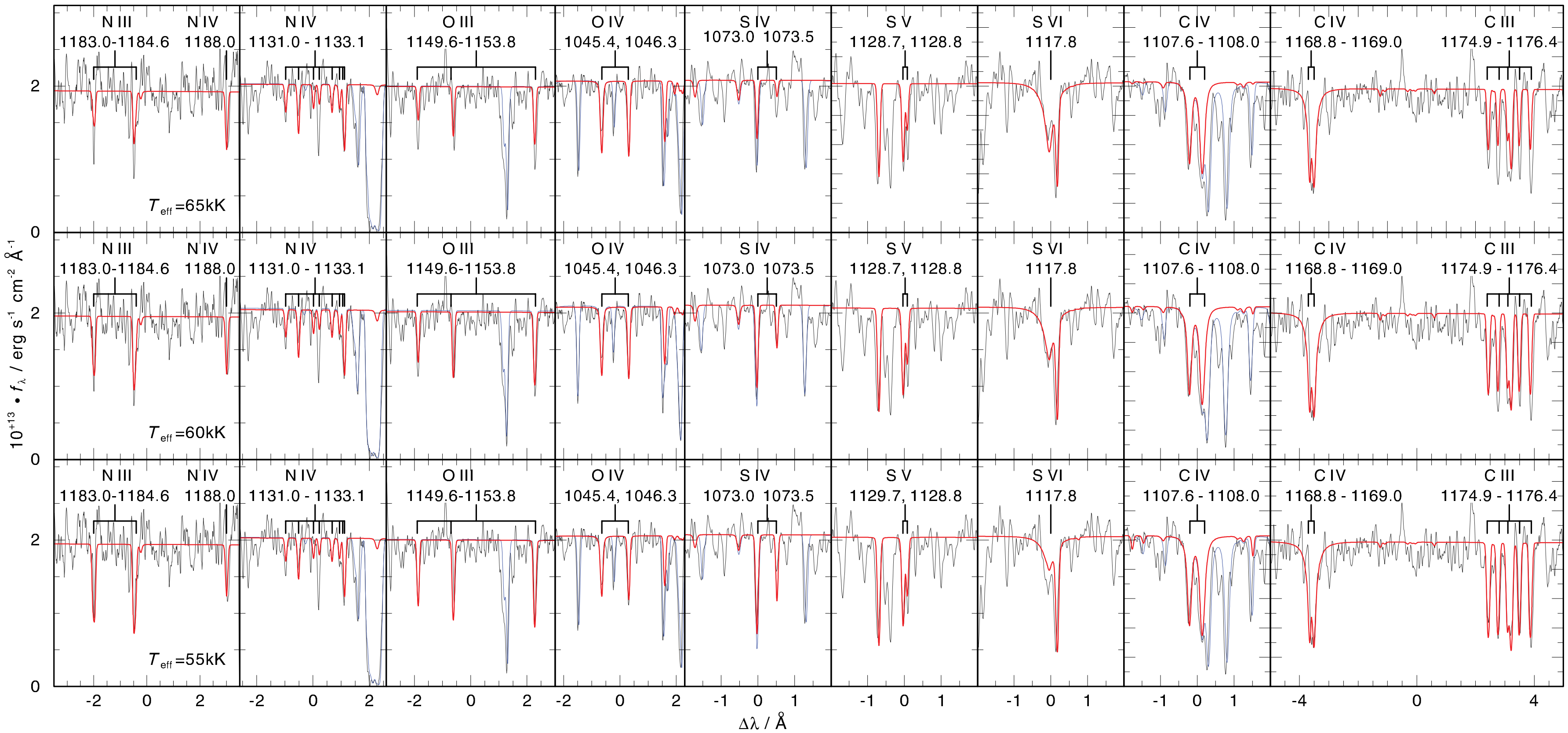

Fig. 4. Determination of $T_{\rm eff}$ using the ionization equilibria of N, O, S and C in the FUSE spectrum taken in 2002. The red (thick) lines indicate the pure stellar spectrum, the blue (thin) lines also include the interstellar lines. N III–IV, O III–V, S IV–VI and C III–IV lines are marked.

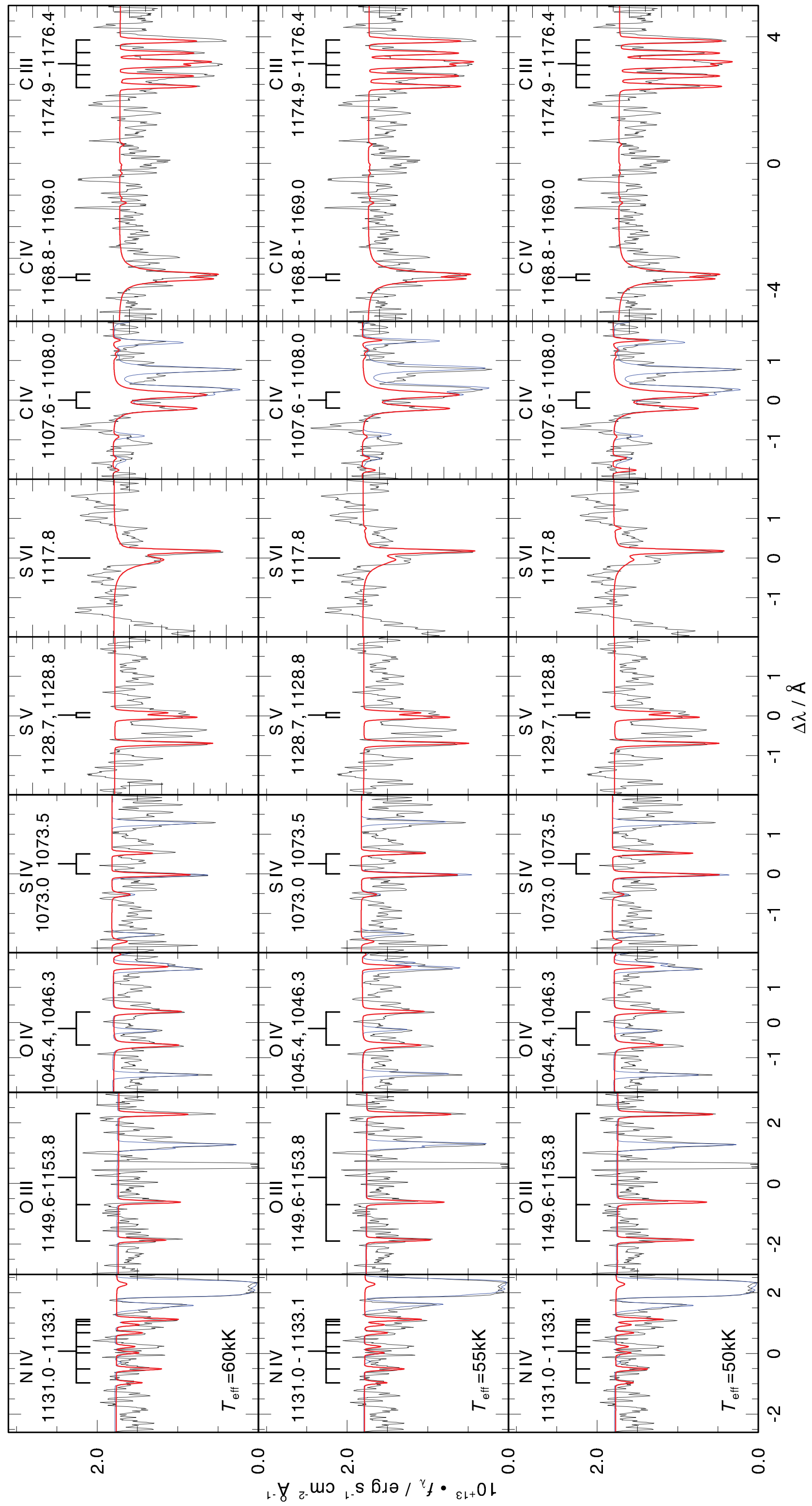

Fig. 5. Same as Fig. 4, but for the year 2006.

Table 3. Statistics of our model atoms.

Ion		NLTE levels	Lines	Sample lines
H	I	5	10	
	II	1	–	
He	I	29	69	
	II	20	190	
	III	1	–	
C	III	58	329	
	IV	54	295	
	V	1	0	
N	III	34	129	
	IV	90	546	
	V	54	297	
	VI	1	0	
O	III	72	322	
	IV	38	173	
	V	53	255	
	VI	54	291	
	VII	1	0	
Ne	II	14	19	
	III	14	17	
	IV	14	24	
	V	14	18	
	VI	1	0	
Si	III	17	28	
	IV	16	44	
	V	25	59	
	VI	1	0	
P	IV	15	9	
	V	18	12	
	VI	1	0	
S	IV	20	25	
	V	23	33	
	VI	30	42	
	VII	1	0	
Fe	IV	5	12	3 102 371
	V	7	25	3 266 247
	VI	7	25	991 935
	VII	1	0	
Ni	IV	5	14	2 512 561
	V	7	25	2 766 664
	VI	7	22	7 408 657
	VII	1	0	
	Total	467	1022	20 048 435

Notes. For iron and nickel, we used a statistical superline/superlevel approach (Rauch & Deetjen 2003) in the subsequent NLTE level population calculations. The original number of the so-called "sample lines" from Kurucz's line list, which are combined to super-lines, is also given.

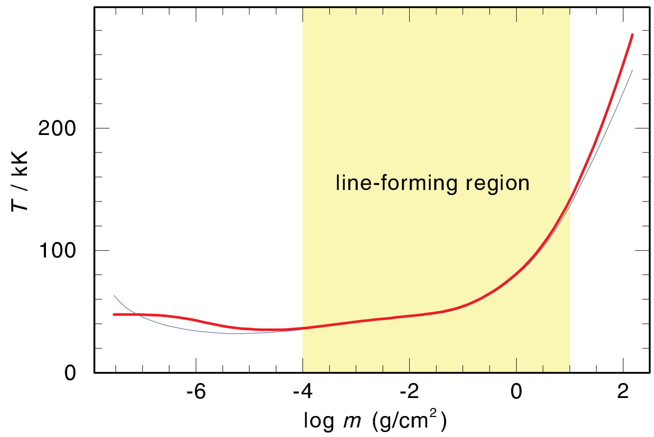

Fig. 6. Comparison of the temperature structures of a HHeCNO (blue, thin) and the final HHeCNONeSiPSFeNi model (red, thick) with $T_{\rm eff}$ = 60 kK and log g = 6.0.

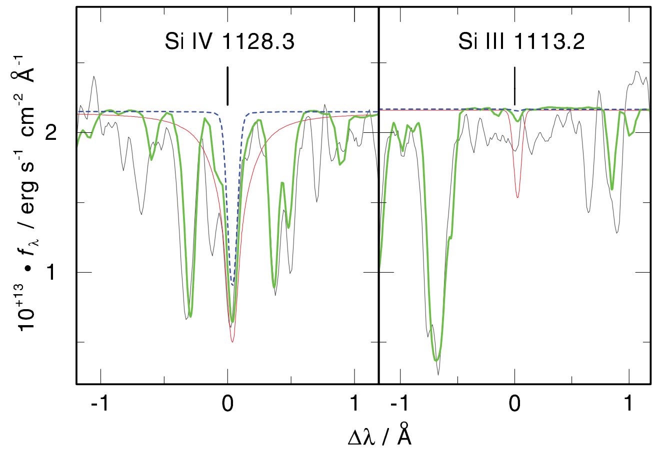

Fig. 7. Determination of the Si abundance. Synthetic line profiles calculated from models with 0.1× solar (blue, dashed), solar (green, light gray, including ISM absorption lines), and 10× solar (red, dark) Si abundance are compared with the observed Si IV (*left*) and Si III (*right*) line profiles.

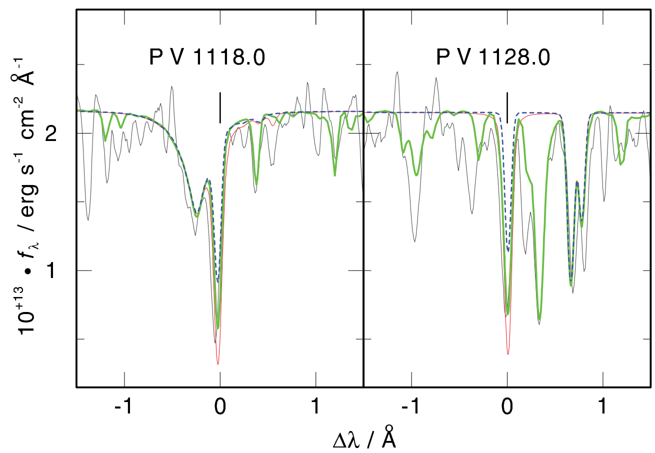

Fig. 8. Determination of the P abundance. Synthetic line profiles calculated from models with 0.01× solar (blue, dashed), 0.1× solar (green, light gray, including ISM absorption lines), and solar (red, dark) P abundance are compared with the observed P V line profiles.

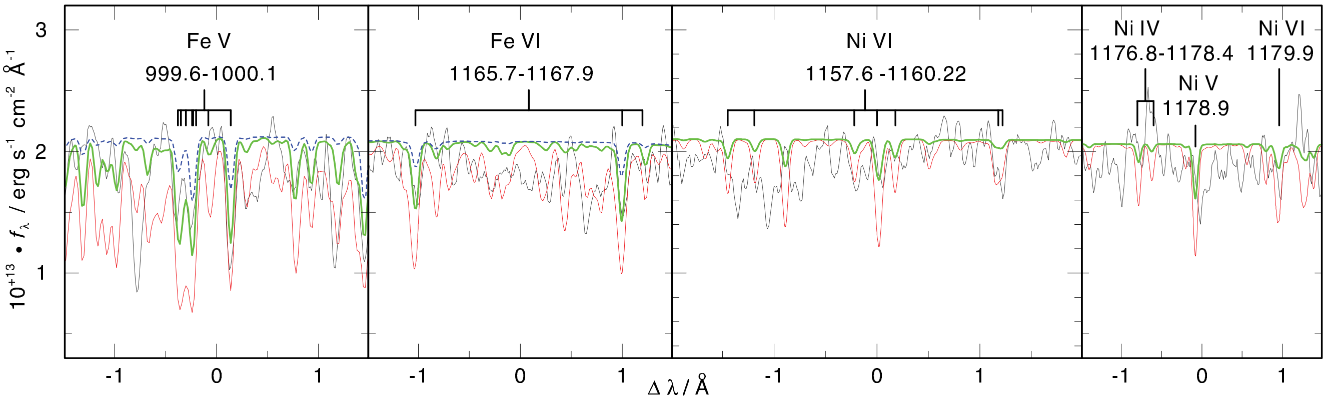

Fig. 9. Determination of the Fe abundance and the upper limit for the Ni abundance. Synthetic spectra calculated from models with 0.1× solar (blue, dashed), solar (green, light) and 10× solar (red, dark) Fe and Ni abundances are compared with the observation.

A&A 566, A116 (2014)
DOI: 10.1051/0004-6361/201423498

Astronomy & Astrophysics

On helium-dominated stellar evolution: the mysterious role of the O(He)-type stars⋆,⋆⋆

N. Reindl[1], T. Rauch[1], K. Werner[1], J. W. Kruk[2], and H. Todt[3]

[1] Institute for Astronomy and Astrophysics, Kepler Center for Astro and Particle Physics, Eberhard Karls University, Sand 1, 72076 Tübingen, Germany
e-mail: reindl@astro.uni-tuebingen.de
[2] NASA Goddard Space Flight Center, Greenbelt, MD 20771, USA
[3] Institute for Physics and Astronomy, University of Potsdam, Karl-Liebknecht-Str. 24/25, 14476 Potsdam, Germany

Received 23 January 2014 / Accepted 28 April 2014

ABSTRACT

Context. About a quarter of all post-asymptotic giant branch (AGB) stars are hydrogen-deficient. Stellar evolutionary models explain the carbon-dominated H-deficient stars by a (very) late thermal pulse scenario where the hydrogen-rich envelope is mixed with the helium-rich intershell layer. Depending on the particular time at which the final flash occurs, the entire hydrogen envelope may be burned. In contrast, helium-dominated post-AGB stars and their evolution are not yet understood.

Aims. A small group of very hot, helium-dominated stars is formed by O(He)-type stars. A precise analysis of their photospheric abundances will establish constraints to their evolution.

Methods. We performed a detailed spectral analysis of ultraviolet and optical spectra of four O(He) stars by means of state-of-the-art non-LTE model-atmosphere techniques.

Results. We determined effective temperatures, surface gravities, and the abundances of H, He, C, N, O, F, Ne, Si, P, S, Ar, and Fe. By deriving upper limits for the mass-loss rates of the O(He) stars, we found that they do not exhibit enhanced mass-loss. The comparison with evolutionary models shows that the status of the O(He) stars remains uncertain. Their abundances match predictions of a double helium white dwarf (WD) merger scenario, suggesting that they might be the progeny of the compact and of the luminous helium-rich sdO-type stars. The existence of planetary nebulae that do not show helium enrichment around every other O(He) star precludes a merger origin for these stars. These stars must have formed in a different way, for instance via enhanced mass-loss during their post-AGB evolution or a merger within a common-envelope (CE) of a CO-WD and a red giant or AGB star.

Conclusions. A helium-dominated stellar evolutionary sequence exists that may be fed by different types of mergers or CE scenarios. It appears likely that all these pass through the O(He) phase just before they become WDs.

Key words. stars: AGB and post-AGB – stars: evolution – stars: fundamental parameters – stars: abundances

1. Introduction

Quantitative spectral analyses of hot, post-asymptotic giant branch (AGB) stars revealed two distinct evolutionary sequences. Besides the well understood H-rich sequence, a H-deficient sequence was discovered. It is composed of Wolf-Rayet-type stars that evolve into PG 1159-type stars and finally might evolve into non-DA white dwarfs (WDs). While (very) late thermal pulse ((V)LTP) evolutionary models can explain the observed He, C, and O abundances in these stars (the typical abundance pattern for PG 1159 stars is He:C:O = 0.30−0.85:0.15−0.60:0.02−0.20 by mass, Werner & Herwig 2006) they do not reproduce the abundances in He-dominated stars, such as subdwarf O (sdO) stars, R Coronae Borealis (RCB) stars, extreme helium (EHe) stars, and the O(He) stars.

Two evolutionary scenarios for the origin of RCB and EHe stars were suggested. They might either be formed by a final He-shell flash or be the merger product of a CO WD with a He WD (Jeffery et al. 2011). The significant Li content in the atmospheres of RCB stars supports the idea of an LTP to explain their origin. However, the relatively high inferred masses of RCB stars and their high F abundance supports a WD merger (Clayton et al. 2011). Zhang & Jeffery (2012a) suggested that a double He-WD merger might also explain RCB and EHe stars. Recently, Kameswara Rao et al. (2013) found the RCB star DY Cen to be the first and only binary system among the RCB stars and their probable relatives. DY Cen is one of the hottest and most H-rich members of the RCB stars. Kameswara Rao et al. (2013) suggested that this system might have evolved from a common-envelope system to its current form. Therefore it may be possible that RCB stars form in various ways.

RCB and EHe stars are not the only He-rich stars for which a merger origin was suggested. Zhang & Jeffery (2012b) presented the results of a double He-WD merger to explain the formation of He-rich, hot sdOs. These can be divided into three

⋆ Based on observations with the NASA/ESA *Hubble* Space Telescope, obtained at the Space Telescope Science Institute, which is operated by the Association of Universities for Research in Astronomy, Inc., under NASA contract NAS5-26666. Based on observations made with the NASA-CNES-CSA Far Ultraviolet Spectroscopic Explorer. Based on observations made with ESO Telescopes at the La Silla Paranal Observatory under programme IDs 091.D-0663, 090.D-0626.
⋆⋆ Figures 1−12, 21−23 and Table 1 are available in electronic form at http://www.aanda.org

subgroups, one C-rich and N-poor, the other N-rich and C-poor, and the third one enriched in C and N (Hirsch 2009). In their numerical experiments, Zhang & Jeffery (2012b) showed that in terms of $T_{\rm eff}$, $\log g$, C, and N abundances, the origin of the two sdO groups can be explained by different double He-WD merger models. Zhang & Jeffery (2012b) distinguished between three types of mergers. In a slow-merger process the less massive He WD transfers its entire mass within a few minutes to form a disk around the primary He WD, which then accretes from it at a rate similar to the Eddington-accretion rate. The surface composition of the resulting star retains the N-rich composition of the accreted WD. In the fast-merger model, the secondary directly transfers its entire mass quickly to the primary surface, where heating up to 10^8 K causes the material to expand and form a hot corona within a few minutes. The fast-merger model produces C-rich stars, in which N is hardly observable. The composite merger includes both processes. In general, models with a merged mass below 0.7 $M_\odot$ produce an N-rich star, while more massive ones produce a C-rich star with a significant N content. Other origins of He-rich sdO stars are discussed as well. Because the merger of a He WD with a post-sdB star is predicted in one of the important binary channels for the formation of sdB stars (Han et al. 2002, 2003), Justham et al. (2011) proposed this formation channel for the previously unexplained He-rich sdO stars. Their models also reproduced the properties of the He-rich sdO stars in terms of $T_{\rm eff}$ and $\log g$. However, in contrast to Zhang & Jeffery (2012b), they did not include nuclear evolution in their calculations.

A more exotic group of He-dominated stars is formed by the O(He) stars. This spectroscopic class is defined by an almost pure He II absorption-line spectrum in the optical wavelength range (Méndez et al. 1986; Rauch et al. 1998). For more than 15 years, only the two central stars of planetary nebulae (CSPNe) K 1−27[1] (WD 0558−756) and LoTr 4, as well as HS 1522+6615 (WD 1522+662), and HS 2209+8229 (WD 2209−8229) were known (Rauch et al. 1994, 1996, 1998). Recently, Werner et al. (2014) found four more of these objects, namely SDSS J 172854.34+361958.62, SDSS J 171916.97+365326.70, SDSS J 141812.50+024426.92, and SDSS J 075732.18+184329.28. They also pointed out that KPD 0005+5106 is a pre-WD. Because of the He-rich surface composition of KPD 0005+5106 (98% by mass, Wassermann et al. 2010), we also consider it as an O(He) star. The evolutionary status of these objects has been studied only rarely. Rauch et al. (1998) proposed that O(He) stars might be successors of the luminous He-rich sdO stars and that because of ongoing mass loss, the low-gravity O(He) stars might envolve into PG 1159 stars. This possibility was studied by Miller Bertolami & Althaus (2006). They had to assume mass-loss rates, that were higher than predicted by radiation-driven wind theory, to turn O(He) stars into helium-enriched PG 1159 stars. An alternative scenario was suggested by Rauch et al. (2006). They invoked the idea that the O(He) stars could also be the offspring of a merging event of two WDs and thus, the direct descendants of RCB stars.

In this paper, we present the analysis of K 1−27, LoTr 4, HS 1522+6615, and HS 2209+8229. In Sect. 2, we briefly describe the available observations. We then present a detailed spectral analysis of the O(He) stars based on optical and ultraviolet spectra (Sect. 3) and derive stellar parameters and distances (Sect. 4). In Sect. 5 we discuss possible evolutionary channels for the O(He) stars and those of other helium-dominated objects. We conclude in Sect. 5.3.

[1] In the following, we use the PNe names to identify their central stars.

2. Observations

In January, June and July 2013, we performed observations of K 1−27 and LoTr 4 with the ESO/NTT (ProgIDs 091.D-0663, 090.D-0626) using the EFOSC2 spectrograph (resolving power $R = \lambda/\Delta\lambda \approx 3000$) with the grisms GR#19 (4400 to 5100 Å) and GR#20 (6000 to 7100 Å). The data reduction was done by using IRAF[2]. The previous optical spectra of the O(He) stars were already described and analyzed by Rauch et al. (1994, 1996, 1998) to determine effective temperature ($T_{\rm eff}$), surface gravity ($\log g$), and the H/He ratio for all four stars as well as the C abundance for K 1−27, LoTr 4 (upper limits), HS 1522+6615, and the N abundance for K 1−27 and LoTr 4.

We have taken FUV spectra with FUSE[3] ($R \approx 20\,000$) in 2002 (all O(He) stars, 49 ks exposure time in total, ProgID: C178) and 2005 (only HS 1522+6615, 4 ks, ProgID: U103) using the LWRS aperture (Figs. 1−4). Additional 204 ks of FUSE observations (K 1−27, HS 1522+6615, HS 2209+8229) were scheduled for summer 2007, but were not performed because of the FUSE failure on July 12. The FUSE spectra show a strong contamination by interstellar (IS) line absorption and the S/N ratio is very poor (Rauch et al. 2006, 2009). To reduce the pixel-to-pixel variation, they were co-added and then slightly smoothed with a low-pass filter (Savitzky & Golay 1964).

Because of the poor quality of the FUSE spectra, we obtained HST/COS[4] spectra (Proposal Id: 11699, Figs. 5−8) during April to July 2010 using the grating G140L ($2000 < R < 3500$ within 1150 Å $< \lambda <$ 1800 Å) and the primary science aperture.

3. Spectral analysis

Motivated by the new COS spectra, we decided to comprehensively re-analyze all available data of the O(He) stars. Since the time when Rauch et al. (1998) presented their analysis of optical, ultraviolet (IUE[5]), and X-ray (ROSAT[6]) data, our Tübingen NLTE Model Atmosphere Package TMAP[7] (Sect. 3.1) as well as the atomic data, that is taken from TMAD[8], the Tübingen Model Atom Database, have continuously improved. Moreover, in a standard procedure, we modeled photospheric and interstellar line-absorption spectra to correctly identify the pure atmospheric lines. Absorption by interstellar gas was modeled using the program Owens (Hébrard & Moos 2003; Hébrard et al. 2002). Owens allows for multiple independent interstellar clouds, each with its own radial and turbulent velocities, temperature, and column densities for each of any number of constituent gas species. All properties of each cloud are adjusted by fitting Voigt profiles to the data by chi-squared minimization.

3.1. Model atmospheres

We used TMAP (Werner et al. 2003; Rauch & Deetjen 2003) to compute plane-parallel, line-blanketed non-LTE model atmospheres in radiative and hydrostatic equilibrium. In the previous

[2] IRAF is distributed by the National Optical Astronomy Observatory, which is operated by the Associated Universities for Research in Astronomy, Inc., under cooperative agreement with the National Science Foundation.

[3] Far Ultraviolet Spectroscopic Explorer.

[4] Cosmic Origins Spectrograph.

[5] International Ultraviolet Explorer.

[6] Röntgensatellit.

[7] http://astro.uni-tuebingen.de/~TMAP

[8] http://astro.uni-tuebingen.de/~TMAD

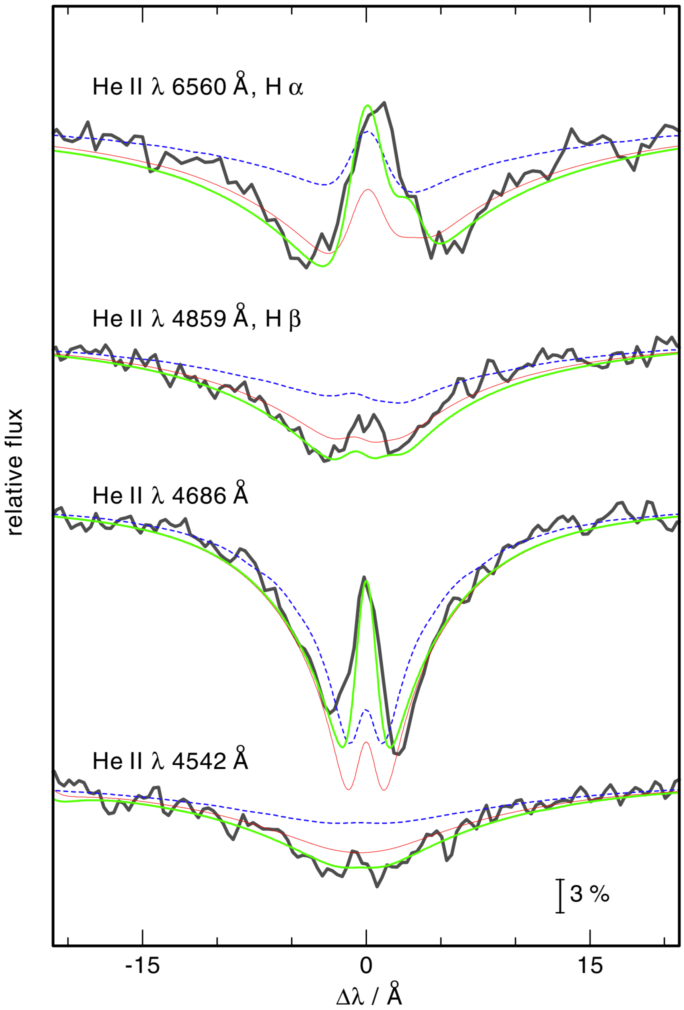

Fig. 13. Comparison of optical H I and He II lines calculated from models including H+He (dashed, blue), H+He+C+N+O (thin, red), and H+He+C+N+O+Ne (thick, green) with $T_{\rm eff} = 135$ kK and $\log g = 6.4$, overplotted on the EFOSC2 spectrum of K 1−27. The vertical bar indicates 3% of the continuum flux.

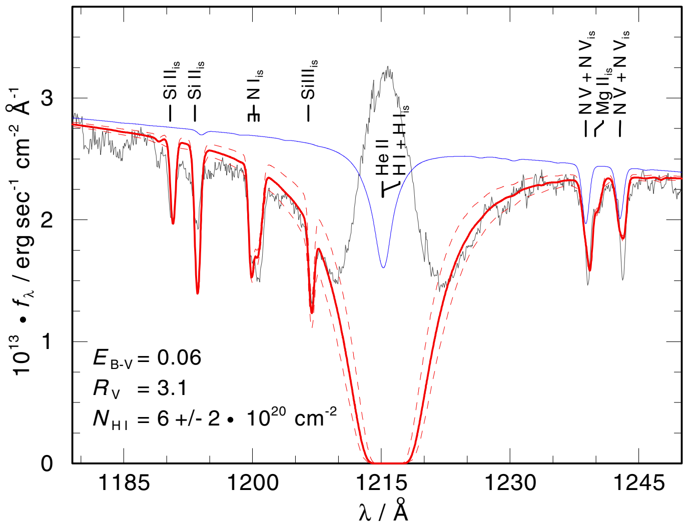

Fig. 14. Determination of the interstellar H I column density toward K 1−27. The dashed lines indicate the error limits. The thin (blue) line is the pure photospheric spectrum. Prominent spectral lines are marked at top, "is" indicates interstellar origin. The line center of Ly α is dominated by geocoronal emission.

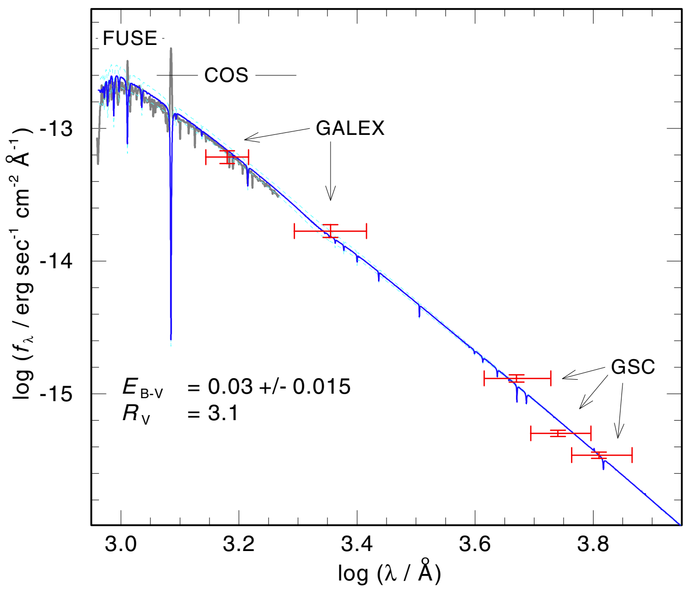

Fig. 15. Determination of E_{B-V} for HS 1522+6615. The FUSE and COS spectra and GALEX and BVR brightnesses from the GSC 2.3 catalog are used for comparison. The thick (blue) line is the spectrum of the final photospheric model. The dashed lines indicate the error limits.

analysis of the O(He) stars, Rauch et al. (1994, 1996, 1998) used only H+He model atmospheres to derive $T_{\rm eff}$, $\log g$, and the H/He ratio. In our analysis, we also included the elements C, N, O, F, Ne, Si, P, S, and Ar with their dominant ionization stages (Table 1, Figs. 9–12) to study their impact on the model atmospheres and the resulting line profiles. We found that C, N, O, and Ne have a strong influence on the atmospheric structure. In Fig. 13 we demonstrate the strong effect of additional opacities on the resulting line profiles. The impact of F, Si, P, S, and Ar turned out to be negligible. Dreizler & Werner (1994) have shown that line blanketing by iron-group elements hardly affects the hydrogen and helium lines in hot central stars. To compute a model grid in reasonable time, we therefore decided to include only H, He, C, N, O, and Ne in our model atmospheres to derive $T_{\rm eff}$, $\log g$, and the element abundances of these elements. To determine the abundances of F, Si, P, S, Ar, and Fe, we kept the values of $T_{\rm eff}$ and $\log g$ fixed. The upper limits (Table 3) were derived by test models where the respective lines in the model contradict the non-detection of the lines in the observation (at the abundance limit).

3.2. Interstellar neutral hydrogen and reddening

The interstellar H I column density was measured from Ly α (Fig. 14). Interstellar reddening was determined using the reddening law of Fitzpatrick (1999). Since its impact is negligible in the infrared, the model flux was normalized to the most reddest brightness found in the literature. Figure 15 shows the example of HS 1522+6615, where the GSC[9] R brightness is used. Table 2 summarizes $N_{\rm H\,I}$ and E_{B-V} of the O(He) stars compared with GALEX[10] values, which agree well. Within the error limits, our values agree with those of Rauch et al. (1998).

[9] Guide Star Catalogue, Bucciarelli et al. (2001).
[10] Galaxy Evolution Explorer, http://www.galex.caltech.edu/

Table 2. Interstellar H I column density and reddening.

Object	$N_{\rm H\,I}$ [10^{20} cm^{-2}]	E_{B-V} this work	E_{B-V} GALEX
K 1−27	6.0 ± 2.0	0.06 ± 0.020	0.0797
LoTr 4	10.0 ± 1.5	0.20 ± 0.020	0.1893
HS 1522+6615	2.0 ± 1.0	0.03 ± 0.015	0.0250
HS 2209+8229	5.0 ± 1.0	0.23 ± 0.040	

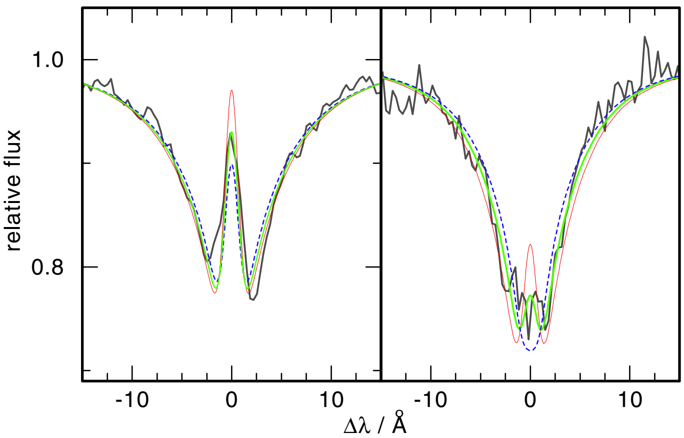

Fig. 16. Determination of $T_{\rm eff}$ of K 1−27 (*left*) and LoTr 4 (*right*) using the central emission of He II λ 4686 Å. The EFOSC2 observation (solid black line) is compared with models with $T_{\rm eff}$ = 130/110 kK (dashed, blue), 135/120 kK (thick, green), and 140/130 kK (thin, red).

3.3. Effective temperature and surface gravity

To determine of $T_{\rm eff}$ and $\log g$, we used the optical H I and He II lines. For HS 1522+6615 and HS 2209+8229 we additionally used the O ionization equilibria to constrain $T_{\rm eff}$. The new optical observations of K 1−27 and LoTr 4 allowed us to use the central emission of He II λ 4686 Å to derive $T_{\rm eff}$ for the two CSPNe (Fig. 16).

For K 1−27, $T_{\rm eff}$ = 135 kK and $\log g = 6.4$ (cm/s) were found. The value of $\log g$ agrees with Rauch et al. (1994, 1998, $\log g = 6.5 \pm 0.5$), but for $T_{\rm eff}$ we found a large deviation from the result of Rauch et al. (1998, $T_{\rm eff}$ = 105 ± 10 kK). However, Rauch et al. (1994, 1998) encountered problems with the lower value of $T_{\rm eff}$ which can be solved with $T_{\rm eff}$ = 135 kK: first, with $T_{\rm eff}$ = 105 kK the star did not provide enough hard photons to ionize its nebula. With the higher $T_{\rm eff}$ for K 1−27, we achieve a more consistent PN ↔ CSPN model. Second, N V $\lambda\lambda$ 4604, 4620 Å do not appear in emission at $T_{\rm eff}$ = 105 kK (as the observation shows), but for $T_{\rm eff}$ = 135 kK they do. Finally, Rauch et al. (1994) had the problem that the central depression of the He II λ 4686 Å ($n-n'$ = 3−4) line was too strong, while other H I and He II lines were almost perfectly reproduced. The addition of Ne to the models solves this problem. Furthermore, the central He II λ 4686 Å and H α emission can only be reproduced with a supersolar Ne abundance, which causes a strong decrease of the temperature in the outer atmosphere. He II λ 4686 Å and H α are most affected by this because they are formed at lower Rosseland optical depths. We stress that the large deviation from the previous $T_{\rm eff}$ value is a result of the additional opacities used in our model atmospheres, as mentioned above.

For LoTr 4, we confirmed the value of $T_{\rm eff}$ = 120 kK (Rauch et al. 1996) but increased the lower limit to $T_{\rm eff}$ = 115 kK because for lower values, N V $\lambda\lambda$ 4604, 4620 Å do not appear in emission as in the observation. The new optical spectra allowed us a better determination of the surface gravity (Fig. 17). We found $\log g = 5.8 \pm 0.2$, which is within the error limits of the literature value (Rauch et al. 1996, $\log g = 5.5 \pm 0.5$).

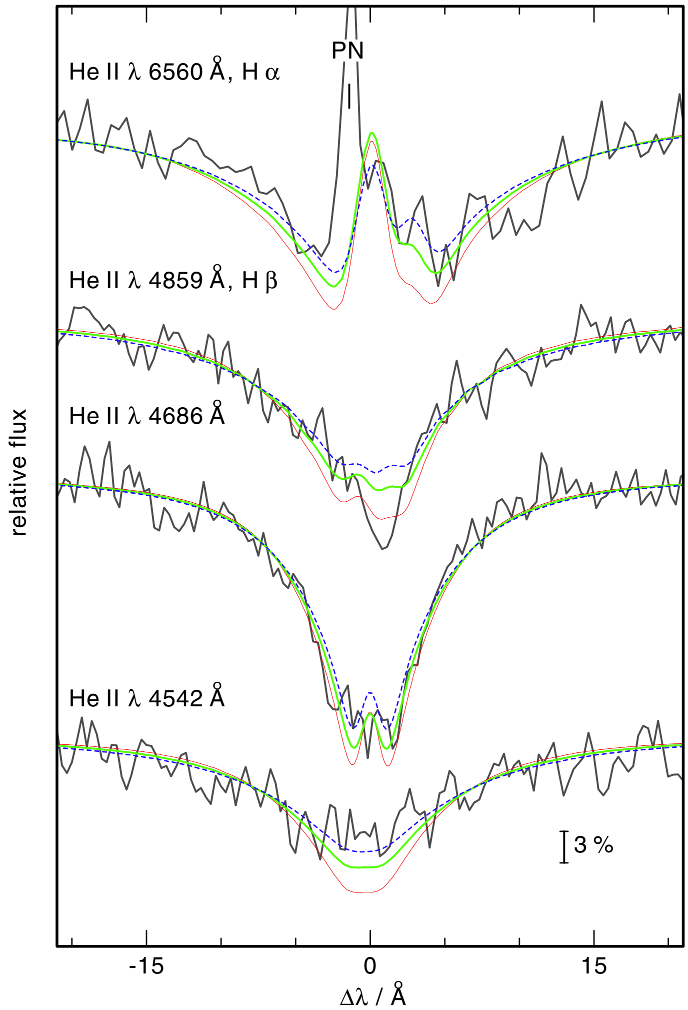

Fig. 17. Determination of $\log g$ of LoTr 4. The EFOSC2 observation (solid black line) is compared with models with $\log g$ = 6.0 (dashed, blue), 5.8 (thick, green), and 5.6 (thin, red). The vertical bar indicates 3% of the continuum flux.

For HS 1522+6615, we determined a lower value of $T_{\rm eff}$ = 130 kK at a higher $\log g = 5.9$ (compared with Rauch et al. 1998, $T_{\rm eff}$ = 140 ± 10 kK, $\log g = 5.5 \pm 0.5$). The errors of $\log g$ were reduced to ±0.2.

Based on the O IV/O V ionization equilibrium (Fig. 18), we found a higher $T_{\rm eff}$ = 110 kK compared with the literature value ($T_{\rm eff}$ = 100 ± 10 kK) for HS 2209+8229. The value of $\log g = 6.0$ is verified and the errors were reduced to ± 0.3.

3.4. Element abundances

The H/He abundance ratio (by mass) was determined using H I $\lambda\lambda$ 6563, 4861, 4340 Å and He II $\lambda\lambda$ 6560, 5412, 4859, 4686, 4542, 4339 Å. It was difficult to fix because the quality of the available optical observations is poor. For LoTr 4 and K 1−27, we reverified the literature values of 0.5 and 0.2, respectively. Figure 19 shows that for HS 1522+6615 the model with H/He = 0.03 fits the observation better than H/He = 0.10 (literature value) where H α appears in emission while for H/He = 0.01

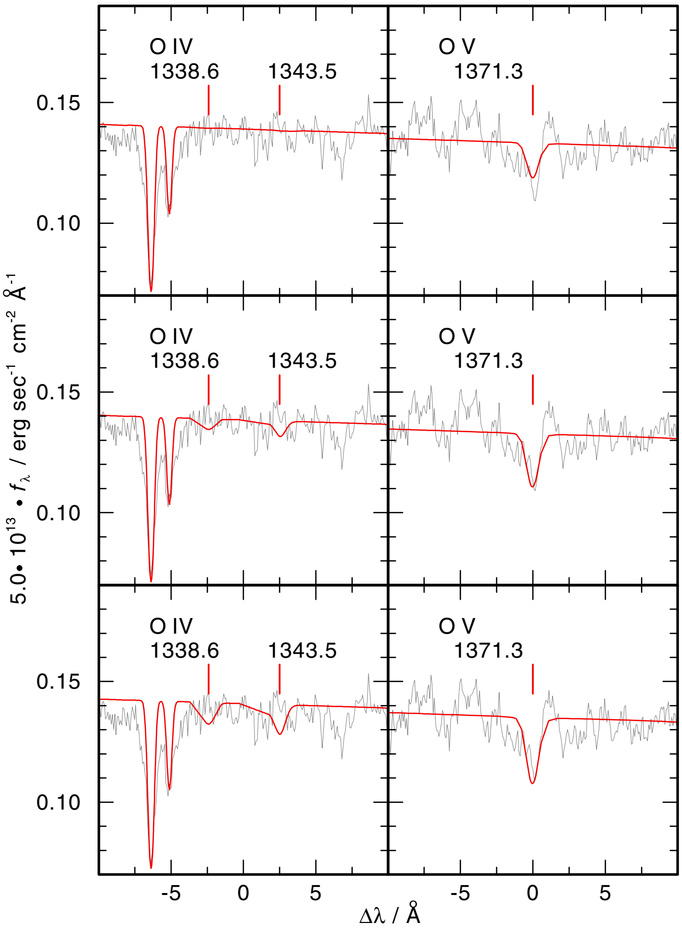

Fig. 18. Determination of $T_{\rm eff}$ of HS 2209+8229 from the O IV/O V ionization equilibrium. *Top panels*: $T_{\rm eff}$ = 100 kK, *middle*: $T_{\rm eff}$ = 110 kK; *bottom*: $T_{\rm eff}$ = 120 kK.

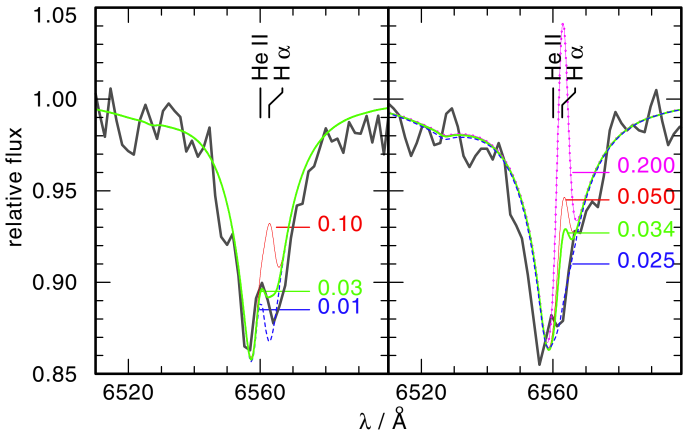

Fig. 19. Determination of the H/He ratio of HS 1522+6615 (*left panel*) and HS 2209+8229 (*right*). The observed H α and He II line blend is compared with models with different H/He mass ratios, as indicated by the labels.

H α is too deep in absorption. For HS 2209+8229, we found that the upper limit of the H/He ratio must be lower because of the strong H α emission for H/He > 0.025 (Table 3, Fig. 20).

Carbon. The C IV $\lambda\lambda$ 1548.2, 1550.8 Å resonance doublet in the COS spectra of all four stars is contaminated by the respective interstellar lines and therefore unsuited for determining the C abundance. In the spectra of LoTr 4 and HS 2209+8229 no other C lines were identified and we derived only upper limits of [C][11] < −0.53 and [C] < −1.50, respectively. In the spectrum of K 1−27, we identified C IV $\lambda\lambda$ 1168.8, 1168.9 Å and determined [C] = −0.62. For HS 1522+6615, C IV $\lambda\lambda$ 1168.9, 1169.0 Å in the COS spectrum and C IV $\lambda\lambda$ 5801.33, 5811.98 Å in the optical spectrum were evaluated, and we achieve the best agreement between model and observation at [C] = 0.62. HS 1522+6615 shows the highest, supersolar C abundance (Fig. 21) while the upper limits of the other stars in our sample indicate subsolar abundances.

Nitrogen. The N abundance for K 1−27 and LoTr 4 was determined from the N V $\lambda\lambda$ 4603.7, 4619.7, 4933.6, 4943.2, 4945.7 Å emission lines. For HS 2209+8229, we used N V $\lambda\lambda$ 1616.1 Å, 1616.4, 1619.6, 1619.7. As for case of C IV, the resonance doublet N V $\lambda\lambda$ 1238.8, 1242.8 Å is blended by the respective ISM lines. The N abundances of K 1−27 ([N] = 1.28, Fig. 22), LoTr 4 ([N] = 1.07), and HS 2209+8229 ([N] = 2.89) were found to be supersolar, in contrast to the upper limit for HS 1522+6615 ([N] < −0.78), which is subsolar.

Oxygen. For K 1−27 and LoTr 4, we derived only upper limits because no O lines except the resonance doublet O VI $\lambda\lambda$ 1031.9, 1037.7 Å were identified, which might be of ISM origin similar to the C IV and N V resonance doublets (Sect. 3.4) We used the O VI $\lambda\lambda$ 1124.7, 1124.8 Å and O VI λ 5290.6 Å to determine the upper limits of [O] < −2.06 for K 1−27 and [O] < −1.47 for LoTr 4. For HS 1522+6615, Rauch et al. (1998) discovered a variability of the O VI λ 5290.6 Å emission feature. Mickaelian et al. (2011) also classified HS 1522+6615 as "possible" variable by comparing the brightness measurements from the Palomar Observatory Sky Survey (POSS) epochs 1 and 2. In view of its variability, we adjusted the O abundance to the co-added optical spectra using O VI $\lambda\lambda$ 3811.4, 3834.2 Å and found [O] = −0.64. A precise determination of the O abundance was possible for HS 2209+8229 using O V λ 1371.3 Å, which is prominent in the COS spectrum (Fig. 23). We found [O] = −1.46 (Table 3).

Fluorine. F is not identified in the O(He) star spectra. We used F VI λ 1139.5 Å and found [F] < −1.00 for all O(He) stars.

Neon. We only derived upper limits using Ne VII $\lambda\lambda$ 1438.8, 1440.5, 1445.0 Å for K 1−27, LoTr 4, and HS 1522+6615 and Ne V $\lambda\lambda$ 1718.2, 1718.3 Å for HS 2209+8229 because of its lower $T_{\rm eff}$. We determined [Ne] < 0.60 for K 1−27, [Ne] < −0.09 for LoTr 4, [Ne] < −0.62 for HS 1522+6615, and [Ne] < −1.10 for HS 2209+8229.

Silicon. An upper limit for the Si abundance was determined using Si IV λ 1128.3 Å, Si V λ 1118.8 Å, and Si VI λ 1130.4 Å. For K 1−27, it is [Si] < −0.56. For LoTr 4, HS 1522+6615, and HS 2209+8229, we derived [Si] < 0.18.

Phosphorus. We identified P V $\lambda\lambda$ 1118.0, 1128.0 Å only in the FUSE spectra of LoTr 4 and HS 2209+8229, and we determined

[11] [X] denotes log (abundance by mass/solar abundance by mass) of species X. Solar abundances were taken from Asplund et al. (2009).

Table 3. Photospheric parameters of the O(He) stars.

	K 1–27		LoTr 4		HS 1522+6615		HS 2209+8229	
	R14	R98	R14	R98	R14	R98	R14	R98
$T_{\rm eff}$ / kK	135^{+5}_{-5}	105^{+10}_{-10}	120^{+10}_{-5}	120^{+12}_{-12}	130^{+10}_{-10}	140^{+14}_{-14}	110^{+10}_{-10}	100^{+10}_{-10}
$\log g$ / cm s^{-2}	$6.4^{+0.2}_{-0.3}$	$6.5^{+0.5}_{-0.5}$	$5.8^{+0.2}_{-0.2}$	$5.5^{+0.5}_{-0.5}$	$5.9^{+0.2}_{-0.2}$	$5.5^{+0.5}_{-0.5}$	$6.0^{+0.3}_{-0.3}$	$6.0^{+0.5}_{-0.5}$
H	$-1.33^{+0.41}_{-0.28}$	<-1.30	$-0.92^{+0.21}_{-0.20}$	$-0.90^{+0.30}_{-0.30}$	$-2.08^{+0.47}_{-0.52}$	$-1.60^{+0.30}_{-0.30}$	<-2.21	<-1.30
He	$-0.03^{+0.03}_{-0.03}$	>-0.02	$-0.06^{+0.02}_{-0.05}$	$-0.06^{+0.3}_{-0.3}$	$-0.009^{+0.005}_{-0.009}$	$0.004^{+0.3}_{-0.3}$	>-0.004	>-0.02
C	$-3.25^{+0.45}_{-0.55}$	<-1.82	<-3.14	<-1.92	$-2.00^{+0.68}_{-0.30}$	$-2.05^{+0.3}_{-0.3}$	<-4.13	
N	$-1.88^{+0.36}_{-0.42}$	$-1.76^{+0.3}_{-0.3}$	$-2.10^{+0.60}_{-0.92}$	$-2.45^{+0.3}_{-0.3}$	<-3.94		$-2.89^{+0.89}_{-0.50}$	
O	<-4.30		<-3.73	<-1.50	$-2.88^{+0.60}_{-0.50}$		$-3.00^{+0.70}_{-0.70}$	
F	<-7.30		<-7.29		<-7.30		<-7.45	
Ne	<-2.30		<-2.99		<-3.53		<-4.00	
Si	<-4.06		<-3.00		<-3.00		<-3.00	
P	<-5.52		$-4.54^{+0.40}_{-1.00}$		<-5.20		$-6.00^{+1.00}_{-1.00}$	
S	<-4.07		$-3.43^{+0.61}_{-1.00}$		<-3.59		$-3.40^{+0.88}_{-1.27}$	
Ar	<-5.30		<-4.92		<-5.10		<-6.26	
Fe	<-2.89		<-1.89		<-2.89		<-2.89	

Notes. Our values (R14) are compared with those given by Rauch et al. (1998, R98). Abundances are given as logarithmic mass fraction.

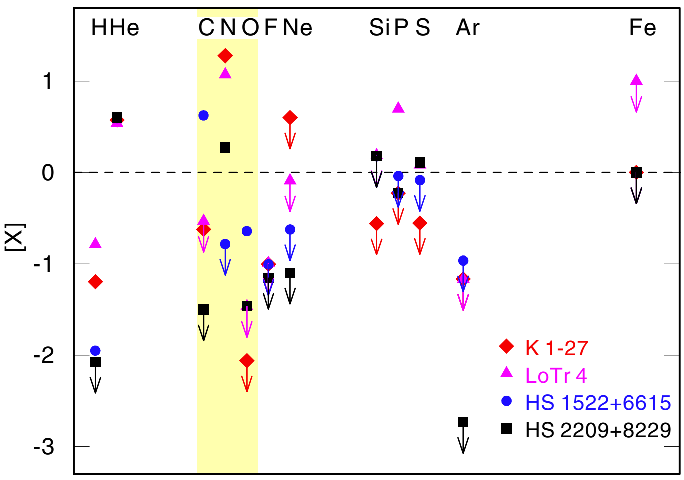

Fig. 20. Abundances of the O(He) stars (Table 3). The shaded (yellow) region emphasizes the CNO differences.

[P] = 0.70 and [P] = −0.76, respectively. For K 1−27 and HS 1522+6615, only upper limits can be given, which are about solar.

Sulfur. S VI λ 1117.8 Å was identified in the FUSE spectra of LoTr 4 and HS 2209+8229 and we determined [S] = −0.08 and [S] = −0.11, respectively. For K 1−27 and HS 1522+6615, only upper limits can be given, which are 0.3 times solar and solar, respectively.

Argon. Is not identified in the O(He) star spectra. We employed Ar VII λ 1535.7, 1537.1, 1537.9 Å and Ar VIII λ 1164.1 Å and derived subsolar upper limits.

Iron. The quality of the FUSE spectra is not sufficient to identify individual Fe lines. Therefore, we only included the iron model atom (ionization stages V – IX) in the line-formation calculations (i.e. fixed atmospheric structure) based on our final model and calculated NLTE occupation numbers for the atomic levels of iron. We found that the resulting upper limits of the Fe abundances are solar for K 1−27, HS 1522+6615, and HS 2209+8229. For LoTr 4, we found an upper limit of ten times solar.

3.5. Mass-loss rates

One aim of our COS observations was to follow up on the suggestion of Miller Bertolami & Althaus (2006) that O(He) stars might be post early-AGB stars. The high mass-loss rates invoked in their calculations were not confirmed by our FUSE observations. We performed test calculations based on the final parameters of our analysis (Table 3) using the Potsdam Wolf-Rayet model-atmosphere code, PoWR[12]. This code solves the NLTE radiative transfer in a spherically expanding atmosphere simultaneously with the statistical equilibrium equations and accounts at the same time for energy conservation. Like in TMAP, iron-group line blanking is treated by means of the superlevel approach (Gräfener et al. 2002), and a wind clumping in first-order approximation is taken into account (Hamann & Gräfener 2004). We did not calculate hydrodynamically consistent models, but assumed a velocity field following a β-law with $\beta = 1$.

For our calculations, we first used the predicted mass-loss rates ($\dot{M}$) of Pauldrach et al. (1988, Table 4) using the stellar masses determined from comparison with evolutionary tracks of VLTP stars (Fig. 24, Miller Bertolami & Althaus 2006). We considered the terminal wind velocities (v_∞) to be 2.51 times the escape velocities of the stars (Lamers et al. 1995). To then determine an upper limit we increased the mass-loss rate until the synthetic spectra no longer agreed with the observations. We

[12] http://www.astro.physik.uni-potsdam.de/~wrh/PoWR/

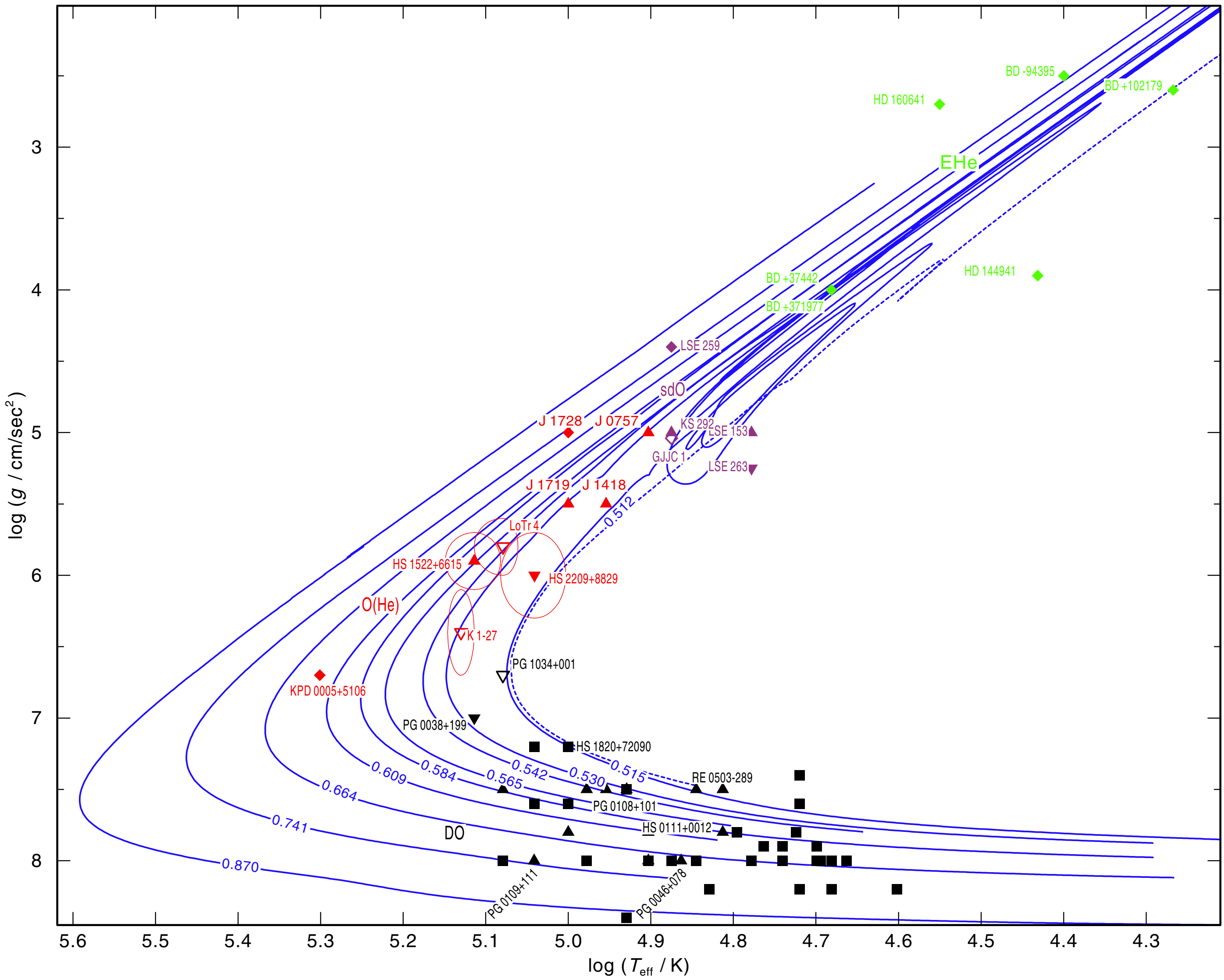

Fig. 24. Locations of EHe stars (green, Jeffery & Hamann 2010) the luminous sdO-stars (purple, Müller-Ringat 2013; Rauch et al. 1998, 1991; Husfeld et al. 1989) and O(He) stars (red, this work, Werner et al. 2014; Wassermann et al. 2010) as well as the DO WDs (black, Werner et al. 2014; Mahsereci 2011; Hügelmeyer et al. 2006; Dreizler & Werner 1996) in the log $T_{\rm eff}$ – log g plane compared with an LTP (dashed line) and VLTP post-AGB (solid lines) evolutionary tracks (labeled with stellar masses in $M_\odot$) of Miller Bertolami & Althaus (2006). Open symbols indicate CSPNe, filled ones indicate that no PN was detected. C-rich objects are represented by triangles, N-rich objects by inverted triangles, C- and N-rich objects by diamonds. Squares specify objects that are neither enriched in C nor in N.

Table 4. Predicted mass-loss rates of the O(He) stars interpolated from Fig. 6a of Pauldrach et al. (1988, P+88) compared with upper limits determined in our analysis (cf. Fig. 25).

Object	log($\dot{M}/M_\odot$ / yr)	
	P+88	this work
K 1-27	−10.0	≤−9.0
LoTr 4	−9.4	≤−9.4
HS 1522+6615	−8.8	≤−8.8
HS 2209+8229	−10.4	≤−10.4

exmained all strategic wind lines that are located in the FUSE and COS wavelength ranges (Fig. 25) and found that only the mass-loss rate of K 1−27, which shows a weak P-Cygni profile at Ne VII λ 973.3 Å in the FUSE spectrum, could be at most an order of magnitude higher than predicted by radiative-driven wind theory. The highest possible $\dot{M}$ values for all O(He) stars are given in Table 4.

4. Stellar parameters and distances

To derive the stellar parameters, we compared the position of the O(He) stars in the log $T_{\rm eff}$ – log g plane with different evolutionary tracks. Figure 24 shows the location of the O(He) stars and related He-dominated objects compared with an LTP evolutionary track (Miller Bertolami & Althaus 2007) and VLTP post-AGB tracks (Miller Bertolami & Althaus 2006). The LTP and VLTP tracks only differ at low surface gravities, and the masses derived from H-rich post-AGB evolutionary tracks (Miller Bertolami & Althaus 2007) also agree well within the error limits with the VLTP masses. Therefore it is justified to derive the masses of the O(He) stars from these tracks although the VLTP scenario cannot be valid for these stars, as we show below.

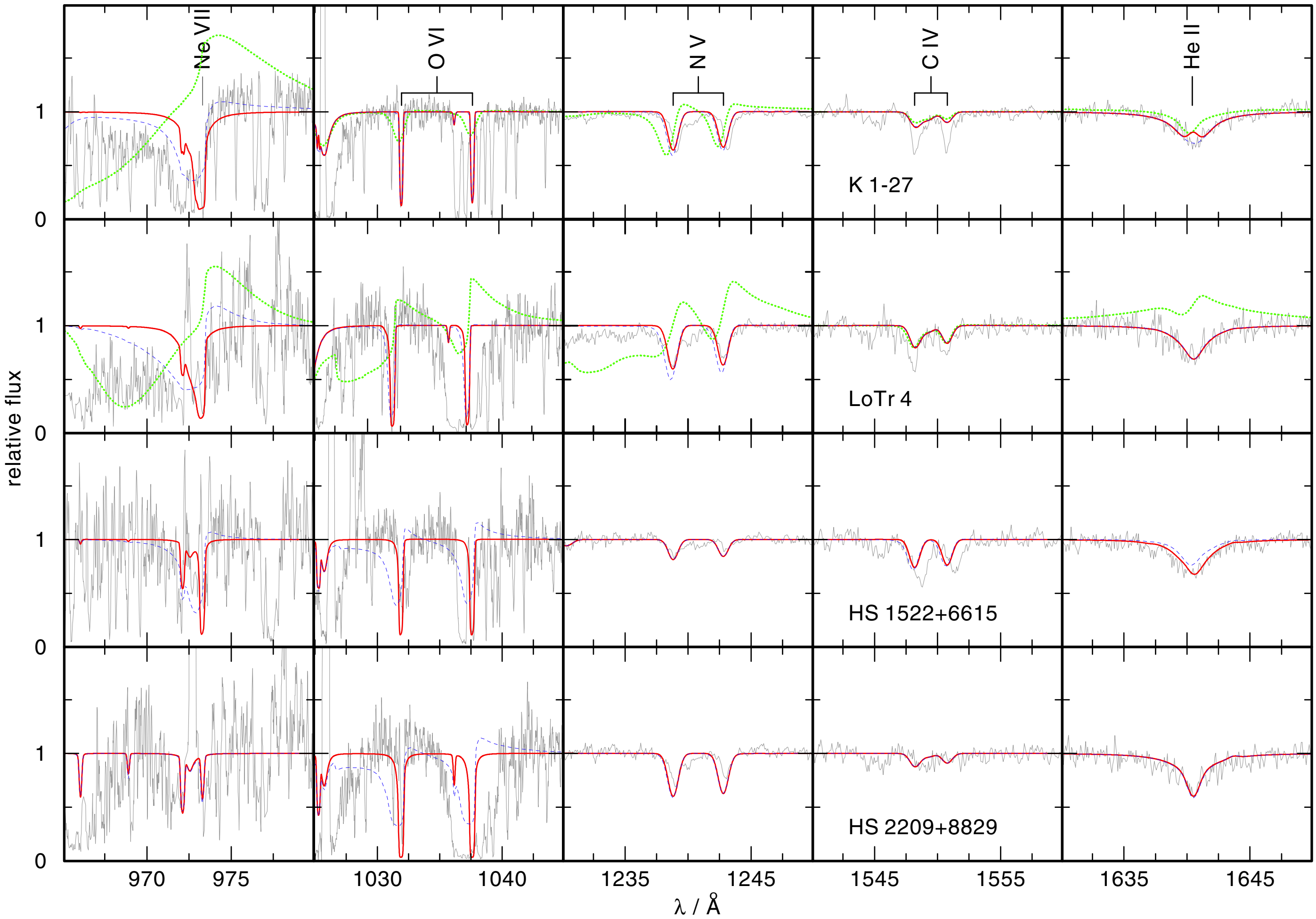

Fig. 25. Synthetic PoWR line profiles of Ne VII 2p ^{1}P^o – 2p ^{1}D, of the resonance doublets of O VI, N V, C IV, and of He II λ 1640 Å calculated with mass-loss rates from Pauldrach et al. (1988, red lines) and $10\times$ and $100\times$ (K 1−27 and LoTr 4 only) enhanced mass-loss rates (blue, dashed and green, dotted lines, respectively), compared with the observations of the four O(He) stars.

We also derived the stellar parameters of the O(He) stars using the evolutionary tracks for double He-WD mergers (Zhang & Jeffery 2012b, Fig. 26). For K 1−27, LoTr 4, and HS 2209+8829, we used the tracks from the slow-merger models because they reproduce the surface abundances of theses stars. For HS 1522+6615 the fast-merger models were used, because they result in C-enriched atmospheres (Sect. 5.2.1). Compared with what we found by comparison with VLTP calculations, luminosities and radii, which were derived from merger processes agree quite well, but the masses are up to $\Delta M = 0.16\,M_\odot$ higher (Table 5).

Based on these masses, we calculated the distances (Table 5) by using the flux calibration of Heber et al. (1984) for λ_eff = 5454 Å,

$$d[\mathrm{pc}] = 7.11\times10^4\cdot\sqrt{H_\nu\cdot M\times10^{0.4\,m_{\mathrm{V}_0}-\log g}},$$

with $m_{\mathrm{V}_0} = m_\mathrm{V} - 2.175c$, $c = 1.47E_{B-V}$, and the Eddington flux H_ν at λ_eff of our final model atmospheres. All O(He) stars and in particular HS 1522+6615 are located far above or below the Galactic plane (Table 5). K 1−27, LoTr 4, and HS 2209+8829 may belong to the thick disk, which dominates in the region $1\,\mathrm{kpc} \lesssim z \lesssim 4\,\mathrm{kpc}$ (Kordopatis et al. 2011). HS 1522+6615 has a high radial velocity of $-180\,\mathrm{km\,s^{-1}}$ (measured by the shift of e.g. C IV $\lambda\lambda$ 1168.9, 1169.0 Å and He II λ 1640.4 Å in the COS spectrum). Using the proper motions from the Sloan Digital Sky Survey Photometric Catalog (Release 9, Ahn et al. 2012), we calculated the space velocities to $U = 95\,\mathrm{km\,s^{-1}}$, $V = -116\,\mathrm{km\,s^{-1}}$, and $W = -121\,\mathrm{km\,s^{-1}}$, which are typical for halo stars (Kordopatis et al. 2011). From the large height above

Table 5. Masses M_m and M_V interpolated from double He-WD mergers (Fig. 26) and evolutionary tracks of VLTP post-AGB stars (Fig. 24), respectively, luminosities L, radii R, Galactic coordinates l and b, distances d, and heights above the Galactic plane z of the O(He) stars, as well as the kinematical ages t_PN of the two PNe.

	K 1−27	LoTr 4	HS 1522+6615	HS 2209+8829
$M_\mathrm{m}/M_\odot$	$0.60^{+0.08}_{-0.03}$	$0.70^{+0.08}_{-0.05}$	$0.70^{+0.05}_{-0.05}$	$0.60^{+0.10}_{-0.05}$
$M_\mathrm{V}/M_\odot$	$0.53^{+0.03}_{-0.01}$	$0.54^{+0.10}_{-0.01}$	$0.57^{+0.07}_{-0.03}$	$0.52^{+0.02}_{-0.01}$
$\log L/L_\odot$	3.2 ± 0.4	3.6 ± 0.3	3.7 ± 0.2	3.2 ± 0.2
$R/R_\odot$	$0.08^{+0.03}_{-0.03}$	$0.14^{+0.05}_{-0.03}$	$0.14^{+0.06}_{-0.02}$	$0.12^{+0.07}_{-0.04}$
$l/°$	286.877	291.434	102.481	117.849
$b/°$	−29.577	+19.258	+44.561	+21.545
d/kpc	$2.00^{+0.63}_{-0.84}$	$4.27^{+1.00}_{-1.15}$	$7.86^{+1.72}_{-2.27}$	$2.90^{+0.90}_{-1.24}$
z/kpc	$-0.99^{-0.31}_{+0.41}$	$1.41^{+0.33}_{-0.38}$	$5.51^{+1.21}_{-1.59}$	$1.07^{+0.33}_{-0.45}$
t_PN/yr	10867^{+3421}_{-4553}	16184^{+3794}_{-4360}		

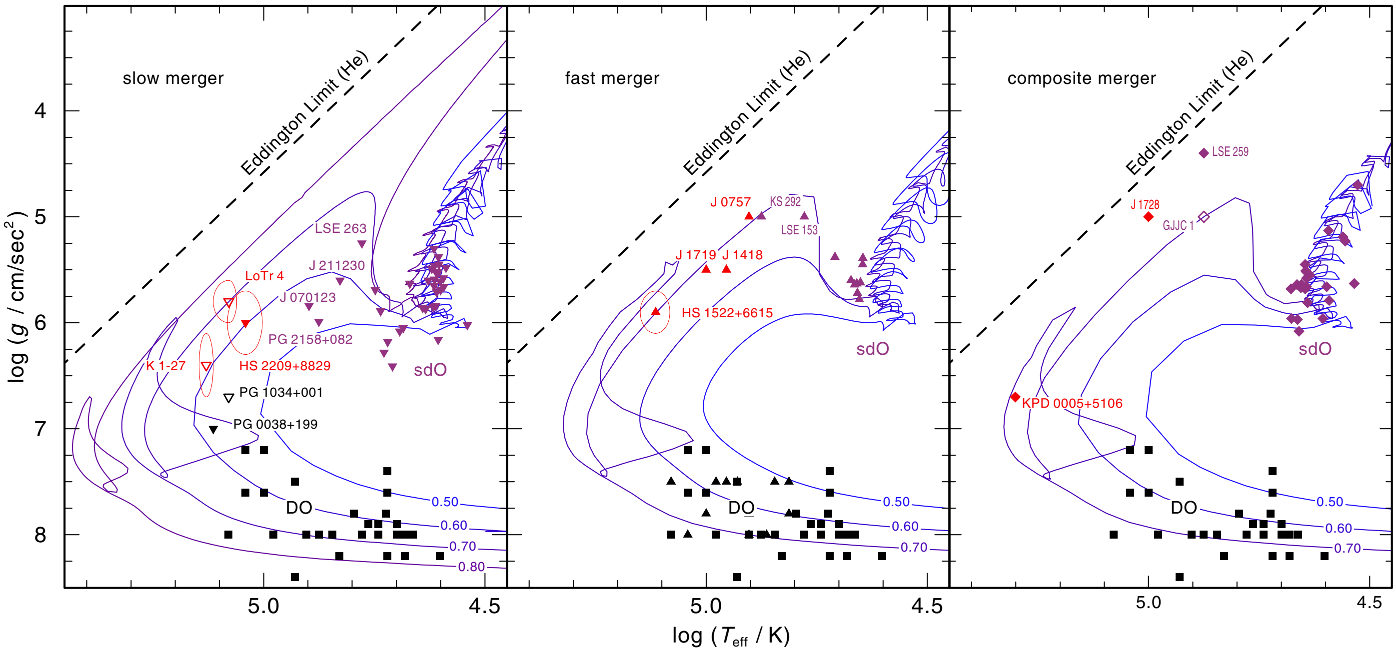

Fig. 26. Evolutionary tracks for a slow-merger (*left*), a fast-merger (*middle*) and a composite-merger (*right*) scenario of two He-WDs, marked with the merger mass in $M_\odot$ (Zhang & Jeffery 2012b). The locations of the sdB-, sdO-stars, (purple, Müller-Ringat 2013; Németh et al. 2012; Naslim et al. 2010; Hirsch 2009; Ahmad et al. 2004; Rauch et al. 1998, 1991; Husfeld et al. 1989; Stroeer et al. 2007) and O(He) stars (red this work, Werner et al. 2014; Wassermann et al. 2010) as well as the DO WDs (black, Werner et al. 2014; Mahsereci 2011; Hügelmeyer et al. 2006; Dreizler & Werner 1996) are marked. Open symbols indicate CSPNe, filled ones that no PN was detected. C-rich objects are represented by triangles, N-rich objects by inverted triangles, C- and N-rich objects by diamonds. Squares specify objects that are neither enriched in C nor in N.

the Galactic plane (z = 5.51 kpc) of HS 1522+6615 and its fast space velocities, we conclude that it belongs to the Galactic halo.

Using a typical expansion velocity of 20 km s^{-1} for the PNe of K 1−27 and LoTr 4, we also calculated their kinematical ages. The results are given in Table 5.

5. Results and discussion

We re-analyzed all known O(He) stars based on the available spectra and improved the determination of their properties (Tables 3, 5). We found that C, N, O, and Ne have a strong impact on the atmospheric structure and thus a strong effect on the resulting line profiles. This mostly affected K 1−27, for which we found a 30 kK higher T_{eff} than in literature. The COS observations allowed us to determine the N and O abundances for HS 2209+8229 for the first time. The FUSE observation of K 1−27 allowed us to determine the C abundances for this star for the first time. We derived upper abundance limits for F, Ne, Si, P, S (for LoTr 4 and HS 2209+8229 the actual abundance values for P and S, measured from the FUSE spectrum), Ar, and Fe.

By examining all strategic wind-lines located in the FUSE and COS wavelength ranges, we found that the upper limits for mass-loss rates of the O(He) stars agree well with predictions by radiative-driven wind theory. Only K 1−27 might have a ten times higher mass-loss rate than predicted (only there did we find spectral signatures). From comparison with stellar-evolution calculations we found that the masses of the O(He) stars range from 0.52 $M_\odot$ to 0.57 $M_\odot$ considering (V)LTP tracks, or from 0.60 $M_\odot$ to 0.70 $M_\odot$ considering double He-WD merger tracks.

Before considering possible evolutionary scenarios, it is worth to mention, that the CNO abundance patterns are similar for all O(He) stars exept HS 1522+6615 (Fig. 20), which exhibits strongly deviating CNO abundances. This suggests a dichotomy within the O(He) class. Interestingly, we find that other He-dominated objects (e.g. He-rich subdwarfs; Müller-Ringat 2013; Németh et al. 2012; Naslim et al. 2010; Hirsch 2009; Ahmad et al. 2004; Rauch et al. 1998, 1991; Husfeld et al. 1989; Stroeer et al. 2007, DO WDs Werner et al. 2014; Mahsereci 2011; Hügelmeyer et al. 2006; Dreizler & Werner 1996) also show these differences in the CNO abundances[13].

Some objects are enriched in N but not in C, some C-enriched objects do not show N, but there also are objects which are enriched in both. This suggests that there exist subclasses within the He-dominated objects. Each of them might have a different evolutionary history. From the He-dominated post-AGB objects (Fig. 24), it seems that there is no correlation of the stellar mass and the C-enriched objects. There is no star among N-enriched objects with a higher mass than 0.542 $M_\odot$. This might be because for low-mass stars no third dredge-up is predicted during the AGB evolution (Mello et al. 2012). The C- and N-enriched sdO and O(He) stars have masses greater than 0.64 $M_\odot$.

Rauch et al. (1998) already proposed the

sdO(He) → O(He) → DO WD

evolutionary channel that runs parallel to the PG 1159 evolution in the HRD. However, they were unable to present stringent clues on the evolution of O(He) stars. In the following we discuss different evolutionary channels to explain the origin of the O(He) stars, but also investigate the origin of other He-dominated objects to find possible progenitors and successors. First we will mention single-star evolutionary channels (Sect. 5.1), such as enhanced mass-loss of post early-AGB stars, (V)LTP scenarios, and the hot-flasher scenario. In Sect. 5.2 we consider to formation channels in binary systems, starting with the merger

[13] A list of all analyzed He-rich sdO stars, that are enriched in N and/or C, O(He) stars and DO WDs can be found at http://astro.uni-tuebingen.de/~reindl/He

scenarios (Sect. 5.2.1). We also discuss problems of this formation channel and some other possible binary formation channels such as enhanced mass-loss triggered by a planet or brown dwarf and the merger of a He and a CO WD (Sect. 5.2.2).

5.1. Single-star evolution

Assuming single-star evolution, Rauch et al. (2009) suggested that low-mass O(He) stars might be post early-AGB stars that experienced an enhanced mass-loss which removed the H-rich envelope. In these stars, the first thermal pulse occurs after their departure from the AGB. A numerical experiment for a $0.512\,M_\odot$ star by Miller Bertolami & Althaus (2006) has shown that an artificially increased mass-loss rate can cause the hydrogen deficiency and, in the later evolution, might turn the O(He) stars into PG 1159 stars. However, to achieve that Miller Bertolami & Althaus (2006) had to assume $\log \dot{M}/(M_\odot\,/\,\mathrm{yr}) = -8$ for $\log T_\mathrm{eff} > 3.8$. Such a strong wind is not predicted by radiative-driven wind theory nor is it seen in the spectra of the O(He) stars. Only K 1−27 could have a ten times higher mass-loss rate than predicted, but the derived upper limited ($\log \dot{M}/(M_\odot\,/\,\mathrm{yr}) = -9$) is still too low to overcome the He-buffer and consequently turn the O(He) star into a PG 1159 star. The previous mass-loss history of the O(He) stars is of course unknown and we can therefore only rule out PG 1159 stars as possible successors of O(He) stars. However, the different H-abundances of the N-enriched O(He) stars, show a correlation with stellar mass and hence the post-AGB times and the remaining H in the atmospheres of these stars. While LoTr 4 still shows 12% H (by mass), the more evolved and lower mass K 1−27 only shows 5% H. No H can be detected in the spectrum in the lowest mass O(He) star, HS 2209+8229. Although the predicted mass-loss rates are lower for stars with lower mass, their evolutionary timescales are much longer, and that is why the correlation of stellar mass and remaining H seems plausible if enhanced mass-loss is assumed.

Within this scenario, good candidates for successors are C-enriched DO WDs (e.g. PG 0108+101, HS 0111+0012, Dreizler & Werner 1996) for HS 1522+6615 or N-enriched DO WDs (e.g. PG 0038+199, PG 1034+001, Mahsereci 2011) for the three other O(He) stars. However, because of gravitational settling they might also turn into DOs, which do not show C or N anymore, or even, depending on the remaining H, into DA WDs.

Possible progenitors might be luminous helium-rich sdO-type stars, for example LSE 153 (Müller-Ringat 2013) for HS 1522+6615 or LSE 263 (Müller-Ringat 2013) for the N-enriched O(He) stars.

Other interesting objects that fit into this sequence, might be the [WN]-type CSPNe IC 4663 (Miszalski et al. 2012) and Abell 48 (Todt et al. 2013; Frew et al. 2014). Because of the strong similarity of the element abundances of [WN] stars and the N-enriched O(He) stars, an analog to the H-deficient, but C-rich post-AGB sequence [WCL] → [WCE] → PG 1159 (e.g. Werner & Herwig 2006), a second, H-deficient sequence [WN] → O(He) was suggested (cf. Werner 2012). By examining He II λ 4686 Å and Ne VII λ 3890 Å, Miszalski et al. (2012) determined $T_\mathrm{eff} = 140$ kK for IC 4663. Their values for the mass and the surface gravity ($M = 0.6\,M_\odot$ and $\log g = 6.1$) are only estimates, however. With $T_\mathrm{eff} = 140$ kK, IC 4663 would be in a similar or even later evolutionary state than the O(He) stars. Abell 48 ($T_\mathrm{eff} = 70$ kK), on the other hand, is in an earlier evolutionary stage than the O(He) stars. Still, it is necessary to clarify why IC 4663 and Abell 48 show a much stronger stellar wind (IC 4663: $\log \dot{M}/M_\odot/\mathrm{yr} = -7.7$, Abell 48: $\log \dot{M}/M_\odot/\mathrm{yr} = -6.4$) than the O(He) stars. We speculate that [WN] stars are O(He) stars with higher masses. According to Pauldrach et al. (1988, Fig. 6b), the high mass-loss rate found for IC 4663 and Abell 48 would correspond to $M \approx 0.7\,M_\odot$ and $M > 1.0\,M_\odot$, respectively.

Rauch et al. (2008) suggested that RCB stars might be possible progenitors of the O(He) stars. This could be true for the two C and N enriched O(He) stars SDSS J 172854.34+361958.62 (Werner et al. 2014) and KPD 0005+5106 (Wassermann et al. 2010). In between evolutionary objects could be the C- and N-enriched luminous sdO stars LSE 259 (Husfeld et al. 1989), GJJC 1 (Rauch et al. 1998), and KS 292 (Rauch et al. 1991).

The VLTP scenarios that were successfully applied to explain the origin of the H-deficient, but C-rich objects (e.g. PG 1159 stars) cannot explain the origin of the O(He) stars because these scenarios always produce C-rich atmospheres with more than about 20% of C by mass (in contrast, the most C-rich O(He) stars only show 3% of C in their atmospheres). The relatively young kinematical age of the H-rich PNe of K 1−27 and LoTr 4 (around 10 000 yrs) strongly contradict a VLTP scenario.

A third conceivable way for a single-star evolutionary channel is the hot-flasher scenario, which was invoked by Miller Bertolami et al. (2008) to explain the helium-rich sdO stars. This scenario is able to explain C- or N-enriched He-sdOs, but these stellar models never reach the high effective temperatures found for the O(He) stars.

5.2. Binary evolution

Since none of the previously mentioned single-star formation channels seems convincing for the O(He) stars, binary formation channels become interesting. We discuss merger scenarios and suggest alternatives.

5.2.1. Merger scenarios

As mentioned above, Zhang & Jeffery (2012b,a) showed that in terms of T_eff, $\log g$, C, and N abundances, the origin of the three sdOs groups, but also the properties of RCB and EHe stars, can be explained by different double He-WD merger models. Zhang & Jeffery (2012a) compared their result with He-rich sdO stars from the sample of Hirsch (2009) and He-rich sdB stars from the sample Naslim et al. (2010). We extended this comparison to all He-rich sdB and sdO stars, that are enriched in C and/or N (Müller-Ringat 2013; Németh et al. 2012; Naslim et al. 2010; Hirsch 2009; Ahmad et al. 2004; Rauch et al. 1998, 1991; Husfeld et al. 1989; Stroeer et al. 2007), the O(He) stars of our work, and those of Werner et al. (2014); Wassermann et al. (2010), and the known DO WDs (Werner et al. 2014; Mahsereci 2011; Hügelmeyer et al. 2006; Dreizler & Werner 1996). We found that all of them fit this scenario. Figure 27 shows the CNO abundances resulting from a slow and a fast merger of two He WDs according to the numerical experiments of Zhang & Jeffery (2012a). These abundances are compared with those of the O(He) stars analyzed in our work. We found that those of the two CSPNe and HS 2209+8229 can be explained by the slow-merger model and the CNO abundances of HS 1522+6615 are reproduced by the fast-merger because of the high C abundance. The three O(He) stars SDSS J 171916.97+365326.70, SDSS J 141812.50+024426.92, and SDSS J 075732.18+184329.28 that were found by Werner et al. (2014) also fit the fast-merger scenario. SDSS J 172854.34+361958.62 (Werner et al. 2014) and

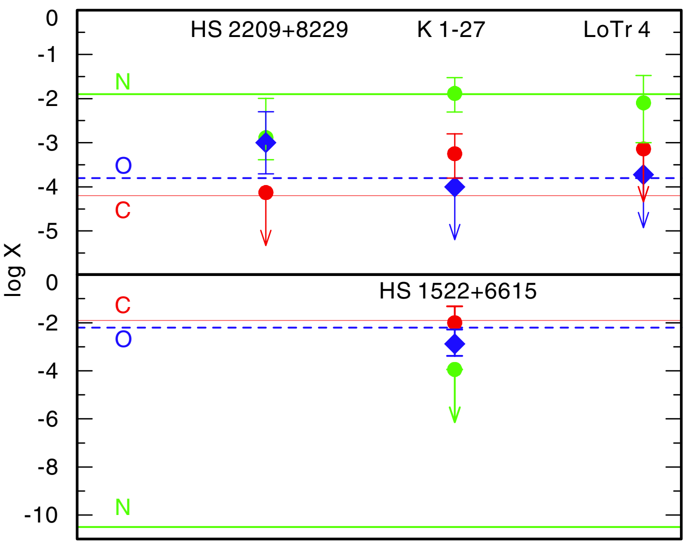

Fig. 27. Comparison of the CNO abundances of the O(He) stars (N: light, green dots, C: dark, red dots, O: dark, blue rhombi) with those resulting form a slow (*top*) and a fast (0.7 $M_\odot$ model, *bottom*) merger of two He WDs (N: light, green, solid line, C: dark, red, solid line, O: dashed, blue, gray line).

KPD 0005+5106 (Wassermann et al. 2010) would fit the composite merger model. Concerning the CNO abundances, the O(He) stars can be explained much better by this double He WD merger scenario than by V(LTP) scenarios.

Figure 26 shows the evolutionary tracks of Zhang & Jeffery (2012a) for their different merger models. According to their surface abundances, which are produced in a certain merger model, we marked the locations of the N-enriched He-dominated objects in the panel for the slow merger, C-enriched ones in the fast-merger panel, and C- and N-enriched objects are shown in the composite merger panel. These evolutionary tracks connect the subluminous sdO with the luminous sdO stars (in contrast to the VLTP calculations), the O(He) stars, and DO WDs.

Other points that support the merger scenario are the very low binary fraction among He-rich sdO-stars (4%, Napiwotzki et al. 2004), O(He) stars, and DO WDs (only PG 0046+078 and PG 0237+116 have been found to be in a binary system). A different evolution scenario probably applies for binary systems.

The position of HS 1522+6615 in the Galactic halo corroborates the merger scenario, because only very old stars are expected there. Napiwotzki (2008) found that a considerable part (20%) of the He-rich sdO stars belongs to the halo population. The fact that no PN is detected around HS 1522+6615, SDSS J 171916.97+365326.70, SDSS J 141812.50+024426.92, and SDSS J 075732.18+184329.28 although their theoretical post-AGB evolutionary times would be shorter than those of K 1−27 or LoTr 4, might be explained considering that these objects are merger products.

We note that the WD+post-sdB star merger channel, proposed by Justham et al. (2011) to explain He-rich sdO stars, can explain the O(He) stars in terms of $T_{\rm eff}$ and $\log g$ as well.

5.2.2. Alternative scenarios

Within the merger models mentioned above it is not possible to explain the PNe of K 1−27 and LoTr 4. Even if a PN would have been ejected during the merger process, it would have dissipated into the ISM a long time ago because the post-merger time of LoTr 4 is about 3.7×10^7 years. In addition, the solar compositions of the PNe of K 1−27 and LoTr 4 and the remaining hydrogen in their atmospheres contradicts a merger origin of these objects. The same holds for GJJC 1, IC 4663, and PG 1034+001. For these reasons common envelope (CE) scenarios become interesting. Soker (2013) speculated that R CrB itself and similar RCB stars are formed from the merger of a WD with the core of an AGB star. The previous common-envelope ejection (CEE) then would have caused the H-deficiency. This scenario would also be possible for the O(He) stars. The merger within a CE of a CO-WD and a RG or AGB star might produce a similar outcome as a He- and CO-WD merger but within a H-rich envelope. The CE ejected during the merger process could then first reproduce the H-rich PNe of K 1−27 and LoTr 4 and then, the post-merger times would be much shorter because no central helium burning phase is expected for a He- and CO-WD merger.

Another possibility for a O(He) star origin is that an RG or AGB star lost its H-rich envelope with the help of a planet or a brown dwarf. If a low-mass companion enters the atmosphere of an RG or AGB star, it spirals inwards and transfers orbital energy and angular momentum to the envelope and, thus, parts or all of it are removed. The companion then either stops in a close orbit or even merges with the more massive star (Diehl et al. 2008; Soker 1998).

5.3. Conclusions

The evolutionary status of the O(He) stars, but also those of other He-dominated stars, is still not understood. It is most likely that they are part of a second H-deficient evolutionary sequence. It appears plausible that there are three subclasses within this He-dominated sequence. For objects that are either enriched in C or N, we propose the channels

sdO(He) → O(He) → DO WD

or

sdO(He) → O(He) → DA WD

if there is some remaining H. For C- and N-rich objects, we propose

RCB → EHe → sdO(He) → O(He) → DO WD

or

RCB → EHe → sdO(He) → O(He) → DA WD

if that there is some remaining H.

This He-dominated sequence has most likely various formation channels. For single-star objects, merger scenarios seem most promising. He-dominated CSPNe must have formed in a different way, for example via enhanced mass-loss during their post-AGB evolution or a merger within a CE of a CO-WD and an RG or AGB star.

To make progress, it would be highly desirable that more O(He) stars and other He-dominated objects were discovered to improve the statistics. Additional quantitative investigations on the binarity of these objects and on the mass-loss rates of RCB, EHe, and sdO stars may help to distinguish between different formation channels. A comprehensive systematic calculation of evolutionary models for thermal pulse and merger scenarios is a pre-requisite for comparision with results of spectral analysis.

Acknowledgements. N.R. is supported by the German Research Foundation (DFG, grant WE 1312/41-1), T.R. by the German Aerospace Center (DLR, grant 05 OR 1301). We thank Marcelo Miguel Miller Bertolami, Simon Jeffery, Stephan Geier, and Geoffrey Clayton for helpful discussions and comments. This research has made use of the SIMBAD database, operated at CDS, Strasbourg, France. This research has made use of NASA's Astrophysics Data System. This work used the profile-fitting procedure OWENS developed by M. Lemoine and the FUSE French Team. Some of the data presented in this paper were obtained from the Mikulski Archive for Space Telescopes (MAST). STScI is operated by the Association of Universities for Research in Astronomy, Inc., under NASA contract NAS5-26555. Support for MAST for non-HST data is provided by the NASA Office of Space Science via grant NNX09AF08G and by other grants and contracts.

References

Ahmad, A., Jeffery, C. S., & Fullerton, A. W. 2004, A&A, 418, 275
Ahn, C. P., Alexandroff, R., Allende Prieto, C., et al. 2012, ApJS, 203, 21
Asplund, M., Grevesse, N., Sauval, A. J., & Scott, P. 2009, ARA&A, 47, 481
Bucciarelli, B., García Yus, J., Casalegno, R., et al. 2001, A&A, 368, 335
Clayton, G. C., Sugerman, B. E. K., Stanford, S. A., et al. 2011, ApJ, 743, 44
Diehl, S., Fryer, C., & Herwig, F. 2008, in Hydrogen-Deficient Stars, eds. K. Werner & T. Rauch, ASP Conf. Ser., 391, 221
Dreizler, S., & Werner, K. 1994, in Evolution of Massive Stars, eds. D. Vanbeveren, W. van Rensbergen, & C. De Loore, 147
Dreizler, S., & Werner, K. 1996, A&A, 314, 217
Fitzpatrick, E. L. 1999, PASP, 111, 63
Frew, D. J., Bojičić, I. S., Parker, Q. A., et al. 2014, MNRAS, 440, 1345
Gräfener, G., Koesterke, L., & Hamann, W.-R. 2002, A&A, 387, 244
Hamann, W.-R., & Gräfener, G. 2004, A&A, 427, 697
Han, Z., Podsiadlowski, P., Maxted, P. F. L., Marsh, T. R., & Ivanova, N. 2002, MNRAS, 336, 449
Han, Z., Podsiadlowski, P., Maxted, P. F. L., & Marsh, T. R. 2003, MNRAS, 341, 669
Heber, U., Hunger, K., Jonas, G., & Kudritzki, R. P. 1984, A&A, 130, 119
Hébrard, G., & Moos, H. W. 2003, ApJ, 599, 297
Hébrard, G., Lemoine, M., Vidal-Madjar, A., et al. 2002, ApJS, 140, 103
Hirsch, H. A. 2009, Ph.D. Thesis, University Nuremberg
Hügelmeyer, S. D., Dreizler, S., Homeier, D., et al. 2006, A&A, 454, 617
Husfeld, D., Butler, K., Heber, U., & Drilling, J. S. 1989, A&A, 222, 150
Jeffery, C. S., & Hamann, W.-R. 2010, MNRAS, 404, 1698
Jeffery, C. S., Karakas, A. I., & Saio, H. 2011, MNRAS, 414, 3599
Justham, S., Podsiadlowski, P., & Han, Z. 2011, MNRAS, 410, 984
Kameswara Rao, N., Lambert, D. L., García-Hernández, D. A., & Manchado, A. 2013, MNRAS, 431, 159
Kordopatis, G., Recio-Blanco, A., de Laverny, P., et al. 2011, A&A, 535, A107
Lamers, H. J. G. L. M., Snow, T. P., & Lindholm, D. M. 1995, ApJ, 455, 269
Mahsereci, M. 2011, Diploma Thesis, University Tübingen
Mello, D. R. C., Daflon, S., Pereira, C. B., & Hubeny, I. 2012, A&A, 543, A11
Méndez, R. H., Miguel, C. H., Heber, U., & Kudritzki, R. P. 1986, in Hydrogen Deficient Stars and Related Objects, eds. K. Hunger, D. Schönberner, & N. Kameswara Rao, Astrophys. IAU Colloq. 87, Space Sci. Lib., 128, 323
Mickaelian, A. M., Mikayelyan, G. A., & Sinamyan, P. K. 2011, MNRAS, 415, 1061
Miller Bertolami, M. M., & Althaus, L. G. 2006, A&A, 454, 845
Miller Bertolami, M. M., & Althaus, L. G. 2007, A&A, 470, 675
Miller Bertolami, M. M., Althaus, L. G., Unglaub, K., & Weiss, A. 2008, A&A, 491, 253
Miszalski, B., Crowther, P. A., De Marco, O., et al. 2012, MNRAS, 423, 934
Müller-Ringat, E. 2013, Dissertation, University of Tübingen, Germany, http://tobias-lib.uni-tuebingen.de/volltexte/2013/6774/
Napiwotzki, R. 2008, in Hydrogen-Deficient Stars, eds. K. Werner & T. Rauch, ASP Conf. Ser., 391, 257
Napiwotzki, R., Karl, C. A., Lisker, T., et al. 2004, Ap&SS, 291, 321
Naslim, N., Jeffery, C. S., Ahmad, A., Behara, N. T., & Şahìn, T. 2010, MNRAS, 409, 582
Németh, P., Kawka, A., & Vennes, S. 2012, MNRAS, 427, 2180
Pauldrach, A., Puls, J., Kudritzki, R. P., Méndez, R. H., & Heap, S. R. 1988, A&A, 207, 123
Rauch, T., & Deetjen, J. L. 2003, in Stellar Atmosphere Modeling, eds. I. Hubeny, D. Mihalas, & K. Werner, ASP Conf. Ser., 288, 103
Rauch, T., Heber, U., Hunger, K., Werner, K., & Neckel, T. 1991, A&A, 241, 457
Rauch, T., Köppen, J., & Werner, K. 1994, A&A, 286, 543
Rauch, T., Köppen, J., & Werner, K. 1996, A&A, 310, 613
Rauch, T., Dreizler, S., & Wolff, B. 1998, A&A, 338, 651
Rauch, T., Reiff, E., Werner, K., et al. 2006, in Astrophysics in the Far Ultraviolet: Five Years of Discovery with FUSE, eds. G. Sonneborn, H. W. Moos, & B.-G. Andersson, ASP Conf. Ser., 348, 194
Rauch, T., Reiff, E., Werner, K., & Kruk, J. W. 2008, in Hydrogen-Deficient Stars, eds. K. Werner & T. Rauch, ASP Conf. Ser., 391, 135
Rauch, T., Werner, K., & Kruk, J. W. 2009, in AIP Conf. Ser. 1135, eds. M. E. van Steenberg, G. Sonneborn, H. W. Moos, & W. P. Blair, 168
Savitzky, A., & Golay, M. J. E. 1964, Anal. Chem., 36, 1627
Soker, N. 1998, AJ, 116, 1308
Soker, N. 2013, New Astron., 18, 18
Stroeer, A., Heber, U., Lisker, T., et al. 2007, A&A, 462, 269
Todt, H., Kniazev, A. Y., Gvaramadze, V. V., et al. 2013, MNRAS, 430, 2302
Wassermann, D., Werner, K., Rauch, T., & Kruk, J. W. 2010, A&A, 524, A9
Werner, K. 2012, in Planetary Nebulae: An Eye to the Future, IAU Symp., 283, 196
Werner, K., & Herwig, F. 2006, PASP, 118, 183
Werner, K., Deetjen, J. L., Dreizler, S., et al. 2003, in Stellar Atmosphere Modeling, eds. I. Hubeny, D. Mihalas, & K. Werner, ASP Conf. Ser., 288, 31
Werner, K., Rauch, T., & Kepler, S. O. 2014, A&A, 564, A53
Zhang, X., & Jeffery, C. S. 2012a, MNRAS, 426, L81
Zhang, X., & Jeffery, C. S. 2012b, MNRAS, 419, 452

Pages 13 to 23 are available in the electronic edition of the journal at http://www.aanda.org

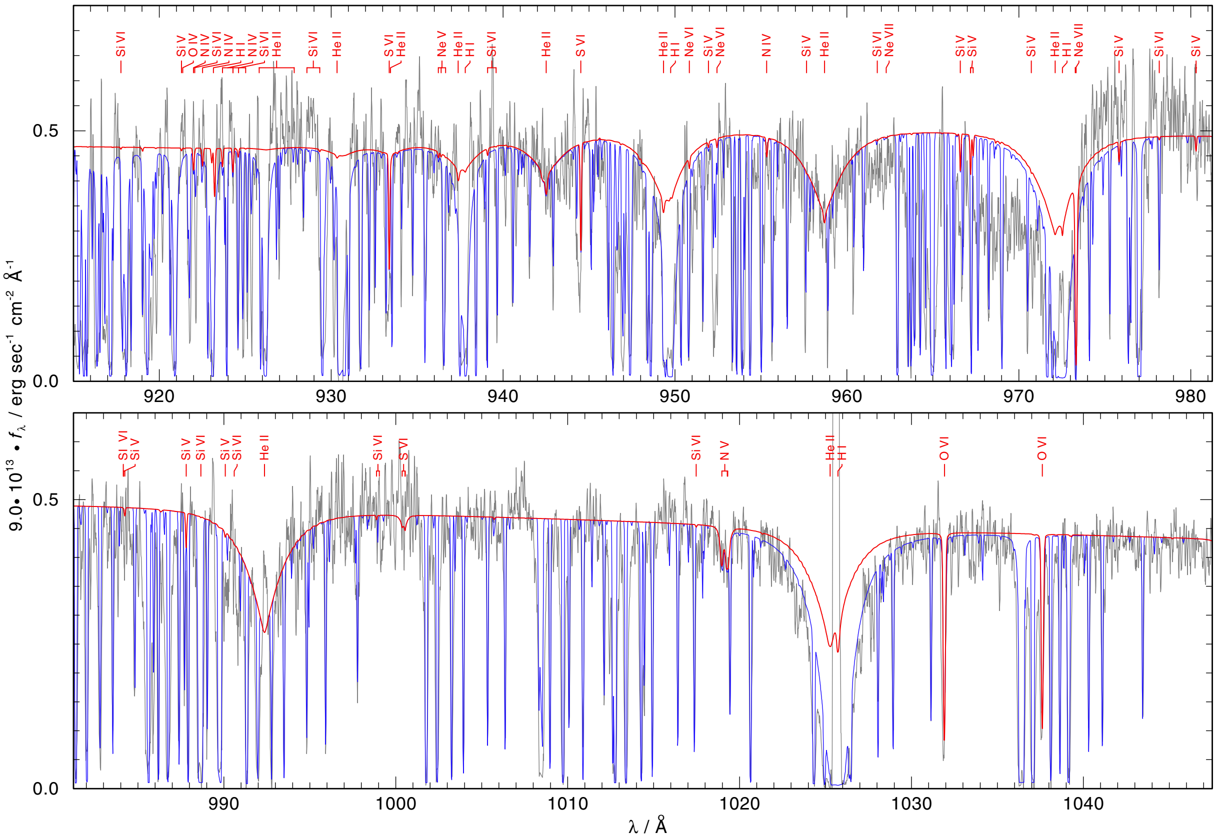

Fig. 1. FUSE spectrum of K 1−27 (gray) compared with final synthetic spectra (red: pure stellar, blue: combined stellar and interstellar). The locations of photospheric lines appearing in the synthetic spectrum are marked.

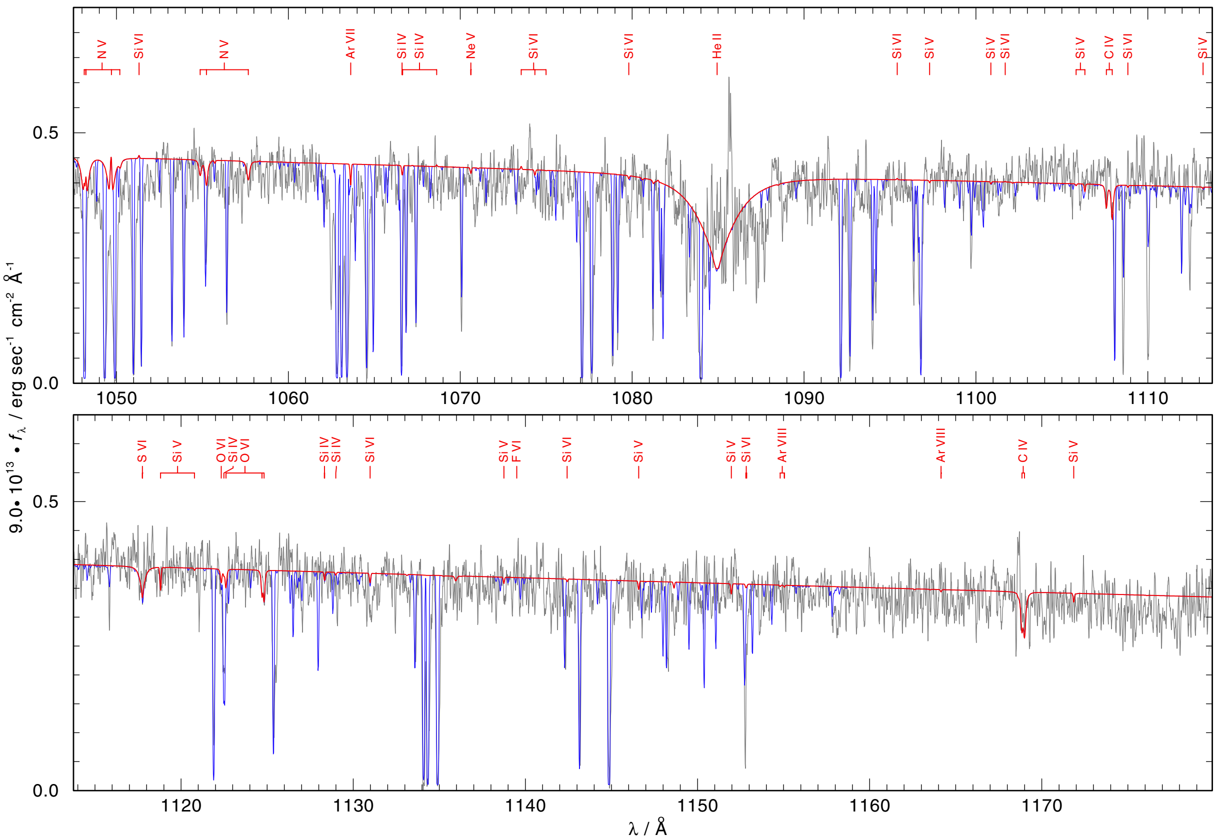

Fig. 1. continued.

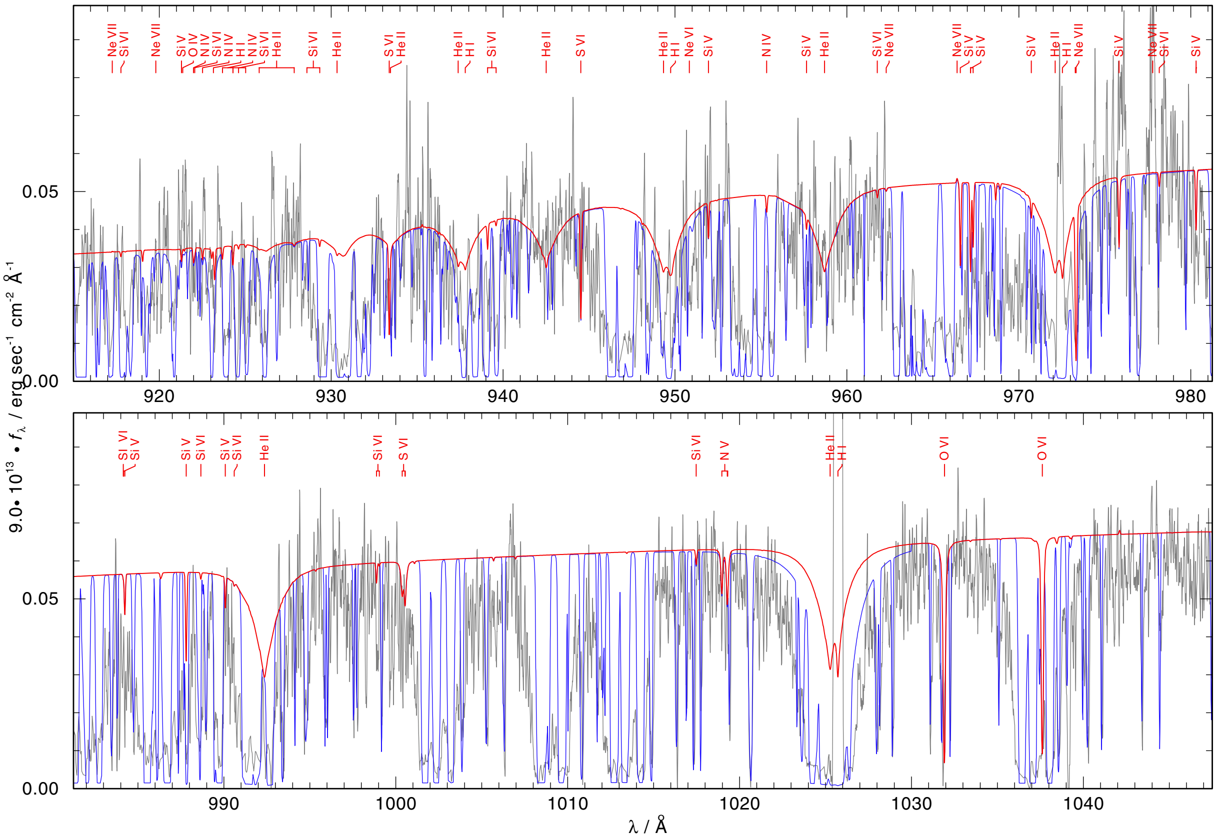

Fig. 2. Same as Fig. 1 for LoTr 4.

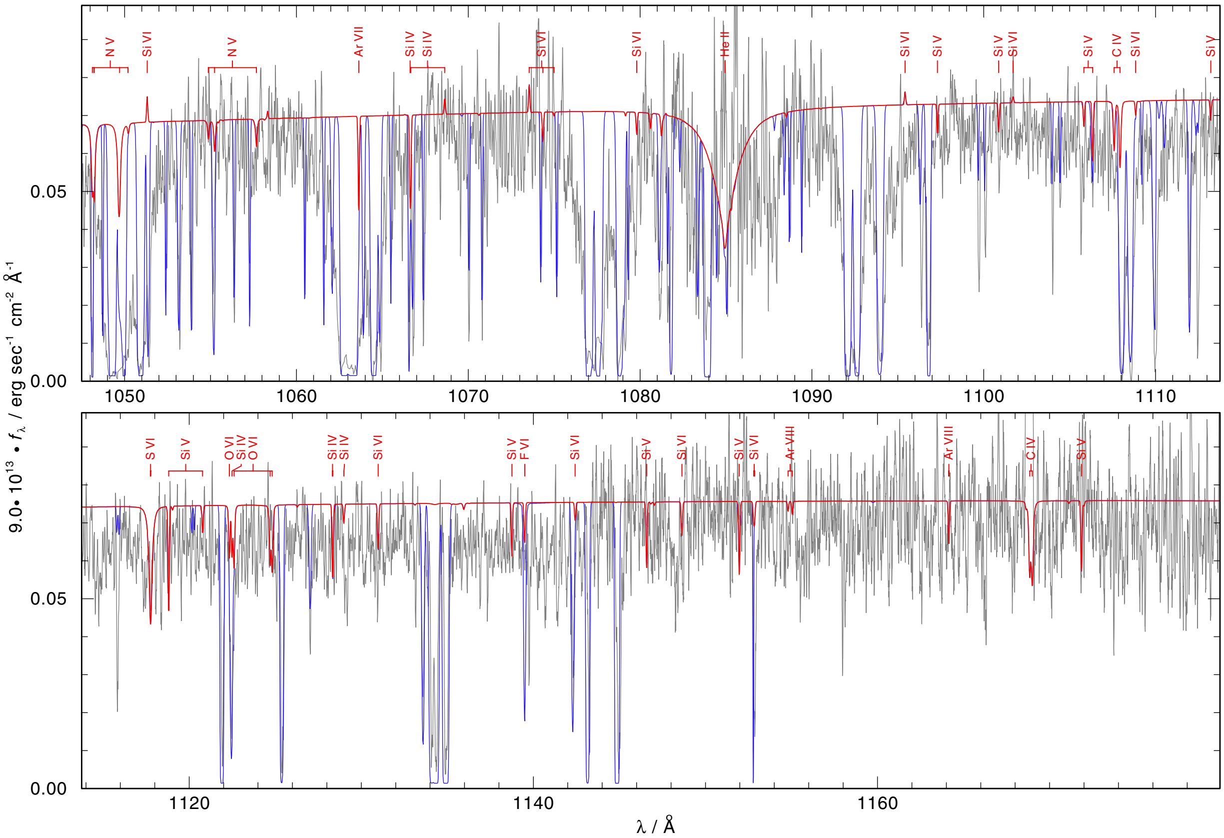

Fig. 2. continued.

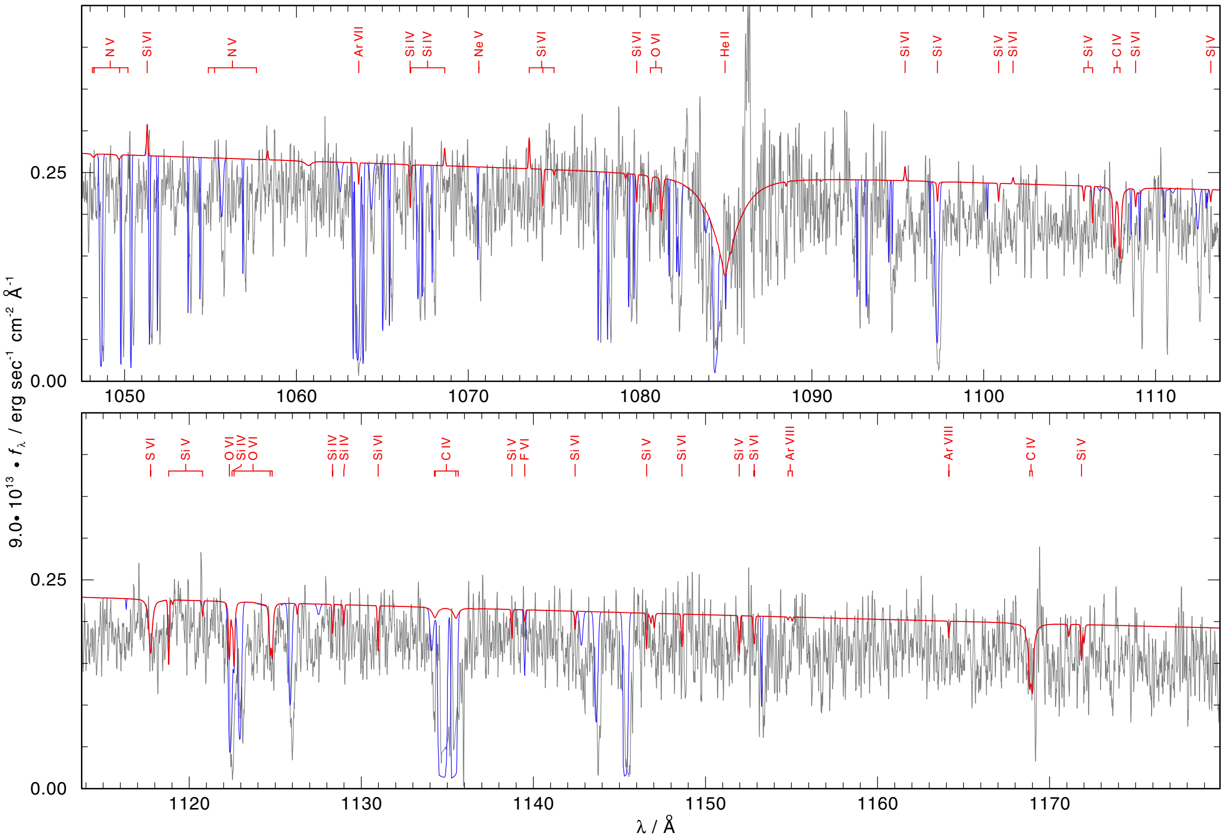

Fig. 3. Same as Fig. 1 for HS 1522+6615.

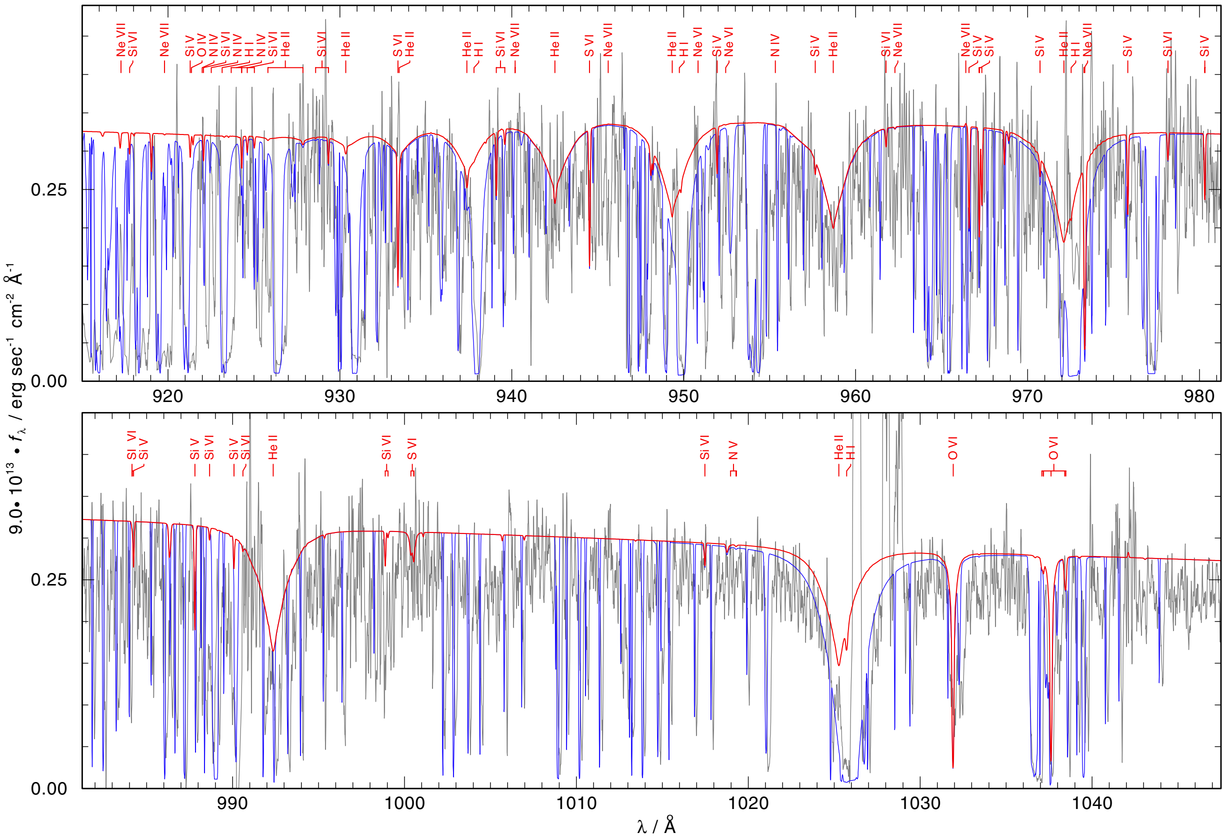

Fig. 3. continued.

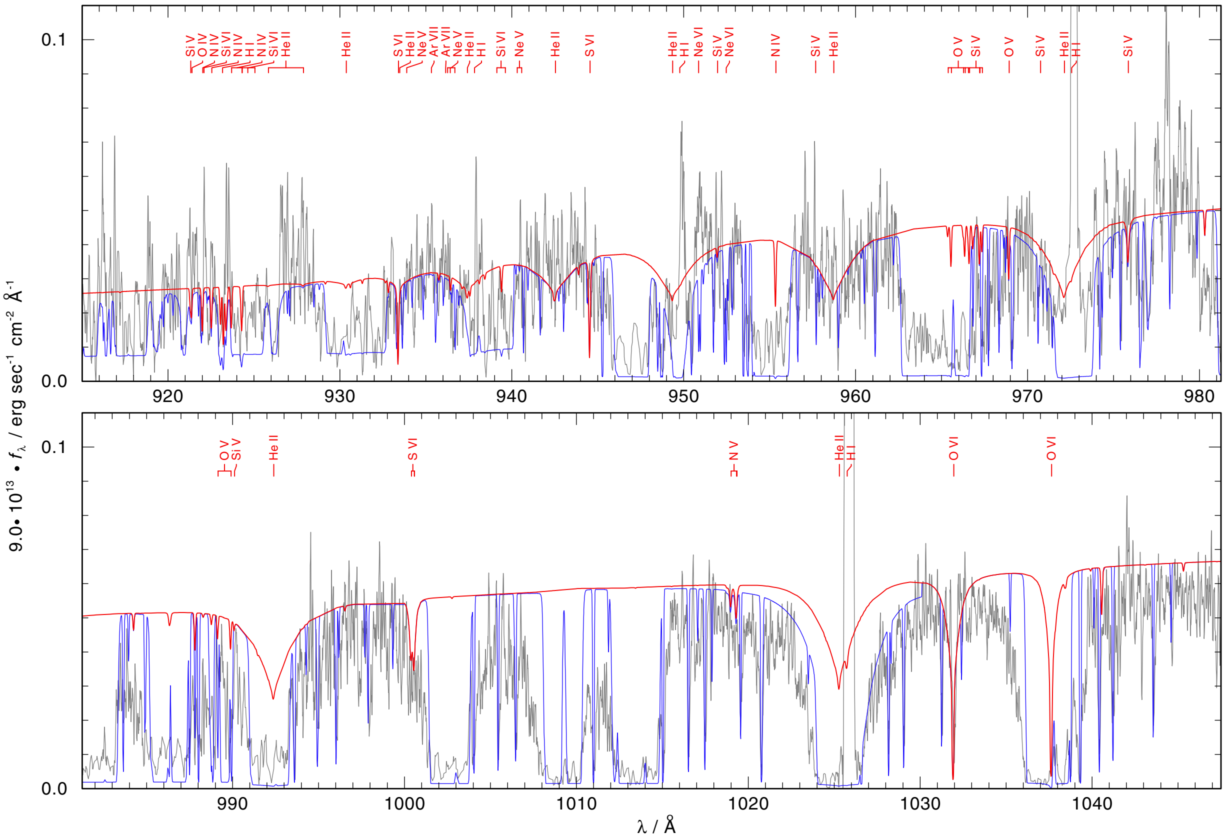

Fig. 4. Same as Fig. 1 for HS 2209+8229.

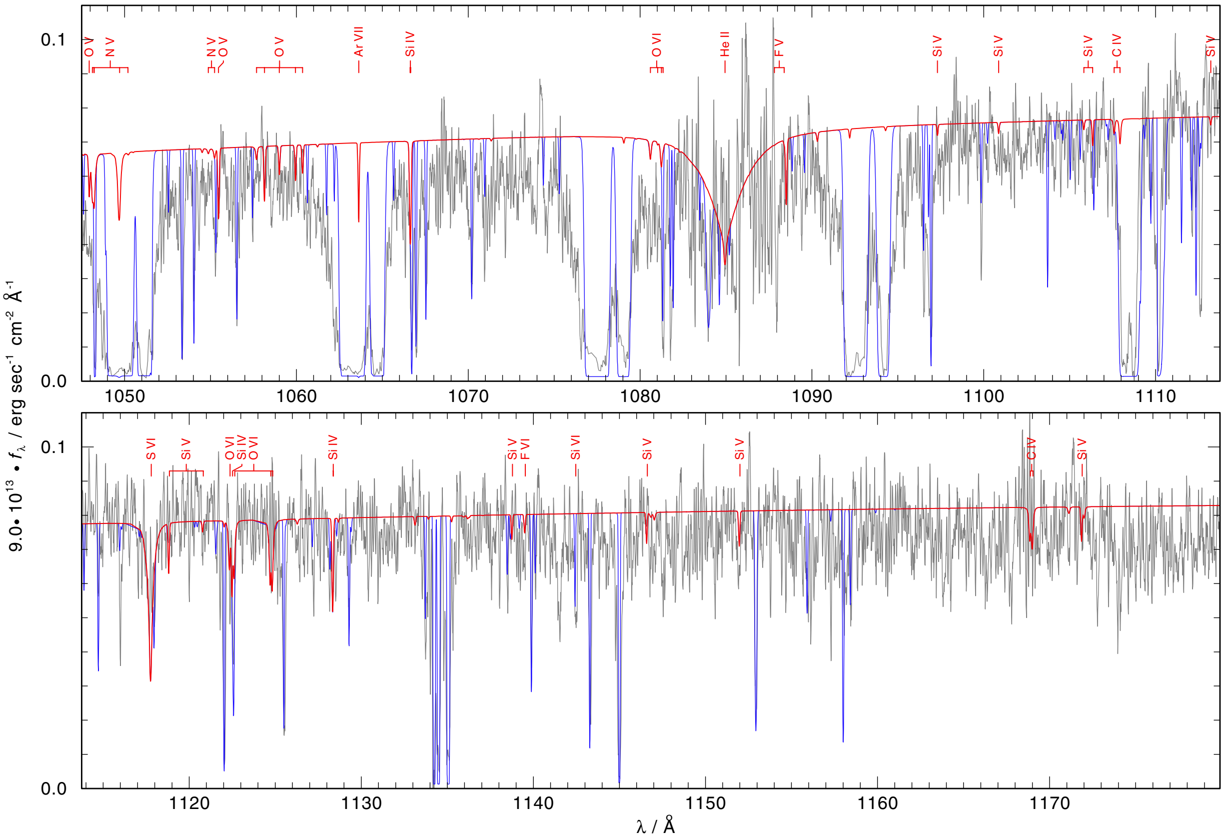

Fig. 4. continued.

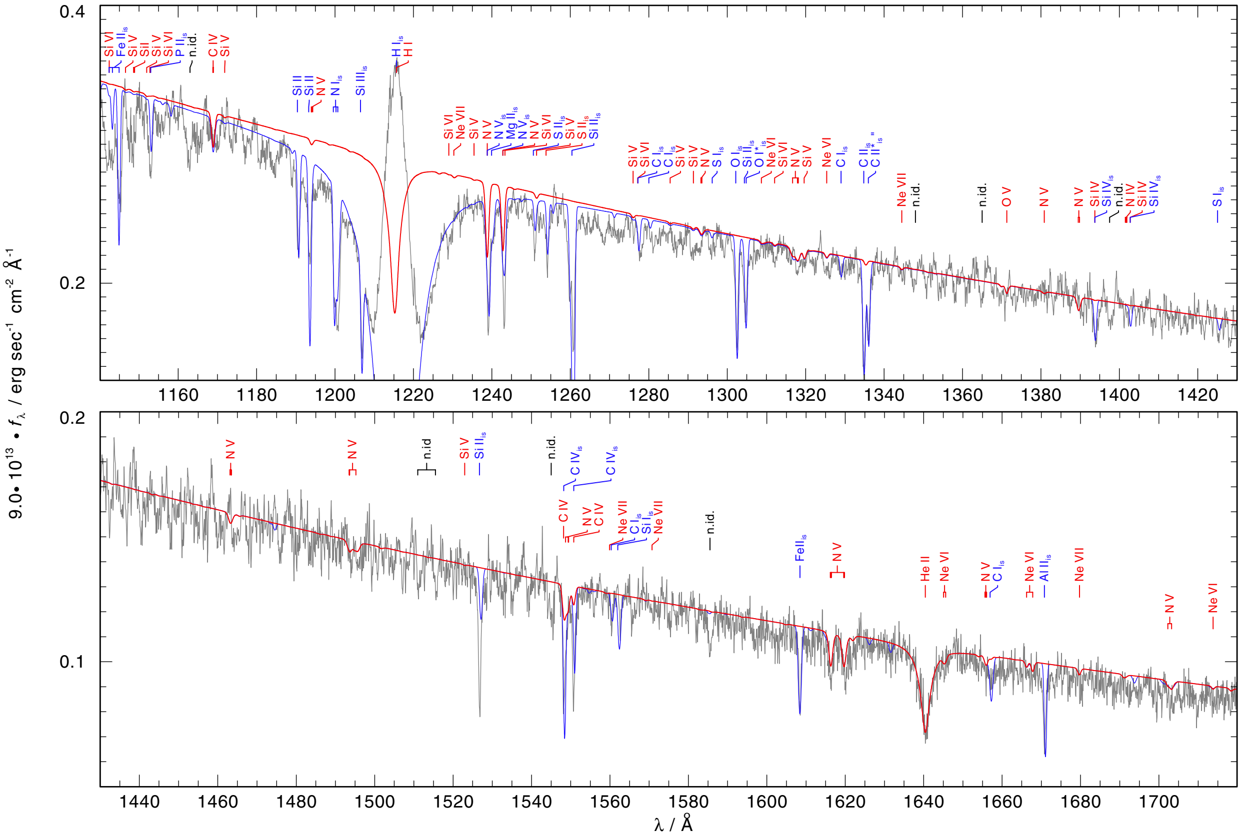

Fig. 5. HST/COS spectrum of K 1−27 (gray) compared with final synthetic spectra (red: pure stellar, blue: combined stellar and interstellar). The locations of photospheric (red) and interstellar (blue) lines reproduced by the synthetic spectrum are marked.

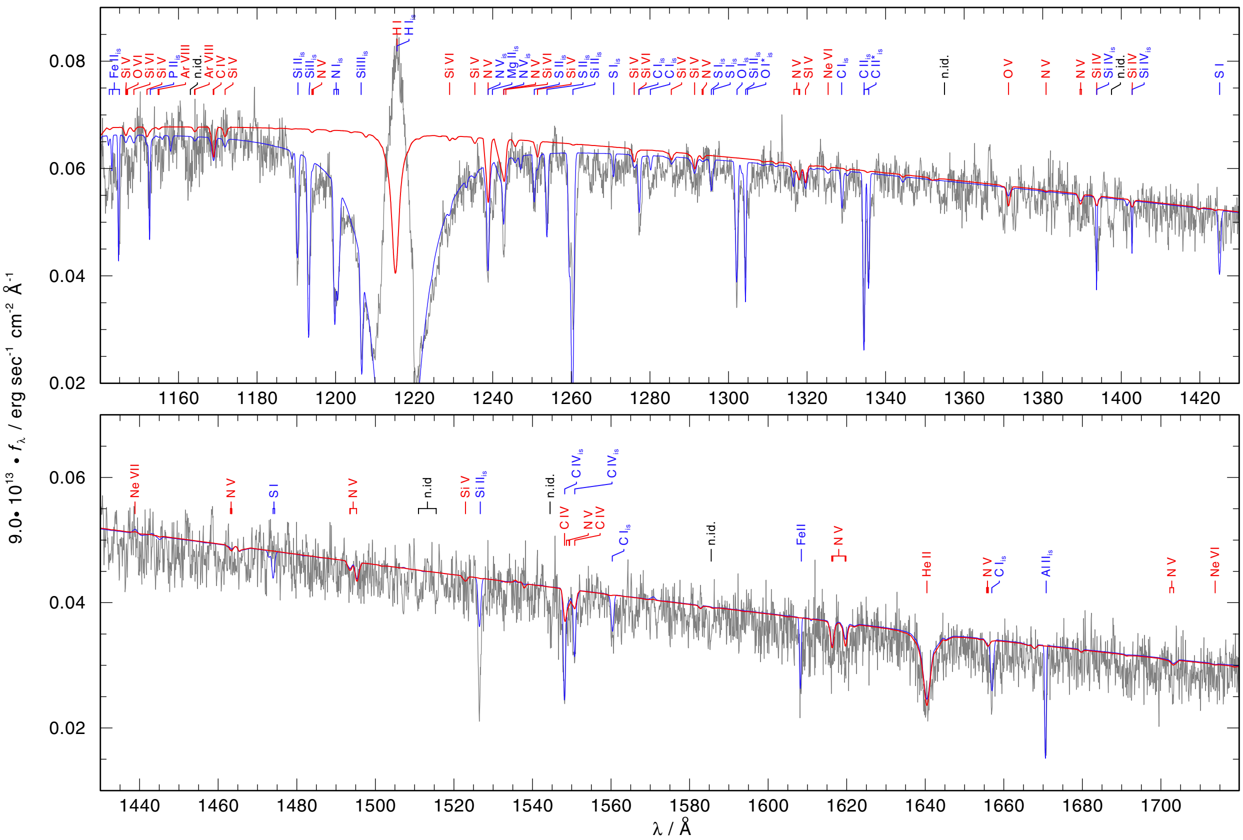

Fig. 6. Same as Fig. 5 for LoTr 4.

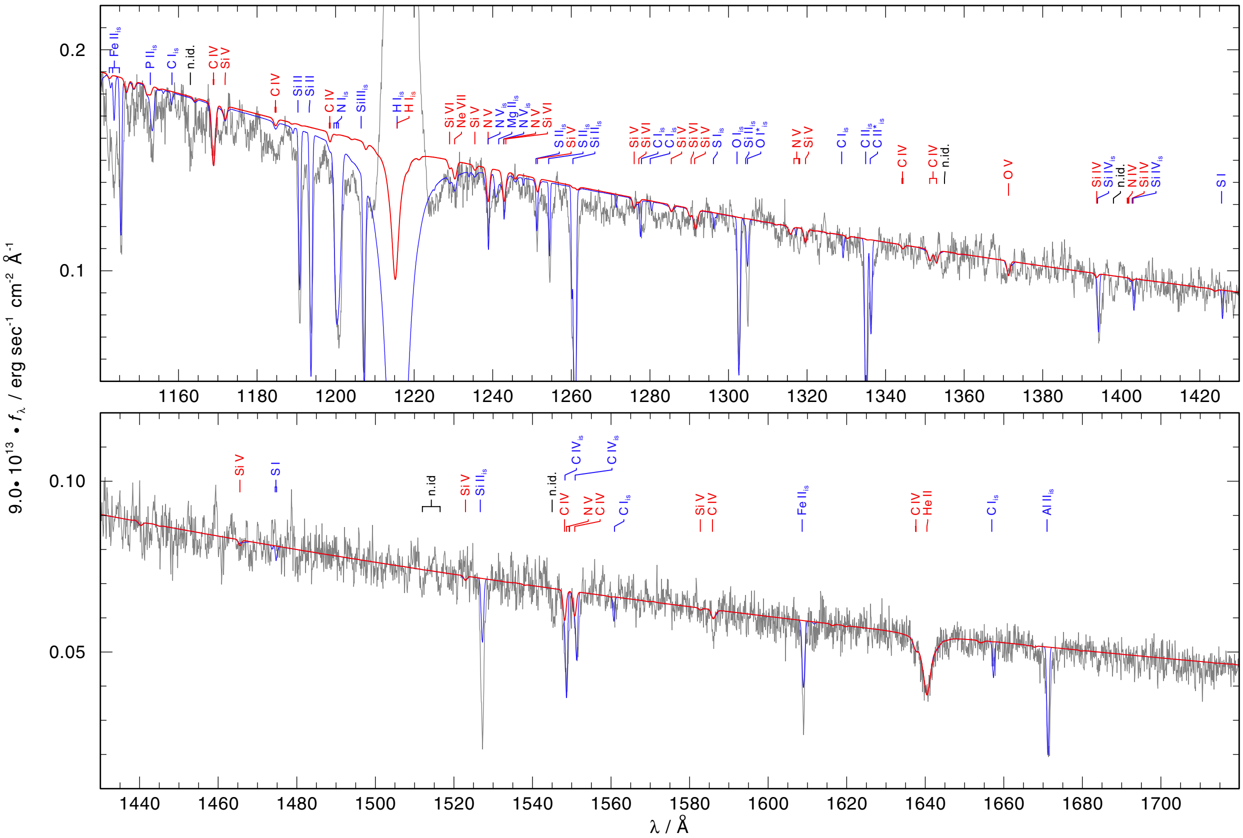

Fig. 7. Same as Fig. 5 for HS 1522+6615.

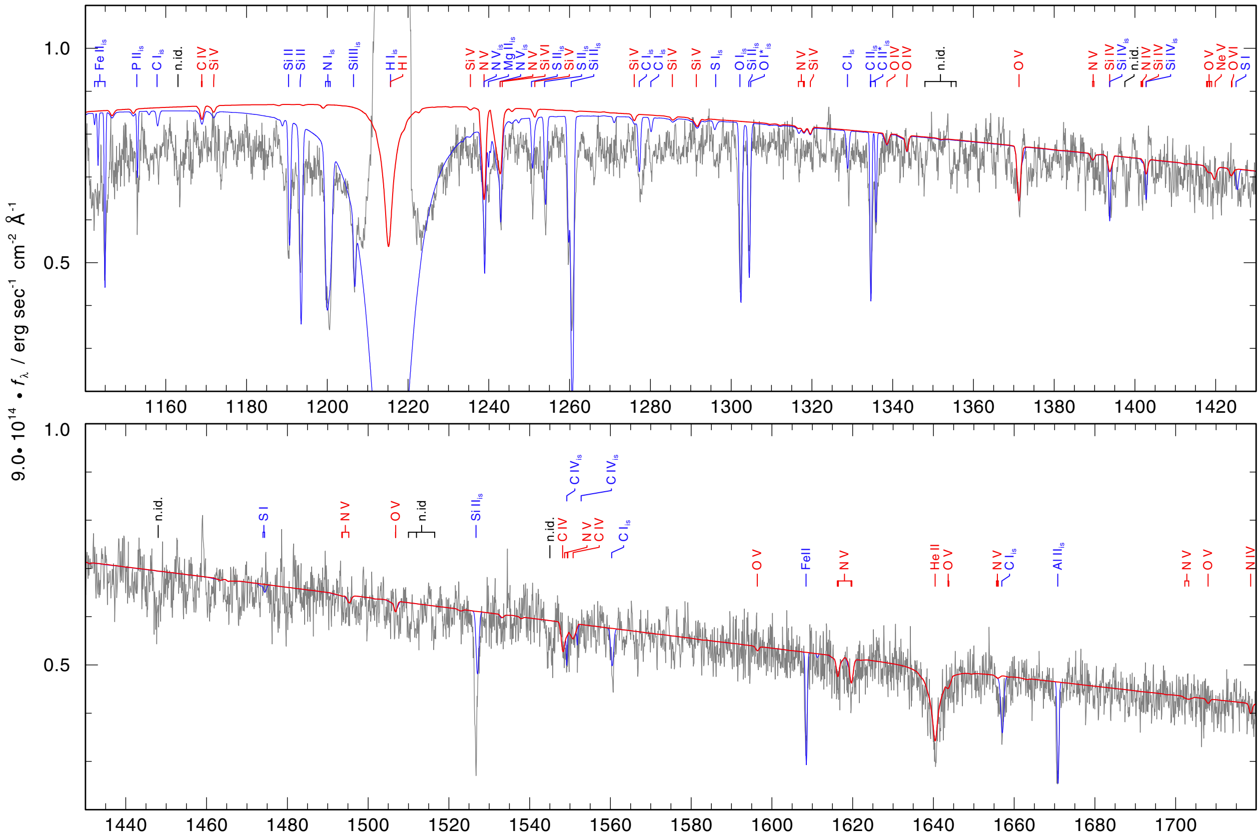

Fig. 8. Same as Fig. 5 for HS 2209+8229.

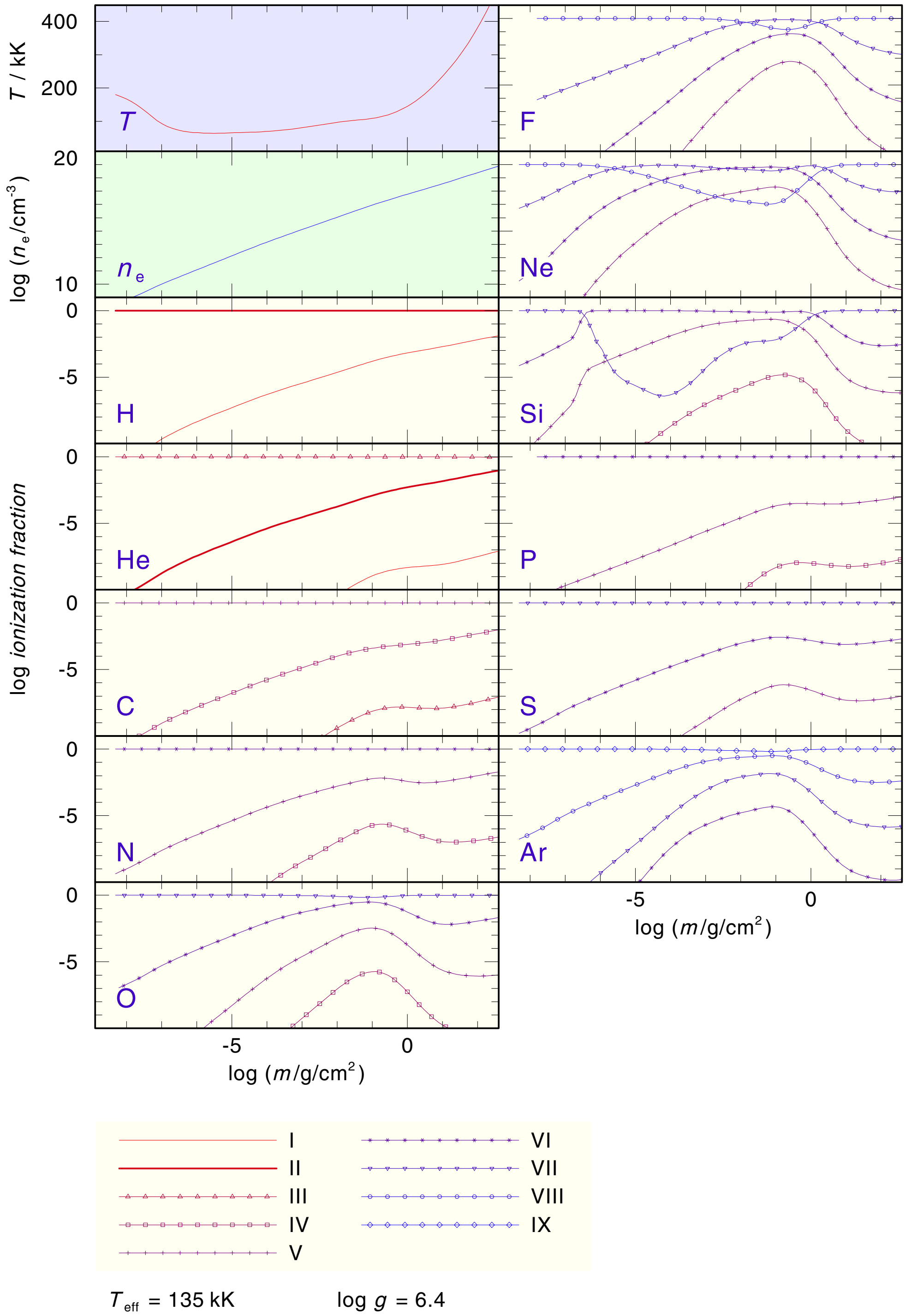

Fig. 9. Temperature, electron density stratification, and ionization fractions of all elements in our final model of K 1−27.

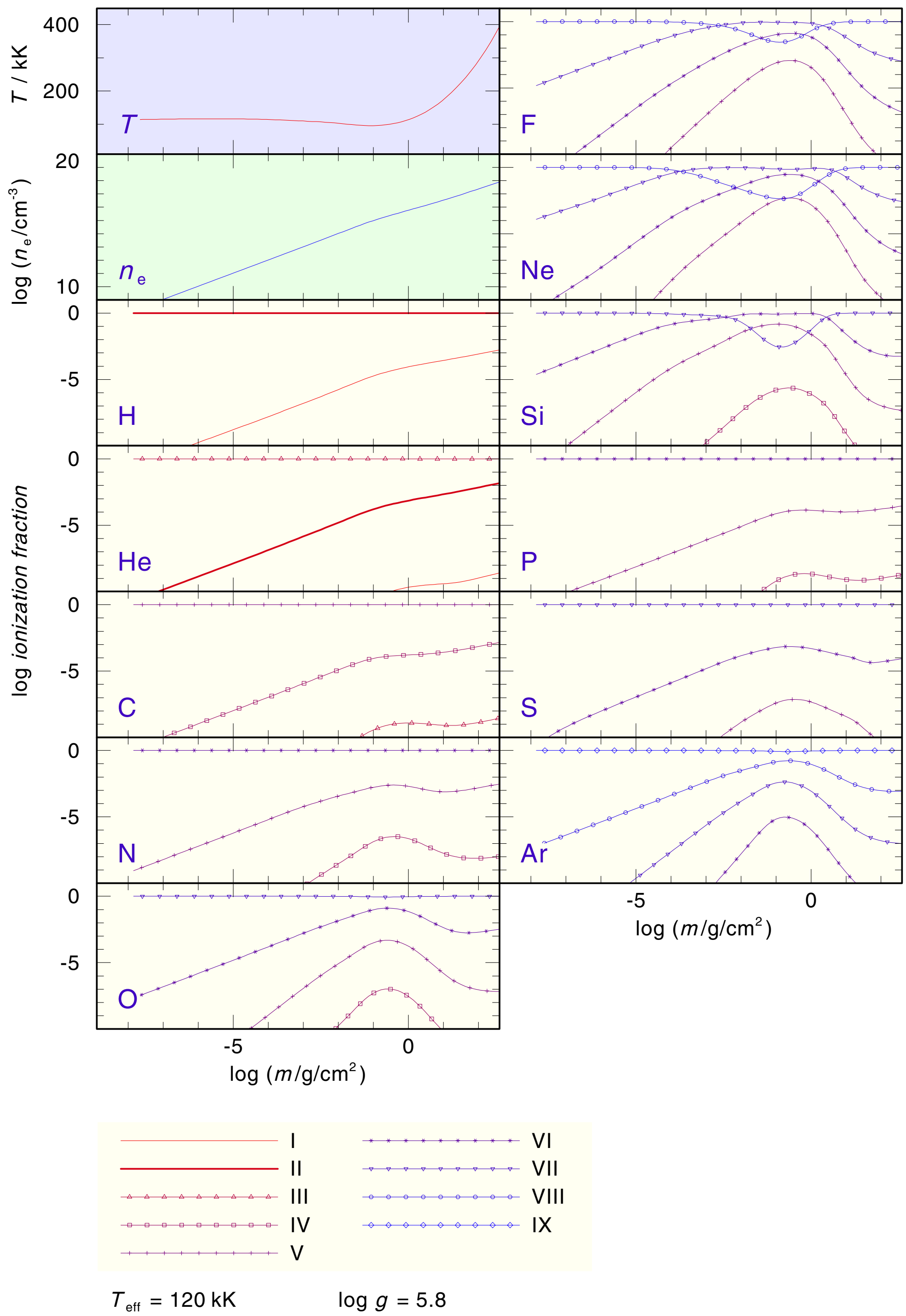

Fig. 10. Like Fig. 9, for LoTr 4.

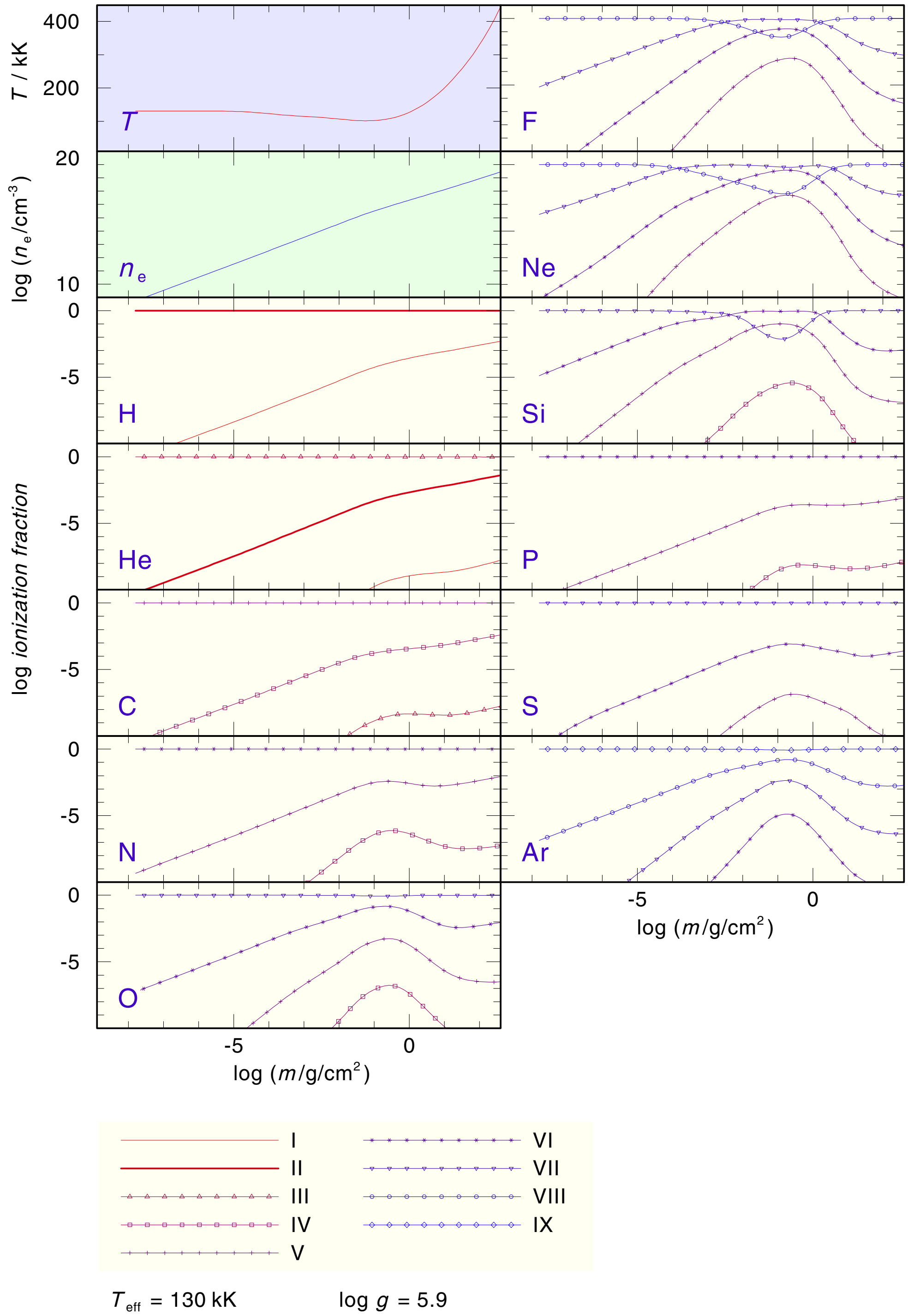

Fig. 11. Like Fig. 9, for HS 1522+6615.

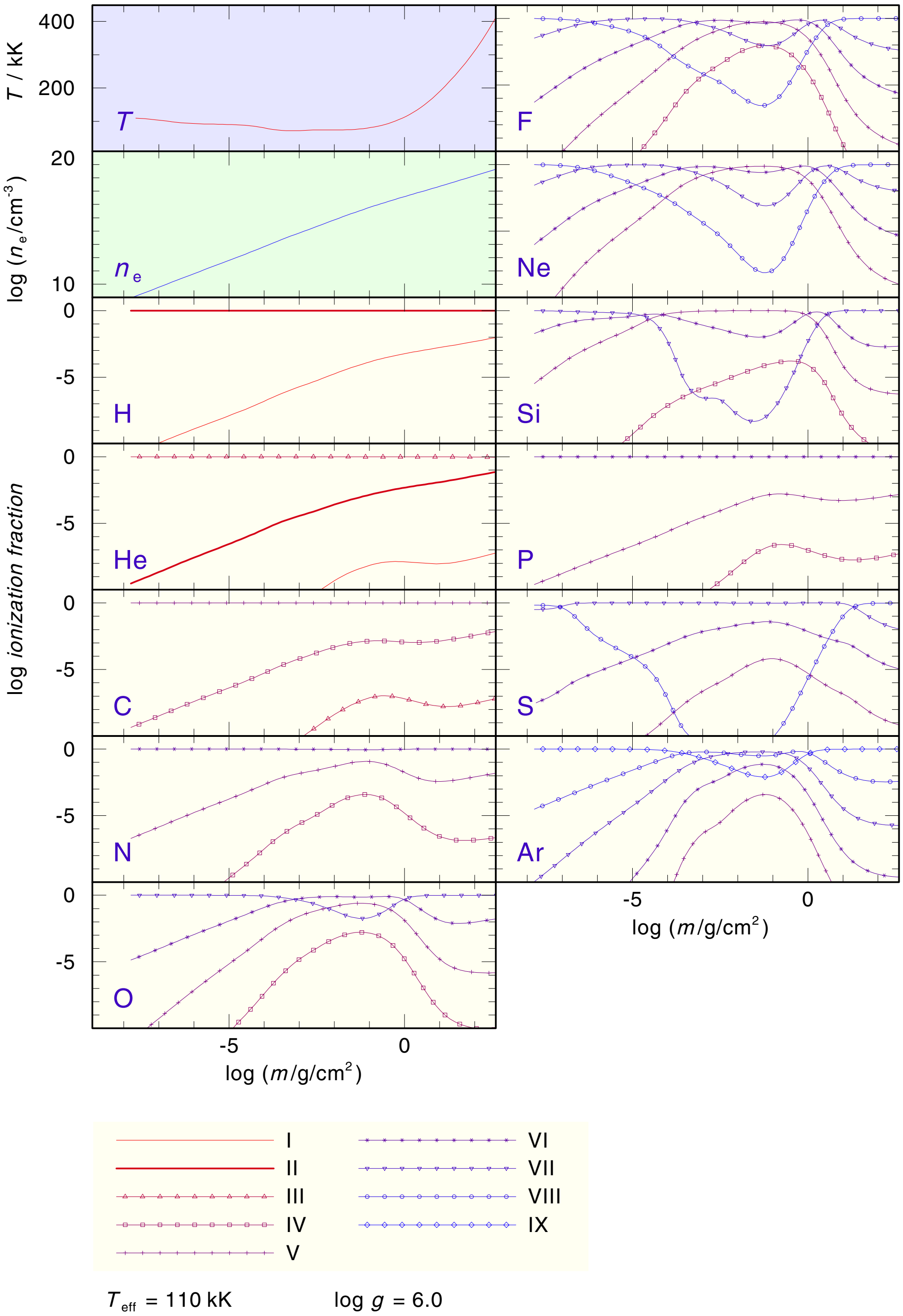

Fig. 12. Like Fig. 9, for HS 2209+8229.

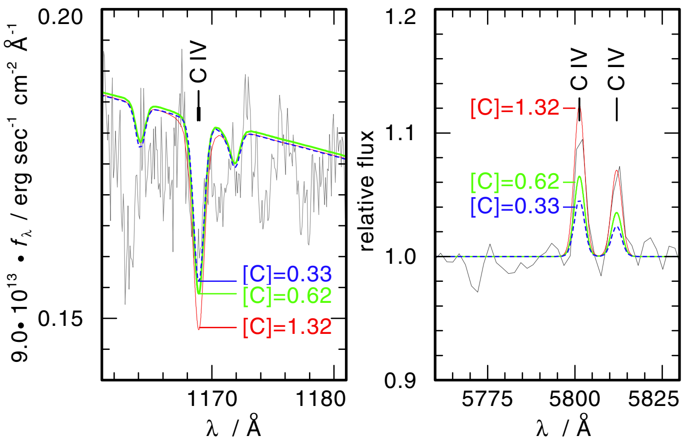

Fig. 21. Determination of the C abundance of HS 1522+6615. C IV lines are compared with models with different C abundances as indicated by the labels.

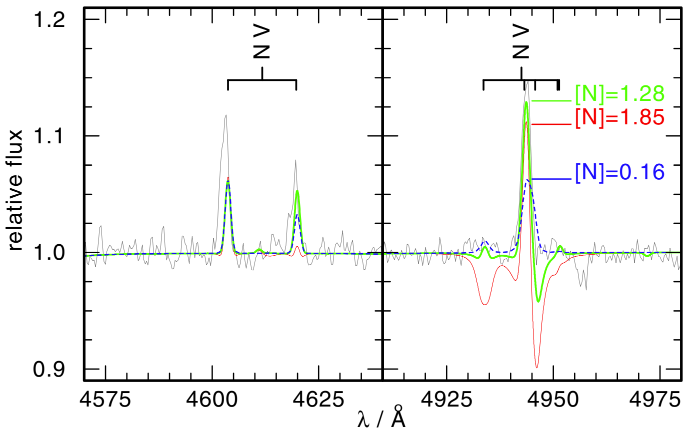

Fig. 22. Determination of the N abundance of K 1−27. N V lines in the EFOSC2 observation are compared with models with different N abundances as indicated by the labels.

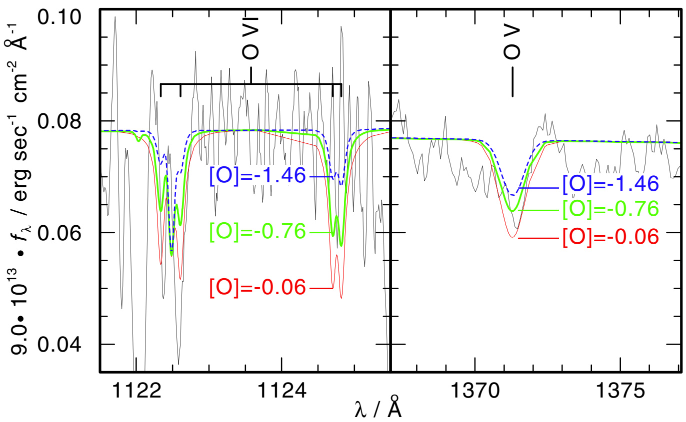

Fig. 23. Determination of the O abundance of HS 2209+8229. O V and O VI lines are compared with models with different O abundances as indicated by the labels.

Table 1. Statistics of the model atoms used in our TMAP calculations.

	$T_{\rm eff}$					
	>110 kK			≤110 kK		
ion	NLTE	LTE	lines	NLTE	LTE	lines
H I	10	6	45	10	6	45
H II	1	–	–	1	–	–
He I	5	98	3	5	98	3
He II	14	18	91	14	18	91
He III	1	–	–	1	–	–
C III	13	54	32	13	54	32
C IV	14	44	35	14	44	35
C V	1	0	0	1	0	0
N III	1	65	0	1	65	0
N IV	16	78	30	16	78	30
N V	14	48	35	14	48	35
N VI	1	0	0	1	0	0
O IV	18	76	39	18	76	39
O V	17	109	35	17	109	35
O VI	14	48	33	14	48	33
O VII	1	0	0	1	0	0
F V	1	10	0	1	10	0
F VI	6	6	0	6	6	0
F VII	2	4	0	2	4	0
F VIII	1	0	0	1	0	0
Ne IV	0	0	0	2	39	0
Ne V	14	80	18	14	80	18
Ne VI	14	17	30	14	17	30
Ne VII	15	94	27	15	94	27
Ne VIII	14	90	35	1	0	0
Ne IX	1	0	0	1	0	0
Si IV	12	11	24	12	11	24
Si V	25	0	59	25	0	59
Si VI	45	195	193	45	195	193
Si VII	1	0	0	1	0	0
P IV	15	36	9	15	36	9
P V	18	7	12	18	7	12
P VI	1	0	0	1	0	0
S V	23	87	47	23	87	47
S VI	25	12	25	25	12	25
S VII	1	0	0	1	0	0
Ar V				1	359	0
Ar VI	1	183	0	14	170	16
Ar VII	40	112	130	40	112	130
Ar VIII	13	28	24	13	28	24
Ar IX	1	0	0	1	0	0

A&A 572, A117 (2014)
DOI: 10.1051/0004-6361/201424861

Astronomy & Astrophysics

Analysis of cool DO-type white dwarfs from the Sloan Digital Sky Survey data release 10

N. Reindl[1], T. Rauch[1], K. Werner[1], S. O. Kepler[2], B. T. Gänsicke[3], and N. P. Gentile Fusillo[3]

[1] Institute for Astronomy and Astrophysics, Kepler Center for Astro and Particle Physics, Eberhard Karls University, Sand 1, 72076 Tübingen, Germany
e-mail: reindl@astro.uni-tuebingen.de
[2] Instituto de Física, Universidade Federal do Rio Grande do Sul, 91501-900 Porto Alegre, RS, Brazil
[3] Department of Physics, University of Warwick, Coventry, CV4 7AL, UK

Received 26 August 2014 / Accepted 17 October 2014

ABSTRACT

We report on the identification of 22 new cool DO-type white dwarfs (WDs) detected in data release 10 (DR10) of the Sloan Digital Sky Survey (SDSS). Among them, we found one more member of the so-called hot-wind DO WDs, which show ultrahigh excitation absorption lines. Our non-LTE model atmosphere analyses of these objects and two not previously analyzed hot-wind DO WDs, revealed effective temperatures and gravities in the ranges $T_{\rm eff} = 45-80$ kK and $\log g = 7.50-8.75$. In eight of the spectra we found traces of C (0.001−0.01, by mass). Two of these are the coolest DO WDs ever discovered that still show a considerable amount of C in their atmospheres. This is in strong contradiction with diffusion calculations, and probably, similar to what is proposed for DB WDs, a weak mass-loss is present in DO WDs. One object is the most massive DO WD discovered so far with a mass of 1.07 $M_\odot$ if it is an ONe-WD or 1.09 $M_\odot$ if it is a CO-WD. We furthermore present the mass distribution of all known hot non-DA (pre-) WDs and derive the hot DA to non-DA ratio for the SDSS DR7 spectroscopic sample. The mass distribution of DO WDs beyond the wind limit strongly deviates from the mass distribution of the objects before the wind limit. We address this phenomenon by applying different evolutionary input channels. We argue that the DO WD channel may be fed by about 13% by post-extreme-horizontal branch stars and that PG 1159 stars and O(He) stars may contribute in a similar extent to the non-DA WD channel.

Key words. stars: abundances – stars: evolution – stars: AGB and post-AGB – white dwarfs

1. Introduction

The vast majority of stars is expected to end as a white dwarf (WD), most of them (≈80%) with H-rich atmospheres, corresponding to the DA spectral type. These can be found all along the WD cooling sequence, that is, they have $4\,500 \le T_{\rm eff} \le 170\,000$ K (Sion 2011). In addition, there are the H-deficient WDs (non-DA WDs), which are usually divided into three subclasses: the DO spectral type ($45\,000 \le T_{\rm eff} \le 200\,000$ K), with the hot DO WDs showing strong He II lines, whereas in the spectra of cool DO WDs He I lines can also be seen; the DB type ($11\,000 \le T_{\rm eff} \le 45\,000$ K) showing strong He I lines; and the DC (featureless spectra), DQ, and DZ types ($T_{\rm eff} \le 11\,000$ K) showing traces of carbon and other metals in their spectra (Sion 2011). The overlap in temperature of the hottest DA and non-DA WDs strongly suggests the existence of a separate evolutionary channel for both classes. While a direct evolutionary connection for the H-rich central stars of planetary nebulae to the DA WDs is very likely (Napiwotzki & Schönberner 1995), the formation and evolution of non-DA WDs is less well understood.

DO WDs are commonly believed to be the successors of the PG 1159 stars (e.g., Werner et al. 2014; Althaus et al. 2009), which are hot ($75\,000 \le T_{\rm eff} \le 200\,000$ K) stars that show H-deficient and He-, C-, and O-rich surface compositions (typically He : C : O = 0.30−0.85 : 0.15−0.60 : 0.02−0.20 by mass, Werner & Herwig 2006). These abundances can be explained by a very late thermal pulse (VLTP), experienced by a WD during its early cooling phase (Iben et al. 1983; Althaus et al. 2005b). Most of the residual hydrogen envelope is engulfed by the helium-flash convection zone and completely burned at the beginning of this thermal pulse. The star is then forced to rapidly evolve back to the AGB and finally into a hydrogen-deficient, helium-burning PG 1159 star (Althaus et al. 2005b). As the star cools down, gravitational settling removes heavy elements from the photosphere and turns it into a DO WD (Unglaub & Bues 2000, unless it is of the subtype hybrid-PG 1159, then it turns into a DA WD).

In the past years it became more clear that the non-DA WDs are fed by distinct H-deficient evolutionary channels. In addition to the carbon-dominated sequence, a helium-dominated sequence exists (Althaus et al. 2009; Miszalski et al. 2012; Reindl et al. 2014; Frew et al. 2014). VLTP scenarios fail to reproduce the helium-rich atmospheres (He ≥ 95%, by mass) of He-rich subdwarf O (sdO) stars, R Coronae Borealis (RCB) stars, extreme helium (EHe) stars, [WN]-type central stars, and O(He) stars, suggesting that these objects have a different formation history. The origin of these stars remains uncertain. Their abundances match predictions of a double-helium WD merger scenario (Zhang & Jeffery 2012a,b), suggesting the evolutionary channel sdO(He) → O(He) → DO WD or, in case of C- and N-rich sdO and O(He) stars, RCB → EHe → sdO(He) → O(He) → DO WD (Reindl et al. 2014). The existence of planetary nebulae that do not show helium enrichment around every other O(He) star or [WN]-type central star, however, precludes a double-helium WD merger origin for these stars. These stars must have formed in a different way, for instance, by enhanced mass-loss during their post-AGB evolution, or a merger within a common envelope of a CO-WD and a red giant or AGB star (Reindl et al. 2014).

Dufour et al. (2007) reported the discovery of several WDs with atmospheres primarily composed of carbon, with little or no trace of hydrogen or helium. These stars do not fit satisfactorily in any of the currently known theories of post-AGB evolution. They are considered to be the cooler counterpart of the unique and extensively studied PG1159 star H1504+65 (Nousek et al. 1986; Werner 1991; Werner et al. 2004a) and might form a new evolutionary sequence that follows the AGB. Another case of H-deficient WDs that need to fit into the evolutionary picture are the oxygen-dominated WDs discovered by Gänsicke et al. (2010).

As a result of their fast evolutionary rate, there are only a few very hot H-deficient stars. A literature study revealed that there are currently only 46 known PG 1159 stars, 10 O(He) stars, and 52 DO WDs[1,2]. The detection and analysis of new DO WDs improve their statistics and thus helps to understand the origin of those objects. Furthermore, it is of importance for the construction of the hot end of the WD luminosity function. Its shape is an excellent tool for constraining the emission of particles in the core of hot DO WDs, for example, and to check for the possible existence of DFSZ axions, a proposed but not yet detected type of weakly interacting particles (Miller Bertolami et al. 2014; Miller Bertolami 2014).

In this paper, we first describe the observations and line identifications (Sect. 2). The spectral analysis follows in Sect. 3. The results are discussed in Sect. 4, where we mention the phenomenon of the so-called hot-wind DO WDs (Sect. 4.1) and debate the evolution of the C abundances before and along the non-DA WD cooling sequence (Sect. 4.2). The mass distribution of all known O(He) stars, PG 1159 stars, and DO WDs is presented in Sect. 4.3 and the hot DA to non-DA ratio in Sect. 4.4.

In the text, we use abbreviated versions of the object names. Full names are given in the Tables 1 and 2.

2. Observations and line identifications

Until 1996, only 22 DO WDs[3] were known (Dreizler & Werner 1996). Hügelmeyer et al. (2005, 2006) almost doubled this number with objects from the SDSS DR1, DR2, DR3, and DR4. Recently, Werner et al. (2014) detected ten new hot DO WDs in the SDSS DR 10. To complete the sample of DO WDs, we have visually scanned a color-selected sample of WD candidates in the SDSS DR10 and also searched for cool DO WDs. These are distinguished from the hot WDs by the presence of He I lines. To distinguish cool DO WDs from sdO stars, we only considered spectra with broad and only weak higher order ($n \geq 10$) He II lines. We found 24 objects (Figs. 1 and 2) that have not previously been analyzed with non-local thermodynamic equilibrium (LTE) model atmospheres. This sample includes two previously not analyzed hot-wind DO WDs (see below) and almost doubles the number of cool DO WDs below 80 kK.

Of the 24 stars, 14 were already included in the DR7 and also found by Kleinman et al. (2013). These authors classified 11 of the stars as DO WDs, two as DOBAH (J1442, J1509) and one as DBAH (J0005). The latter was already included in the SDSS DR4 catalog of spectroscopically confirmed WDs (Eisenstein et al. 2006) and classified as an sdO star. The analyses of Kleinman et al. (2013) and Eisenstein et al. (2006) were only based on LTE models and, thus do not provide reliable atmospheric parameters for DO WDs. Kleinman et al. (2013) listed 52 additional DO WDs, 28 of them previously analyzed with non-LTE model atmospheres. The remaining 24 had spectra with a too low signal-to noise ratio (S/N) or were either a misclassified cataclysmic variable (CV), misclassified He-sdO stars ($\log g \leq 7.0$), or DAO WDs. J0839 is listed as DAO WD, but might be a good candidate for a DO WD. The poor S/N, however, does not allow a precise spectral analysis. All these objects are listed in Table 1 and were rejected from our sample.

Table 1. DO WD candidates from the SDSS DR7 WD catalog (Kleinman et al. 2013) that were rejected from our sample.

SDSS name	g [mag]	S/N	Comment
J012602.53−004834.5	17.97	20	misclassified He−sdO
J014531.86+010629.7	20.15	8	poor quality spectrum
J024323.23+275045.5	19.48	12	poor quality spectrum
J025622.18+330944.7	19.70	10	poor quality spectrum
J065745.83+834958.5	19.18	18	poor quality spectrum
J080846.19+313106.0	19.44	53	misclassified CV
J081533.08+264646.4	19.48	19	poor quality spectrum
J083959.93+142858.0	18.61	6	poor quality spectrum
J094526.91+172917.2	20.28	5	poor quality spectrum
J102907.31+254008.4	17.35	16	misclassified DAO
J130249.00-013309.5	19.15	9	poor quality spectrum
J130249.00-013309.5	18.71	11	poor quality spectrum
J131816.55+485741.3	19.15	7	poor quality spectrum
J151246.56+071517.3	19.41	13	poor quality spectrum
J154829.87+203139.1	16.81	35	misclassified DAO
J155642.95+501537.5	15.81	43	misclassified He−sdO
J161512.22+110240.0	16.89	36	misclassified DAO
J163200.32−001928.3	18.37	20	misclassified DAO
J171600.52+422131.1	18.19	16	poor quality spectrum
J173027.20+265639.5	17.07	33	misclassified He−sdO
J173824.64+581801.8	18.36	13	poor quality spectrum
J205030.40−061957.9	17.98	21	misclassified DAO
J205930.25−052848.9	17.64	25	misclassified DAO
J213932.49+112611.3	19.29	9	poor quality spectrum

Table 2 lists all the DO WDs from our sample. In the spectra of six newly discovered objects (J0742, J0902, J1107, J1531, J1707, and J1717), we were able to detect the C IV $\lambda\lambda$ 4647, 4657, 4658, 4659, 4660, 5803, 5814 Å lines. For the first time, we identified C III lines in the spectra of two DO WDs. In the spectrum of J2239, we found C III $\lambda\lambda$ 4515, 4516, 4517, 4647, and 4650 Å, and in the spectrum of J0301, we additionally identified C III $\lambda\lambda$ 4056, 4068, 4069, 4070, 4187, and 4326 Å.

Our sample furthermore includes three members of the so-called hot-wind DO WDs, which show ultrahigh excitation (uhei) absorption lines. The uhei lines in the spectrum of J0747 (HS 0742+6520) were identifed for the first time. This star was first classified as an O(He) star by Heber et al. (1996), who discovered it in the Hamburg-Schmidt survey. However, because of the low S/N, the uhei features were not clearly visible in this spectrum. Sinamyan (2011) used empirical formulas to estimate $T_{\rm eff}$ and $\log g$ for 87 First Byurakan Survey (FBS) WDs. Based on the SDSS colors, he found for J0747 $T_{\rm eff} = 85\,279$ K and $\log g = 7.78$. J0201 (HS 0158+2335, discovered by Dreizler et al. 1995) and J0717 (also known as HS 0713+3958, discovered by Werner et al. 1995) are known DO WDs with uhei features. Since their SDSS spectra range up to 10 000 Å, we were able to identify additional lines beyond the hitherto observed Hα region (Table 3). Figure 2 shows the spectra of these DO WDs.

[1] This excludes the 22 new DO WDs from this paper.
[2] A list of all analyzed DO WDs can be found at http://astro.uni-tuebingen.de/~reindl/He
[3] This excludes KPD 0005+5106 which was recently reclassified as a pre-WD (Werner et al. 2014) and is now considered as an O(He) star (Reindl et al. 2014).

Table 2. Parameters of the new cool DO WDs.

SDSS name	$T_{\rm eff}$ [kK]	$\log g$ [cm/s^2]	C	M [$M_\odot$]	g [mag]	Remarks
J000509.93+003809.6	51^{+2}_{-2}	8.00 ± 0.25	<0.003	$0.64^{+0.14}_{-0.10}$	18.181	
J020127.20+234952.7	70^{+10}_{-10}	7.75 ± 0.50	<0.002	$0.58^{+0.11}_{-0.06}$	16.633	HS 0158+2335, uhei
J030130.10+050802.9	50^{+2}_{-1}	7.75 ± 0.25	$0.01^{+0.01}_{-0.005}$	$0.54^{+0.10}_{-0.07}$	18.392	
J071644.59+395808.9	60^{+10}_{-5}	8.25 ± 0.50	<0.05	$0.75^{+0.15}_{-0.09}$	18.591	
J071702.72+395323.6	80^{+10}_{-10}	7.75 ± 0.50	<0.003	$0.60^{+0.09}_{-0.07}$	16.295	HS 0713+3958, uhei
J072025.52+370336.3	52^{+2}_{-2}	7.75 ± 0.25	<0.01	$0.54^{+0.10}_{-0.07}$	18.271	
J073849.46+485126.6	60^{+10}_{-5}	8.00 ± 0.50	<0.01	$0.66^{+0.26}_{-0.16}$	18.695	
J074203.59+493333.8	60^{+10}_{-5}	7.75 ± 0.25	$0.002^{+0.001}_{-0.001}$	$0.56^{+0.10}_{-0.06}$	16.707	
J074725.15+651301.1	80^{+10}_{-10}	7.50 ± 0.50	<0.002	$0.53^{+0.16}_{-0.08}$	15.414	HS 0742+6520, uhei
J075633.77+163359.0	50^{+2}_{-2}	7.50 ± 0.25	<0.005	$0.49^{+0.05}_{-0.04}$	18.891	
J081739.99+163117.1	60^{+10}_{-9}	7.50 ± 0.50	<0.05	$0.50^{+0.06}_{-0.04}$	19.184	
J090227.65+125206.0	60^{+5}_{-5}	7.75 ± 0.25	$0.003^{+0.002}_{-0.001}$	$0.56^{+0.10}_{-0.06}$	17.049	
J090958.98+011105.4	51^{+2}_{-2}	7.50 ± 0.25	<0.003	$0.49^{+0.05}_{-0.04}$	16.660	
J103041.44+401312.6	55^{+5}_{-3}	8.00 ± 0.25	<0.005	$0.65^{+0.13}_{-0.16}$	17.348	
J110747.86+383550.8	60^{+5}_{-5}	8.00 ± 0.25	$0.003^{+0.002}_{-0.001}$	$0.66^{+0.12}_{-0.10}$	17.173	
J113816.30+382635.1	65^{+10}_{-10}	8.75 ± 0.50	<0.01	$1.08^{+0.18}_{-0.29}$	18.080	
J130717.27+004151.6	60^{+10}_{-10}	8.00 ± 0.50	<0.01	$0.66^{+0.26}_{-0.16}$	17.188	
J142440.79+330439.5	50^{+2}_{-2}	7.50 ± 0.25	<0.005	$0.49^{+0.05}_{-0.04}$	18.572	
J150927.22+292206.3	50^{+2}_{-1}	7.75 ± 0.25	<0.003	$0.54^{+0.10}_{-0.07}$	17.321	
J152943.01+183722.8	52^{+3}_{-3}	7.50 ± 0.25	<0.005	$0.49^{+0.05}_{-0.04}$	18.432	
J153133.11+343327.5	70^{+10}_{-5}	8.00 ± 0.25	$0.003^{+0.002}_{-0.001}$	$0.69^{+0.09}_{-0.11}$	15.834	
J170723.85+450009.9	60^{+10}_{-5}	8.00 ± 0.50	$0.003^{+0.002}_{-0.001}$	$0.66^{+0.26}_{-0.16}$	18.644	
J171720.52+373605.9	60^{+5}_{-5}	7.75 ± 0.25	$0.003^{+0.002}_{-0.001}$	$0.56^{+0.10}_{-0.06}$	17.880	
J223939.44+225925.9	45^{+1}_{-2}	7.50 ± 0.25	$0.001^{+0.002}_{-0.0009}$	$0.47^{+0.05}_{-0.05}$	18.248	

Notes. C abundances are given as mass fraction. uhei indicates objects with ultrahigh excitation features.

3. Spectral analysis

We used the Tübingen non-LTE model-atmosphere package (TMAP[4], Werner et al. 2003; Rauch & Deetjen 2003) to compute non-LTE, plane-parallel, fully metal-line-blanketed model atmospheres in radiative and hydrostatic equilibrium. The model atoms for this analysis were taken from the Tübingen model-atom database TMAD[5]. To calculate synthetic line profiles, we used Stark line-broadening tables provided by Barnard et al. (1969) for He I $\lambda\lambda$4026, 4388, 4471, 4921 Å, Barnard et al. (1974) for He I λ4471 Å and Griem (1974) for all other He I lines, and for He II and C IV we used the tables provided by Schöning & Butler (1989) and Schöning (1993). To account for the spectral resolution of the observations, synthetic spectra were convolved with Gaussians ($FWHM$ = 2.5 Å). All observed spectra were shifted to rest wavelengths by applying radial-velocity corrections by centroiding the He I and He II lines.

First, we calculated a pure-He model grid, spanning from $T_{\rm eff} = 45-90$ kK (in steps of 5 kK) and $\log g = 6.75-8.75$ (in steps of 0.25). Because the He I / He II ionization equilibrium is very sensitive around $T_{\rm eff} = 50$ kK, we refined the model grid from $T_{\rm eff} = 43-55$ kK to 1 kK steps. We reproduced all He lines and chose the best-fit models by visual comparison with the whole rectified observed WD spectra. To determine $T_{\rm eff}$, we used the He I / He II ionization equilibrium, and for the $\log g$ determination the wings of the He lines.

Then, we also included C (C = 0.0001, 0.0005, C = 0.001−0.01, in 0.001 steps, and C = 0.01−0.05, in 0.01 steps, by mass) into our best-fit models to derive C abundances by fitting all identified C lines (Sect. 2). Upper limits were derived by test models where the respective lines in the model contradicted the non-detection of the lines in the observation (at the abundance limit). For five stars (J0902, J1107, J1531, J1707, and J1717), we derived C = 0.003, which is slightly supersolar (solar abundance according to Asplund et al. 2009). For J0742 we found C = 0.002 (about solar). Two of our objects are the coolest DO WDs ever discovered that still show a considerable amount of C. J0301 ($T_{\rm eff} = 50$ kK) was found to have the highest C abundance in our sample (C = 0.01, about four times solar), and for J2239 ($T_{\rm eff} = 45$ kK) we found C = 0.001 (slightly subsolar).

[4] http://astro.uni-tuebingen.de/~TMAP
[5] http://astro.uni-tuebingen.de/~TMAD

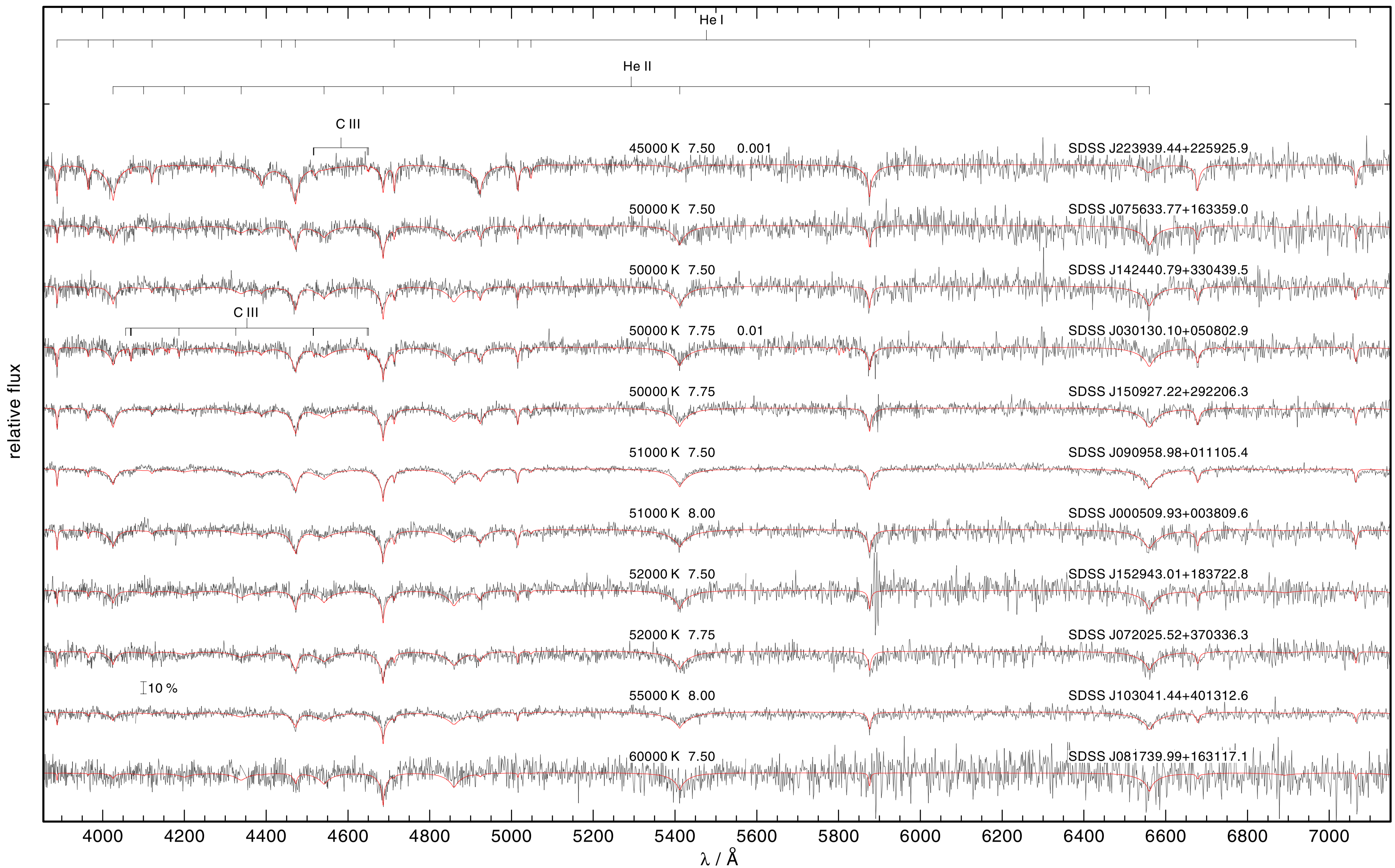

Fig. 1. Spectra of new cool DO WDs together with best-fit models. Each spectrum is labeled with $T_{\rm eff}$, $\log g$, the C abundance (mass fractions, where determined), and the SDSS name. The locations of photospheric lines are marked. The vertical bar indicates 10% of the continuum flux.

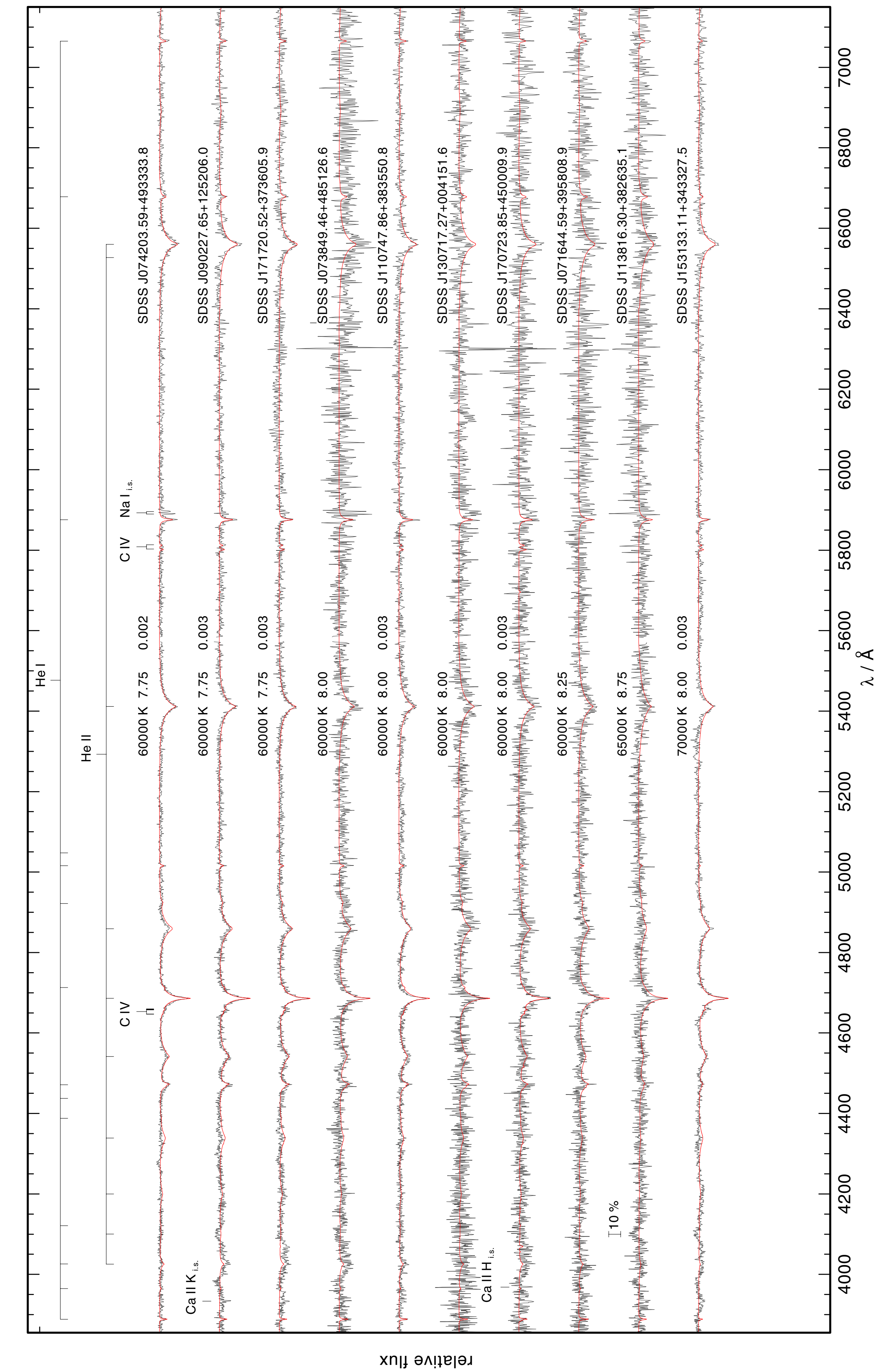

Fig. 1. continued.

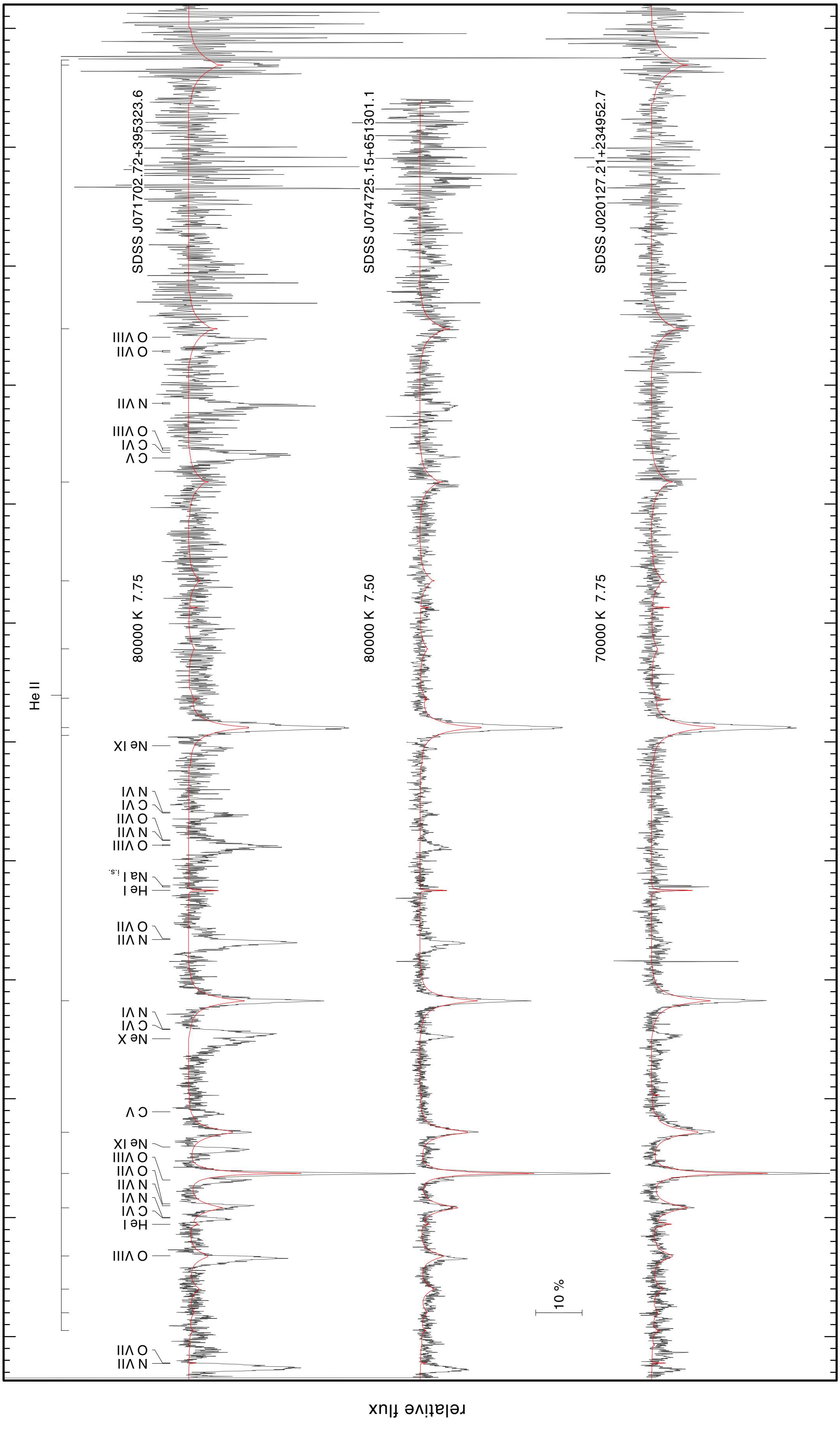

Fig. 2. DO WDs with ultrahigh excitation absorption lines. Each spectrum is labeled with $T_{\rm eff}$, $\log g$, and the SDSS name. The locations of photospheric lines and ultrahigh excitation features are marked. The vertical bar indicates 10% of the continuum flux.

The three DO WDs with uhei features clearly show He I λ5875.7 Å; the high S/N of the spectra of J0747 and J0201 also allowed the identification of He I λ4471.5 Å. We used these lines to constrain $T_{\rm eff}$ and found $T_{\rm eff} = 70$ kK for J0201 and $T_{\rm eff} = 80$ kK for J0717 and J0747. For the surface gravity of these objects we estimate $\log g = 7.75$ (for J0717 and J0201) and $\log g = 7.50$ (for J0747). For lower values of $\log g$, the Pickering lines below 4500 Å become too strong. Upper limits for $\log g$ were derived using He II $\lambda\lambda$4542, 4860, 8237 Å, which form deep in the atmosphere and might thus be least affected by the process that creates the too-deep He II lines. We summarize the results of our analysis in Table 2.

The additional opacities of C do not affect the theoretical He I and He II line profiles. We also investigated a possible impact of line blanketing by iron-group elements. For that, we calculated two test models with $T_{\rm eff} = 60, 80$ kK, and $\log g = 7.0$. Iron-group elements were included with a generic model atom (Rauch & Deetjen 2003) containing the elements Ca, Sc, Ti, V, Cr, Mn, Fe, Co, and Ni at solar abundance values. For the $T_{\rm eff} = 60$ kK model the ionization stages IV – VII were considered and for the $T_{\rm eff} = 80$ kK model the ionization stages V – IX. The model atom was calculated via the Tübingen iron-group opacity interface TIRO[6] (Müller-Ringat 2013). This has recently been developed in the framework of the Virtual Observatory (VO[7]) and is provided as a registered service by the German Astrophysical Virtual Observatory[8]. We found that for the pure-He models, the central depression of He II λ4686 Å is stronger than in the model that includes the iron-goup elements (42% stronger in the $T_{\rm eff} = 60$ kK model and 10% stronger in the $T_{\rm eff} = 80$ kK model). However, the profiles of all the other He I and He II lines remain unaffected.

4. Discussion

4.1. Hot-wind DO WDs

The discovery of uhei lines and unusually deep He II lines in the spectrum of J0747 makes it the eleventh member of the so-called hot-wind DO WDs. This class so far included eight other DO WDs: SDSS J105956.00+404332.4 (Werner et al. 2014), SDSS J151026.48+610656.9, SDSS J025403.75+005854.4 (Hügelmeyer et al. 2006), HS 0158+2335, HS 0727+6003, HS 2027+0651 (Dreizler et al. 1995), HE 0504-2408, HS 0713+3958 (Werner et al. 1995), one PG 1159 star: SDSS J121523.09+120300.8 (Hügelmeyer et al. 2006), and one DAO WD HS 2115+1148 (Dreizler et al. 1995). In addition, there are five other DO WDs known that also show too deep He II lines that they cannot be fitted by any model, but have no clear uhei features in their spectra: SDSS J082134.95+173919.40, SDSS J082724.44+585851.68, SDSS J094722.49+101523.62, SDSS J151215.72+065156.34 (Werner et al. 2014), and HE 1314+0018 (Werner et al. 2004b; Hügelmeyer et al. 2006). Werner et al. (2014) speculated that the same unknown process is at work here, affecting the He II lines, but failing to generate the strong uhei lines.

An attempt was made by Werner et al. (1995) to explain the uhei absorptions lines by extremely hot, static, plane-parallel non-LTE model atmospheres. The results showed that the observed spectra cannot have a photospheric origin assuming such an extreme $T_{\rm eff}$. Since the strongest of the uhei lines often show a very broad blue wing, it is believed that they are formed in a hot stellar wind that is optically thick in these transitions along the line of sight toward the stellar disk.

From constraining atmospheric parameters for these stars with the method described in Sect. 3, we cannot find any correlation of the temperature (e.g., the presence of He I lines), and the presence or strength of uhei features in these DO WDs.

The fraction of DO WDs showing this phenomenon is significant (19% show too deep He II lines, 11% show additional uhei features) and awaits an explanation.

4.2. C abundances

The detection of C in cool DO WDs is of particular interest in studying the chemical evolution of WDs and to place constraints on possible progenitors and successors of DO WDs.

The chemical evolution of hot WDs in the presence of diffusion and mass loss was studied by Unglaub & Bues (2000). Using the luminosity dependence of the mass-loss rate of Blöcker (1995), they predicted that until $T_{\rm eff} = 65$ kK the C abundance of a 0.529 $M_\odot$ star is reduced only by a factor of two. For stars with higher mass this occurs somewhat earlier, as indicated by the upper dashed line in Fig. 3. This figure also shows the locations of all analyzed DO WDs, PG 1159, and O(He) stars compared with VLTP evolutionary tracks from Althaus et al. (2009). As a consequence of increasing gravity and decreasing mass-loss rates, the effect of gravitational settling becomes more and more apparent. When the star has reached the lower dashed line in Fig. 3, the C abundance is expected to be reduced by a factor of ten. If the dependence of mass loss on the chemical composition is considered, an even sharper transition of PG 1159 stars into DO WDs is expected. We also show in Fig. 3 the corresponding theoretical wind limit for PG 1159 stars in which gravitational settling overcomes radiation-driven mass loss (thin solid line). The thick solid line in Fig. 3 corresponds to a ten times lower mass-loss rate and relates to the *observed* PG 1159 wind limit because no PG 1159 star is observed beyond that region. Assuming a lower mass-loss rate, however, also implies that the decrease of C abundances in DO WDs occurs earlier. Unglaub & Bues (2000) claimed that the co-existence of PG 1159 stars and DO WDs with various compositions and similar stellar parameters does not contradict an evolutionary link. Depending on their mass-loss rates, some objects may evolve into DO WDs somewhat earlier, others later.

Figure 4 illustrates the observed (logarithmic) C abundances as a function of $T_{\rm eff}$ for PG 1159 stars (values taken from Geier et al. in prep.; Werner & Rauch 2014; Werner et al. 2014; Schuh et al. 2008; Werner & Herwig 2006; Hügelmeyer et al. 2006), O(He) stars (Reindl et al. 2014; Werner et al. 2014; Wassermann et al. 2010), C-rich He-sdOs (Németh et al. 2012; Hirsch 2009), DO WDs, (this work; Werner et al. 2014; Hügelmeyer et al. 2006; Dreizler & Werner 1996), DB WDs (Provencal et al. 1996, 2000; Dufour et al. 2002; Petitclerc et al. 2005; Desharnais et al. 2008; Koester et al. 2014) and DQ WDs (Koester & Knist 2006; Dufour et al. 2005). Although there are some He-rich luminous PG 1159 stars, the vast majority of the luminous, that is, less evolved, PG 1159 stars (black, open triangles) display $C \approx 0.5$. Obviously, PG 1159 stars close to the wind limit ($T_{\rm eff} \leq 120$ kK and $\log g \geq 7.5$, black, filled triangles) display the lowest C abundances ($C \leq 0.22$, by mass), which means that they are lower by about a factor of two than the average of the luminous stars. This observational fact indeed supports the theory of advancing gravitational settling.

[6] http://astro.uni-tuebingen.de/~TIRO
[7] http://www.ivoa.net
[8] http://www.g-vo.org

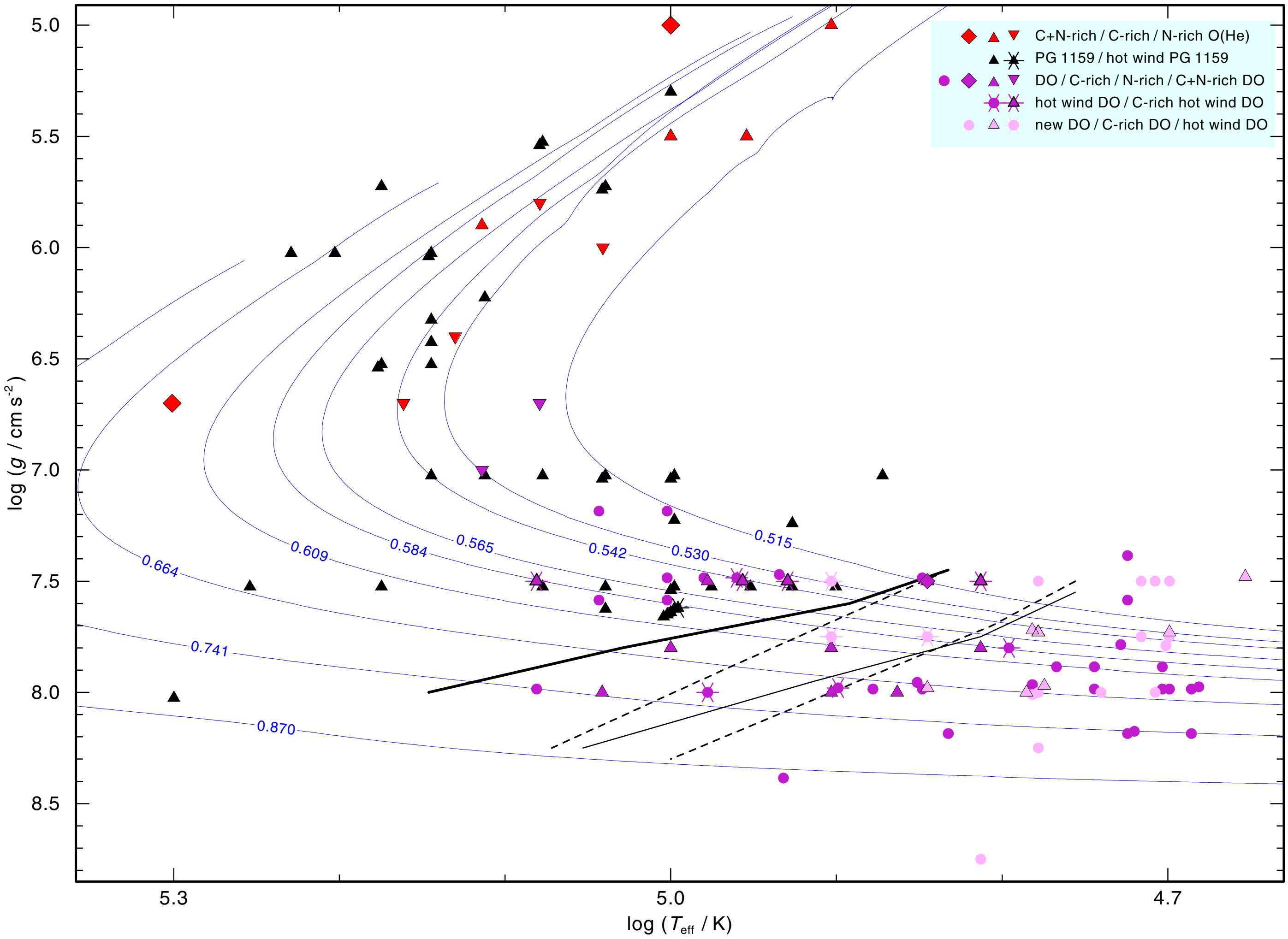

Fig. 3. Locations of O(He) stars (red, Reindl et al. 2014; Werner et al. 2014; Wassermann et al. 2010; De Marco et al. 2014), PG 1159 stars (black, Geier et al. in prep.; Werner et al. 2014; Gianninas et al. 2010; Werner & Herwig 2006; Schuh et al. 2008) and DO WDs (purple, this work, Werner et al. 2014; Mahsereci 2011; Hügelmeyer et al. 2006; Dreizler & Werner 1996; Nagel et al. 2006) in the log $T_{\rm eff}$–log g plane compared to VLTP post-AGB (solid lines) evolutionary tracks (labeled with stellar masses in $M_\odot$) of Althaus et al. (2009). The black solid and dashed lines indicate theoretical wind limits for abundance changes as predicted by Unglaub & Bues (2000) and discussed in Sect. 4.2.

On the other hand, the typical C abundances in DO WDs (0.001–0.01 by mass) do not change along the WD cooling track and are much closer to the C abundances observed in C-rich O(He) stars (typically 0.1–0.03 by mass, Werner et al. 2014; Reindl et al. 2014; Wassermann et al. 2010) than to those of PG 1159 stars. The discovery of a significant amount of C in the atmosphere of J0301, and still some detectable C in the atmosphere of J2239, emphasizes that gravitational settling might work less well than predicted by theory in the DO WD cooling region. According to Unglaub & Bues (2000), the C abundances of J0301 and J2239 should already have dropped far below the detectable limit. Dreizler (1999) also found no evidence for gravitational settling. By analyzing HST spectra of DO WDs ranging from $T_{\rm eff} = 50–100$ kK, he found that DO WDs can best be fitted with chemically homogeneous models, whereas the stratified models significantly deviated from the observations.

It is also interesting to note that the hot-wind DO WDs are located around the PG 1159–DO transition region predicted by Unglaub & Bues (2000). Given that the cause for their spectral anomaly is a fast wind, this would additionally stress that some mass-loss must still be occurring in DO WDs.

The observed C abundances found in DO WDs are also very similar to those observed in C-rich He-sdO stars. A non-LTE analysis of a large sample of these stars revealed C abundances in the range of 0.001–0.03 (Németh et al. 2012; Hirsch 2009). Especially J2239, for which we derived a mass of 0.47 $M_\odot$, might be a good candidate for a successor of a C-rich He-sdO star.

Traces of C ($0.9–9.5 \times 10^{-6}$, by mass) are also found in some hot DB WDs (Provencal et al. 1996, 2000; Dufour et al. 2002; Petitclerc et al. 2005; Desharnais et al. 2008; Koester et al. 2014) and cannot be easily explained either by any physical processes currently thought to operate in the envelopes of DB stars. Numerical simulations of Fontaine & Brassard (2005) showed that assuming a weak stellar wind of about 10^{-13} $M_\odot$/yr would sufficiently slow down the settling of C. However, their wind model has no physical basis and is not compatible with the thin radiatively driven winds discussed by Unglaub & Bues (2000) at much higher $T_{\rm eff}$. Moreover, the mass-loss rates are far below the detection limit.

The monotonic decrease of the C abundance with decreasing temperature in DQ stars, uncovered by Dufour et al. (2005)

Table 3. Identification of ultrahigh excitation features in J0717, J0747, and J0201.

Ion	λ/Å	J0717	J0747	J0201
C V	4945[4]	×		
	7694[2]	⋆	⋆	⋆
C VI	4499[5]	×		
	5291[5]	×	⋆	
	6201[5]	×	⋆	
	7717[2]	⋆	⋆	
N VI	4501[1]	×		
	5293[1]	×	⋆	×
	6204[1]	×	⋆	×
N VII	3887[5]	×	⋆	×
	4550[5]	×	⋆	×
	5669[5]	×	⋆	×
	6085[5]	×	⋆	×
	7921[1]	⋆	⋆	
	7926[1]	⋆	⋆	
O VII	3889[1]	×	⋆	×
	4558[1]	×	⋆	×
	5673[1]	×	⋆	×
	6088[1]	×	⋆	×
	8139[3]	⋆		
	8146[3]	⋆		
O VIII	4340[5]	×	⋆	
	4658[5]	×	⋆	×
	6064[5]	×	⋆	×
	6068[5]	×	⋆	×
	7726[1]	⋆	⋆	
	7736[1]	⋆	⋆	×
	8202[1]	⋆	⋆	
Ne IX	4797[1]	×	⋆	⋆
	6484[1]	×	⋆	×
Ne X	5252[1]	×	⋆	×

Notes. × denotes that these lines were already identified in J0717 by Werner et al. (1995) and in J0201 by Dreizler et al. (1995), while ⋆ denotes newly identified lines. [(1)] Hydrogenic value; [(2)] Engstrom et al. (1992); [(3)] Accad et al. (1971); [(4)] Moore (1970); [(5)] Garcia & Mack (1965).

and confirmed by Koester & Knist (2006), can be explained in terms of the dredge-up model developed by Pelletier et al. (1986). They predicted that the highest contamination occurs at around $T_{\rm eff} = 12$ kK, approximately the $T_{\rm eff}$ at which the base of the He convection zone reaches its highest depth. Below this $T_{\rm eff}$, C pollution decreases with further cooling, mainly because C sinks back into the star as a result of its partial recombination. The tight observational sequence found by Dufour et al. (2005) and Koester & Knist (2006) allowed Brassard et al. (2007) to pin down the masses of the He-dominated envelopes in DQ stars (10^{-2} to $10^{-3.75}$ $M_\odot$), which agrees with (V)LTP models. Hence, they reaffirmed the natural connection between PG 1159 stars, DO, DB, and DQ WDs. A completely different result was obtained by Scóccola et al. (2006). They found that PG 1159 stars cannot be related to any DQ WDs with low C abundances and instead suggested that the latter could be successors of RCB stars or C-poor post-extreme horizontal branch (EHB) stars. In that sense, we propose that O(He) stars should also be investigated as possible progenitors of DQ WDs. It is important to note, however, that Scóccola et al. (2006) failed to reproduce the decrease of the C abundance with decreasing temperature in DQ stars and instead found an *increase* of the C abundance with decreasing temperature.

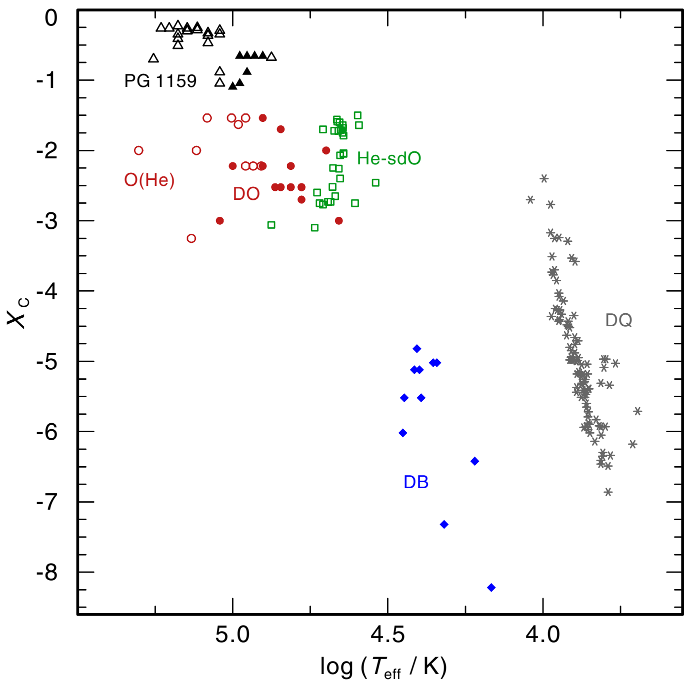

Fig. 4. Carbon abundances (in logarithmic mass fractions) before and along the non-DA WD cooling track. Luminous PG 1159 stars with $T_{\rm eff}$ > 120 kK and log g < 7.5 are represented by open, black triangles, PG 1159 stars close to the wind limit with $T_{\rm eff} \leq 120$ kK and log $g \geq 7.5$ by filled, black triangles, O(He) stars and DO WDs before the wind limit by open, red circles, DO WDs beyond the wind limit by filled, red circles, DB WDs by blue rhombs, and DQ WDs by gray stars.

4.3. Mass distribution

We derived the masses of the new cool DO WDs by comparing their positions in the log $T_{\rm eff}$–log g plane with VLTP evolutionary tracks from Althaus et al. (2009, Fig. 3). With $T_{\rm eff} = 65$ kK and log $g = 8.75$, J1138 clearly lies outside of the region covered by the VLTP tracks. Considering J1138 as CO-WD, we used CO-WD evolutionary tracks of Wood (1994), which extend up to 1.10 $M_\odot$. We found M = 1.09 $M_\odot$ with a lower limit of 0.79 $M_\odot$. Considering J1138 as an ONe-WD we used ONe-WD tracks of Althaus et al. (2005a) and derive M = 1.07 $M_\odot$ with an upper limit of 1.26 $M_\odot$. Lau et al. (2012) showed that because of instabilities in the late thermally pulsing-AGB phase of massive AGB stars with zero-age main-sequence masses of 7–10 $M_\odot$ and envelope masses of about 1–2 $M_\odot$, most of the envelope of these stars can be ejected. The outcome might be a central star (CS) of around 1 $M_\odot$ with a relatively massive planetary nebula (PN), like the so-far unique He-rich CS N66 (SMP 83), whose luminosity corresponds to a core mass of about 1.2 $M_\odot$ (Hamann et al. 2003). J1138 could be a successor of such a star. The very low frequency of massive DO WDs could be consistent with the fact that not all AGB stars going through such an ejection mechanism would eject all of their envelope and thus would instead become a massive DA WD.

The derived masses together with their errors (as resulting from the uncertainties in $T_{\rm eff}$ and log g) are given in Table 2. For J1138, we adopted the mean value given by both sets of tracks.

In the upper panel of Fig. 5, we show the mass distribution of the DO WDs of our sample. We derived a mean mass of $\langle M \rangle$ = 0.60 $M_\odot$ with a standard deviation of σ = 0.13 $M_\odot$. In the middle panel of Fig. 5 we show the mass distribution of all analyzed PG 1159 stars, O(He) stars, and DO WDs before the observed

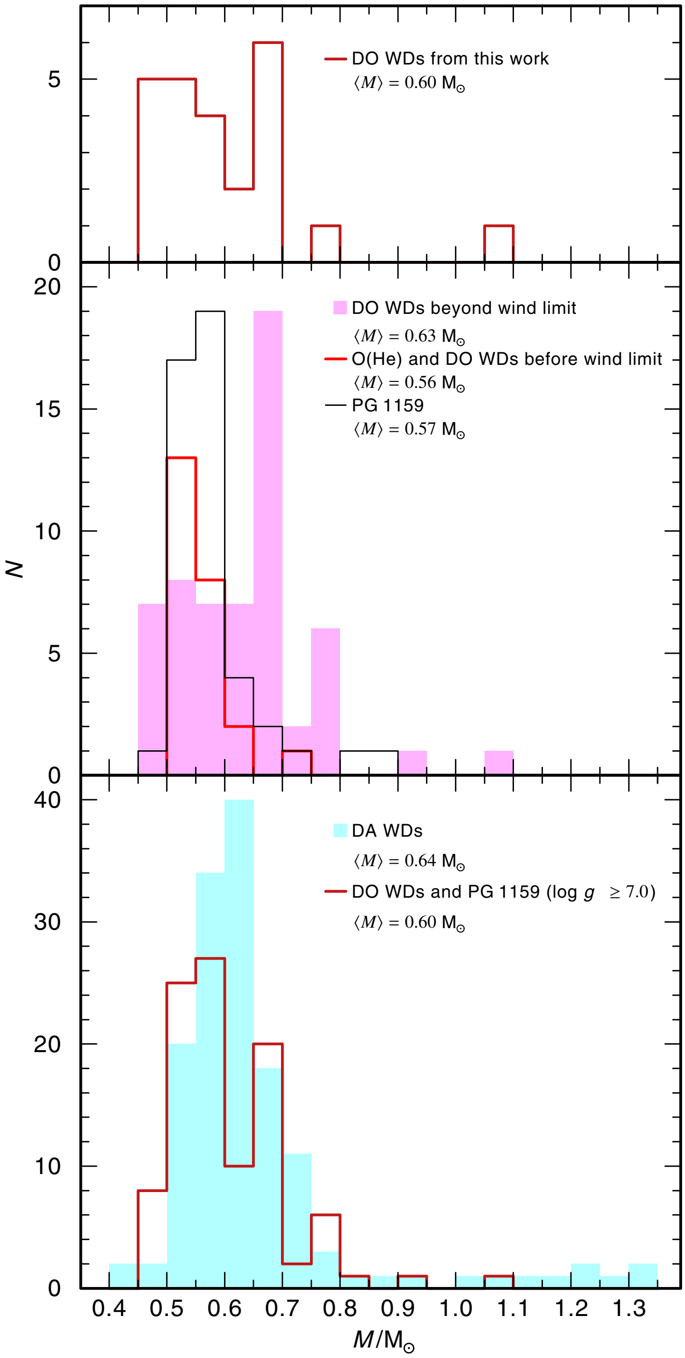

Fig. 5. *Upper panel*: mass distribution of all DO WDs from our sample. *Middle panel*: mass distribution of PG 1159 stars (thin black line), O(He) stars and DO WDs before the wind limit (thick red line), and DO WDs beyond the wind limit (gray area, light pink in the online version). *Lower panel*: mass distribution of the hot ($T_{\rm eff}$ $\geq$ 45 kK) DA WDs (gray area, light blue in the online version) from the sample of Giannias et al. (2011) compared with the mass distribution of non-DA WDs (PG 1159 and DO WDs with $\log g$ $\geq$ 7, thick red line).

wind limit[9] and DO WDs beyond the wind limit. To avoid systematic errors introduced by using different evolutionary tracks, we derived the masses for PG 1159 and O(He) stars by additionally using the VLTP tracks from Althaus et al. (2009). The mean mass of the O(He) stars and DO WDs before the wind limit ($\langle M\rangle$ = 0.56 $M_\odot$, with σ = 0.04 $M_\odot$) is slightly lower than the mean mass of the PG 1159 stars ($\langle M\rangle$ = 0.57 $M_\odot$, σ = 0.08 $M_\odot$). The mean mass of DO WDs beyond the wind limit is slightly higher ($\langle M\rangle$ = 0.63 $M_\odot$, σ = 0.11 $M_\odot$) than those of the objects before the wind limit. This trend continues in the mass distribution of DB WDs. Using only the spectra with S/N $\geq$ 15 out of their sample of 923 DB stars, Kleinman et al. (2013) found a mean mass of $\langle M\rangle$ = 0.685 $\pm$ 0.013 $M_\odot$. By restricting this sample to just those hotter than $T_{\rm eff}$ = 16 kK, they found a slightly lower mean mass of $\langle M\rangle$ = 0.676 $\pm$ 0.014 $M_\odot$. Bergeron et al. (2011) presented a detailed analysis of 108 DB WDs based on model atmosphere fits to high S/N optical spectroscopy. They derived an almost identical mean mass of 0.67 $M_\odot$ for their sample.

The phenomenon of increasing mean mass with decreasing $T_{\rm eff}$ is not restricted to non-DA WDs. Gianninas et al. (2011) presented the spectroscopic analysis of over 1100 bright ($V \geq 17.5$) DA white dwarfs. They found a mean mass of $\langle M\rangle$ = 0.661 $M_\odot$, with σ = 0.160 $M_\odot$, but by dividing their sample into objects with $T_{\rm eff}$ > 13 kK and $T_{\rm eff}$ < 13 kK, they also found that the mean mass of the hot objects ($\langle M\rangle$ = 0.638 $M_\odot$, σ = 0.145 $M_\odot$) is significantly lower than the mean mass of the cool DA WDs ($\langle M\rangle$ = 0.736 $M_\odot$, σ = 0.183 $M_\odot$). Tremblay et al. (2013) showed that this problem can be solved using 3D hydrodynamical models to compute spectra for the cool DA WDs. In the lower panel of Fig. 5 we therefore compare only the mass distributions of DA WDs with $T_{\rm eff}$ > 45 kK with those of the DO WDs and PG 1159 stars with $\log g \geq 7.0$. We derived mean masses of both classes to $\langle M\rangle$ = 0.64 $M_\odot$ (hot DA WDs) and $\langle M\rangle$ = 0.60 $M_\odot$ (non-DA WDs). The slightly higher mean mass for DA WDs results from the larger number of massive WDs, while a larger number of non-DA WDs with M < 0.5 $M_\odot$ is known. Seven out of the 55 (about 13%) DO WDs beyond the wind limit have M < 0.5 $M_\odot$, thus they are most likely post-EHB stars. The progenitors of these DO WDs might be He-sdO stars or low mass PG 1159 stars, such as HS 0704+6153 (Dreizler & Heber 1998). However, we emphasize that the errors on the masses are still large and that only a better $\log g$ determination can provide better constraints.

Another interesting feature that can be seen in the middle panel of Fig. 5 is that the mass distribution of the DO WDs beyond the wind limit compared with the mass distribution of the objects before the wind limit strongly disagree. While the flat plateau around 0.6 $M_\odot$ in the mass distribution of the DO WDs beyond the wind limit agrees with the mass distribution of PG 1159 stars, O(He) stars, and DO WDs before the wind limit, two additional peaks at 0.675 $M_\odot$ and 0.775 $M_\odot$ can be seen. The significant difference in the mass distributions is confirmed by a Kolmogorov-Smirnov test. The result of this test is that the probability that both samples are taken from the same mass distribution is rather small ($<10^{-4}$). The shape of the mass distributions before and beyond the wind limit are also preserved if we divide the stars into objects younger and older than 0.4 Myr, which approximately corresponds to a vertical line at $T_{\rm eff}$ = 80 kK (Althaus et al. 2009). This shows that the discrepancy in the mass distributions does not arise because the wind limit is reached earlier for more massive stars. Althaus et al. (2009) noted that the mass distribution of young DO WDs differs considerably from that of the older WDs. Werner et al. (2014) attributed the higher mean mass for DOs found by Hügelmeyer et al. (2006) to a calibration problem in the SDSS DR4. However, we found that using only the DO WDs from our analysis, we also see a peak around 0.675 $M_\odot$. Thus

[9] Since no gravitational settling is predicted for DO WDs before the wind limit, we placed them in the O(He) group.

we believe that this peak is real and not an artifact of a poor flux calibration.

This poses the question whether these two high-mass peaks display different input channels of DO WDs. Althaus et al. (2009) suggested that some DO WDs might result from evolutionary channels that do not involve PG 1159 stars. For instance, they could be the result of post-merger evolution involving RCB, EHe, luminous He-sdO stars, and O(He) stars. Reindl et al. (2014) found that using double He-WD merger tracks from Zhang & Jeffery (2012b) instead of VLTP tracks, the masses of O(He) stars are $0.07-0.16\,M_{\odot}$ higher. This would indeed shift the mean mass of these stars closer to the higher mass peaks of DO WDs beyond the wind limit. Comparing the evolutionary tracks of Zhang & Jeffery (2012b) and Althaus et al. (2009), we found that they differ significantly only in the luminous part ($T_{\rm eff} > 100$ kK) in the log $T_{\rm eff}$–log g plane. We again derived the masses of all O(He) stars and DO WDs before the wind limit using the tracks of Zhang & Jeffery (2012b) and found a mean mass of $\langle M \rangle = 0.62\,M_{\odot}$ instead of the $\langle M \rangle = 0.56\,M_{\odot}$ found using the tracks of Althaus et al. (2009). Although a double He-WD merger can be excluded for some O(He) stars, we claim that a contribution of post-double He-WD mergers to the observed higher mass peaks in the mass distribution of the DO WDs beyond the wind limit is possible. We also stress that determining the mass through evolutionary tracks requires knowing the evolutionary history of an object, which is very unclear at least for the He-dominated objects.

Another possible origin of DO WDs with higher masses are H-deficient [WC] or [WN]-type central stars. A spectroscopic mass determination for these objects is, however, extremely difficult since log g cannot be derived from photospheric lines. Wind emission lines do not depend on the first approximation of L and M. For the spectral analysis of these stars, it is common practice to assume standard values of log g or M (e.g., log $g = 6.0$ or $M = 0.6\,M_{\odot}$), which are equivalent input parameters for wind codes. The two currently known [WN]-type central stars IC 4663 (Miszalski et al. 2012) and Abell 48 (Todt et al. 2013; Frew et al. 2014) are in an evolutionary state similar to or even later than the O(He) stars, but show much stronger stellar winds. Reindl et al. (2014) speculated that [WN] stars are O(He) stars, but with higher masses and hence higher luminosity, which could explain the higher mass-loss rates of [WN] stars.

4.4. Ratio of DAs to non-DAs for hot WDs

The sample of Gianninas et al. (2011) comprised 131 DA WDs with $T_{\rm eff} > 45$ kK, while there are 49 PG 1159 stars with log $g \geq 7.0$, and DO WDs (hot non-DA WDs) known with $V \leq 17.5$. This would lead to a ratio of hot DAs to non-DAs of 2.7. However, neither sample can be considered complete. To correctly calculate the ratio of hot DAs to non-DAs, it is necessary to compare samples with the same the magnitude limit, sky coverage, and completeness. No systematic search for hot DA WDs in the SDSS DR 10 was presented so far, therefore we restricted ourselves to the SDSS DR7 spectroscopic sample. Since we compare objects in the same $T_{\rm eff}$ range, incompleteness should affect both subclasses in the same manner. Atmospheric parameters derived by Kleinman et al. (2013) are only based on LTE models, and thus they show large differences for $T_{\rm eff} \gtrsim 50$ kK compared with the objects they had in common with the sample of Gianninas et al. (2011). However, to distinguish whether a DA WD is hotter or cooler than $T_{\rm eff} = 45$ kK, LTE models are probably good enough. By comparing pure He and H model atmosphere fluxes, we found that at $T_{\rm eff} = 45$ kK DA WDs are about 0.1 mag brighter than DO WDs. Accordingly, we set the magnitude limit for DA WDs to $g < 17.4$ and for DO WDs to $g < 17.5$. We found in total 117 DA WDs with $T_{\rm eff} > 45$ kK, with 81 of them clean DA WDs (no subtypes, e.g. DAO, DAM, DAH). On the other hand we found 23 hot non-DA WDs in the SDSS DR7 spectroscopic sample with $g < 17.5$, leading to DA/non-DA = 5.1, with a lower limit of 3.5 if we consider clean DA WDs alone.

Among the H-deficient objects before the wind limit that are included in the SDSS DR 10 spectroscopic sample, we find 18 PG 1159 stars and 12 O(He) stars and DO WDs, which leads to a ratio of C-dominated to He-dominated objects of 1.5. Including log $g > 7.0$ objects alone, the ratio of C-dominated to He-dominated objects is 0.75. This suggests that DO WDs beyond the wind limit may be fed to a similar extent by PG 1159 and O(He) stars.

4.5. Conclusions

We have visually scanned a color-selected sample of white dwarf candidates in the SDSS DR10 and identified 22 new cool DO white dwarfs. Effective temperatures, surface gravities, and C abundances (or at least upper limits) for 24 DO WDs were derived with non-LTE model atmospheres. Among the newly identified DO WDs, we found one more member of the so-called hot-wind DO WDs, which shows uhei absorption lines. One of the DO WDs is the most massive DO WD ever discovered with a mass of 1.07 $M_{\odot}$ if it is an ONe-WD or 1.09 $M_{\odot}$ if it is a CO-WD. Two of our objects are the coolest DO WDs ever discovered that still show a considerable amount of C in the atmosphere ($C = 0.001-0.01$). This strongly contradicts the diffusion calculations of Unglaub & Bues (2000). We suggest that – similar to what has been proposed for the cooler DB stars – a weak mass-loss is present in cool DO WDs. Furthermore, we presented the mass distribution of all hitherto analyzed DO WDs, PG 1159, and O(He) stars. We found that the mass distribution of DO WDs beyond the wind limit strongly deviates from the mass distribution of the objects before the wind limit and explained this phenomenon with a scenario of different input channels. The plateau around $0.6\,M_{\odot}$ in the mass distribution of DO WDs beyond the wind limit agrees with the mass distribution of PG 1159 stars, O(He) stars, and DO WDs before the wind limit. The two additional higher mass peaks might reflect a merger origin of some O(He) stars and DO WDs and/or the possibility that [WN] and [WC] type central stars are more massive than PG1159 and O(He) stars. The non-DA WD channel may be fed by about 13% by low-mass PG 1159 stars and post-EHB He-sdO stars. PG 1159 stars and O(He) stars may contribute to a similar extent to the non-DA WD channel.

Acknowledgements. N.R. is supported by the German Research Foundation (DFG, grant WE 1312/41-1), T.R. by the German Aerospace Center (DLR, grant 05 OR 1401). The research leading to these results has received funding from the European Research Council under the European Union's Seventh Framework Programme (FP/2007-2013)/ERC Grant Agreement No. 320964 (WDTracer). B.T.G. was supported in part by the UK's Science and Technology Facilities Council (ST/I001719/1). Funding for SDSS-III has been provided by the Alfred P. Sloan Foundation, the Participating Institutions, the National Science Foundation, and the US Department of Energy Office of Science. The SDSS-III web site is http://www.sdss3.org/. SDSS-III is managed by the Astrophysical Research Consortium for the Participating Institutions of the SDSS-III Collaboration including the University of Arizona, the Brazilian Participation Group, Brookhaven National Laboratory, Carnegie Mellon University, University of Florida, the French Participation Group, the German Participation Group, Harvard University, the Instituto de Astrofisica de Canarias, the Michigan State/Notre Dame/JINA Participation Group, Johns

Hopkins University, Lawrence Berkeley National Laboratory, Max Planck Institute for Astrophysics, Max Planck Institute for Extraterrestrial Physics, New Mexico State University, New York University, Ohio State University, Pennsylvania State University, University of Portsmouth, Princeton University, the Spanish Participation Group, University of Tokyo, University of Utah, Vanderbilt University, University of Virginia, University of Washington, and Yale University. This research has made use of the SIMBAD database, operated at CDS, Strasbourg, France. This research has made use of the VizieR catalogue access tool, CDS, Strasbourg, France.

References

Accad, Y., Pekeris, C. L., & Schiff, B. 1971, Phys. Rev. A, 4, 516
Ahn, C. P., Alexandroff, R., Allende Prieto, C., et al. 2012, ApJS, 203, 21
Althaus, L. G., García-Berro, E., Isern, J., & Córsico, A. H. 2005a, A&A, 441, 689
Althaus, L. G., Serenelli, A. M., Panei, J. A., et al. 2005b, A&A, 435, 631
Althaus, L. G., Panei, J. A., Miller Bertolami, M. M., et al. 2009, ApJ, 704, 1605
Asplund, M., Grevesse, N., Sauval, A. J., & Scott, P. 2009, ARA&A, 47, 481
Barnard, A. J., Cooper, J., & Shamey, L. J. 1969, A&A, 1, 28
Barnard, A. J., Cooper, J., & Smith, E. W. 1974, J. Quant. Spectr. Rad. Transf., 14, 1025
Bergeron, P., Wesemael, F., Dufour, P., et al. 2011, ApJ, 737, 28
Blöcker, T. 1995, A&A, 299, 755
Brassard, P., Fontaine, G., Dufour, P., & Bergeron, P. 2007, in 15th European Workshop on White Dwarfs, eds. R. Napiwotzki, & M. R. Burleigh, ASP Conf. Ser., 372, 19
De Marco, O., Long, J., George, H. J., et al. 2014, MNRAS, submitted
Desharnais, S., Wesemael, F., Chayer, P., Kruk, J. W., & Saffer, R. A. 2008, ApJ, 672, 540
Dreizler, S. 1999, A&A, 352, 632
Dreizler, S., & Heber, U. 1998, A&A, 334, 618
Dreizler, S., & Werner, K. 1996, A&A, 314, 217
Dreizler, S., Heber, U., Napiwotzki, R., & Hagen, H. J. 1995, A&A, 303, L53
Dufour, P., Wesemael, F., & Bergeron, P. 2002, ApJ, 575, 1025
Dufour, P., Bergeron, P., & Fontaine, G. 2005, ApJ, 627, 404
Dufour, P., Liebert, J., Fontaine, G., & Behara, N. 2007, Nature, 450, 522
Eisenstein, D. J., Liebert, J., Harris, H. C., et al. 2006, ApJS, 167, 40
Engstrom, L., Bengtsson, P., Jupen, C., & Westerlind, M. 1992, J. Phys. B At. Mol. Phys., 25, 2459
Fontaine, G., & Brassard, P. 2005, in 14th European Workshop on White Dwarfs, eds. D. Koester, & S. Moehler, ASP Conf. Ser., 334, 49
Frew, D. J., Bojičić, I. S., Parker, Q. A., et al. 2014, MNRAS, 440, 1345
Gänsicke, B. T., Koester, D., Girven, J., Marsh, T. R., & Steeghs, D. 2010, Science, 327, 188
Gianninas, A., Bergeron, P., Dupuis, J., & Ruiz, M. T. 2010, ApJ, 720, 581
Gianninas, A., Bergeron, P., & Ruiz, M. T. 2011, ApJ, 743, 138
Griem, H. R. 1974, Spectral line broadening by plasmas (New York: Academic Press), 39, 421
Hamann, W.-R., Peña, M., Gräfener, G., & Ruiz, M. T. 2003, A&A, 409, 969
Heber, U., Dreizler, S., & Hagen, H.-J. 1996, A&A, 311, L17
Hirsch, H. A. 2009, Ph.D. Thesis, University Nuremberg, Germany
Hügelmeyer, S. D., Dreizler, S., Werner, K., et al. 2005, A&A, 442, 309
Hügelmeyer, S. D., Dreizler, S., Homeier, D., et al. 2006, A&A, 454, 617
Iben, Jr., I., Kaler, J. B., Truran, J. W., & Renzini, A. 1983, ApJ, 264, 605
Kleinman, S. J., Kepler, S. O., Koester, D., et al. 2013, ApJS, 204, 5
Koester, D., & Knist, S. 2006, A&A, 454, 951
Koester, D., Provencal, J., & Gänsicke, B. T. 2014, A&A, 568, A118
Lau, H. H. B., Gil-Pons, P., Doherty, C., & Lattanzio, J. 2012, A&A, 542, A1
Mahsereci, M. 2011, Diploma thesis, University Tübingen, Germany
Miller Bertolami, M. M. 2014, A&A, 562, A123
Miller Bertolami, M. M., Melendez, B. E., Althaus, L. G., & Isern, J. 2014, JCAP, 10, 069
Miszalski, B., Crowther, P. A., De Marco, O., et al. 2012, MNRAS, 423, 934
Moore, C. E. 1970, Selected tables of atomic spectra (NSRDS-NBS)
Müller-Ringat, E. 2013, Dissertation, University of Tübingen, Germany, http://tobias-lib.uni-tuebingen.de/volltexte/2013/6774/
Nagel, T., Schuh, S., Kusterer, D.-J., et al. 2006, A&A, 448, L25
Napiwotzki, R., & Schönberner, D. 1995, A&A, 301, 545
Németh, P., Kawka, A., & Vennes, S. 2012, MNRAS, 427, 2180
Nousek, J. A., Shipman, H. L., Holberg, J. B., et al. 1986, ApJ, 309, 230
Pelletier, C., Fontaine, G., Wesemael, F., Michaud, G., & Wegner, G. 1986, ApJ, 307, 242
Petitclerc, N., Wesemael, F., Kruk, J. W., Chayer, P., & Billères, M. 2005, ApJ, 624, 317
Provencal, J. L., Shipman, H. L., Thejll, P., Vennes, S., & Bradley, P. A. 1996, ApJ, 466, 1011
Provencal, J. L., Shipman, H. L., Thejll, P., & Vennes, S. 2000, ApJ, 542, 1041
Rauch, T., & Deetjen, J. L. 2003, in Stellar Atmosphere Modeling, eds. I. Hubeny, D. Mihalas, & K. Werner, ASP Conf. Ser., 288, 103
Reindl, N., Rauch, T., Werner, K., Kruk, J. W., & Todt, H. 2014, A&A, 566, A116
Schöning, T. 1993, A&A, 267, 300
Schöning, T., & Butler, K. 1989, A&AS, 78, 51
Schuh, S., Traulsen, I., Nagel, T., et al. 2008, Astron. Nachr., 329, 376
Scóccola, C. G., Althaus, L. G., Serenelli, A. M., Rohrmann, R. D., & Córsico, A. H. 2006, A&A, 451, 147
Sinamyan, P. K. 2011, Astrophysics, 54, 413
Sion, E. M. 2011, in White Dwarf Atmospheres and Circumstellar Environments (Wiley-VCH), 1
Todt, H., Kniazev, A. Y., Gvaramadze, V. V., et al. 2013, MNRAS, 430, 2302
Tremblay, P.-E., Ludwig, H.-G., Steffen, M., & Freytag, B. 2013, A&A, 559, A104
Unglaub, K., & Bues, I. 2000, A&A, 359, 1042
Wassermann, D., Werner, K., Rauch, T., & Kruk, J. W. 2010, A&A, 524, A9
Werner, K. 1991, A&A, 251, 147
Werner, K., & Herwig, F. 2006, PASP, 118, 183
Werner, K., & Rauch. 2014, A&A, 569, A99
Werner, K., Dreizler, S., Heber, U., et al. 1995, A&A, 293, L75
Werner, K., Deetjen, J. L., Dreizler, S., et al. 2003, in Stellar Atmosphere Modeling, eds. I. Hubeny, D. Mihalas, & K. Werner, ASP Conf. Ser., 288, 31
Werner, K., Rauch, T., Barstow, M. A., & Kruk, J. W. 2004a, A&A, 421, 1169
Werner, K., Rauch, T., Napiwotzki, R., et al. 2004b, A&A, 424, 657
Werner, K., Rauch, T., & Kepler, S. O. 2014, A&A, 564, A53
Wood, M. A. 1994, in Am. Astron. Soc. Meet. Abstr., BAAS, 26, 1382
Zhang, X., & Jeffery, C. S. 2012a, MNRAS, 426, L81
Zhang, X., & Jeffery, C. S. 2012b, MNRAS, 419, 452

Mon. Not. R. Astron. Soc. **000**, 1–?? (2014) Printed 8 January 2015 (MN LaTeX style file v2.2)

Identifying close binary central stars of PN with *Kepler*

Orsola De Marco[1,2]⋆ , J. Long[3], George H. Jacoby[3], T. Hillwig[4], M. Kronberger[5], Steve B. Howell[6], N. Reindl[7,8] and Steve Margheim[9]

[1] *Department of Physics and Astronomy, Macquarie University, Sydney NSW 2109, Australia*
[2] *Astronomy, Astrophysics and Astrophotonics Research Centre, Macquarie University, Sydney NSW 2109, Australia*
[3] *Giant Magellan Telescope / Carnegie Observatories, Pasadena, CA 91101, USA*
[4] *Valparaiso University, 700 Chapel Dr, Valparaiso, IN 46383, USA*
[5] *Deepskyhunters Collaboration*
[6] *NASA Ames Research Centre Moffett Field, CA 94035, USA*
[7] *Tübingen University, Geschwister-Scholl-Platz 72074 Tübingen, Germany*
[8] *Institute for Astronomy and Astrophysics, Kepler Center for Astro and Particle Physics, Eberhard Karls University, 72076, Tübingen, Germany*
[9] *Gemini Observatory, Southern Operations Center, Casilla 603, La Serena, Chile*

Received; Accepted

ABSTRACT

Only three planetary nebulae (PN) were known in the *Kepler* space telescope field of view at the time of launch. Two additional objects were discovered by the *Deep Sky Hunters* amateur collaboration while an additional PN was recently found by Aller et al.. Despite this low tally, we have identified a substantial amount of binary-related and anomalous behaviour. Of the 5 central stars of PN with useful data, one, J 193110888+4324577, is a short-period, post common envelope binary exhibiting relativistic beaming effects. A second, the central star of the newly identified PN Pa 5, has a consistent variability that may be explained by magnetic activity or the influence of an orbiting planet. A model of the stellar spectrum classifies it among the very rare O(He) class. The third PN, NGC 6826 has a central star whose *Kepler* light curve was previously analysed with the conclusion that it is due to rotational modulation implying a surface velocity of 78 km s^{-1}, something that can only be achieved in a merger. Fourth, the central star of the newly identified PN Kn 61, exhibits a rare PG1159, hydrogen-deficient spectrum and a peculiar light variability with approximately triangular brightness peaks of ∼0.08-0.14 magnitudes and lasting 1-2 days, spaced irregularly at intervals of a few days. We considered several single star and binary explanations for the variability, although none is fully convincing. Finally the central star of the circular PN A 61 does not appear to have a photometric variability above 2 mmag. With the possible exception of the variability of Kn 61, all other variability behaviour, whether due to binarity or not, would not easily have been detected from the ground. We conclude, based on very low numbers, that there may be many more close binary or close binary products to be discovered with ultra-high precision photometry. With a larger number of high precision photometric observations we will be able to determine how much higher than the currently known 15 per cent, the short period binary fraction for central stars of PN is likely to be.

Key words: techniques: photometric; stars: evolution; binaries: close; planetary nebulae: individual: Kn 61; planetary nebulae: individual: Pa 5; planetary nebulae: individual: J193110888+4324577.

1 INTRODUCTION

What is a planetary nebula? The textbooks are clear and definitive that a planetary nebula (PN) is a common, short-lived, phase of a typical star like the Sun that occurs as it burns up the last of its available nuclear fuel. During the next 1000 years or so, the star blows off its outer layers to reveal a central core that becomes hot enough to ionise the ejected layers. That ionised gas then glows due to recombination and collisional excitation. This simple scenario likely has some validity. However, we still do not have a satisfactory physical explanation for how single stars create PN with

⋆ E-mail: orsola.demarco@mq.edu.au

non-spherical shapes, which amount to 80-85 percent of the entire population (Parker et al. 2006).

García-Segura et al. (1999, 2005) argued that stellar rotation and magnetic fields in *single* stars can alter the morphology of a mass-losing asymptotic giant branch (AGB) star, but Soker (2006) and Nordhaus et al. (2007) argued that in a large majority of cases, single AGB stars are unlikely to be able to sustain large-scale magnetic fields for long enough to affect shaping, because the field embedded in an expanding plasma, drains the star of angular momentum on short time scales and quenches itself. Without an angular momentum source, the field would vanish. In the models of García-Segura et al. (1999) and García-Segura et al. (2005) the field strength was assumed constant and was not coupled to the negative feedback action of the stellar envelope. In fact, recently García-Segura et al. (2014) have re-examined this issue and have determined, using stellar structure and evolution simulations, including the effect of angular momentum transport, that AGB stars cannot maintain rotation profiles that allow the formation of bipolar PN. A stellar or substellar companion, though, can provide the angular momentum source (Soker 2006; Nordhaus et al. 2007).

A host of related conundrums that also may find explanations in the presence of a binary companion, are the unexplained intensifying of mass-loss at the end of the AGB (but see Lagadec & Zijlstra 2008), linear momenta in post-AGB outflows 1000 times in excess of what can be explained by radiation pressure on dust (Bujarrabal et al. 2001), or the lack of an explanation for the constant bright edge of the PNLF in old elliptical and young spiral populations (Jacoby et al. 1992; Marigo et al. 2004, but see also Schönberner et al. (2007)). Finally, the population synthesis studies of Moe & De Marco (2006) and Moe & De Marco (2010) show that the current scenario predicts too many PN in the Galaxy by a factor of 5 at the 3σ level, while the binary interactions (from strong, such as common envelope [CE] interactions to weak, such as gravitational focussing) can explain $\sim$70 per cent of all PN.

The *binary hypothesis* (De Marco 2009) therefore argues that some single AGB stars do not make a PN, which implies that binarity is over-represented in the PN population compared to the progenitor main sequence population. To test this emerging hypothesis, several groups are actively working together to determine the true frequency of binary central stars and the properties of those systems (Bond 2000; De Marco et al. 2004; Miszalski et al. 2009; De Marco et al. 2013; Hillwig et al. 2010; Jones et al. 2014).

The only binary fraction that is reasonably well constrained today is that of very close central star binaries: $\sim$15 per cent of all central stars are in post-CE binaries (periods typically shorter than a day) and are detected with periodic flux variability due to irradiation, ellipsoidal variability, or eclipses (Bond 2000; Miszalski et al. 2009). Almost all of the photometric variables detected have amplitudes larger than $\sim$0.1 mag, mostly due to suboptimal sampling due to telescope scheduling and weather constraints.

It has therefore been asked how many objects have remained undetected as one would expect that inclination, companion size and orbital distance would all play a role in the variability amplitude (De Marco et al. 2008). It is likely that there is a dearth of central star close binaries with periods just longer than those detected so far (i.e., between a couple of days and a couple of months). It is likely that with our current detection limits we would have easily detected binaries with periods up to two weeks (De Marco et al. 2008). In addition, studies of post-CE white dwarf (WD) binaries, the progeny of post-CE central stars of PN binaries, seem to indicate a dearth of objects in that period range (Schreiber et al. 2009). However, short period, post-CE binaries with smaller companions, with an unfavourable orbital inclination, or with a weak irradiation effect should be there, with variability below the ground-based threshold. We have therefore embarked in a study to find new post-CE central star binaries with *Kepler* to determine whether we can get an indication of the frequency of the undetected, low amplitude binaries.

While a sample of 6 central stars in the *Kepler* field precludes the statistical revision of the short-period binary fraction, it would be indicative to find even just one photometric variable that would *not* have been detected from the ground. Any indication that such binaries exist would motivate further studies to quantify how much larger the post-CE binary fraction is than the 15 per cent currently known.

In § 2 we present the PN sample in the *Kepler* field of view, while in § 3 we describe the observations. In § 4 to § 7 we present the *Kepler* lightcurves, atmosphere model analyses, as well as combined analysis of the light and radial velocity curves to derive stellar and binary parameters for five of the six central stars of PN in the *Kepler* field of view that have adequate data. We conclude in § 8.

2 THE PN SAMPLE

We have monitored (programme # GO30018) six PN in the *Kepler* field. Three were known (Abell 61, hereafter A 61, NGC 6742 and NGC 6826). One was recently discovered by Aller et al. (2013, the central star is known as J193110888+4324577, hereafter J19311, while the nebula may be indicated as AMU 1 after the discoverers, but we shall use the star's name to indicate this object). Two were found by the *Deep Sky Hunter* team (Jacoby et al. 2010, Kronberger 61, hereafter Kn 61 and Patchick 5, hereafter Pa 5), partly during an effort targeting the *Kepler* field in support of this study. A seventh object, PaTe 1, also found by the Deep Sky Hunters, is in an area of extended emission but is not seen in [O III] images, and therefore cannot be confirmed as a PN at this time. Available data for these objects are summarised in Table 1 while images are presented in Fig. 1.

A 61 is an old, circular PN first presented by Abell (1966). Its central star spectrum was modelled by Napiwotzki (1999) and the following parameters were derived: $T_{\rm eff} = (88\,000 \pm 7900)$ K, $\log g = 7.10 \pm 0.37$, $R = 0.67$ $R_\odot$ at a distance of 1380 pc. Drummond (1980) lists the central star of A 61 as a variable and the Russian catalogue of variable stars (Kukarkin et al. 1981) designates it as NSV 11917.

Kepler data for the central star J19311 were first presented by Østensen et al. (2010), who showed that it has a periodically variable light curve. The PN was only recently discovered by Aller et al. (2013) who showed it to consist of two elongated structures at 90 deg from one another and

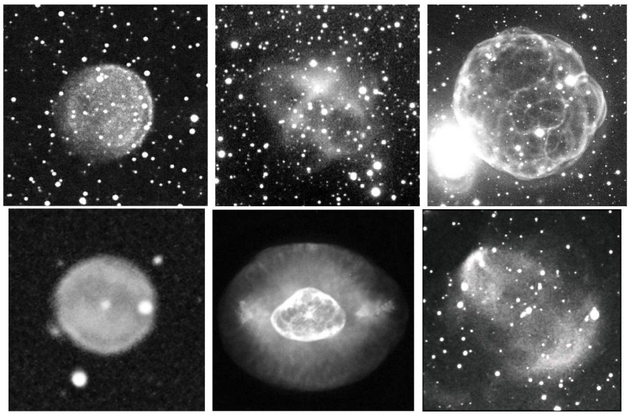

Figure 1. A mosaic of the six PN in the *Kepler* field that were observed by our programme (the nebular diameters can be found in Table 1; North is towards the top, East to the left, except for Kn 61 - see caption to Figure 2). Top left: A 61, courtesy of Jim Shuder; Top centre: J19311+4324, Aller et al. (2013); Top right: Kn 61, courtesy of Travis Rector and the Gemini Observatory; Bottom left: NGC 6742, courtesy of Adam Block. Bottom centre: NGC 6826, courtesy of Bruce Balick; Bottom right: Pa 5, from Jacoby et al. (2010)

with kinematics indicating that they were ejected almost at the same time.

Kn 61 is a PN discovered by the *Deep Sky Hunters* (Kronberger et al. 2012) and already studied by Gonzalez Buitrago et al. (2014), who showed it to have a hydrogen poor, PG1159-type central star. Its central star's spectrum was originally presented by Jacoby et al. (2012), Long et al. (2013) and García-Díaz et al. (2014). García-Díaz et al. (2014) discuss extensively the PN, concluding that it is hydrogen poor, a quality shared by only a handful of other known objects (Harrington et al. 1997).

NGC 6742 is a little studied, circular PN with a morphology which is very similar to that of A 61 (Fig. 1). Its central star's light is diluted in the bright nebula and in § 3 we question whether the *Kepler* photometry could even identify the star itself.

NGC 6826 is a very well studied PN. Its central star was detected to vary by Bond & Ciardullo (1990) and classified as a ZZ Leporii star by Handler (2003). The stellar spectrum was modelled by Kudritzki et al. (2006, $T_{\rm eff}$=46 kK, $\log g$ = 3.8, consistent with a mass of 0.74 M$_{\odot}$). The PN consisted of two, well defined, elliptical structures and two jet-like structures aligned with the long axis of the PN. The *Kepler* light curve of the central star was presented by Handler et al. (2013) who demonstrated convincingly that its variability behaviour is not consistent with a short period binary, but instead with a fast rotating central star.

The *Kepler* lightcurve of the central star of Pa 5 (also known as J19195+4445), was already presented by Østensen et al. (2010). The PN was discovered by the *Deep Sky Hunters* (DSH J1919.5+4445; Kronberger et al. 2006). Østensen et al. (2010) also presented a spectrum of the central star and remarked on this star being a very hot PG1159 star, a classification that we will revise in § 7.

In Fig. 1 and 2 we present images of the six PN. The image of Kn 61 was obtained with the Gemini telescope in July 2011 after a confirmation image was obtained by us at the KPNO 2.1-m telescope.

Figure 2. A Gemini-north GMOS, 500-second exposure image of the newly-discovered PN Kn 61 obtained with the Gemini telescope. [OIII] is blue, Hα is red. North is 21 degrees West of the vertical, West is 90 degrees left of North and the field of view is 2.2 x 4.4 arcminutes. Image curtesy of the Gemini Observatory and Travis Rector (see Gemini Office press release http://www.gemini.edu/node/11656)

3 DESCRIPTION OF THE OBSERVATIONS

3.1 *Kepler* photometry, periodicity analysis, and non-detections

The *Kepler* space telescope was launched on March 7, 2009 with the aim of monitoring approximately 115 sq. degrees of sky centred on the Cygnus-Lyra region of the sky. The telescope aperture is 1.4 m. The filter bandpass has a full width at half maximum between 4300 and 8900 Å. The monitoring cadence of our targets was approximately 30 minutes while each exposure time was equivalent to 1626 sec. The *Kepler* pixel scale is 3.98 arcsec/pix. The *Kepler* data is distributed by quarters, each three months long. The quarters available for a particular object vary: A 61 was observed in quarters #2-7 and #10-13, J19311 was observed in quarters #1-6 and #13, Kn 61 in quarters #10-13, NGC 6742 was only observed for a single quarter (#13). NGC 6826 has data

	A 61	J 19311	Kn 61	NGC 6742	NGC 6826	Pa 5
Kepler Input Catalogue	9583158	7755741	3231337	10963135	12071221	8619526
RA	19 19 10.22	19 31 08.89	19 21 38.93	18 59 20.03	19 44 48.15	19 19 30.52
Dec	+46 14 52.03	+43 24 57.74	+38 18 57.36	+48 27 55.24	+50 31 30.26	+44 45 43.08
Distance (kpc)	1.38[c]	1.82[e]	4::	4.86[e]	1.3[e]	1.4
PN diameter (arcsec)	200[d]	∼300[f]	104	27[g]	27x24[e]	120[i]
PN morphology	circular	bipolar/elliptical	∼circular	circular	elliptical/jets	bipolar/torus
V-band magnitude[a]	17.389	13.697	18.416	16.567[h]	10.41[g]	15.670[j]
Kepler magnitude	17.321	13.752	18.283	16.255[h]	10.757	15.839
Central star spectral type[b]	DAO	O(H)	PG1159	?	O3f(H)	O(He)
# of *Kepler* "quarters"	10	7	4	1	7	8
Light curve period (days)	–	2.928	2-12	–	0.619,1.236	1.12
Light curve amplitude (mmag)	<2	0.729	∼80-140	–	∼2-8	0.5

[a]From Everett et al. (2012) unless otherwise stated; [b]We stay away from sub-dwarf classifications for these objects, which confuses them with post-RGB stars, and use instead the classification system used by, e.g., Mendez et al. (1988); [c]Napiwotzki 1999; [d]ESO catalogue; [e]Frew (2008); [f]This nebula was decomposed into two elliptical/bipolar shells approximately 5×2 arcmin^2 with axes perpendicular (Aller et al. 2013) to each other and with similar expansion velocities and kinematic ages; [g]Acker et al. (1992); [h]Likely too bright because of the bright nebula; [i]Width of the torus' long axis; [j]but see § 5.2 for an alternative value.

Table 1. Available literature data and results for the sample of PN in the *Kepler* field of view

from quarters #1-7 and #10-13 and Pa 5 was observed in quarters #1, #5-7, and #10-13.

Although *Kepler* 's detectors contain over 95 million pixels, only a small fraction can be captured for the creation of long cadence light curves due to spacecraft onboard storage and downlink constraints. As a result, targets chosen by observers are assigned a mask, and only pixels within the mask are stored and eventually downloaded for analysis. Light curves from *Kepler* are obtained through simple aperture photometry on the recorded pixels, and processed by the *Kepler* "pre-search data conditioning" (PDC) pipeline to remove systematic errors. The same measures in the pipeline that try to minimise false positives for exoplanet transit detection also risk removing intrinsic star variability. However, comparing PDC light curves to ones extracted from the original target pixel files and detrended with the cotrending basis vectors provided with the data release showed them to be very similar, leading us to conclude that PDC light curves were acceptable for our purposes without additional reduction.

Each quarter of data was analysed to detect possible periodic components in the signal using the Lomb-Scargle periodogram algorithm. The resulting periodograms were used to identify the strongest periodic component in the light curve. In order to combine different quarters of data for an object, it was necessary to normalise the light curves by the median values. Otherwise, differences between quarters result in discontinuities when stitching the light curves. A periodogram was also generated for the stitched light curve, to get a better signal to noise ratio in detecting the periodic signal. To generate the folded light curve, the stitched data was folded at the strongest period from the periodogram. In the phasing process, the data were binned to form median flux values, with 50 bins per light curve cycle.

The central star of A 61 has no detected variability to a limit of 2 mmag, which is curious given its designation as NSV 11917.

For the central star of NGC 6742 we did not detect any variability. However, we were unable to distinguish any difference between the flux in pixels centred on the central star coordinates from pixels a few arcsec away. For the other PN, the nebulae have very low surface brightnesses relative to the central stars. In the case of NGC 6742, however, *Kepler* 's large pixel size and broad bandpass results in a high background noise that degrades the contrast between the nebula and star. We therefore must conclude that this target could not measured accurately enough to draw any conclusion as to the variability of the stellar light.

3.2 Spectroscopy

Spectra were obtained for the central star J19311 and the central star of PN Pa 5 at the Gemini North telescope with GMOS in long-slit mode using the B1200 grating between 8 and 16 July, and 3–5 September, 2012. The spectral range was 4020–5480 Å and the spectral resolution was R=4200. Both central stars were observed in queue observing mode via phase windows defined by the photometric period from the *Kepler* photometry. The central star of Pa 5 was observed in 9 out of 15 evenly spaced phase bins over *twice* the photometric period. Twice the photometric period was used in the event that the photometric variability was caused by an ellipsoidal effect. The central star J19311 was observed in 6 out of 10 evenly spaced phase bins over its photometric period. The spectra of the central star of Pa 5 were taken in pairs of 900-second exposures while the spectra of J19311 were taken in pairs of 600-second exposures.

One spectrum of the central star of Pa 5 was also acquired at the 3.6-m WIYN telescope on Kitt Peak, on 2009, September 12, using the bench spectrograph with a resolution of R=700 and a spectral range of 4300-7000 Å.

We also observed the central star of Kn 61 on 2012, June 16, using the National Optical Astronomy Observatory, Mayall 4-m telescope on Kitt Peak and the facility RCSpec long-slit spectrograph with the T2KA CCD. The slit was 1 arcsec wide by 49 arcsec long and oriented with a position angle of 90 deg. The KPC-22b grating in second order was used to disperse the spectra with 0.72 Å pixel^{-1} at a nominal resolution of $\Delta\lambda$ = 1.7 Å. The spectra covered an effective wavelength range of 4100 to 5000 Å, being slightly

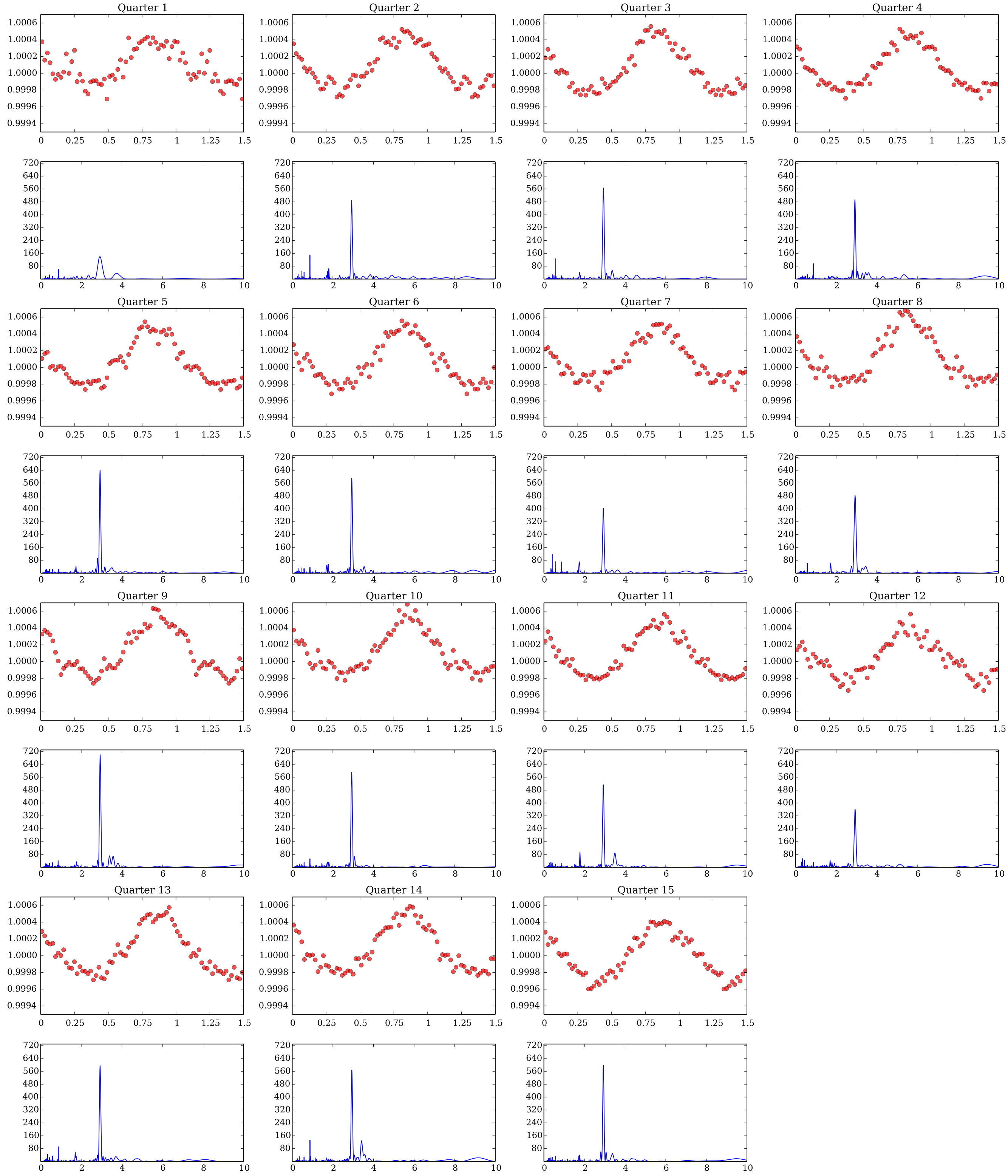

Figure 3. The folded lightcurves (upper rows) and periodograms (lower rows) for the central star of J19311, for each individual quarter of data, using a period of 2.928 days. The light curves' x-axes values are phase, while those of the periodograms are time in days. The light curve fluxes are median-normalised, while the periodograms' y-axes measure the signal detection efficiency

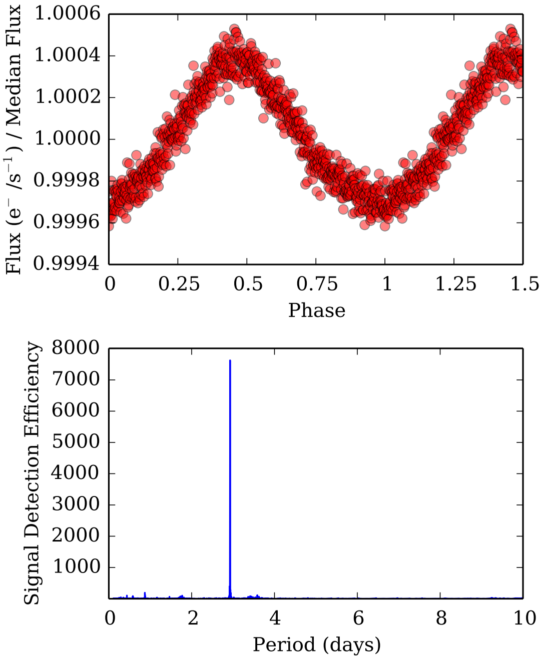

Figure 4. The folded lightcurve (upper panel) and periodogram (lower panel) for the central star of J19311, for all quarters of data, using a period of 2.928 days

out of focus at both ends where the fluxes could not be reliably calibrated. The spectrum of Kn 61 was immediately proceeded with a comparison arc lamp spectrum (FeAr) for wavelength calibration. The exposure time was 1200 sec. At least one spectrophotometric standard star was observed on the night providing a relative flux value. Calibration data consisting of bias frames, quartz lamp flat field exposures, and comparison lamp exposures were taken during the daytime. The data reduction is based on various IRAF packages for performing image reduction and the *onedspec* package for extracting and calibrating the spectra.

4 THE ANALYSIS OF J 19311

4.1 The light curve of the central star J 19311

In Fig. 3 we present the period analysis using individual quarters for the central star J19311 (the flux units in these plots are electrons per 30 minute exposure). In Fig. 4 we present the lightcurve phased using the most prominent period. J 19311 is almost certainly a short period binary. All quarters give consistently the same period of 2.928 days with an amplitude of 0.729 mmag. In § 4.2 we examine the radial velocity curve of this star together with its light curve and we will interpret this variability as due to both Doppler beaming and an ellipsoidal effect.

4.2 Modelling of the atmosphere, light and radial velocity curves of the central star J19311

We used TMAP[1] (Werner et al. 2003; Rauch & Deetjen 2003) atmosphere models to fit the spectrum of J19311 with a pure hydrogen and helium composition, with a helium mass fraction of 0.4 which best fit the helium lines. TMAP calculates non-LTE, plane-parallel, fully metal-line blanketed model atmospheres in radiative and hydrostatic equilibrium. Model parameters of effective temperature and gravity, $T_{\rm CS}$ = 80 kK and $\log g_{\rm CS}$ = 5.0 fit the data well. We show the fit in Figure 5, alongside the fits of Pa 5 and Kn 61 which will be presented in § 5 and 7. The lack of He I lines indicates a temperature in excess of 70 kK, while the presence of NV lines in absorption (lines that we do not fit) indicates a temperature less than 115 kK. This model is only approximate but it is sufficient for a crucial constraint on the WD model below.

Within the temperature range described above we find the lower values to be more likely, based on reported distances for the nebula. Frew (2008) gives the distance to the PN around J19311 to be d = 1.82 kpc. For $T_{\rm CS}$ = 70 kK and our minimum radius arrived at below, we calculate M_V = 1.98. Using the interstellar reddening value of Frew (2008), A_V = 0.26, we find the minimum distance to be d_{min} = 1.91 kpc. Higher temperatures will result in an intrinsically brighter central star and a greater distance required to give the same observed brightness. If we take an uncertainty in the distance of Frew (2008) of 0.6 kpc the allowed range in temperatures is larger, but we are still limited to $T_{\rm CS} \lesssim 115$ kK.

Comparing bolometric luminosity and effective temperature values for central stars in our temperature and gravity ranges with the evolutionary models of Schönberner (1983) and (Blöcker 1995), we rule out masses below ∼0.55 M$_\odot$. Post-AGB stars with masses lower than this limit are intrinsically too faint. Likewise, stars with masses above ∼0.85 M$_\odot$ are intrinsically too bright for these temperatures. We therefore conclude that the central star mass is largely unconstrained , i.e., in the range $0.55 < M_{\rm CS} < 0.85$ M$_\odot$.

The spectral features in J19311 show strong radial velocity variability on the same period as the *Kepler* photometry with a semi-amplitude of 88 km s^{-1} (Figure 6). The star is clearly in a binary system, though there is no obvious signature of the companion star in our optical spectrum. While the radial velocity curve is not well sampled, it is well fit by a sine curve and shows no clear sign of eccentricity in the orbit so we assume for the remainder of our analysis that the orbit is circular. We find then that the mass function is $f(m) = (m_2 \sin i)^3/(m_1 + m_2)^2 = 0.207$ M$_\odot$, with m_1 and m_2 the masses of the primary and secondary, respectively, while i is the orbital inclination.

The light curve for J19311 demonstrates the exquisite precision of *Kepler* photometry. By coadding the photometry into 100 evenly spaced bins folded on the photometric, and orbital, period of 2.928151 days, we find a nearly sinusoidal light curve with amplitude 0.729 mmag. Surprisingly, the photometric light curve is out of phase with the radial

[1] astro.uni-tuebingen.de/ rauch/TMAF/flux_H+He.html.

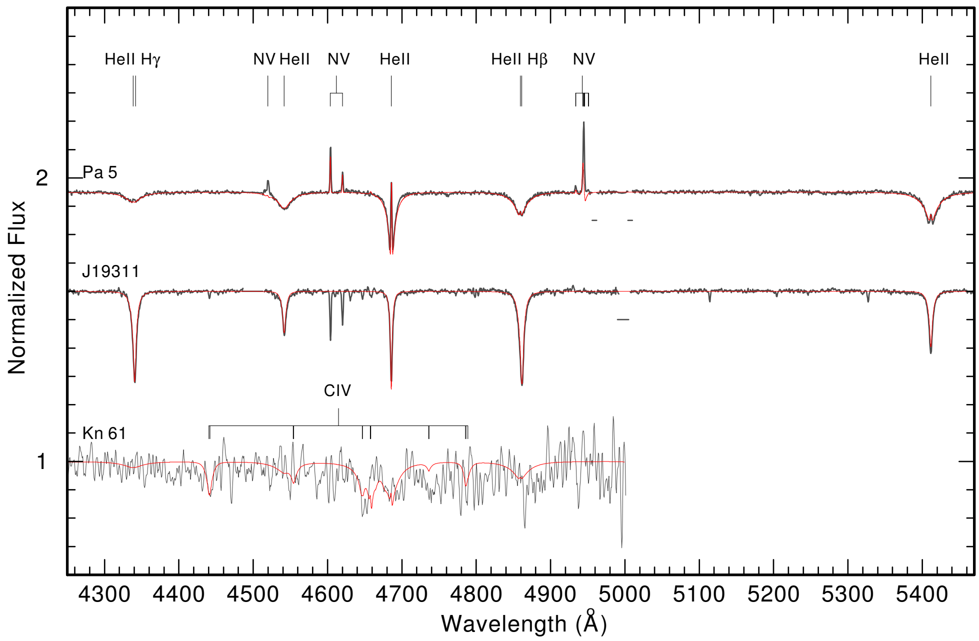

Figure 5. The rectified spectra of three central stars (black lines) overlaid with the best fitting TMAP models (red lines). The spectrum of J19311 is shifted by 0.6 units, that of Pa 5's central star by 0.95

velocities by exactly π. This phase shift means that the photometric variability is not due to irradiation of the companion star, in which case the phase shift would be $\pi/2$. We can also rule out ellipsoidal variability as the primary cause of the sinusoid. For ellipsoidal variability in which one star is distorted due to the gravity of its companion, the photometric period is half the orbital period, unlike the case here.

It is possible that the variability is due to accretion of material from the companion, producing a cool spot on the central star. However, it is not clear why the spot would be aligned perfectly with the axis connecting the two stars or why it would be so consistent over the duration of the *Kepler* observations. There is one source of variability which we would expect to produce the observed phase shift between the radial velocities and photometry. Relativistic effects caused by the radial motion of the star in its orbit, dominated by Doppler beaming, are known to result in photometric variability at small levels (Shporer et al. 2010; Bloemen et al. 2011, 2012; Herrero et al. 2014).

Using the equation for relativistic variability from Zucker et al. (2007) and Shporer et al. (2010), with the expected temperature range, we find that our observed photometric amplitude can be described by relativistic effects given our current limits for the physical parameters of the central star. We conclude that the system's photometric variability is due primarily to Doppler beaming. In typical WD binaries the relativistic beaming effects of the two components are exactly out of phase and likely to nearly cancel one another out. However, in cases such as J19311, where one of the two stars has not yet contracted to the WD cooling track and is therefore much more luminous than its companion, it dominates the system luminosity and the relativistic effects.

Given our mass function for the system and a post-AGB central star with mass $\gtrsim 0.55$ M$_\odot$, the smallest possible companion mass, for an inclination angle, $i = 90^\circ$ is $M_2(min) = 0.68$ M$_\odot$. Assuming the companion and central star to be coeval, and that the companion was less massive than the progenitor of the central star, we require that the maximum companion mass is $M_2(max) \approx 8$ M$_\odot$. Again, from our mass function we find then a minimum system inclination of $i = 18^\circ$. Using the Wilson-Devinney modeling code (Wilson 1990; Wilson & Devinney 1971) with main sequence stars in the mass range $0.68 < M_2 < 8.0$ M$_\odot$ and central stars with the limits we have determined above, any such companion produces an irradiation effect at least an order of magnitude larger than our observed photometric variability. We conclude that the companion is not a main sequence star but must be a compact star, most likely a white dwarf. If this is the case, we then also expect that the companion will have had a greater mass during the main sequence phase than the mass of the observed star's progenitor. So we expect today's mass ratio, $q = M_2/M_{\rm CS} > 1.0$ With this requirement, a maximum WD mass of ≈ 1.4 M$_\odot$, and our mass function derived above, we find a minimum possible inclination for the system of $i_{\rm min} = 40^\circ$. Since no eclipses are observed in the *Kepler* light curve, if the companion is on the WD cooling track, the inclination of the system would need to be $\lesssim 88^\circ$ for the two stars not to eclipse one another.

Alone, the relativistic variability does not provide strong constraints on the physical parameters of either star in the binary system. The relativistic effects depend largely upon the temperatures of the two stars and their flux ratio. With our current ranges for temperature and radius of the central star we cannot place further constraints on the binary parameters. However, we also see that the *Kepler* light curve is not precisely fit by a sinusoid. If relativistic effects are the sole cause of the light variability, the shape of the observed light curve should mimic that of the radial velocity curve, in this case a sine curve. If we subtract a sine curve from the binned data we find that the residuals are distributed in a nearly sinusoidal curve, with a period that is half of the orbital period and maxima that align with maxima and minima of the Doppler beaming variability. This behaviour is what we would expect from ellipsoidal variability. The semi-amplitude of the variability of the residuals is approximately ten times smaller than that of the variability before subtraction.

Ellipsoidal variability is caused by a difference in the projected surface area of the star, thus the amplitude of the effect depends on the geometry of the star, but not typically on the temperature. Again we use the Wilson-Devinney code starting with our limits from above, $i > 40°$ and $0.55 < M_{\rm CS} < 0.85$ M$_\odot$ to find limits on the stellar radius (and surface gravity) that produce the observed ellipsoidal variations. We then check the results for consistency with evolutionary models and iterate the process. A central star with $R_{\rm CS}$ ≈8–9 per cent of its Roche lobe volume radius (depending on inclination) produces the ellipsoidal variability amplitudes we observe. The iteration process reduces the mass and radius ranges, and we find that the radius of the central star can be constrained to $0.27 < R_{\rm CS} < 0.35$ R$_\odot$, the surface gravity must be $5.2 < \log g < 5.4$, in good agreement with the preliminary model of the spectrum discussed above, and the central star mass falls in the range $0.55 < M_{CS} < 0.70$ M$_\odot$. In Fig. 6 we show two model curves (solid lines). One is an example ellipsoidal variable curve, showing the amplitude of the observed ellipsoidal effect. The second is the final model combining the Doppler beaming, as a sine curve with semi-amplitude 0.337 mmag, and the ellipsoidal effect.

Using this information for the central star and assuming the companion is either a WD or an evolved pre-WD, the relativistic variability produces our observed amplitudes best for the higher end of our temperature range. In fact, if the companion provides less than 0.1 per cent of the total flux then the central star's temperature must be $\gtrsim$ 100 kK to produce the observed amplitude. Lower central star temperatures and smaller radii within our range do work, though we find that the companion would then contribute a few percent to the system's luminosity. The companion then must either not have reached the WD cooling track (or have expanded again possibly due to accreted material from the PN ejection), or the temperature of the companion must be very high, with $T_2 \gtrsim 130$ kK. Studies of other double-degenerate central stars, such as those of NGC 6026 (Hillwig et al. 2010), Abell 41 (Shimanskii et al. 2008), and TS 01 (Tovmassian et al. 2010) show companions that are either roughly coeval with the central star or have expanded and been reheated from a more evolved stage. Since it is unlikely that all of these systems, or perhaps *any* of the systems, have two stars with nearly identical masses as to both be in the post-AGB/pre-WD stage simultaneously, it is more likely that compact companions to stars going through the PN stage are reheated and expand, possibly in response to accreted material (for a summary of the fit parameters see Table 2).

Parameter	Value
M$_{\rm CS}$ (M$_\odot$)	0.55 – 0.70
M$_2$ (M$_\odot$)	0.68 – 1.4
R$_{\rm CS}$ (R$_\odot$)	0.27 – 0.35
T$_{\rm CS}$(K)	80 000
log(g/cm s^{-2})	5.2 – 5.4
i (deg)	40 – 88
$v_{\rm CS} \sin i$ (km s^{-1})	88

Table 2. Model parameters to fit the light and radial velocity curves of the central star J19311. The subscript "CS" stands for central star

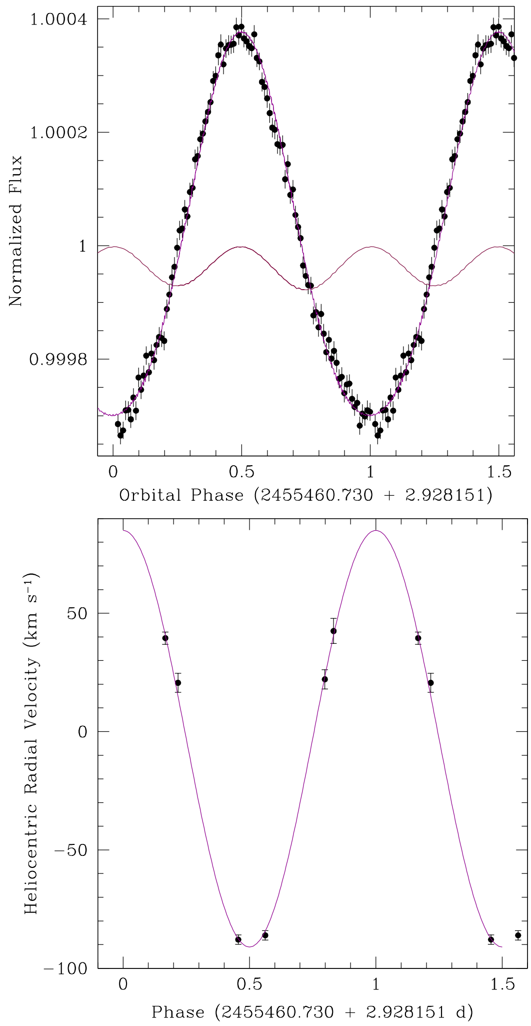

Figure 6. The folded light (upper panel) and radial velocity (lower panel) curves of J19311 with overlaid the fit corresponding to the model parameters in Table 2

5 THE ANALYSIS OF KRONBERGER 61

5.1 The light curve of the central star of Kn 61

The central star of Kn 61 has a light curve characterised by peaks that occur with spacings of 2 to 12 days. In Fig 7 we present the period analysis using individual quarters for the central star of Kn 61 (the flux units in these plots are elec-

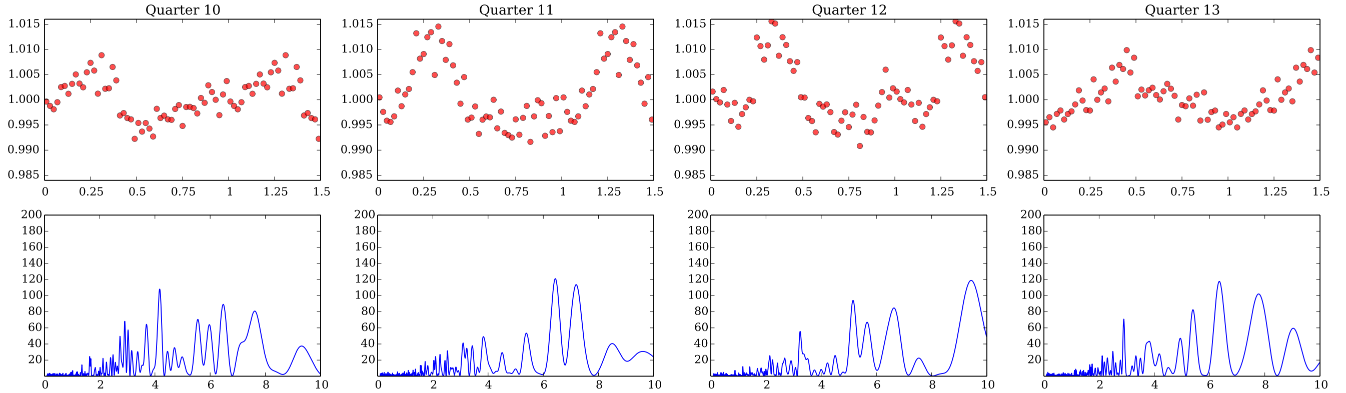

Figure 7. The folded lightcurve (upper rows) and periodogram (lower rows) for the central star of Kn 61, for each individual quarter of data, using a period of 6.4 days. The light curves' x-axes values are phase, while those of the periodograms are time in days. The light curves fluxes are median-normalised, while the periodogram's y-axes measure the signal detection efficiency

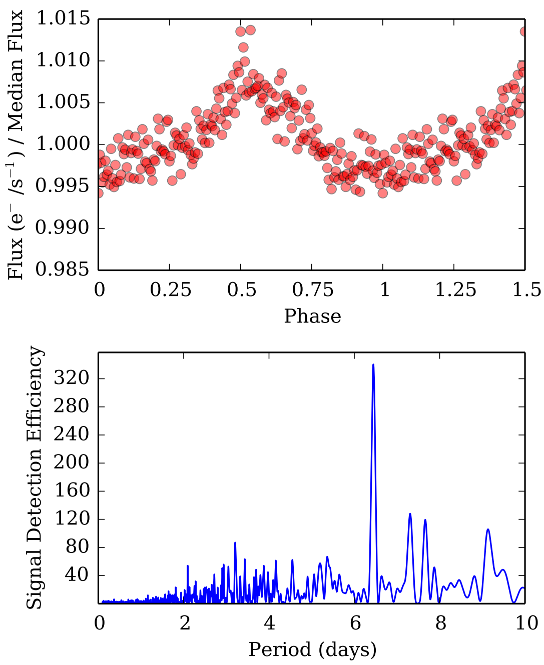

Figure 8. The folded lightcurve (upper panel) and periodogram (lower panel) for the central star of Kn 61, for all quarters of data, using a period of 6.4 days

trons per 30 minute exposure), while in Fig. 8 we have folded all quarters using a period of 6.4 days. However, inspecting the light curve (see Fig. 9), this cadence is clearly not any more likely than other peak recurrence times. The peaks rise from an unvarying baseline and have approximately triangular shapes, although they appear to rise faster than they decay (the smaller amplitude, shorter-duration peaks have only few data points and lower signal-to-noise ratio so it is harder to determine their shape). Brightness peaks have a width at the base between 1 and 2 days. Their height is $\sim$80-140 mmag. This type of variability is not interpretable as irradiation, ellipsoidal variability nor eclipses. In fact this variability is unprecedented and we have not been able to determine its origin. In § 8 we will discuss this variability in

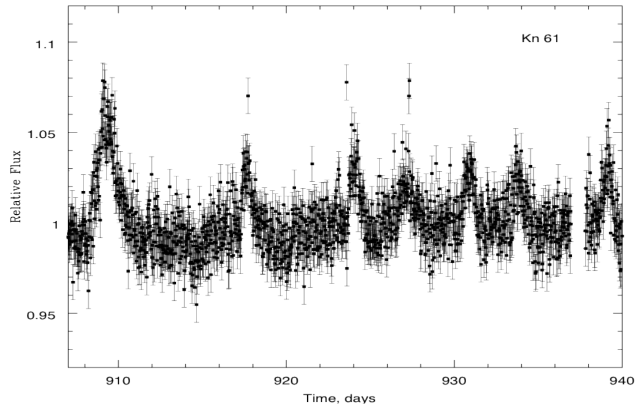

Figure 9. A representative part of the lightcurve of the central star of Kn 61 showing its variability

the context of another object also discovered using *Kepler* data, which has similar characteristics.

5.2 The spectrum of the central star of Kn 61 and energetics of the light outbursts

Our spectrum of the central star of Kn 61 shows an almost featureless continuum. However we discern the following features (see Fig. 5): CIV $\lambda\lambda$4440,4442,4647,4658 and HeII λ4686. Hβ is absent. We modelled this low signal-to-noise spectrum using a hydrogen-free synthetic spectrum with $T_{\rm eff}$=120 kK, $\log g$=7.0 and He/C=1 (by mass). These are only indicative, but we know that the temperature must be in excess of 100 kK because García-Díaz et al. (2014) report to have observed the CIV lines at 5801 and 5012 Å in emission.

Together with the mass-luminosity relation of Vassiliadis & Wood (1994), we obtain a radius of 0.04 R$_\odot$, a mass of 0.5 M$_\odot$ and a luminosity of 250 L$_\odot$. If we then interpret the light behaviour in the *Kepler* band as a similar increase in the bolometric luminosity, we derive that each peak emits 20 L$_\odot$, or 3-7$\times$10^{39} ergs, assuming that the peaks are 1.1 times the quiescence brightness, have a base 1-2 days wide

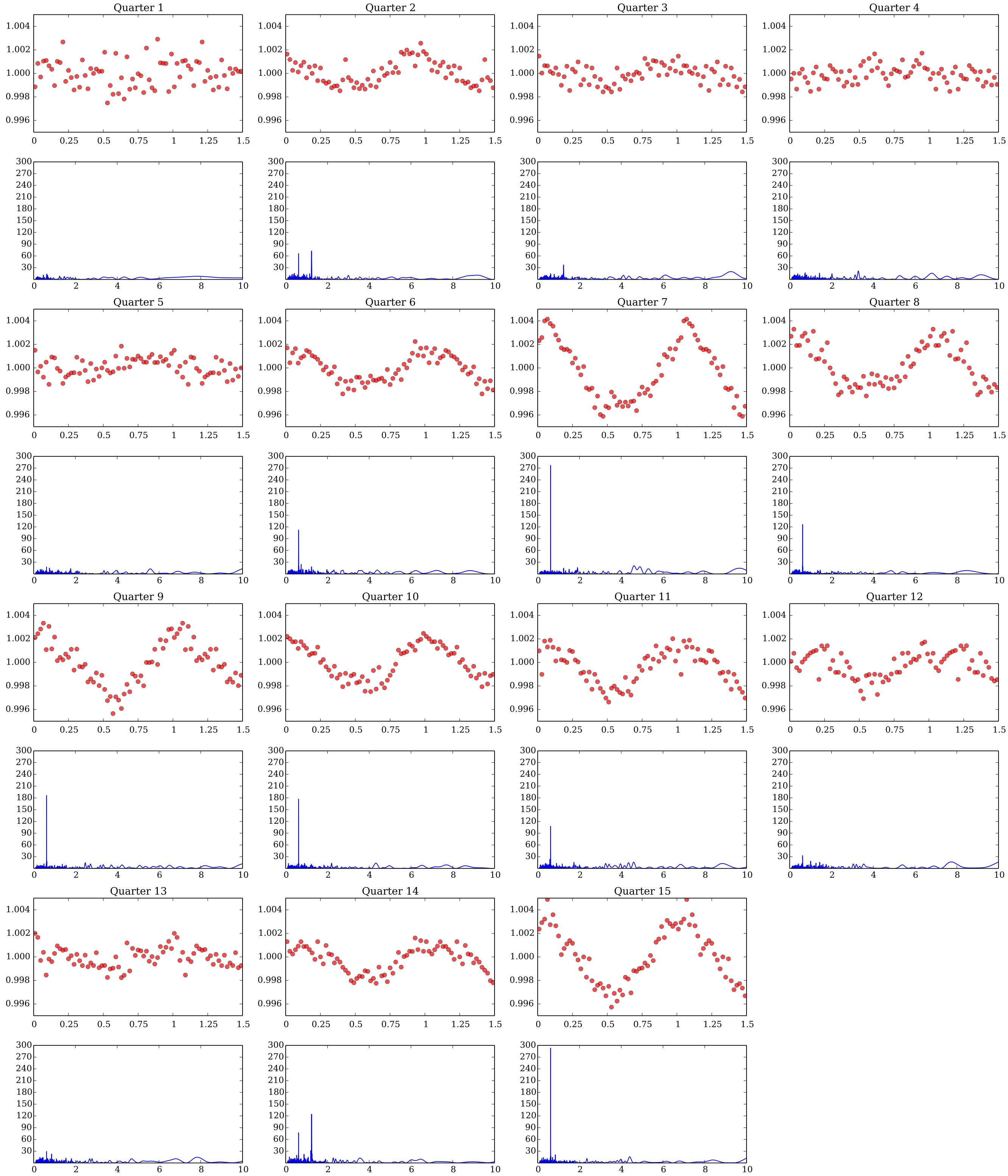

Figure 10. A sample of light curves (upper rows) folded using a period of 0.61895 days, for the central star of NGC 6826, for the 11 quarters of data, with corresponding periodograms (lower rows). No consistent periodicity could be detected for this star, but see the studies of Handler et al. (2013) and Jevtić et al. (2012). The light curves' x-axes values are phase, while those of the periodograms are time in days. The light curve fluxes are median-normalised, while the periodograms' y-axes measure the signal detection efficiency

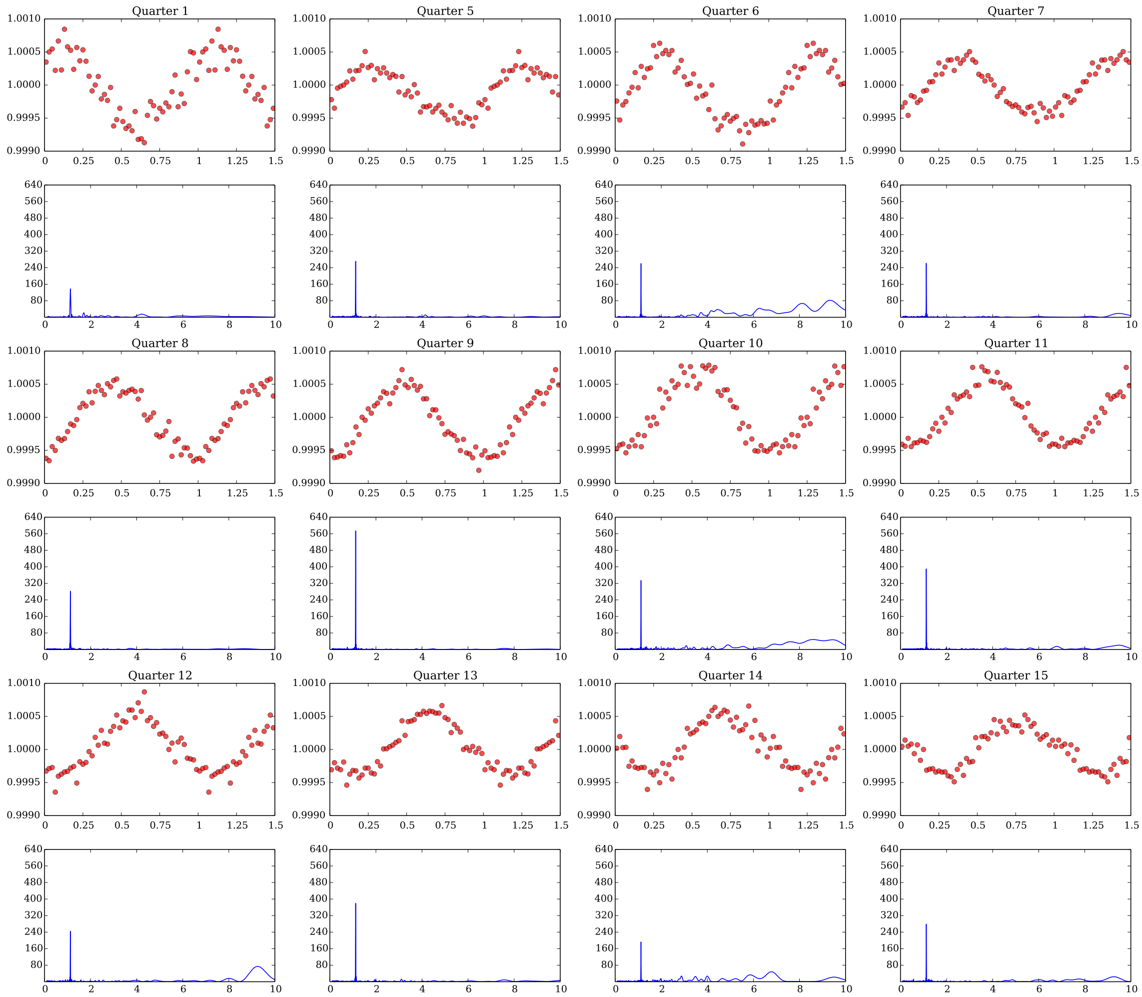

Figure 11. The folded lightcurves (upper rows) and periodograms (lower rows) for the central star of Pa 5, for each individual quarter of data, using a period of 1.12 days. The light curves' x-axes values are phase, while those of the periodograms are time in days. The light curves fluxes are median-normalised, while the periodogram's y-axes measure the signal detection efficiency

and have a triangular shape. If each outburst were due to an accretion event, the accreted mass would be:

$$m = 1 \times 10^{-11} \left(\frac{R}{0.04R_{\odot}}\right) \left(\frac{E_{acc}}{10^{39}\mathrm{erg}}\right) \left(\frac{M}{0.5M_{\odot}}\right) M_{\odot}$$

We note that this calculation is quite insensitive to the value of temperature and gravity adopted. The accretion rate would be only $\sim 10^{-16}$ $M_{\odot}$ yr^{-1} on average over a one-day-long accretion episode and these episodes would be semi-regularly spaced.

Accretion onto the central star, however would quickly provide a hydrogen layer, which would change the PG1159 classification. Accretion onto the companion from the PG1159 star would be difficult to envisage because it would imply a compact companion and a very short periastron passage which would imply very high eccentricity. Alternative scenarios could be accretion onto the companion of material from a circumbinary disk for a light companion in an eccentric orbit. Alternatively the outbursts are caused by wind instabilities, the cause of which would require a semi-periodic nature.

6 THE ANALYSIS OF NGC 6826

In Figs. 10 we present the period analysis using individual quarters for the central star of NGC 6826 (the flux units in these plots are electrons per 30 minute exposure). This star is peculiar. It has a strong, yet not consistent variability, exhibiting two periods: 0.619 and 1.236 days, where one is a harmonic of the other, with an amplitude varying between 2 and 8 mmag. The longer periodicity appears in only about half of the analysed quarters of data. We also measured a weak radial velocity variability with a best period of 0.238 days (which is equivalent to one fifth of the 1.236 day periodcity), using measurements from the catalogue of Acker et al. (1982). We discuss this peculiar behaviour further in § 8.3 where we compare our measurements with those of Jevtić et al. (2012) and Handler et al. (2013).

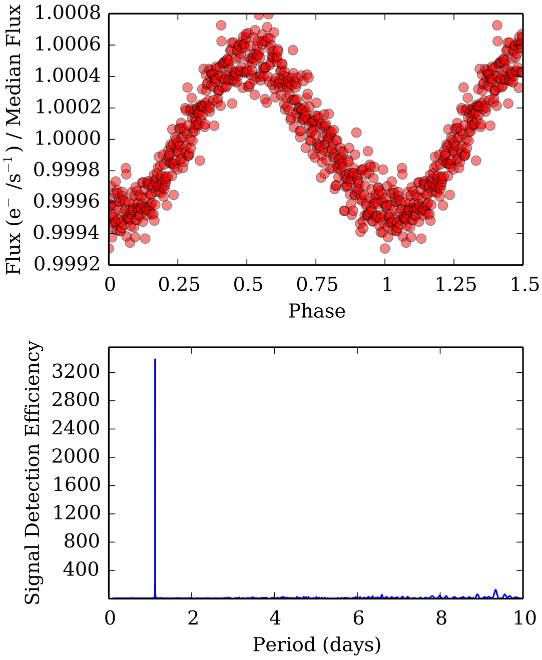

Figure 12. The folded lightcurve (upper panel) and periodogram (lower panel) for the central star of Pa 5, for all quarters of data, using a period of 1.12 days

7 THE ANALYSIS OF PATCHICK 5

7.1 The light and radial velocity curves of the central star of Pa 5

In Fig. 11 we present the period analysis using individual quarters for the central star of Pa 5 (the flux units in these plots are electrons per 30 minute exposure). In Fig. 12 we present the lightcurve phased using the most prominent period. The lightcurve of the central star of Pa 5 gives a consistent period of 1.12 days with an amplitude of 0.5 mmag. No radial velocity variability is detected larger than $\sim$5 km s^{-1}. It is entirely possible this is a binary seen close to pole on, but even so, the small amplitude of the curve implies a planetary or evolved companion.

7.2 Stellar atmosphere modelling of the central star of Pa 5

The optical spectrum of Pa 5 strongly resembles that of the O(He) central star of PN K 1-27 (Reindl et al. 2014). The only photospheric lines in the spectrum of Pa 5 are HeII lines at 4339, 4542, 4686, 4859, 5412 Å and NV lines at 4513-4530, 4604, 4620, 4934 and 4943-4951 Å (note that the Balmer lines are actually HeII lines and that emission lines in the trough of absorption lines are of stellar origin). The fact that the N V $\lambda\lambda\,4604, 4620$ lines appear in emission already indicates $T_{\rm eff} \geqslant 115$ kK. The central emission of He II $\lambda\,4686$ Å is stronger than the one observed in K 1−27, suggesting that Pa 5 is hotter than $T_{\rm eff} = 135$ kK. To further constrain the surface parameters of Pa 5, we calculated TMAP atmosphere models by extending the model grid calculated for K 1−27 (Reindl et al. 2014) up to $T_{\rm eff} = 160$ kK. It included opacities of the elements H, He, C, N, O, and Ne, which were taken from the Tübingen model-atom database TMAD[2]. While we achieved a good fit for the He II and the N V $\lambda\lambda\,4604, 4620$ lines with $T_{\rm eff} = 145$ kK, $\log g = 6.7$, a helium mass fraction of 0.9835, N/He $= 1.3 \times 10^{-2}$, C/He=5x10^{-4} and O/He=4x10^{-4} (by mass), we could not reproduce the remaining N V lines perfectly. Since the aim of our analysis was a coarse estimation of the surface parameters rather than a precise spectral analysis, we will leave the solution of this problem to future work. It is worth noting that, differently from the case of K 1−27, we could not find any hint of hydrogen in the atmosphere of Pa 5. Upper limits for the abundances of carbon and oxygen were derived by test models where the respective lines in the model contradict the non-detection of the lines in the observation (at the abundance limit). For the determination of an upper limit for the carbon abundance we used C IV $\lambda\lambda\,4441, 4646, 4658, 4660$ and found C/He $\leqslant 5 \times 10^{-4}$ (by mass) and for oxygen we used O V $\lambda\lambda\,5114$ and found O/He $\leqslant 4 \times 10^{-4}$. Thus, Pa 5 displays a similar CNO abundance pattern (nitrogen supersolar, carbon and oxygen subsolar, with solar abundances according to Asplund et al. (2009)) as the O(He) stars K 1−27, LoTr 4, and HS 2209+8229 (Reindl et al. 2014).

We calculated the spectroscopic distance of Pa 5 using the flux calibration of Heber et al. (1984) for $\lambda_{\rm eff} = 5454$ Å,

$$d[\mathrm{pc}] = 7.11 \times 10^4 \cdot \sqrt{H_\nu \cdot M \times 10^{0.4\, m_{\rm V_0} - \log g}} \ ,$$

with $m_{\rm V_o} = m_{\rm V} - 2.175c$, $c = 1.47E_{\rm B-V}$, and the Eddington flux H_ν (2.348.15 $\times$ 10^{-3} erg/cm^2/s/Hz) at 5454 Å of our best fit model atmosphere. We use the visual brightness ($m_{\rm V}$ = 15.719) obtained from the US Naval Observatory CCD Astrograph Catalogue (UCAC4, Zacharias et al. 2013), which is similar to the one listed in Table 1 obtained by Everett et al. (2012). The reddening, E_{B-V} = 0.1058, was taken from the Galactic dust extinction maps from Schlafly & Finkbeiner (2011). The mass of Pa 5 (0.54 $M_\odot$) was derived by comparing its position in the $\log T_{\rm eff} - \log g$ plane with evolutionary tracks from Althaus et al. (2009). We derive a distance of 1.4 kpc. From the angular diameter of 2 arcmin, a linear radius of the PN of $R = 0.3$ pc results. Using an expansion velocity of 45 km s^{-1}(García-Díaz et al. 2014), the kinematic age of the PN is about 6500 years.

Our spectrum also exhibits PN lines of [OIII] $\lambda\lambda$4959,5007. The Hβ emission line in the trough of the HeII λ4859 absorption is reasonably fitted with our stellar atmosphere model, but while other HeII emission components in the trough of absorption lines are completely unchanged by the sky subtraction process, showing them to be stellar, the emission in the trough of the HeII line at 4859 Å is completely removed by the sky subtraction as are the lines of [OIII], showing these to be from the nebula.

The systemic velocity determined via the two [OIII] nebular lines is 26.9 km s^{-1}. García-Díaz et al. (2014) quote a systemic velocity value of 12.4 $\pm$ 2 km s^{-1} obtained from Hα and [OIII] lines. We note that the HeII emission lines in the trough of absorption lines, as well as the Hβ emission indicate a smaller systemic velocity of (9.6$\pm$1.3) km s^{-1}, in agreement with the value of García-Díaz et al. (2014). Finally the three emission lines we have identified as NV have positions corresponding with 19, 13 and 3 km s^{-1},

[2] http://astro.uni-tuebingen.de/ TMAD

for the $\lambda\lambda$4604,4620 and λ4945, respectively. The nebular expansion velocity obtained from HWHM of the [OIII] lines is 76 km s^{-1}, while García-Díaz et al. (2014) obtained 45.2$\pm$2 km s^{-1} from their position-velocity diagram, a value that is more reliable and which we have adopted above.

The WIYN spectrum of the central star of Pa 5 confirms the presence of all spectral lines. In the longer spectral range we also see Hα, both in absorption and emission (once again the absorption component is due to HeII, while the emission could be of mixed stellar and nebular origin) and the CIV doublet centred at λ5806, which appears as a blue shifted absorption, with possibly a red shifted weak emission. This line was first noted by Østensen et al. (2010), but could not be confirmed by García-Díaz et al. (2014). We also see the interstellar Na D lines, blended together. These were incorrectly identified as CaII lines by García-Díaz et al. (2014).

We detected no orbital radial velocity shift to within $\pm$5 km s^{-1}. Our observations cover phases related to the photometric variability of 0.0–0.25 and 0.55–0.75, where phase zero occurs at minimum light. If the photometric variability were caused by an irradiation effect, then the radial velocity minimum and maximum would occur at phases 0.25 and 0.75, so we are sensitive to the full radial velocity range in that case. For an ellipsoidal effect, our radial velocities are sensitive to about two-thirds of the full radial velocity amplitude range, thus we are highly sensitive to those variations as well. If this is a close binary, its orbital rotation axis is approximately aligned with the line of sight, a geometry that would be consistent with the small amplitude of the photometric variability, despite the short period.

7.3 Wilson-Devinney models of the photometric variability of the central stars of Pa 5

The sinusioidal variability in the *Kepler* light curve of the central star of Pa 5 seems to indicate the presence of a binary companion. However, there are several post-AGB and WD stars such as WD 1953-011 (Wade et al. 2003; Valyavin et al. 2011), BOKS 53586 (Holberg & Howell 2011), and WD 0103+732, (Hillwig et al., in preparation) that exhibit a consistent periodic behaviour in which the variability has been attributed to magnetic spots. In these cases the periods reflect the rotation of the star rather than an orbital modulation.

We have explored the potential binary origins for the photometric variability in the central star of Pa 5. We can effectively rule out most stellar companions because of the lack of radial velocity variation of the spectral lines and because of the lack of emission lines in the spectrum that would be caused by irradiation. While we can find arbitrarily low inclinations for which the amplitude of an irradiation effect matches the observed *Kepler* photometry, for such a hot central star the spectrum should exhibit very strong emission lines from the irradiated stellar hemisphere. The emission lines may not be as strong if the companion is hotter than an M or K dwarf, but then the companion's visual luminosity would approach or surpass the visual luminosity of the central star and we should see spectral features from the companion. Therefore it is unlikely that the central star of Pa 5 has a main sequence companion in a 1.12 day orbital period.

Given the case of J19311 discussed in § 4.2 and the relatively large number of double-degenerate binary central stars known (Hillwig 2011), it is possible that Pa 5 could have a WD or pre-WD companion. While a cooler WD companion *might* exhibit an irradiation effect without strong emission lines, our limit on the radial velocity amplitude means that for a stellar mass companion the potential binary system would have an inclination $i < 2.5^\circ$.

Another possibility may be a planetary mass companion. Using the mass, radius, and temperature values above for the central star and a representative "hot Jupiter" companion, we find that for $M_2 = 0.001$ M$_\odot$, $R_2 = 0.13$ R$_\odot$, and $T_2 = 1200$ K and an albedo of 0.3 for the companion, we also need to resort to a very low inclination to match the photometric amplitude, arriving at $i = 1.5^\circ$.

Yet another alternative is that the variability is caused by a spot of constant size and constant temperature contrast, at a constant location on the surface of the star. This would almost certainly have to be due to magnetic fields. However, the relatively narrow spectral lines do not show evidence of a strong magnetic field and the effective temperature is *much* too high to expect a convective atmosphere which may help produce spots (for a recent review see Brinkworth et al. 2013). Weak magnetic fields ($\sim$100 G) have only been detected once in a PN central star (Todt et al. 2014), while several searches have returned either false positives (Jordan et al. 2005) or upper limits of few $\times$100 G (Jordan et al. 2012; Asensio Ramos et al. 2014).

8 DISCUSSION AND CONCLUSIONS

Below we explore scenarios to explain the photometric and spectroscopic behaviour of our four central stars. The central star of A 61 was not observed to vary above 2 mmag, and that of NGC6742 could not be analysed at all. Below we discuss the four objects that were found to vary.

8.1 The short period binary J19311

J19311 is a short period, post-common envelope (post-CE), binary where the light variability is due to Doppler beaming rather than irradiation, and to an additional, weak, ellipsoidal variability effect. This is the first time such an effect has been detected in a central star of PN, undoubtedly because its weakness would be difficult to see with the precision and sporadic cadence of ground-based observations. The companion is almost certainly an evolved star. Despite the predicted rarity of these double degenerate central stars, they appear to be rather common among the post-CE central stars of PN (Hillwig et al. 2010). The star itself is hot, but does not appear to have any other peculiarities. Finally, the PN consists of two separate ejections, close in time and with a 90 degree angle between them (Aller et al. 2013). Common envelope ejections are far from being understood (e.g., Ricker & Taam 2012; Passy et al. 2012; Ivanova et al. 2013), and this object with its two degenerate stars and the peculiar nebular morphology indicating two almost simultaneous ejections at 90 deg from one another, bears witness to the complexity of the phenomenon.

8.2 The nature of Kn 61's central star

The central star of Kn 61 is a variable PG1159, hydrogen-deficient star, with a variability amplitude of 0.08-0.14 mag. The approximately-triangular brightness peaks recur typically every 2-12 days. The width of the peaks at their base varies between 1 and 2 days. The shape of the light curve is very different from those of irradiated or ellipsoidal variables.

Only one other object to our knowledge may be similar to this: the DA WD J1916+3938 (KIC 4552982). Aside from pulsations (Hermes et al. 2011), it shows a *Kepler* light curve variability very similar to that exhibited by the central star or Kn 61, except with a slightly larger amplitude of 0.15 mag from base to peak (JJ Hermes, private communication). The peaks repeat approximately every 3 days (cf. our 2-12 days) and they are narrower, only $\sim$10 hours vs. our 24-48 hours. This star is an 11-kK WD with a $\log g = 8.3$ and as such is very different from our hot pre-WD. Interpreting the brightness peaks of J1916+3938 as accretion events the median accreted mass per episode is $5{\times}10^{-18}$ M$_\odot$, or an accretion rate of 10^{-22} M$_\odot$ yr^{-1}, over 10 hour-long events, substantially less than equivalent numbers deduced for Kn 61's central star.

Another PG1159 star is known to have outbursts, Lo 4 (Werner et al. 1992). Bond (2014) measured them to recur approximately every 100 days and to occupy approximately 5 per cent of the monitoring period. These outbursts do not appear to have any relationship with the pulsations of the star, which are of the order of minutes, nor to be caused by them. If the outbursts on Kn 61's central star are due to accretion episodes, each would accrete $\sim 10^{-11}$ M$_\odot$(assuming the accretion happens onto the central star). Accretion of, presumably, hydrogen-rich material onto a hydrogen deficient, PG1159 star would rapidly change its spectral type.

If the light curve peaks were instead caused by accretion onto a companion orbiting the PG1159 primary, caused perhaps by periastron passages, then the companion would have to be more compact than the PG1159 star, hence a WD. However, in order to have an orbit with a period of the order of days and with periastron passages that allow a very small star to overflow its Roche lobe, the eccentricity would have to be unreasonably high. Another alternative are accretion from a circumbinary disk onto a companion that, being lighter than the central star and in an eccentric orbit, moves periodically away from the centre of mass and into the region of the disk. Alternatively these 20-L$_\odot$ light outbursts are semi-periodic wind outbursts, which may also have been responsible for the nebular morphology (see Fig. 2), but we then wonder what causes them to recur. It is possible that wind outbursts are triggered by a companion in an eccentric orbit, generating a mechanism similar to the so-called "heartbeat" stars (Thompson et al. 2012). All of these scenarios involve a short-period eccentric binary having evolved through a CE interaction,but so far our understanding of CE interactions is that the eccentricity of the post-CE binary would be relatively low ($\lesssim 0.2$; Passy et al. 2012).

We have considered the possibility that a foreign, non-associated object affected the light curve. We have carefully investigated this possibility by reanalysing the *Kepler* data and we found no indication that this is the case. However, a chance alignment remains a possibility given *Kepler*'s low spatial resolution. This said, this light curve is not just odd for a central star of PN, it is unique of its own right. We therefore appeal to Occam's Razor and argue that it is unlikely that a chance alignment was observed between a rare central star of PN and a unique object with light properties that have not been observed before.

We must in the end conclude that we have at this point no definitive explanation for the light behaviour of the central star of Kn 61.

8.3 The fast-rotating central star of NGC6826

The *Kepler* data of the central star of NGC 6826 was carefully analysed by Jevtić et al. (2012) and Handler et al. (2013). While the former study ascribes the incoherent variability to a combination of binarity and wind variability, the latter concluded that the variability is due to rotationally-induced wind variability. We have measured a distinct (2-8 mmag) dominant periodicity of 0.619 days with an occasional periodicity of 1.236 days, appearing in only about half of the analysed quarters of data. We also measured a weak radial velocity variability with a best period of 0.238 days (which is equivalent to one fifth of the 1.236 days). Handler et al. (2013) on the other hand measured several periodicities but a persistent periodicity emerges in their data at 1.23799 days, which, as the lowest harmonic, they conclude is related to the underlying cause of the phenomenon. Their spectra show primarily non periodic variability, although their HeII lines show a period at 0.13 days. They exclude any spectral variability on the dominant photometric period of 1.24 days.

The conclusion for this object is that the variability is not due to a short period binary. However, it may be due to a modulation of the wind caused by rotation of the star. Handler et al. (2013) concluded that a rotation rate can be inferred from the 1.24-d period and results in a rotation rate of 73 km s^{-1} assuming a radius of 1.8 R$_\odot$ measured by Kudritzki et al. (2006). Using a projected rotation rate of the star of $v \sin i$ = 50 km s^{-1} determined by Prinja et al. (2012) an inclination angle of $\sim$45 deg was derived. Such a fast rotation would be extremely high for a post-AGB star. Measurements show that white dwarfs rotate with projected rotation velocities smaller than 10 km s^{-1} (Berger et al. 2005) with measurements from pulsating white dwarf showing even lower values (Kawaler 2004). Such low rotation rates are understood today by the effects of mass-loss and angular momentum transport (Suijs et al. 2008; Cantiello et al. 2014). These central stars have slightly larger radii compared to WDs and their rotation rates should be smaller still. It is likely that this star's rotation was caused by a merger. Mergers have been proposed to explain high rotation rates and magnetic activity in post-giant stars by, e.g., Nordhaus et al. (2011) and Geier et al. (2013).

8.4 The periodically-variable central star of Pa 5

The lightcurve of the central star of Pa 5 gives a consistent period of 1.12 days with an amplitude of 0.5 mmag. No radial velocity variability is detected larger than $\sim$5 km s^{-1}. It is entirely possible this is a binary seen close to pole on, but even so, the small amplitude of the curve implies a planetary or evolved companion. A planetary companion so close to the central star would imply that planetary companions can survive a common envelope phase. Despite the fact that close planets have been announced around post-giant stars (e.g., Silvotti et al. 2014) we remain suspicious that survival is possible under common envelope conditions (De Marco et al. 2012).

It is possible that the variability is due to a star spot. However, the regularity of the light curve would imply a constant spot, which is unlikely. Also, the strong magnetic fields implied are not consistent with negative searches for magnetic fields in central stars of PN (Jordan et al. 2012; Asensio Ramos et al. 2014; Todt et al. 2014). The central star is a rare O(He) star, in other words a star made almost entirely of helium. It is only the tenth known star in the class (four more objects have recently been found; Werner et al. 2014). O(He) stars are likely the descendant of the R Coronae Borealis stars considered mergers of two white dwarfs (Reindl et al. 2014; Clayton et al. 2005). However, the central star of Pa 5 seems to have too much nitrogen and too little carbon to descend from the carbon-rich R Coronae Borealis stars. If they were mergers we may expect that the rotation rate would be higher than usual for WDs. Interpreting the 1.12 days as the rotation period, the surface velocity this star would be v=0.4-4.5 km s^{-1}, for radii of 0.01 to 0.1 R$_\odot$, therefore not particularly large.

Maoz et al. (2014) analysed 14 WDs and 7 had a variability very similar to the one of the central star of Pa 5. They reviewed several scenarios, some similar to those we have considered. Their best scenario is one where accretion of debris material along the poles increases the UV opacity generating some optically-bright spots. A misalignment between the magnetic and rotational axis would bring the spots in and out of view as the star rotates. The fact that half of their stars show the phenomenon and that this is approximately the fraction of WD that show active debris disk accretion reinforces that conclusion. It would be however unlikely to find debris disks around Pa 5's central star since, contrary to the situation in WDs, its sublimation radius is much larger than the tidal disruption radius.

At this time, the most plausible hypothesis is that Pa 5 has a central star with an evolved companion in a nearly-pole-on orbit.

8.5 General discussion on the entire sample

There is no way to obtain a measure of the binary fraction from a sample of five objects. So, where does this small *Kepler* sample take us? One, possibly two, of the 5 central stars with usable data are likely binaries that would not have been detected from the ground in photometric variability surveys (though J 19311 would have been detected from the ground using radial velocity variability, a technique which is not readily used in survey mode due to its time-intensive nature (De Marco et al. 2007)). The very fast rotating central star of NGC 6826 can only be explained with current theories as the product of a merger and hence as a star that has evolved via a binary channel. Finally, the enigmatic PG1159 central star of Kn 61 with its semi-periodic small outbursts remains largely a puzzle, though it is possible that this behaviour is binary-induced.

With three out of the 4 variable objects displaying amplitudes below the ground-based detectability threshold we now know that many discoveries await surveys sporting the precision of *Kepler*. We also suspect that low level, periodic or semi-periodic variability is often binary related. We therefore wonder how much larger than 15 per cent the binary fraction would have been found, had *Kepler* surveyed the entire samples surveyed by Bond (2000) or Miszalski et al. (2009).

A short period binary fraction of 15 per cent is already higher than one would expect. This statement is based on the period distribution of intermediate mass stars (Duquennoy & Mayor 1991; Raghavan et al. 2010), the tidal capture radii of giant stars (e.g., Villaver & Livio 2009; Mustill & Villaver 2012) and the fact that binaries that go through a CE on the RGB tend not to ascend the AGB (Heber 1986; Dorman et al. 1993), and thus never become PN central stars. The prediction is of the order of a few percent, although the exact number depends on the mean mass of the central star population: a lower mass results in a lower number of post-CE central stars, while a higher mean mass results in a higher number. Depending on how much larger than 15 per cent this fraction becomes, we may face a situation where a CE phase is a preferred channel to form PN. The "*Kepler* 2" mission data will include an additional ∼20 PN central stars that will improve the statistics on this matter.

ACKNOWLEDGMENTS

We wish to thank Martin Still and Thomas Barclay of NASA Ames for providing in-depth guidance of the *Kepler* reduction pipeline so that we could devise the data analysis pathway for our program, and Jim Shuder and Adam Block for providing images of NGC 6742 and A 61, respectively. The Gemini Observatory and Travis Rector are acknowledged for the acquisition of the image of Kn 61. Boris Gaensicke, JJ Hermes and Klaus Werner are thanked for advising us on the light curve of the central star of Kn 61. Dan Maoz is thanked for sharing the content of his paper before its publication. Some of the synthetic spectra were obtained from the German Astrophysical Virtual Observatory through the TheoSSA web interface.

This research was supported in part by NASA grant NNX12AC86G, and by the Carnegie Observatories, Pasadena, CA and includes data collected by the *Kepler* mission. Funding for the *Kepler* mission is provided by the NASA Science Mission directorate. This research made use of PyKE (Still & Barclay 2012), a software package for the reduction and analysis of *Kepler* data. This open source software project is developed and distributed by the NASA *Kepler* Guest Observer Office. This research also made use of the NASA Exoplanet Archive, which is operated by the California Institute of Technology, under contract with the National Aeronautics and Space Administration under the Exoplanet Exploration Program. This material is based in part upon work supported by the National Science Foundation under Grant No. AST-1109683 (TH,OD). Any opinions, findings, and conclusions or recommendations expressed in this material are those of the author(s) and do not necessarily reflect the views of the National Science Foundation. NR is supported by the German Research Foundation (DFG, grant WE 1312/41-1).

Based in part on observations obtained at the Gemini Observatory, which is operated by the Association of Universities for Research in Astronomy, Inc., under a cooperative agreement with the NSF on behalf of the Gemini partnership: the National Science Foundation (United States), the National Research Council (Canada), CONICYT (Chile), the Australian Research Council (Australia), Ministério da Ciência, Tecnologia e Inovação (Brazil) and Ministerio de Ciencia, Tecnología e Innovación Productiva (Argentina).

REFERENCES

Abell G. O., 1966, ApJ , 144, 259
Acker A., Gleizes F., Chopinet M., Marcout J., Ochsenbein F., Roques J. M., 1982, Publication Speciale du Centre de Donnees Stellaires, 3
Acker A., Marcout J., Ochsenbein F., Stenholm B., Tylenda R., 1992, Strasbourg - ESO catalogue of galactic planetary nebulae. Part 1; Part 2. Garching: European Southern Observatory, 1992
Aller A. et al., 2013, A&A , 552, A25
Althaus L. G., Panei J. A., Romero A. D., Rohrmann R. D., Córsico A. H., García-Berro E., Miller Bertolami M. M., 2009, A&A , 502, 207
Asensio Ramos A., Martínez González M. J., Manso Sainz R., Corradi R. L. M., Leone F., 2014, ApJ , 787, 111
Asplund M., Grevesse N., Sauval A. J., Scott P., 2009, Annual Reviews in Astronomy and Astrophysics, 47, 481
Berger L., Koester D., Napiwotzki R., Reid I. N., Zuckerman B., 2005, A&A , 444, 565
Blöcker T., 1995, A&A , 299, 755
Bloemen S. et al., 2012, MNRAS , 422, 2600
Bloemen S. et al., 2011, MNRAS , 410, 1787
Bond H. E., 2000, in ASP Conf. Ser. 199: Asymmetrical Planetary Nebulae II: From Origins to Microstructures, p. 115
Bond H. E., 2014, ArXiv e-prints
Bond H. E., Ciardullo R., 1990, in Astronomical Society of the Pacific Conference Series, Vol. 11, Confrontation Between Stellar Pulsation and Evolution, Cacciari C., Clementini G., eds., pp. 529–533
Brinkworth C. S., Burleigh M. R., Lawrie K., Marsh T. R., Knigge C., 2013, ApJ , 773, 47
Bujarrabal V., Castro-Carrizo A., Alcolea J., Sánchez Contreras C., 2001, A&A , 377, 868
Cantiello M., Mankovich C., Bildsten L., Christensen-Dalsgaard J., Paxton B., 2014, ApJ , 788, 93
Clayton G. C., Herwig F., Geballe T. R., Asplund M., Tenenbaum E. D., Engelbracht C. W., Gordon K. D., 2005, ApJL , 623, L141
De Marco O., 2009, PASP , 121, 316
De Marco O., Bond H. E., Harmer D., Fleming A. J., 2004, ApJL , 602, L93
De Marco O., Hillwig T. C., Smith A. J., 2008, AJ, 136, 323
De Marco O., Passy J.-C., Frew D. J., Moe M., Jacoby G. H., 2013, MNRAS , 428, 2118
De Marco O., Passy J.-C., Herwig F., Fryer C. L., Mac Low M.-M., Oishi J. S., 2012, in IAU Symposium, Vol. 282, IAU Symposium, Richards M. T., Hubeny I., eds., pp. 517–520
De Marco O., Wortel S., Bond H. E., Harmer D., 2007, in Asymmetrical Planetary Nebulae IV, IAC Elec. Pub.
Dorman B., Rood R. T., O'Connell R. W., 1993, ApJ , 419, 596
Drummond J. D., 1980, PhD thesis, New Mexico Univ., Albuquerque.
Duquennoy A., Mayor M., 1991, A&A , 248, 485
Everett M. E., Howell S. B., Kinemuchi K., 2012, PASP , 124, 316
Frew D. J., 2008, PhD thesis, Department of Physics, Macquarie University.
García-Díaz M. T., González-Buitrago D., López J. A., Zharikov S., Tovmassian G., Borisov N., Valyavin G., 2014, ArXiv e-prints
García-Segura G., Langer N., Różyczka M., Franco J., 1999, ApJ , 517, 767
García-Segura G., López J. A., Franco J., 2005, ApJ , 618, 919
García-Segura G., Villaver E., Langer N., Yoon S.-C., Manchado A., 2014, ApJ , 783, 74
Geier S., Heber U., Heuser C., Classen L., O'Toole S. J., Edelmann H., 2013, A&A , 551, L4
Gonzalez Buitrago D., García-Díaz M. T., López J. A., Zharikov S., Tovmassian G., Borisov N., Valyavin G., 2014, in Asymmetrical Planetary Nebulae VI conference, Proceedings of the conference held 4-8 November, 2013. Edited by C. Morisset, G. Delgado-Inglada and S. Torres-Peimbert. Online at http://www.astroscu.unam.mx/apn6/PROCEEDINGS/, id.34
Handler G., 2003, in IAU Symposium, Vol. 209, Planetary Nebulae: Their Evolution and Role in the Universe, Kwok S., Dopita M., Sutherland R., eds., p. 237
Handler G., Prinja R. K., Urbaneja M. A., Antoci V., Twicken J. D., Barclay T., 2013, MNRAS , 430, 2923
Harrington J. P., Borkowski K. J., Tsvetanov Z. I., 1997, in IAU Symposium, Vol. 180, Planetary Nebulae, Habing H. J., Lamers H. J. G. L. M., eds., p. 235
Heber U., 1986, A&A , 155, 33
Heber U., Hunger K., Jonas G., Kudritzki R. P., 1984, A&A , 130, 119
Hermes J. J. et al., 2011, ApJL , 741, L16
Herrero E., Lanza A. F., Ribas I., Jordi C., Collier Cameron A., Morales J. C., 2014, A&A , 563, A104
Hillwig T. C., 2011, in Asymmetric Planetary Nebulae 5 Conference
Hillwig T. C., Bond H. E., Afşar M., De Marco O., 2010, AJ, 140, 319
Holberg J. B., Howell S. B., 2011, AJ, 142, 62
Ivanova N. et al., 2013, Astronomy & Astrophysics Rev., 21, 59
Jacoby G., De Marco O., Howell S., Kronberger M., 2012, in American Astronomical Society Meeting Abstracts, Vol. 219, American Astronomical Society Meeting Abstracts, p. 418.02
Jacoby G. H. et al., 1992, PASP , 104, 599
Jacoby G. H. et al., 2010, PASA , 27, 156
Jevtić N., Stine P., Nilsen W., Schweitzer J. S., Jenkins J. M., Klaus T. C., Lie J., McCauliff S., 2012, ApJ , 756, 9

Jones D., Boffin H. M. J., Miszalski B., Wesson R., Corradi R. L. M., Tyndall A. A., 2014, A&A , 562, A89
Jordan S., Bagnulo S., Werner K., O'Toole S. J., 2012, A&A , 542, A64
Jordan S., Werner K., O'Toole S. J., 2005, A&A , 432, 273
Kawaler S. D., 2004, in IAU Symposium, Vol. 215, Stellar Rotation, Maeder A., Eenens P., eds., p. 561
Kronberger M. et al., 2012, in IAU Symposium, Vol. 283, IAU Symposium, pp. 414–415
Kronberger M. et al., 2006, A&A , 447, 921
Kudritzki R. P., Urbaneja M. A., Puls J., 2006, in IAU Symposium, Vol. 234, Planetary Nebulae in our Galaxy and Beyond, Barlow M. J., Méndez R. H., eds., pp. 119–126
Kukarkin B. V. et al., 1981, in Moscow, Acad. of Sciences USSR Sternberg,1951 (1981), p. 0
Lagadec E., Zijlstra A. A., 2008, MNRAS , 390, L59
Long J., Jacoby G., De Marco O., Hillwig T. C., Kronberger M., Howell S. B., 2013, in American Astronomical Society Meeting Abstracts, Vol. 221, American Astronomical Society Meeting Abstracts #221, p. #249.07
Maoz D., Mazeh T., McQuillan A., 2014, ArXiv e-prints
Marigo P., Girardi L., Weiss A., Groenewegen M. A. T., Chiosi C., 2004, A&A , 423, 995
Mendez R. H., Kudritzki R. P., Herrero A., Husfeld D., Groth H. G., 1988, A&A , 190, 113
Miszalski B., Acker A., Moffat A. F. J., Parker Q. A., Udalski A., 2009, A&A , 496, 813
Moe M., De Marco O., 2006, ApJ , 650, 916
Mustill A. J., Villaver E., 2012, ApJ , 761, 121
Napiwotzki R., 1999, A&A , 350, 101
Nordhaus J., Blackman E. G., Frank A., 2007, MNRAS , 376, 599
Nordhaus J., Wellons S., Spiegel D. S., Metzger B. D., Blackman E. G., 2011, Proceedings of the National Academy of Science, 108, 3135
Østensen R. H. et al., 2010, ArXiv e-prints
Parker Q. A. et al., 2006, MNRAS , 373, 79
Passy J.-C. et al., 2012, ApJ , 744, 52
Prinja R. K., Massa D. L., Cantiello M., 2012, ApJL , 759, L28
Raghavan D. et al., 2010, ApJ Supp. , 190, 1
Rauch T., Deetjen J. L., 2003, in Astronomical Society of the Pacific Conference Series, Vol. 288, Stellar Atmosphere Modeling, Hubeny I., Mihalas D., Werner K., eds., p. 103
Reindl N., Rauch T., Werner K., Kruk J. W., Todt H., 2014, A&A , 566, A116
Ricker P. M., Taam R. E., 2012, ApJ , 746, 74
Schlafly E. F., Finkbeiner D. P., 2011, ApJ , 737, 103
Schönberner D., 1983, ApJ , 272, 708
Schönberner D., Jacob R., Steffen M., Sandin C., 2007, A&A , 473, 467
Schreiber M. R. et al., 2009, Journal of Physics Conference Series, 172, 012024
Shimanskii V. V., Borisov N. V., Sakhibullin N. A., Sheveleva D. V., 2008, Astronomy Reports, 52, 479
Shporer A., Kaplan D. L., Steinfadt J. D. R., Bildsten L., Howell S. B., Mazeh T., 2010, ApJL , 725, L200
Silvotti R. et al., 2014, A&A , 570, A130
Soker N., 2006, PASP , 118, 260
Suijs M. P. L., Langer N., Poelarends A.-J., Yoon S.-C., Heger A., Herwig F., 2008, A&A , 481, L87
Thompson S. E. et al., 2012, ApJ , 753, 86
Todt H., Steffen M., Hubrig S., Schöller M., Hamann W.-R., Sandin C., Schönberner D., 2014, in Asymmetrical Planetary Nebulae VI conference, Proceedings of the conference held 4-8 November, 2013. Edited by C. Morisset, G. Delgado-Inglada and S. Torres-Peimbert. Online at http://www.astroscu.unam.mx/apn6/PROCEEDINGS/, id.103
Tovmassian G. et al., 2010, ApJ , 714, 178
Valyavin G. et al., 2011, ApJ , 734, 17
Vassiliadis E., Wood P. R., 1994, ApJ Supp. , 92, 125
Villaver E., Livio M., 2009, ApJL , 705, L81
Wade G. A., Bagnulo S., Szeifert T., Brinkworth C., Marsh T., Landstreet J. D., Maxted P., 2003, in Astronomical Society of the Pacific Conference Series, Vol. 307, Solar Polarization, Trujillo-Bueno J., Sanchez Almeida J., eds., p. 569
Werner K., Deetjen J. L., Dreizler S., Nagel T., Rauch T., Schuh S. L., 2003, in Astronomical Society of the Pacific Conference Series, Vol. 288, Stellar Atmosphere Modeling, Hubeny I., Mihalas D., Werner K., eds., p. 31
Werner K., Hamann W.-R., Heber U., Napiwotzki R., Rauch T., Wessolowski U., 1992, A&A , 259, L69
Werner K., Rauch T., Kepler S. O., 2014, A&A , 564, A53
Wilson R. E., 1990, ApJ , 356, 613
Wilson R. E., Devinney E. J., 1971, ApJ , 166, 605
Zacharias N., Finch C. T., Girard T. M., Henden A., Bartlett J. L., Monet D. G., Zacharias M. I., 2013, AJ, 145, 44
Zucker S., Mazeh T., Alexander T., 2007, ApJ , 670, 1326

4 Results

4.1 The rapid evolution of the exciting star of the Stingray Nebula

We find that SAO 244567 has steadily increased its effective temperature from 38 kK in 1988 to a peak value of 60 kK in 2002. During the same time, the star was contracting, as concluded from an increase in surface gravity from $\log g = 4.8$ to 6.0 and a drop in luminosity. Simultaneously, the mass-loss rate declined from $\log(\dot{M} \,/\, M_\odot\,\mathrm{yr}^{-1}) = -9.0$ to -11.6 and the terminal wind velocity increased from $v_\infty = 1800\,\mathrm{km/\,s}$ to $2800\,\mathrm{km/\,s}$. Since around 2002, the star stopped heating and has cooled down again to 55 kK by 2006. It has a largely solar surface composition with the exception of slightly subsolar carbon, phosphorus, and sulfur.

The subsolar carbon abundance indicates that the (possible) AGB phase of SAO 244567 was terminated before the third dredge-up. The observed mass-loss values agree well with prediction from radiative-driven wind theory, thus enhanced mass-loss is not responsible for the fast evolution SAO 244567. We cannot confirm the T_eff values found by Arkhipova *et al.* (2013) and argue that the formalism of Kaler (1978) they used to derive T_eff does not provide good estimates for the CS temperature. However, the evaluation of the ionization equilibria found in the FUSE spectra shows that T_eff is declining from 2002 on, supporting the contention by Arkhipova *et al.* (2013) that T_eff has recently peaked and has begun to decline.

By comparison with stellar-evolution calculations, we confirm that SAO 244567 must be a low-mass star ($M < 0.55\,M_\odot$). The observed fast evolution of SAO 244567 and its young PN with a kinematical age of only about 1000 years are in strong contradiction with the slow evolution of the respective stellar evolutionary models. The existence of the PN around SAO 244567 suggests that it is more likely a post-AGB star than an AGB-manqué star because – in general – only these stars are expected to eject a PN. However, the high heating rate of SAO 244567 ($\log(dt/dT_\mathrm{eff}/\mathrm{yrK}^{-1}) = -3$) would imply a CSPN mass of $0.87 M_\odot$ according to post-AGB evolutionary calculations of Blöcker (1995). We speculate that the star could be a late He-shell flash object like FG Sge, because the evolutionary speed of LTP objects is very high (decades). In addition, LTP scenarios predict a solar surface composition in the phase relevant to SAO 244567, because – different to VLTP scenarios – the star becomes hydrogen-deficient only when it has evolved back to the AGB. Alternatively, SAO 244567 could be the outcome of close binary evolution, being a low mass ($0.35\ M_\odot$) pre-He-WD after a CE phase, during which the PN was ejected. In the case the star was in thermal non-equilibrium after the CE ejection, this scenario might also account for its rapid evolution.

4.2 On helium-dominated stellar evolution: the mysterious role of the O(He)-type stars

Thanks to the better resolution of the new optical spectra (1.5 Å instead of 3 Å), we could derive the atmospheric parameters of the two O(He) stars K 1−27 and LoTr 4 more precisely. For instance, the spectrum of K 1−27 now reveals the central emission of He II λ 4686 Å, which could be used to reduce the errors of effective temperature. By that also a more accurate mass and distance determination was possible. The latter was used to derive the kinematical ages of the PNe of K 1−27 and LoTr 4. These provide an important information about time that has passed since the PNe were formed. As PNe are expected to be formed either on the tip of the AGB, or – if sufficient mass is lost – the RGB, the kinematical age of the PNe can tell us when the stars must have left the AGB or RGB. The relatively short kinematical ages of the hydrogen-rich PNe of K 1−27 and LoTr 4 lead to the conclusion, that these stars can not have been formed via double helium WD merger process, because even if the PNe would have been ejected during the merger process the post-merger times would be far too long (several million years) for a PN to survive.
In addition, we derived for the first time upper limits for the mass-loss rates of the four O(He) stars and found, that they agree well with predictions by radiative-driven wind theory. Only K 1−27 could have a ten times higher mass-loss rate than predicted. By that, we could rule out the possibility that O(He) stars can evolve into helium-enriched PG 1159 stars.
Furthermore, a trichotomy within the O(He) class was found. Some O(He) stars are enriched in nitrogen but not in carbon, some carbon-enriched objects do not show nitrogen, but there also are objects which are enriched in both. Interestingly, also other helium-dominated objects (e.g., He-sdO stars, DO WDs) exhibit the same trichotomy, and their carbon and nitrogen abundances are extremely similar to the ones of the O(He) stars. This is a strong hint, that their must be an evolutionary connection between the three subclasses, respectively. RCB stars and extreme helium stars are found to have the same helium/carbon/nitrogen abundance patterns like carbon and nitrogen enriched O(He), thus a evolutionary connection is also possible for them.
In contrast to previous statements, we do not see the two currently known [WN]-type CSPNe as progenitors of the O(He) stars, but rather as objects in a similar evolutionary stage as the O(He) stars because of the overlap in effective temperatures. We speculate that [WN]-type CSPNe might be more massive and by that more luminous than O(He) stars, what could explain their much higher mass-loss rates.
The helium-dominated sequence has most likely various formation channels. For single-star objects, merger scenarios seem most promising. Helium-dominated CSPNe must have formed in a different way, for example via enhanced mass-loss during their post-AGB evolution, or a merger within a CE of a CO-WD and an RGB or AGB star.

4.3 Analysis of cool DO-type white dwarfs from the Sloan Digital Sky Survey Data Release 10

We identified 24 DO WDs in the SDSS DR10, which have not been analyzed by non-LTE model atmospheres before. Our spectral analysis revealed effective temperatures and gravities in the ranges $T_{\rm eff} = 45 - 80\,\rm kK$ and $\log g = 7.50 - 8.75$.
Among them, we found one new and two not previously analyzed members of the so-called hot-wind DO WDs, which show ultrahigh excitation (uhei) absorption lines and too deep He II lines that cannot be fitted by any model. The process, which is responsible for these phenomena is still not understood. A literature study revealed that the fraction of DO WDs showing this phenomenon is significant (19% show too deep He II lines, 11% show additional uhei features), thus it is highly desirable to find an explanation for this phenomenon.
In eight of the spectra we were able to detect C III or C IV lines and we derived carbon abundances $C = 0.001 - 0.01$, by mass. For the other 16 objects upper limits for the carbon abundances were derived. Two of our objects are the coolest DO WDs ever discovered that still show a considerable amount of carbon in the atmosphere. This is in strong contradiction with diffusion calculations, and we suggested that, similar to what is proposed for DB WDs, a weak mass-loss is present in DO WDs.
We found that the additional opacities of C do not affect the theoretical He I and He II line profiles and we also investigated a possible impact of line blanketing by iron-group elements. We found that only the central depression of He II $\lambda\,4686\,\text{Å}$ is affected by the additional opacities of the iron-group elements. Thus, similar to the case of the O(He) stars, He II $\lambda\,4686\,\text{Å}$ might be an indicator for (hidden) opacities in the stellar atmosphere.
About 13% of the DO WDs have masses below $0.5\,M_\odot$ and might be successors of post-EHB He-sdO stars or low-mass PG 1159 stars. The mass distribution of DO WDs beyond the wind limit strongly deviates from the mass distribution of the objects before the observed PG 1159 wind limit. The plateau around $0.6\,M_\odot$ in the mass distribution of DO WDs beyond the wind limit agrees with the mass distribution of PG 1159 stars, O(He) stars, and DO WDs before the wind limit. The two additional higher mass peaks might reflect a merger origin of some O(He) stars and DO WDs and/or the possibility that [WN] and [WC] type central stars are more massive than PG1159 and O(He) stars.
Based on the SDSS DR7 spectroscopic sample, we derived a DA/non-DA ratio of 5.1 for hot WDs, with a lower limit of 3.5 if we consider clean DA WDs (no subtypes) alone. Based on the SDSS DR10 spectroscopic sample, we found that PG 1159 stars and O(He) stars may contribute to a similar extent to the non-DA WD channel. This further stresses the importance of the helium dominated stellar evolutionary channel.
One object is the most massive DO WD discovered so far with a mass of $1.07 M_\odot$ if it is an ONe-WD or $1.09 M_\odot$ if it is a CO-WD. It is a candidate for a massive post-super-AGB star that has just avoided an electron-capture supernova, because instabilities in the late thermally pulsing-AGB phase have led to the ejection of its hydrogen-rich envelope.

4.4 Identifying close binary central stars of PN with Kepler

One of the five investigated CSPNe with useful data, namely J 193110888+4324577, is a short-period (2.928 d), post-CE binary, exhibiting relativistic beaming effects and additionally shows a weak ellipsoidal variability. The binary system consists of a hot, hydrogen-rich pre-WD and – most likely – a more massive, cool WD.
The CSPN of Pa 5 has a consistent photometric period of 1.12 d, but shows no radial velocity shifts larger than 5 km/s. Thus, the photometric variability may be explained by the influence of an orbiting planet or by magnetic activity, but most likley by a evolved companion in a nearly-pole-on orbit. The spectral analysis of the CSPN revealed that it belongs to the class of O(He) stars, making it the tenth member of this small group, and only the third O(He) star with a detected PN. Differently to K 1−27 and LoTr 4, no traces of hydrogen are found in the atmosphere of Pa 5, however it displays the same carbon/nitrogen/oxygen abundance patterns like the other two O(He) CSPNe and HS 2209+8229. The kinematic age of the PN is only 6500 years.
The third CSPN, NGC 6826, has a Kepler light curve that was previously analyzed with the conclusion that it is due to rotational modulation implying a surface velocity of 78 km/s, something that can only be achieved in a merger.
The spectrum of the CSPN of Kn 61 has a too low S/N ratio for a precise spectral analysis, however, we could identify He II λ 4686 Å and several C IV absorption lines, confirming Kn 61 as a PG 1159 star. It exhibits a peculiar light variability with approximately triangular brightness peaks of 0.08−0.14 magnitudes and lasting 1−2 days, spaced irregularly at intervals of few days. The reason for this kind of variability is not understood.
Finally, the central star of the circular PN A 61 does not show a photometric variability above 2 mmag.
With the possible exception of the variability of Kn 61, all other variability behavior, whether due to binarity or not would not easily have been detected from the ground. Based on this very low object number, we conclude, that there are a lot more short periodic close binaries than the currently estimated fraction of 15% and that they can be discovered with ultra-high-precision photometry.

5 Outlook

To resolve the puzzle about the evolutionary status of SAO 244567, i.e., if it has recently suffered a late He-shell flash or a CE evolution, further observations are needed. The detection of a close binary would support the scenario of a CE ejection. Post-CE binaries have orbital periods typically between 0.1 and 10 days (Heber 2009), thus a close companion could be detected via radial velocity shifts in high-resolution spectra taken over this period.
The LTP scenario would predict an evolution back to the AGB, e.g. a decrease of the effective temperature (which is already indicated by the FUSE observations in 2006 and the nebula spectrum in 2013) and an increase of luminosity, i.e. an decrease in surface gravity accompanied by a possible increased mass-loss rate. With accepted UV HST/COS spectroscopy (which will be performed in September 2015), we will be able to follow the evolution of the surface properties of SAO 244567. The derived surface parameters could establish constraints for LTP evolutionary calculations, which would not only explain the nature of SAO 244567, but also provide a deeper insight in the formation process of hydrogen-deficient stars and offer a unique opportunity to directly test the accuracy of stellar evolution modeling.

Further investigations are required the resolve the evolutionary origin of the O(He) stars. It would be particularly interesting to search systematically for close companions to these stars. Firstly, because close binary systems are expected to have undergone a CE evolution and the ejection of a CE in a previous evolutionary stage could explain how O(He) stars could have lost their hydrogen-rich envelope. A comparison of the properties of the companions (masses, periods, eccentricities, ect.) with hydrogen-rich CSPNe close binary companions could also provide information about the CE ejection efficiency, a process that is still not understood (Ivanova *et al.*, 2013). Finally, the confirmation of close companions to O(He) stars would be a significant result, because it would be inconsistent with the merger scenario as triple star systems are arranged hierarchically.
To check if O(He) stars have lost their hydrogen-rich envelope via enhanced mass-loss, it would be worthy to derive mass-loss rates for possible progenitor stars. The O(He) stars recently discovered by Werner *et al.* (2014) have considerably lower surface gravities than those studied in Reindl *et al.* (2014b) and thus they could still show wind signatures in the UV spectra. In addition the mass-loss rates of the luminous He-sdO stars KS 292, LSE 153, and LSE 259 would be interesting to study. In their high-resolution IUE spectra the N V resonance lines display P-Cygni profiles; for LSE 259 even a FUSE spectrum

exists which shows P-Cygni profiles of the O VI resonance lines.
Merger-scenarios are currently the only way to connect O(He) to the compact He-sdO stars. Population synthesis models, that predict the observable numbers of O(He) stars relative to the number of He-sdO stars, could confirm the evolutionary link between these objects. The prediction of absolute numbers of O(He) stars currently observable in our Galaxy could further constrain the contribution of double WD mergers as evolutionary origin of these stars.

The known number of hot (pre-) WDs is still rather low and to draw statistically meaningful conclusions from their derived properties it would be desirable that more of these objects would be discovered. The SDSS DR12 was just made publicly available and is promising more of these objects. Since the SDSS DR4 stellar parameters of hot (pre-) WDs have so far only been derived for the hydrogen-deficient objects by means of NLTE model atmospheres. The NLTE-analysis of also the hot DA WDs would be in particular important to derive the hot end of the WD luminosity function (WDLF). A hot WDLF based on the SDSS DR4 was presented before (Krzesiński *et al.*, 2009), however since the DR10 the number of known hot WDs has more than doubled. Furthermore, Krzesiński *et al.* (2009) neglected the strong impact of the assumed scale height on the shape of especially the hot end of the LF by adopting the same scale height (250 pc, corresponding to the thin disk) for all of them. Rowell and Hambly (2011) took into account the different Galactic population memberships and calculated thin disc, thick disc and spheroid WDLFs from the SuperCOSMOS Sky Survey, however their LFs do not extend to the hot end.
So far, the Galactic distribution of white dwarfs was studied only for relatively cool and by that nearby WDs (e.g., Sion *et al.* 2014; Pauli *et al.* 2006). That is why a study of the Galactic distribution of hot WDs would be an interesting and new research of its own, because due to their high luminosities hot WDs cover a huge space volume (several kpc^3). Studies of WD kinematics can help to determine the fraction of the total mass of our Galaxy contained in the form of thick-disk and halo white dwarfs, an issue which is still under discussion (Pauli *et al.*, 2006). Finally, as show by Kalirai (2012), WDs that have just entered the WD cooling sequence can be used to determine the age of the Milky Way inner halo, a number that is so far based on four local WDs only.

Bibliography

Aller, A., Miranda, L. F., Ulla, A., Vázquez, R., Guillén, P. F., Olguín, L., Rodríguez-López, C., Thejll, P., Oreiro, R., Manteiga, M., and Pérez, E. (2013). Detection of a multishell planetary nebula around the hot subdwarf O-type star 2MASS J19310888+4324577. *A&A*, **552**, A25.

Althaus, L. G., Panei, J. A., Miller Bertolami, M. M., García-Berro, E., Córsico, A. H., Romero, A. D., Kepler, S. O., and Rohrmann, R. D. (2009). New Evolutionary Sequences for Hot H-Deficient White Dwarfs on the Basis of a Full Account of Progenitor Evolution. *ApJ*, **704**, 1605.

Arkhipova, V. P., Ikonnikova, N. P., Kniazev, A. Y., and Rajoelimanana, A. (2013). Rapid photometric and spectroscopic evolution of the young planetary nebula Hen 3-1357 and its central star SAO 244567. *Astronomy Letters*, **39**, 201.

Asplund, M., Lambert, D. L., Kipper, T., Pollacco, D., and Shetrone, M. D. (1999). The rapid evolution of the born-again giant Sakurai's object. *A&A*, **343**, 507–518.

Blöcker, T. (1995). Stellar evolution of low- and intermediate-mass stars. II. Post-AGB evolution. *A&A*, **299**, 755.

Blöcker, T. and Schönberner, D. (1996). Evolutionary post-AGB models: Application to the variable star FG Sge. *Mem. Soc. Astron. Italiana*, **67**, 665.

Blöcker, T. and Schönberner, D. (1997). Stellar evolution of low and intermediate-mass stars. III. an application of evolutionary post-AGB models: the variable central star FG Sagittae. *A&A*, **324**, 991.

Bobrowsky, M. (1994). Narrowband HST imagery of the young planetary nebula Henize 1357. *ApJ*, **426**, L47.

Bond, H. E. (2000). Binarity of Central Stars of Planetary Nebulae. In J. H. Kastner, N. Soker, and S. Rappaport, editors, *Asymmetrical Planetary Nebulae II: From Origins to Microstructures*, volume 199 of *Astronomical Society of the Pacific Conference Series*, page 115.

Brassard, P., Fontaine, G., Dufour, P., and Bergeron, P. (2007). The Origin and Evolution of DQ White Dwarfs: The Carbon Pollution Problem Revisited. In R. Napiwotzki and M. R. Burleigh, editors, *15th European Workshop on White Dwarfs*, volume 372 of *Astronomical Society of the Pacific Conference Series*, page 19.

Brown, T. M., Sweigart, A. V., Lanz, T., Landsman, W. B., and Hubeny, I. (2001). Flash Mixing on the White Dwarf Cooling Curve: Understanding Hot Horizontal Branch Anomalies in NGC 2808. *ApJ*, **562**, 368.

Brown, W. R., Kilic, M., Allende Prieto, C., and Kenyon, S. J. (2010). The ELM Survey. I. A Complete Sample of Extremely Low-mass White Dwarfs. *ApJ*, **723**, 1072.

Brown, W. R., Kilic, M., Allende Prieto, C., and Kenyon, S. J. (2012). The ELM Survey. III. A Successful Targeted Survey for Extremely Low Mass White Dwarfs. *ApJ*, **744**, 142.

Chayer, P., Fontaine, G., and Wesemael, F. (1995). Radiative Levitation in Hot White Dwarfs: Equilibrium Theory. *ApJS*, **99**, 189.

Clayton, G. C., Kerber, F., Pirzkal, N., De Marco, O., Crowther, P. A., and Fedrow, J. M. (2006). V605 Aquilae: The Older Twin of Sakurai's Object. *ApJ*, **646**, L69.

Dawson, K. S., Schlegel, D. J., Ahn, C. P., and et al. (2013). The Baryon Oscillation Spectroscopic Survey of SDSS-III. *AJ*, **145**, 10.

De Marco, O., Farihi, J., and Nordhaus, J. (2009). The WD perspective on the PN binary hypothesis. *Journal of Physics Conference Series*, **172**(1), 012031.

De Marco, O., Long, J., George, H. J., Hillwig, T., Kronberger, M., Howell, S., Reindl, N., and S., M. (2015). Identifying close binary central stars of PN with Kepler. *MNRAS, submitted*.

Dorman, B., Rood, R. T., and O'Connell, R. W. (1993). Ultraviolet Radiation from Evolved Stellar Populations. I. Models. *ApJ*, **419**, 596.

Dreizler, S. (1999). Hubble Space Telescope spectroscopy of hot helium-rich white dwarfs: metal abundances along the cooling sequence. *A&A*, **352**, 632.

Duerbeck, H. W., Benetti, S., Gautschy, A., van Genderen, A. M., Kemper, C., Liller, W., and Thomas, T. (1997). The Final Helium Flash Object Sakurai: Photometric Behavior and Physical Characteristics. *AJ*, **114**, 1657.

Eggen, O. J. and Greenstein, J. L. (1965). Spectra, colors, luminosities, and motions of the white dwarfs. *ApJ*, **141**, 83.

Eisenstein, D. J., Weinberg, D. H., Agol, E., Aihara, H., Allende Prieto, C., Anderson, S. F., Arns, J. A., Aubourg, É., Bailey, S., Balbinot, E., and et al. (2011). SDSS-III: Massive Spectroscopic Surveys of the Distant Universe, the Milky Way, and Extra-Solar Planetary Systems. *AJ*, **142**, 72.

Fontaine, G., Brassard, P., and Bergeron, P. (2001). The Potential of White Dwarf Cosmochronology. *PASP*, **113**, 409.

Frew, D. J., Bojičić, I. S., Parker, Q. A., Stupar, M., Wachter, S., DePew, K., Danehkar, A., Fitzgerald, M. T., and Douchin, D. (2014). The planetary nebula Abell 48 and its [WN] nucleus. *MNRAS*, **440**, 1345.

Fujimoto, M. Y. (1977). On the Origin of R-Type Carbon Stars: Possibility of Hydrogen Mixing during Helium Flicker. *PASJ*, **29**, 331.

Gingerich, O. (2005). Tycho Brahe and the Nova of 1572. In M. Turatto, S. Benetti, L. Zampieri, and W. Shea, editors, *1604-2004: Supernovae as Cosmological Lighthouses*, volume 342 of *Astronomical Society of the Pacific Conference Series*, page 3.

Girven, J., Gänsicke, B. T., Steeghs, D., and Koester, D. (2011). DA white dwarfs in Sloan Digital Sky Survey Data Release 7 and a search for infrared excess emission. *MNRAS*, **417**, 1210.

Green, R. F., Schmidt, M., and Liebert, J. (1986). The Palomar-Green catalog of ultraviolet-excess stellar objects. *ApJS*, **61**, 305.

Greenstein, J. L. (1958). The Spectra of the White Dwarfs. *Handbuch der Physik*, **50**, 161.

Hagen, H.-J., Groote, D., Engels, D., and Reimers, D. (1995). The Hamburg Quasar Survey. I. Schmidt observations and plate digitization. *A&AS*, **111**, 195.

Hajduk, M., Zijlstra, A. A., Herwig, F., van Hoof, P. A. M., Kerber, F., Kimeswenger, S., Pollacco, D. L., Evans, A., Lopéz, J. A., Bryce, M., Eyres, S. P. S., and Matsuura, M. (2005). The Real-Time Stellar Evolution of Sakurai's Object. *Science*, **308**, 231.

Hall, P. D., Tout, C. A., Izzard, R. G., and Keller, D. (2013). Planetary nebulae after common-envelope phases initiated by low-mass red giants. *MNRAS*, **435**, 2048.

Heap, S. R. (1975). Spectroscopic studies of very old hot stars. I - NGC 246 and its exciting star. *ApJ*, **196**, 195.

Heber, U. (2009). Hot Subdwarf Stars. *ARA&A*, **47**, 211.

Hermes, J. J., Montgomery, M. H., Winget, D. E., Brown, W. R., Kilic, M., and Kenyon, S. J. (2012). SDSS J184037.78+642312.3: The First Pulsating Extremely Low Mass White Dwarf. *ApJ*, **750**, L28.

Hermes, J. J., Montgomery, M. H., Gianninas, A., Winget, D. E., Brown, W. R., Harrold, S. T., Bell, K. J., Kenyon, S. J., Kilic, M., and Castanheira, B. G. (2013). A new class of pulsating white dwarf of extremely low mass: the fourth and fifth members. *MNRAS*, **436**, 3573.

Iben, Jr., I., Kaler, J. B., Truran, J. W., and Renzini, A. (1983). On the evolution of those nuclei of planetary nebulae that experience a final helium shell flash. *ApJ*, **264**, 605.

Isern, J., García-Berro, E., Torres, S., and Catalán, S. (2008). Axions and the Cooling of White Dwarf Stars. *ApJ*, **682**, L109.

Ivanova, N., Justham, S., Chen, X., De Marco, O., Fryer, C. L., Gaburov, E., Ge, H., Glebbeek, E., Han, Z., Li, X.-D., Lu, G., Marsh, T., Podsiadlowski, P., Potter, A., Soker, N., Taam, R., Tauris, T. M., van den Heuvel, E. P. J., and Webbink, R. F. (2013). Common envelope evolution: where we stand and how we can move forward. *A&A Rev.*, **21**, 59.

Jeffery, C. S. and Schönberner, D. (2006). Stellar archaeology: the evolving spectrum of FG Sagittae. *A&A*, **459**, 885.

Kaler, J. B. (1978). The forbidden O III lines as a quantitative indicator of nebular central-star temperature. *ApJ*, **220**, 887.

Kalirai, J. S. (2012). The age of the Milky Way inner halo. *Nature*, **486**, 90.

Kalirai, J. S., Saul Davis, D., Richer, H. B., Bergeron, P., Catelan, M., Hansen, B. M. S., and Rich, R. M. (2009). The Masses of Population II White Dwarfs. *ApJ*, **705**, 408.

Kleinman, S. J., Harris, H. C., Eisenstein, D. J., Liebert, J., Nitta, A., Krzesiński, J., Munn, J. A., Dahn, C. C., Hawley, S. L., Pier, J. R., Schmidt, G., Silvestri, N. M., Smith, J. A., Szkody, P., Strauss, M. A., Knapp, G. R., Collinge, M. J., Mukadam, A. S., Koester, D., Uomoto, A., Schlegel, D. J., Anderson, S. F., Brinkmann, J., Lamb, D. Q., Schneider, D. P., and York, D. G. (2004). A Catalog of Spectroscopically Identified White Dwarf Stars in the First Data Release of the Sloan Digital Sky Survey. *ApJ*, **607**, 426.

Koester, D., Voss, B., Napiwotzki, R., Christlieb, N., Homeier, D., Lisker, T., Reimers, D., and Heber, U. (2009). High-resolution UVES/VLT spectra of white dwarfs observed for the ESO SN Ia Progenitor Survey. III. DA white dwarfs. *A&A*, **505**, 441–462.

Krzesiński, J., Kleinman, S. J., Nitta, A., Hügelmeyer, S., Dreizler, S., Liebert, J., and Harris, H. (2009). A hot white dwarf luminosity function from the Sloan Digital Sky Survey. *A&A*, **508**, 339.

Lanz, T., Brown, T. M., Sweigart, A. V., Hubeny, I., and Landsman, W. B. (2004). Flash Mixing on the White Dwarf Cooling Curve: Far Ultraviolet Spectroscopic Explorer Observations of Three He-rich sdB Stars. *ApJ*, **602**, 342.

Latour, M., Fontaine, G., Chayer, P., and Brassard, P. (2013). A Non-LTE Analysis of the Hot Subdwarf O Star BD+28°4211. I. The UV Spectrum. *ApJ*, **773**, 84.

Lorimer, D. R. (2008). Binary and Millisecond Pulsars. *Living Reviews in Relativity*, **11**, 8.

Maxted, P. F. L., Anderson, D. R., Burleigh, M. R., Collier Cameron, A., Heber, U., Gänsicke, B. T., Geier, S., Kupfer, T., Marsh, T. R., Nelemans, G., O'Toole, S. J., Østensen, R. H., Smalley, B., and West, R. G. (2011). Discovery of a stripped red giant core in a bright eclipsing binary system. *MNRAS*, **418**, 1156.

Méndez, R. H., Miguel, C. H., Heber, U., and Kudritzki, R. P. (1986). Helium rich subdwarf O stars and central stars of planetary nebulae. In K. Hunger, D. Schönberner, and N. Kameswara Rao, editors, *IAU Colloq. 87: Hydrogen Deficient Stars and Related Objects*, volume 128 of *Astrophysics and Space Science Library*, page 323.

Miller Bertolami, M. M. (2014). Limits on the neutrino magnetic dipole moment from the luminosity function of hot white dwarfs. *A&A*, **562**, A123.

Miller Bertolami, M. M. and Althaus, L. G. (2006). Full evolutionary models for PG 1159 stars. Implications for the helium-rich O(He) stars. *A&A*, **454**, 845.

Miller Bertolami, M. M., Althaus, L. G., Unglaub, K., and Weiss, A. (2008). Modeling He-rich subdwarfs through the hot-flasher scenario. *A&A*, **491**, 253.

Miller Bertolami, M. M., Melendez, B. E., Althaus, L. G., and Isern, J. (2014). Revisiting the axion bounds from the Galactic white dwarf luminosity function. *J. Cosmology Astropart. Phys.*, **10**, 69.

Miszalski, B., Acker, A., Moffat, A. F. J., Parker, Q. A., and Udalski, A. (2009). Binary planetary nebulae nuclei towards the Galactic bulge. I. Sample discovery, period distribution, and binary fraction. *A&A*, **496**, 813.

Miszalski, B., Crowther, P. A., De Marco, O., Köppen, J., Moffat, A. F. J., Acker, A., and Hillwig, T. C. (2012). IC 4663: the first unambiguous [WN] Wolf-Rayet central star of a planetary nebula. *MNRAS*, **423**, 934.

Mowlavi, N. (1999). Stellar evolution in real time: single star evolution. *New A Rev.*, **43**, 389.

Parker, Q. A., Acker, A., Frew, D. J., Hartley, M., Peyaud, A. E. J., Ochsenbein, F., Phillipps, S., Russeil, D., Beaulieu, S. F., Cohen, M., Köppen, J., Miszalski, B., Morgan, D. H., Morris, R. A. H., Pierce, M. J., and Vaughan, A. E. (2006). The Macquarie/AAO/Strasbourg Hα Planetary Nebula Catalogue: MASH. *MNRAS*, **373**, 79.

Parthasarathy, M., Garcia-Lario, P., Pottasch, S. R., Manchado, A., Clavel, J., de Martino, D., van de Steene, G. C. M., and Sahu, K. C. (1993). SAO 244567 - A post-AGB star which has turned into a planetary nebula within the last 40 years. *A&A*, **267**, L19.

Parthasarathy, M., Garcia-Lario, P., de Martino, D., Pottasch, S. R., Kilkenny, D., Martinez, P., Sahu, K. C., Reddy, B. E., and Sewell, B. T. (1995). Fading and variations in the spectrum of the central star of the very young planetary nebula SAO 244567 (Hen 1357). *A&A*, **300**, L25.

Pauli, E.-M., Napiwotzki, R., Heber, U., Altmann, M., and Odenkirchen, M. (2006). 3D kinematics of white dwarfs from the SPY project. II. *A&A*, **447**, 173.

Pelletier, C., Fontaine, G., Wesemael, F., Michaud, G., and Wegner, G. (1986). Carbon pollution in helium-rich white dwarf atmospheres Time-dependent calculations of the dredge-up process. *ApJ*, **307**, 242.

Preval, S. P., Barstow, M. A., Badnell, N. R., Holberg, J. B., and Hubeny, I. (2014). A possible solution to the Lyman/Balmer line problem in hot DA white dwarfs. *ArXiv e-prints*.

Rauch, T. (2012). Recent Investigations on AA Doradus. In D. Kilkenny, C. S. Jeffery, and C. Koen, editors, *Fifth Meeting on Hot Subdwarf Stars and Related Objects*, volume 452 of *Astronomical Society of the Pacific Conference Series*, page 111.

Rauch, T., Köppen, J., and Werner, K. (1994). Spectral analysis of the planetary nebula K 1-27 and its very hot hydrogen-deficient central star. *A&A*, **286**, 543.

Rauch, T., Köppen, J., and Werner, K. (1996). Spectral analysis of the multiple-shell planetary nebula LoTr4 and its very hot hydrogen-deficient central star. *A&A*, **310**, 613.

Rauch, T., Dreizler, S., and Wolff, B. (1998). Spectral analysis of O(He)-type post-AGB stars. *A&A*, **338**, 651.

Rauch, T., Reiff, E., Werner, K., Herwig, F., Koesterke, L., and Kruk, J. W. (2006). On the Evolutionary Status of Extremely Hot Helium Stars — are O(He) Stars Successors of RCrB Stars? In G. Sonneborn, H. W. Moos, and B.-G. Andersson, editors, *Astrophysics in the Far Ultraviolet: Five Years of Discovery with FUSE*, volume 348 of *Astronomical Society of the Pacific Conference Series*, page 194.

Rauch, T., Werner, K., Biémont, É., Quinet, P., and Kruk, J. W. (2012). Stellar laboratories: new Ge V and Ge VI oscillator strengths and their validation in the hot white dwarf RE 0503-289. *A&A*, **546**, A55.

Rauch, T., Werner, K., Quinet, P., and Kruk, J. W. (2014a). Stellar laboratories. II. New Zn iv and Zn v oscillator strengths and their validation in the hot white dwarfs G191-B2B and RE 0503-289. *A&A*, **564**, A41.

Rauch, T., Werner, K., Quinet, P., and Kruk, J. W. (2014b). Stellar laboratories. III. New Ba v, Ba vi, and Ba vii oscillator strengths and the barium abundance in the hot white dwarfs G191-B2B and RE 0503-289. *A&A*, **566**, A10.

Reimers, D. (1975). Circumstellar absorption lines and mass loss from red giants. *Memoires of the Societe Royale des Sciences de Liege*, **8**, 369.

Reindl, N. (2012). *Spektralanalyse von O(He)-Sternen*. Master thesis, University Tübingen, Germany, http://astro.uni-tuebingen.de/publications/diplom/reindl-master.pdf.

Reindl, N. and Rauch, T. (2014). TheoSSA - Model WD Spectra on Demand: The impact of Ne, Na, Mg, and iron-group elements on the Balmer lines. In *to appear in the Proceedings of the 19th European White Dwarf Workshop*.

Reindl, N., Rauch, T., Werner, K., Kepler, S. O., Gänsicke, B. T., and Gentile Fusillo, N. P. (2014a). Analysis of cool DO-type white dwarfs from the Sloan Digital Sky Survey data release 10. *A&A*, **572**, A117.

Reindl, N., Rauch, T., Werner, K., Kruk, J. W., and Todt, H. (2014b). On helium-dominated stellar evolution: the mysterious role of the O(He)-type stars. *A&A*, **566**, A116.

Reindl, N., Rauch, T., Parthasarathy, M., Werner, K., Kruk, J. W., Hamann, W.-R., Sander, A., and Todt, H. (2014c). The rapid evolution of the exciting star of the Stingray nebula. *A&A*, **565**, A40.

Rowell, N. and Hambly, N. C. (2011). White dwarfs in the SuperCOSMOS Sky Survey: the thin disc, thick disc and spheroid luminosity functions. *MNRAS*, **417**, 93.

Schönberner, D. (1979). Asymptotic giant branch evolution with steady mass loss. *A&A*, **79**, 108.

Schönberner, D. (2008). FG Sge, V605 Aql, Sakurai – Facts and Fictions. In A. Werner and T. Rauch, editors, *Hydrogen-Deficient Stars*, volume 391 of *Astronomical Society of the Pacific Conference Series*, page 139.

Sion, E. M., Holberg, J. B., Oswalt, T. D., McCook, G. P., Wasatonic, R., and Myszka, J. (2014). The White Dwarfs within 25 pc of the Sun: Kinematics and Spectroscopic Subtypes. *AJ*, **147**, 129.

Staff, J. E., Menon, A., Herwig, F., Even, W., Fryer, C. L., Motl, P. M., Geballe, T., Pignatari, M., Clayton, G. C., and Tohline, J. E. (2012). Do R Coronae Borealis Stars Form from Double White Dwarf Mergers? *ApJ*, **757**, 76.

Todt, H., Kniazev, A. Y., Gvaramadze, V. V., Hamann, W.-R., Buckley, D., Crause, L., Crawford, S. M., Gulbis, A. A. S., Hettlage, C., Hooper, E., Husser, T.-O., Kotze, P., Loaring, N., Nordsieck, K. H., O'Donoghue, D., Pickering, T., Potter, S., Romero-Colmenero, E., Vaisanen, P., Williams, T., and Wolf, M. (2013). Abell 48 - a rare WN-type central star of a planetary nebula. *MNRAS*, **430**, 2302.

Unglaub, K. and Bues, I. (2000). The chemical evolution of hot white dwarfs in the presence of diffusion and mass loss. *A&A*, **359**, 1042.

Van Hoof, P. A. M., Hajduk, M., Zijlstra, A. A., Herwig, F., Evans, A., van de Steene, G. C., Kimeswenger, S., Kerber, F., and Eyres, S. P. S. (2007). Recent Observations of Sakurai's Object. In *Asymmetrical Planetary Nebulae IV*, page 20.

Wassermann, D., Werner, K., Rauch, T., and Kruk, J. W. (2010). Metal abundances in the hottest known DO white dwarf (KPD 0005+5106). *A&A*, **524**, A9.

Webbink, R. F. (1984). Double white dwarfs as progenitors of R Coronae Borealis stars and Type I supernovae. *ApJ*, **277**, 355–360.

Werner, K. (1996). On the Balmer Line Problem. *ApJ*, **457**, L39.

Werner, K. (2012). Central stars of planetary nebulae: The white dwarf connection. In *Planetary Nebulae: An Eye to the Future*, volume 283 of *IAU Symposium*, page 196.

Werner, K. and Herwig, F. (2006). The Elemental Abundances in Bare Planetary Nebula Central Stars and the Shell Burning in AGB Stars. *PASP*, **118**, 183.

Werner, K., Deetjen, J. L., Dreizler, S., Nagel, T., Rauch, T., and Schuh, S. L. (2003). Model Photospheres with Accelerated Lambda Iteration. In I. Hubeny, D. Mihalas, and K. Werner, editors, *Stellar Atmosphere Modeling*, volume 288 of *Astronomical Society of the Pacific Conference Series*, page 31.

Werner, K., Rauch, T., Ringat, E., and Kruk, J. W. (2012). First Detection of Krypton and Xenon in a White Dwarf. *ApJ*, **753**, L7.

Werner, K., Rauch, T., and Kepler, S. O. (2014). New hydrogen-deficient (pre-) white dwarfs in the Sloan Digital Sky Survey Data Release 10. *A&A*, **564**, A53.

Wesemael, F., Green, R. F., and Liebert, J. (1985). Spectrophotometric and model-atmosphere analyses of the hot DO and DAO white dwarfs from the Palomar-Green survey. *ApJS*, **58**, 379.

Yanny, B., Rockosi, C., Newberg, H. J., and et al. (2009). SEGUE: A Spectroscopic Survey of 240,000 Stars with g = 14-20. *AJ*, **137**, 4377.

York, D. G., Adelman, J., Anderson, Jr., J. E., and et al. (2000). The Sloan Digital Sky Survey: Technical Summary. *AJ*, **120**, 1579.

Zhang, X. and Jeffery, C. S. (2012a). Can R Coronae Borealis stars form from the merger of two helium white dwarfs? *MNRAS*, **426**, L81.

Zhang, X. and Jeffery, C. S. (2012b). Evolutionary models for double helium white dwarf mergers and the formation of helium-rich hot subdwarfs. *MNRAS*, **419**, 452.

Zhang, X., Jeffery, C. S., Chen, X., and Han, Z. (2014). Post-merger evolution of carbon-oxygen + helium white dwarf binaries and the origin of R Coronae Borealis and extreme helium stars. *MNRAS*, **445**, 660.